Dissertation
submitted to the
Combined Faculties for the Natural Sciences and for Mathematics
of the Ruperto-Carola University of Heidelberg, Germany
for the degree of
Doctor of Natural Sciences

Put forward by
Diplom-Physikerin Sophie Friederike Warken, geb. Winterhalder
born in Pforzheim

Oral examination: 19.04.2017

Potentials and limitations of multi-proxy records in speleothem research

-

Case studies in complex climate systems

Referees:
Prof. Dr. Augusto Mangini
Prof. Dr. Werner Aeschbach

Abstract

The central goal of this dissertation is assessing the benefits and limitations of multi-proxy approaches in speleothem research with respect to paleo climate reconstruction. Hence, the aims were evaluating the environmental controls of speleothem proxies such as stable isotopes or trace elements, and the application to samples from locations affected by complex climate interactions. Thus, this thesis provides an important contribution to the recent scientific discussion in speleothem and climate research.

The presented case studies comprise a Holocene stalagmite from southwestern Romania, and two speleothems from the Caribbean realm covering major parts of the last Glacial cycle. All records are based on high-precision dating methods, such as ^{230}Th/U dating, lamina counting or radiocarbon dating. The analysis of stable isotope δ^{18}O and δ^{13}C composition together with trace elemental signatures enables a broad survey of past environmental changes comprising temperature and rainfall variability as well as soil and vegetation dynamics. The studies presented in this thesis demonstrate the strong benefits of the combination of several proxies in speleothems and in the investigated regions, they provide the first speleothem derived climate reconstructions, respectively, combining successfully both stable isotopes and elemental proxies.

In tropical locations, the δ^{18}O values in speleothems may be reliable recorders of past rainfall changes. However, a number of processes such as temperature variability, source effects and disequilibrium fractionation affecting the oxygen isotopic composition have to be carefully evaluated. Under certain circumstances, trace elements such as magnesium and strontium are found to constitute valuable tracers of hydrological variability, whereas phosphorus is most commonly associated with soil and vegetation dynamics. However, the interpretation of P/Ca is found to be diverse in the three case studies. To explain the non-conventional P systematics in the Cuban sample, a mechanism was devised which previously has received little attention.

Stalagmite C09-2 from southwestern Romania emerged as one of the unique samples appropriate for quantitative reconstruction of past climate variability. The Mg/Ca ratio was found to be strongly connected with past winter rainfall, and the reconstructed precipitation estimates for the last 3.6 ka are in agreement with other local and supra-regional records. The δ^{18}O record from stalagmite PR-LA-1 is one of the first speleothem derived long-term reconstructions of rainfall variability from the western tropical Atlantic realm which demonstrates the imprint of both the Heinrich stadials as well as the Dansgaard/Oeschger cycles on Puerto Rico during the last Glacial. In addition, stalagmite CM from western Cuba provides one of the longest speleothem records from the Caribbean region, and the geochemical evidence from the stable isotope and trace element signatures gives a comprehensive picture of past environmental variability over a long time interval of the last Glacial.

Zusammenfassung

Das Hauptthema dieser Dissertation ist die Beurteilung der Vor- und Nachteile der Anwendung von mehreren Spurenstoffen in der Speläothemforschung im Hinblick auf die Rekonstruktion der Klimavariabilität in der Vergangenheit. Die Ziele waren daher die Herausarbeitung der relevanten Umwelteinflüsse auf die angewandten Proxies, wie zum Beispiel stabile Isotopenverhältnisse oder Spurenelemente, und deren Anwendung an Hand von Fallstudien aus Regionen, welche von komplexen Klimawechselwirkungen beeinflusst werden. Die präsentierte Arbeit stellt damit einen wichtigen Beitrag zur aktuellen wissenschaftlichen Diskussion in der Speläothem- und Klimaforschung dar.

Die gezeigten Fallstudien umfassen einen holozänen Stalagmit aus dem Südwesten Rumäniens, sowie zwei Speläotheme aus der Karibik, welche wesentliche Abschnitte des letzten Glazialen Zyklus abdecken. Die erstellten Zeitreihen basieren auf hochpräzisen Datierungstechniken, wie der ^{230}Th/U-Methode, Lagenzählung oder der Radiokarbonmethode. Die Auswertung der stabilen Isotopenverhältnisse δ^{18}O and δ^{13}C zusammen mit bestimmten Spurenelementgehalten ermöglicht einen breiten Überblick über vergangene Umweltveränderungen wie zum Beispiel Temperatur- und Niederschlagsvariabilität oder Boden- und Vegetationsdynamik. In den jeweiligen Gegenden sind die Studien in dieser Arbeit mit die ersten Speläothemzeitreihen, in denen die genannten Proxies erfolgreich kombiniert werden und stellen daher den großen Nutzen der Anwendung mehrerer Indikatoren in Speläothemen dar.

In den Tropen können δ^{18}O Werte in Speläothemen ein verlässlicher Indikator für die Niederschlagsvariabilität in der Vergangenheit sein. Jedoch beeinflussen eine Reihe von weiteren Prozessen die isotopische Zusammensetzung des Sauerstoffs, wie zum Beispiel Temperaturschwankungen, Quelleneffekte oder Ungleichgewichtsfraktionierung. Spurenelemente wie Magnesium oder Strontium können unter bestimmten Umständen wertvolle Indizien auf hydrologische Prozesse in Höhlensystemen liefern. Dagegen wird der Phosphorgehalt in Speläothemen meist mit Boden- und Vegetationsdynamik assoziiert. Interessanterweise unterscheiden sich jedoch in den drei Fallstudien die Interpretationen des P/Ca verhältnisses. Um die unkonventionelle P Systematik im kubanischen Stalagmiten zu erklären, wurde ein bislang wenig beachteter Mechanismus neu beleuchtet.

Der Stalagmit C09-2 aus dem Südwesten Rumäniens hebt sich als eine der wenigen Proben hervor, welche sich für quantitative Klimarekonstruktion eignen. Es stellte sich heraus, dass das Mg/Ca Verhältnis stark mit dem regionalen Winterniederschlag korreliert. Die daraus abgeleitete Niederschlagszeitreihe für die letzten 3,6 ka stimmt in vielen Bereichen mit anderen lokalen und überregionalen Rekonstruktionen überein. Die δ^{18}O Zeitreihe der Probe PR-LA-1 aus Puerto Rico ist eine der ersten Niederschlagsrekonstruktionen aus dem westlichen, tropischen Atlantik, die sowohl den Einfluss der Heinrich Kaltphasen als auch der Dansgaard/Oeschger Zyklen während dem letzten Glazial zeigt. Stalagmit CM aus West-Kuba bietet eine der längsten Speläothemzeitreihen aus der Karibik. Auch hier ergeben die geochemischen Hinweise aus den stabilen Isotopenverhältnissen und Spurenelementen ein zusammenhängendes Bild der Umweltveränderungen der Vergangenheit.

Contents

Part I

Introduction

1 Motivation

Reconstruction of past climate variability from natural archives such as ice cores, marine or lake sediments, tree rings, corals or speleothems offers the possibility to extend the observational records back in time. This knowledge helps to improve the projections for future climate trends and its impacts on the global and regional environments. For this purpose, speleothems are valuable paleo climate archives, which can provide precisely dated reconstructions of past climate on various time scales from sub-annual to glacial-interglacial variability (e.g., Wang et al. (2001); Cruz et al. (2007); Fleitmann et al. (2009); Tan et al. (2014); Baker et al. (2015)).

The formation of speleothems occurs within carbonate rocks and depends on various factors (Fairchild et al., 2006a; Fairchild and Baker, 2012). The main processes controlling the proxies eventually incorporated in speleothem calcite comprise the transport of moisture to the location of the cave and through the soil and karst system until the incorporation in the crystal lattice (Figure 1.1).

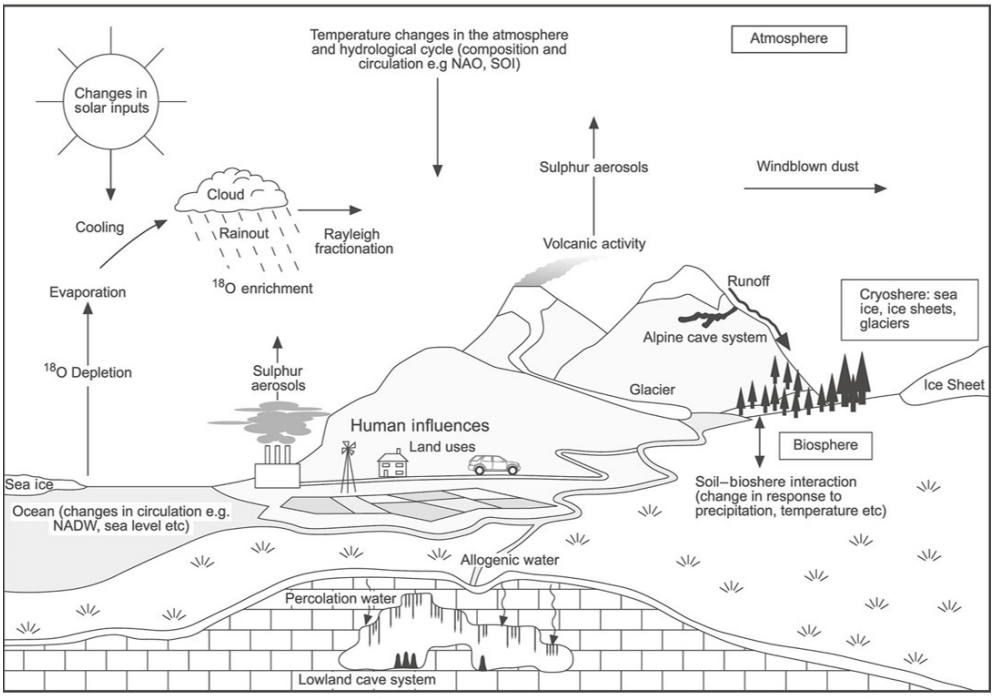

Figure 1.1: *Schematic view on environmental controls on signals recorded by speleothems (after Fairchild et al. (2006a)).*

1 Motivation

For the purpose of climate reconstruction, an increasing number of proxies and methods is applied in speleothem research, amongst the most commonly used stable isotopes of oxygen and carbon (Lachniet and Patterson, 2009; Dreybrodt and Scholz, 2011). A valuable proxy to trace the pathway of the rain water are stable oxygen isotopes ($\delta^{18}O$) which have long been used to reconstruct cave temperature or properties of meteoric precipitation (Fairchild and Treble, 2009; McDermott, 2004). Carbon isotopes ($\delta^{13}C$) are widely applied e.g., to recover information about soil activity and vegetation density (Dorale et al., 1992; Genty et al., 2003). But a much greater variety of parameters can be analyzed and used to consolidate or expand the interpretation of speleothem climate records. The shape of the specimen itself, as well as the mineralogy and petrology of the calcium carbonate crystals can already provide valuable information about past cave environments (Frisia et al., 2000; Kaufmann, 2003; Frisia, 2015).

Recent research also focuses on the analysis and interpretation of trace elements such as magnesium or strontium, which were found to provide hydrological information under certain circumstances (Borsato et al., 2007; Treble et al., 2003; Cruz et al., 2007). Analytical methods such as e.g., laser ablation or synchrotron XRF mapping enable the construction of highly resolved proxy records (Borsato et al., 2007; Tan et al., 2014). Hence, the understanding of the processes determining incorporation and variability of certain elemental proxies has considerably grown in the last decade (e.g., Treble et al. (2005); Borsato et al. (2007); Wassenburg et al. (2012)).

Additionally, new methods and proxies are continuously investigated and improved, such as the direct analysis of fluid inclusions in speleothem calcite (e.g., Dublyansky and Spötl (2009); Krüger et al. (2011); Kluge et al. (2014)) or the measurement of 'clumped isotopes' (Ghosh et al., 2006; Eiler, 2007; Affek et al., 2008). Various more proxies have found application in speleothem research, such as annual lamina width (Baker et al., 2008; Roberts et al., 1998) or growth rate (Tan et al., 2013). Dating information can be retrieved by identifying the 20^{th} century atmospheric radiocarbon bomb peak (Genty et al., 1998; Noronha et al., 2015; Sundqvist et al., 2013) whereas some publications deal with the analysis and interpretation of organic components in speleothems (Blyth et al., 2008; McGarry and Baker, 2000). Growing interest have also found the improvements in the analysis of fluid inclusions in speleothems, e.g. for reconstruction of the isotopic composition of paleo dripwater (Dublyansky and Spötl, 2009; Arienzo et al., 2013; Affolter et al., 2015; Labuhn et al., 2015) or the reconstruction of paleo temperatures (Kluge et al., 2008; Krüger et al., 2011; Kluge et al., 2014).

A very important measure for decoding the climatic imprint in speleothem calcite is the extensive monitoring of cave air and dripwater parameters (Mattey et al., 2010; Riechelmann et al., 2011). But also much effort was made to establish cave or karst-analogue laboratory studies (Huang et al., 2001; Tremaine and Froelich, 2013; Hansen et al., 2013), as well as theoretical and numerical models (Kaufmann, 2003; Mühlinghaus et al., 2009; Scholz et al., 2009; Wackerbarth et al., 2010; Dreybrodt and Scholz, 2011; Deininger et al., 2012). The knowledge of the processes determining speleothem formation greatly improves the interpretation of records deduced from samples from well-understood cave systems (Mattey et al., 2010).

Deciphering the environmental controls on climate parameters may be especially difficult in regions with a complex interplay of different local or interconnected parameters influencing climate variability on varying timescales. Thus, research rather focused on regions within climatological frameworks which can be relatively easy reduced to very few unknowns in the key controls of the proxy parameters. Suitable are for example locations affected by monsoon systems (e.g., southeastern Asia (Wang et al., 2008, 2001)), (semi-)arid regions such as the eastern Mediterranean or the Middle East (e.g.,Affek et al. (2008); Fleitmann et al. (2009)) or the tropical latitudes, which receive its precipitation mainly dependent on the position of the Intertropical Convergence Zone (ITCZ) (Wang et al., 2004; Cruz et al., 2009; Lachniet, 2009b; Strikis et al., 2011). Another site mainly influenced by only very few climate parameters or teleconnection pattern, is for example western Europe (Mangini et al., 2005; Trouet et al., 2009), which was found to be strongly affected by the variability of the North Atlantic Oscillation (NAO) (Wanner et al., 2001; Hurrell et al., 2003). In some cases, it is even possible to derive a transfer function from the proxy to the climate parameter and to quantitatively reconstruct precipitation or temperature variability (Mangini et al., 2005; Tan et al., 2013; Johnson et al., 2006).

However, in order to adjust the predictions of future climate change it is important to improve the understanding of spatial and temporal connections. Thus, it is crucial to fill the gaps in the global network of climate reconstructions, applying also to geographically and climatologically complex regions. Affected are for example locations at the transition between different climate zones, which are influenced by an interplay of atmospheric teleconnection patterns. Other factors complicating the interpretation of climate records may be orographic structures such as mountain chains. Additionally, at many locations, it is most probable that the predominant processes are not temporally stable. hence, establishing robust climate reconstructions for such regions is a challenge.

This thesis is an approach towards a better understanding of the interpretation of speleothem records regarding the application of certain proxies on the basis of case studies also from complex climate systems (section 1.1) and provides an important contribution to the recent discussion in speleothem and climate research.

1.1 Outline of this thesis

The main goals of this dissertation are increasing the spatial coverage of paleo climate data from terrestrial archives, applying speleothem studies to meet the objection of complex climate systems and increasing the knowledge and understanding of past climate conditions in the investigated regions. A further main task is to eventually assess the benefits and limitations of multi-proxy speleothem records. Thus, the extraction of appropriate proxies and methods as well as the improvement of their general understanding is essential.

For this purpose, a range of proxies has been measured from three speleothems from different localities. The tracers comprise the commonly used stable isotope ratios of oxygen and carbon as well as a number of trace elements, with the constructed records basing on high-precision dating methods. The combination of these multiple proxies is evaluated and assessed with respect to their advantages and disadvantages in speleothem research.

After this paragraph, a brief overview of the featured case studies and publications follows together with a statement to the contributions of the authors and co-authors of each case study and publication, respectively. In the introducing Chapter 2, the relevant aspects of the most important processes and proxies for this dissertation are summarized, followed by a short description of the applied methods in Chapter 3. The sites of the case studies are located in the Caribbean region on the greater Antilles (western Cuba and Puerto Rico) and in eastern Europe (southwestern Romania). Both regions are characterized by a complex interplay between atmospheric teleconnection patterns and further - partially competing - climate mechanisms. Hence, the climatological background and current state of research concerning the investigated locations are pointed out in Chapter 4.

Subsequently, the main part consists of the case studies, presented in the format of self-contained paper manuscripts, respectively (Chapters 5 to 7). The thesis concludes with a discussion of the presented results concerning the main methodological (Chapter 8) as well as the climatological inferences (Chapter 9). The dissertation concludes with a final outlook in Chapter 10.

1.2 List of papers

This doctoral dissertation consists of this thesis based on the following manuscripts I to III, supported by the featured publications IV and V.

This dissertation was supervised by Prof. Augusto Mangini (Institute of Environmental Physics, University of Heidelberg) and Prof. Denis Scholz (Institute for Geosciences, University of Mainz).

Paper I

Warken S.F., Scholz, D., Vieten R., Spötl C., Jochum, K.P., Miller T.E., Winter A., Schröder-Ritzrau A. and Mangini A. *Manuscript.* Millennial scale climate variability on Puerto Rico reconstructed from a multi-proxy speleothem record spanning 46 - 15 ka BP.

Paper II

Warken S.F., Scholz, D., Spötl C., Jochum, K.P., Pajón J.M. and Mangini A. *Manuscript.* Variability of the tropical hydrological cycle during the last Glacial deduced from a multi-proxy speleothem record from western Cuba.

Paper III

Warken S.F., Schröder-Ritzrau A., Fohlmeister J., Arps J., Constantin S., Terente M., Spötl C., Gerdes A., Esper J., Frank N., Mangini A. and Scholz D. *Manuscript.* Hydroclimate variability in SW Romania during the last 3.6 ka reconstructed from a high-resolution speleothem multi-proxy record.

Featured publications:

Paper I is based on an extensive monitoring program in Cueva Larga:

Paper IV

Vieten R., Winter A., **Warken S.F.**, Schröder-Ritzrau A., Miller T.E. and Scholz D. (2016). Seasonal temperature variations controlling cave ventilation processes in Cueva Larga, Puerto Rico. International Journal of Speleology, 45(3): 7.

Paper V

Vieten R., **Winterhalder S.**, Winter A., Scholz D., Miller T., Spötl C. and Schröder-Ritzrau A. (in press). Monitoring of Cueva Larga, Puerto Rico - a First Step to Decode Speleothem Climate Records. Karst Groundwater Contamination and Public Health. Selected papers and abstracts of the symposium held January 27 through 30, 2016, San Juan, Puerto Rico. Karst Waters Institute Special Publication, 19: 74.

1.3 General information and author contributions

Paper I

Sample PR-LA-1 originates from Cueva Larga, Puerto Rico. A long-term monitoring program in Cueva Larga since 2012 resulted in two recent publications (Vieten et al., 2016, in press). These papers form a basic framework for interpreting the trace element and stable isotope records of PR-LA-1.

The study was conceived and designed by D. Scholz, A. Mangini and S. Warken. S. Warken wrote the manuscript in close collaboration with D. Scholz.

Stable isotope lab work has been carried out by S. Warken under the guidance of C. Spötl. Trace elemental analysis has been performed by S. Warken under the guidance of K. Jochum. Dating of sample material has been carried out by S. Warken under the guidance of A. Mangini and D. Scholz. Age modeling and statistical analysis has been performed by S. Warken in collaboration with D. Scholz. T. Miller was responsible for the recovery of the sample. Monitoring data and field work has been conducted by R. Vieten in collaboration with T. Miller, A. Winter, S. Warken, A. Schröder-Ritzrau and C. Spötl.

The manuscript of this record is attached to this thesis as Chapter 5 and will be submitted in a peer reviewed journal in 2017.

Paper II

Stalagmite Cuba medio (CM) was collected in western Cuba. It was already investigated by Fensterer et al. (2012), who combined the Holocene part of the $\delta^{18}O$ record with another stalagmite from the same cave system, Cuba Pequeño (CP), in order to provide a millennial-scale climate record covering the last 12.5 ka. In this thesis, the stable isotope record is expanded to the whole last glacial period and the analysis of trace elements is added to the set of proxies. Moreover, the age model was greatly improved for the glacial part of the record.

This study was conceived and designed by D. Scholz, A. Mangini and S. Warken. S. Warken wrote the paper in close collaboration with D. Scholz.

Stable isotope lab work has been carried out by S. Warken under the guidance of C. Spötl. Trace elemental analysis has been performed by S. Warken under the guidance of K. Jochum. Dating of sample material has been carried out by S. Warken under the guidance of A. Mangini and D. Scholz. Age modeling and statistical analysis has been performed by S. Warken in collaboration with D. Scholz. Field work has been carried out by J. Pajón. All authors contributed with commenting on the manuscript.

This manuscript was submitted to Geophysical Research Letters in November 2016. The revised manuscript is attached to this thesis as Chapter 6 and will be resubmitted in a peer reviewed journal in March 2017.

Paper III

Sample C09-2 was collected from Cloşani Cave in SW Romania. Cloşani Cave is also subject of a long-term monitoring program since 2010 (Constantin et al., unpublished data).

This study was conceived and designed by A. Schröder-Ritzrau, J. Fohlmeister, A. Mangini and S. Warken. S. Warken wrote the paper in close collaboration with A. Schröder-Ritzrau and J. Fohlmeister.

Stable isotope lab work has been carried out by C. Spötl. Dating of sample material by J. Arps and S. Warken under the guidance of N. Frank. Radiocarbon dating has been carried out by J. Fohlmeister. Age modeling and statistical analysis has been performed by S. Warken with help of D. Scholz, J. Fohlmeister and J. Esper. Trace element analyses have been performed by A. Gerdes. Field work has been carried out by S. Constantin and M. Terente. All authors contributed with commenting on the manuscript.

This manuscript was submitted to Earth and Planetary Science Letters in July 2016. The revised manuscript is attached to this thesis as Chapter 7 and will be resubmitted in March 2017.

Paper IV

Cueva Larga is subject of an extensive monitoring program since 2012 which resulted in two publications, this study and Paper IV and V.

This paper was conceived and designed by R. Vieten, A. Winter and S. Warken. R. Vieten wrote the paper in close collaboration with A. Winter and S. Warken. Field work carried out by R. Vieten under the guidance of T. Miller. Modeling and statistical analysis was performed by S. Warken. Improvements in structure and discussion on interpretation from D. Scholz. All authors contributed with commenting on the manuscript.

The published version of this paper can be downloaded at: http://scholarcommons.usf.edu/cgi/viewcontent.cgi?article=1983&context=ijs.

Paper V

For general information compare Paper I and IV.

This publication was conceived and designed by R. Vieten, A. Winter and S. Warken. R. Vieten wrote the paper in close collaboration with A. Winter, A. Schröder-Ritzrau and S. Warken. Field work carried out by R. Vieten under the guidance of T. Miller. Stable isotope lab work was performed by C. Spötl. Trace elements in water samples were analyzed by A. Schröder-Ritzrau. Improvements in structure and discussion on interpretation from D. Scholz. All authors contributed with commenting on the manuscript.

The accepted version of this paper is attached to the supplementary material, Appendix D.

2 Speleothems as climate archives

2.1 Formation of speleothems

Speleothems - secondary cave deposits - occur in various forms, such as stalagmites, stalactites or flowstones in caves, where carbonate rocks are present in the host rock, e.g., calcite/aragonite limestone ($CaCO_3$) or dolomite ($CaMg(CO_3)_2$). Another prerequisite for the formation of speleothems is sufficient water and CO_2 supply, which most commonly originates from the vegetation above the cave and accumulates in the soil zone up to values of 100,000 ppm pCO_2 (McDermott, 2004).

As meteoric waters enter this CO_2 rich zone, carbon dioxide is dissolved and carbonic acid is produced (Figure 2.1):

$$CO_{2(g)} + H_2O \rightleftharpoons H_2CO_3 + CO_{2(aq)}. \tag{2.1}$$

Carbonic acid is a 'weak' acid, which progressively dissociates (de-protonates) at higher pH to bicarbonate (HCO_2^-) and carbonate (CO_2^{2-}) ions (Figure 2.2a):

$$H_2CO_3 \rightleftharpoons HCO_3^- + H^+ \rightleftharpoons CO_3^{2-} + 2H^+ \tag{2.2}$$

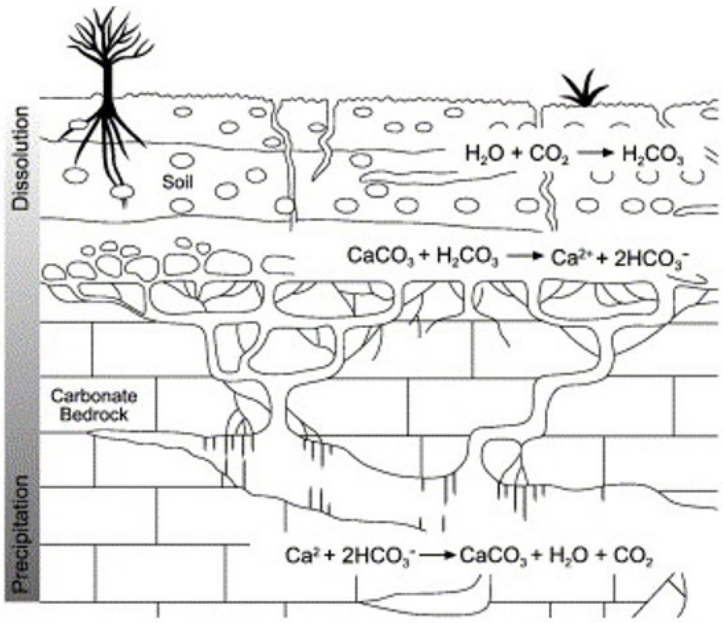

Figure 2.1: *Illustration of dissolution and precipitation regimes in the karst system. Figure adapted from Fairchild et al. (2006a).*

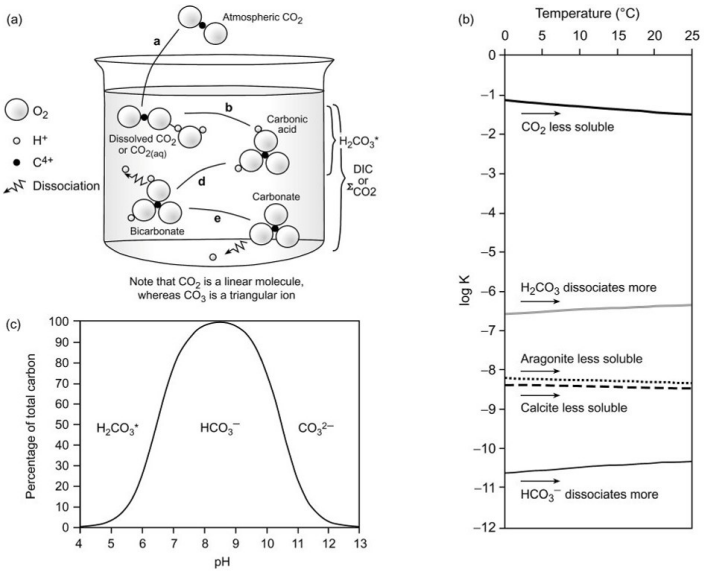

Figure 2.2: *(a) Graphic view of carbonate equilibria (Railsback, 2008). (b) Temperature dependency of equilibrium constants in the carbonate system. (c) Relative importance of different inorganic carbon species in solution as dictated by pH (values plotted for 10°C). Figure from Fairchild and Baker (2012).*

At near-neutral pH values, HCO_3^- is the dominant species of the total dissolved inorganic carbon (DIC) (Figure 2.2c), but the small proportion of CO_3^{2-} is vital for determining the stability of carbonate minerals (Fairchild and Baker, 2012). Figure 2.2 illustrates the carbonate system (Figure 2.2 a) and dependencies of its equilibria from temperature (Figure 2.2 b) and pH values of the solution (Figure 2.2 c). The resulting acid solution dissolves the carbonate host rock (Figure 2.1) following the chemical reaction

$$CO_2 + H_2O + Ca CO_3 \rightleftharpoons Ca^{2+} + 2HCO_3^-, \tag{2.3}$$

and the equilibrium reaction between carbonate dissolution and precipitation can be described as:

$$Ca^{2+} + 2HCO_3^- \rightleftharpoons CO_2 \uparrow + Ca CO_3 \downarrow + H_2O. \tag{2.4}$$

The equilibrium of dissolved Ca^{2+}-ions and bicarbonate HCO_3^- in the dripwater depends on temperature, pCO_2 and whether dissolution occurs in an open or closed system (Kaufmann, 2003; McDermott, 2004). Depending on the ventilation of the cave, the pCO_2 of cave air is much lower than in the soil zone. The water entering the cave atmosphere degases and becomes subsequently supersaturated with respect to calcium carbonate, which precipitates and forms speleothems. Figure 2.1 summarizes the formation processes of speleothems in the karst system. Stalagmite growth was quantitatively described by Dreybrodt (1988) and Dreybrodt (1999). Further work investigating growth rate or the shape of stalagmites dependent on cave temperature, drip rate and pCO_2 was published by Kaufmann (2003), Mühlinghaus et al. (2007) and Romanov et al. (2008).

2.2 Stable isotopes of oxygen and carbon

The interpretation of $\delta^{18}O$ and $\delta^{13}C$ values in speleothems is not straightforward since their stable isotopic composition is influenced by a variety of processes (Dreybrodt and Scholz, 2011; Scholz et al., 2009). In the case of $\delta^{18}O$, the composition of the dripwater feeding the speleothem is determined by the isotopic composition of the infiltrating rain and ground water (Lachniet, 2009a; Vuille, 2003) and is subsequently modulated by various processes in the soil and karst system (Dreybrodt and Scholz, 2011; Scholz et al., 2009; Mühlinghaus et al., 2009; Deininger et al., 2012). The main factors controlling the stable isotopes of oxygen are atmospheric effects from the source of the moisture and during the transport of the air masses to the cave site as well as the conditions under which the calcium carbonate precipitates on the stalagmite's surface. Once arrived in the cave, the conditions controlling the cave environment have a direct impact on the characteristics of calcite precipitation and its composition. Although speleothem $\delta^{13}C$ data are simultaneously available alongside $\delta^{18}O$ analysis, most published $\delta^{13}C$ records lack a convincing interpretation and are indeed often unreported (Fairchild and Baker, 2012). However, important information about soil processes and climate can be provided by the study of carbon isotope variability in speleothems.

2.2.1 Standards and notifications

The most commonly used proxies for paleo climate reconstruction with speleothems are the stable isotopes of carbon and oxygen, which are usually expressed in the δ-notation, which gives the deviation of the isotopic ratio of the sample relative to that of a standard:

$$\delta^{18}O = \frac{^{18}O/^{16}O_{sample} - ^{18}O/^{16}O_{standard}}{^{18}O/^{16}O_{standard}} \times 1000\,[‰] \tag{2.5}$$

Stable isotopes of carbon and hydrogen are analogously expressed as the ratio of the isotopes ^{13}C to ^{12}C and ^{1}H to $^{2}H = D$. The standard for water samples is the Vienna Standard Mean Ocean Water (VSMOW), and for carbonates the Vienna Pee Dee Belemnite (VPDB).

A useful feature to quantify fractionation processes of infiltrating and dripwater at a site is the global meteoric water line (GMWL), which was defined by Craig (1961) as the relationship between the δD and $\delta^{18}O$ values of monthly rainfall water samples around the globe:

$$\delta D = 8 \cdot \delta^{18}O + 10\,‰ \tag{2.6}$$

It results from the proportional fractionation difference during phase changes between δD and $\delta^{18}O$ and kinetic isotope fractionation during evaporation at relative humidity below 100 % creating a d-excess. The d-excess d is caused by the higher diffusivity for the lighter deuterium carrying molecule $^{2}H^{1}H^{16}O$ than for the heavier $^{1}H^{1}H^{18}O$ and defined as:

$$d = \delta D - 8 \cdot \delta^{18}O \tag{2.7}$$

The d-excess of 10 ‰ in the GMWL represents an average relative humidity of 85 % at the water source region (Clark and Fritz, 1997; Merlivat and Jouzel, 1979).

2.2.2 External controls: From the atmosphere into the epikarst zone

Local meteoric precipitation shows a clear connection to climatic parameters such as the air temperature and amount of precipitation (Vuille, 2003; Lachniet, 2009a). In mid to high latitudes, the $\delta^{18}O$ value of the precipitation usually follows the seasonal temperature pattern ('temperature effect'), which is often expressed as a positive correlation with mean annual air temperatures (Dansgaard, 1964; Lachniet, 2009a). In the tropics, the $\delta^{18}O$ and δD value of precipitation was found to be closely related to the amount of rainfall (Lachniet and Patterson, 2006; Lachniet, 2009b; Lachniet and Patterson, 2009; Vuille, 2003), since at low latitudes high temperatures and rainy season are closely related ('amount effect'). The seasonality of meteoric precipitation results in the $\delta^{18}O$ values of the dripwater to be biased towards the $\delta^{18}O$ signal of the season with the highest contribution to the annual amount of meteoric precipitation ('seasonality effect', Cruz et al. (2005b); Johnson et al. (2006); van Beynen and Febbroriello (2006)). Figure 2.3 illustrates the primary processes influencing moisture $\delta^{18}O$ values along its pathway from the source to the speleothem.

Changes of the isotopic composition of the dominant source regions eventually alter the isotopic signature of precipitation ('source effect', Cole et al. (1999); Charles et al. (1994)). Since the d-excess of rain water does not change during condensation it is an indicator of the water vapor source region (Merlivat and Jouzel, 1979).

On longer timescales, the $\delta^{18}O$ values of the oceans have varied significantly, since during the glacial - interglacial cycles, the amount of freshwater stored on the continents has changed tremendously. Subsequently the $\delta^{18}O$ signature of the oceans increased to heav-

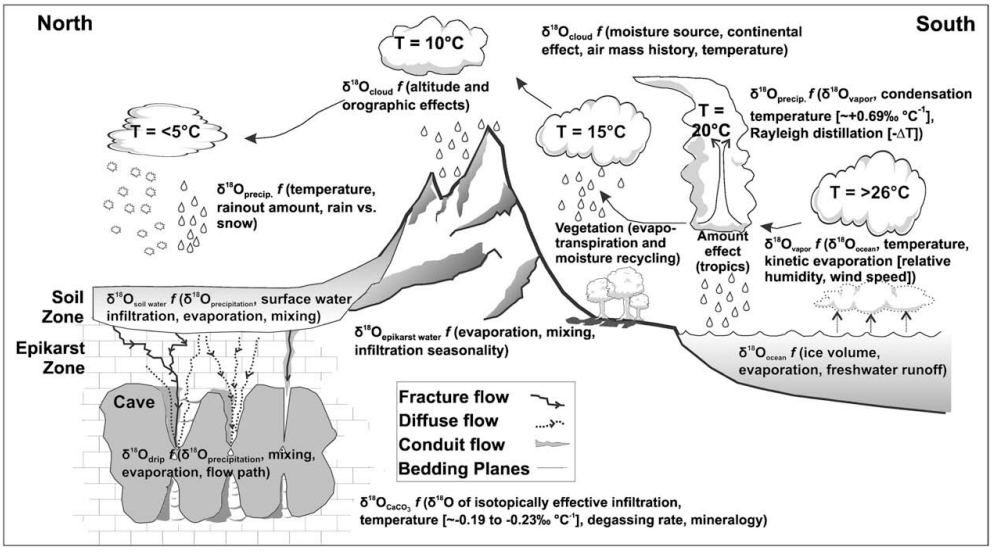

Figure 2.3: *Diagram illustrating the primary processes related to* $\delta^{18}O$ *variations relevant to speleothem paleo climatology. The dominant controls are based on variations in temperature and relative humidity which influence the* $\delta^{18}O$ *values through the various processes and phase changes in the ocean, atmosphere, hydrosphere, soil and epikarst zones, and finally in speleothem* $CaCO_3$*. In the figure, 'f' indicates it is a function of listed variables. From Lachniet (2009a).*

ier values due to the preferential remove of the light stable isotope during evaporation ('ice volume effect', Lea et al. (2002); Sharp (2007)). Eventually, the trajectory of the rainfall is crucial for the evolution of the isotopic composition of the rainfall, since due to the water loss during the movement of oceanic air inland the remaining atmospheric water vapor is progressively depleted in heavy isotopes ('continental effect', Dansgaard (1964); Rozanski et al. (1993); Clark and Fritz (1997)). The same phenomenon is observed when the water vapor reaches an orographic obstacle, because the up-lift of moist air masses is accompanied by an isotopic depletion due to adiabatic cooling and precipitation ('altitude effect', Fleitmann et al. (2004); Gonfiantini et al. (2001); Poage and Chamberlain (2001)).

Processes occurring in the soil and karst above the cave influencing the $\delta^{18}O$ signature are for example averaging meteoric water of several months, calcite dissolution and the recycling of seepage water by evapotranspiration. These processes strongly depend on the type of vegetation above the cave and the constitution of the soil (Lachniet, 2009a; Wackerbarth et al., 2010).

A main driver of $\delta^{13}C$ variability in the soil is the primary carbon production by higher plants which follows the two main photosynthetic pathways C_3 and C_4, which have a very different $\delta^{13}C$ signature (about -10 to -15 ‰ for C_4 and -25 to -30 ‰ for C_3 plants). In contrast, atmospheric (-5 to -8 ‰) and carbonate bedrock (±0 ‰) $\delta^{13}C$ signatures are much higher. The pCO_2 in the soil zone determines the amount of CO_2 to be dissolved in the infiltration waters and is related to biological activity (Spötl et al., 2005; Baskaran and Krishnamurthy, 1993; Frisia et al., 2011). During the proceeding host-rock dissolution, an important feature in the context of carbon isotope variability is the consideration of open and closed system behaviour (Garrels and Christ, 1965; Deines et al., 1974; Clark and Fritz, 1997). The open system is characterized by a continuous equilibration of the solution with a finite gas phase, whereas the under closed system conditions, the solution with high initial pCO_2 set by the soil is subsequently isolated from the gas phase. In a closed system, much higher $\delta^{13}C$ values are reached than under open system conditions, because more $CaCO_3$ is added to the water with a much higher $\delta^{13}C$ composition.

2.2.3 Cave-internal controls: Equilibrium fractionation and kinetic effects

At the point of any phase change, one isotope is favored over the other. This so called fractionation can be described as

$$\alpha_{A-B} = \frac{R_a}{R_B} \tag{2.8}$$

where α is the equilibrium fractionation factor and R is the isotopic ratio (e.g. $^{18}O/^{16}O$) between the substances A and B. Hendy (1971) argued that the precipitated calcite on a speleothem's surface will be in isotopic equilibrium with the water and speleothem $\delta^{18}O$ values will 'depend on climate alone' if the loss of dissolved CO_2 from the solution is slow. Fractionation factors describe the relationships between the involved species, which is e.g.

for carbon dissolved bicarbonate (b), solid calcite (s) and gaseous CO_2 (g). For oxygen isotopic composition, also liquid water (l) is involved. For synthetic calcite, an equilibrium fractionation factor relationship for oxygen isotopes between calcite and water was determined by Kim and O'Neil (1997):

$$1000 * ln\alpha_{s,l} = 18.03 \times (10^3 \cdot T^{-1}) - 32.42. \tag{2.9}$$

Experiments in cave environments have shown, that slightly different relationships are in better agreement with field studies (e.g., Coplen (2007)). For example, a commonly accepted relation was found by Tremaine et al. (2011):

$$1000 * ln\alpha_{s,l} = 16.1 \times (10^3 \cdot T^{-1}) - 24.6. \tag{2.10}$$

In contrast, if degassing of CO_2 is rapid, a kinetic fractionation will occur and the precipitated calcite will show a simultaneous increase in $\delta^{18}O$ and $\delta^{13}C$ values (Hendy, 1971). In fact, rapid degassing of CO_2 from the thin film of dripwater on the speleothem surface is often considered to have a large effect on both $\delta^{18}O$ and $\delta^{13}C$ and is offered as an explanation for higher $\delta^{18}O$ and $\delta^{13}C$ values than expected under conditions of stable isotope equilibrium (e.g., Mattey et al. (2010); Boch et al. (2011); Frisia et al. (2011); Scholz et al. (2012). In order to describe the fractionation processes occurring before and at the point of carbonate precipitation have been the subject of various theoretical model studies (Scholz et al., 2009; Mühlinghaus et al., 2009; Dreybrodt and Scholz, 2011; Deininger et al., 2012) and laboratory experiments (Polag et al., 2010; Hansen et al., 2013).

Speleothem $\delta^{18}O$ and $\delta^{13}C$ values are affected by fractionation effects due to variations of temperature, drip interval (or drip rate), evaporation, the partial pressure of CO_2 (pCO_2) in the dripwater and the cave air. For instance, evaporation at the stalagmite's surface has a significant effect on $\delta^{18}O$ and $\delta^{13}C$ values of the calcite due to the loss of H_2O from the solution layer and the related increase of the Ca^{2+} concentration. This leads to higher precipitation rates and, consequently, larger isotope fractionation effects (Deininger et al., 2012). Strong variability in cave parameters such as cave air pCO_2, relative humidity (RH) or temperature, for example due to ventilation effects, substantially affect evaporation and thus calcite precipitation rates and, as a consequence, isotopic fractionation and the composition of the stalagmite's calcite. Many of these processes may occur on seasonal scale or attached to climatic changes, e.g. generally drier conditions may be accompanied by lower drip rates.

Higher cave temperatures would result in lower (depleted) $\delta^{18}O$ but higher (enriched) $\delta^{13}C$ values in speleothem calcite (Mühlinghaus et al., 2009). In contrast, decreasing drip rates result in higher (enriched) values of $\delta^{13}C$ and $\delta^{18}O$. In tropical locations, these effects would amplify the negative relationship between rainfall amount and speleothem $\delta^{18}O$.

Recent laboratory experiments under conditions similar to those in natural cave systems confirmed the importance of drip rate variability on the stable isotope composition in speleothem calcite (Hansen et al., 2013). Moreover, the authors determined the time constants for

degassing of CO_2, $\tau_{deg} \approx 2$ s, subsequent equilibration to a new pCO_2, τ_{eq} and precipitation of $CaCO_3$, τ_{pr}. Dependent on the time T required until the drop falls onto the surface of the stalagmite after entering the cave, the implications for the interpretation of stable isotopes signals in speleothems are very different (Hansen et al., 2013). For example, if the time T is longer than τ_{pr}, calcite precipitation may already occur prior to deposition on the stalagmite, which is referred to as prior calcite precipitation (PCP) in speleothem literature and may have a large effect on stable isotopes values and trace element signatures (compare the following section and Fairchild et al. (2006a); Fohlmeister et al. (2012); Wassenburg et al. (2012)). In the case of stable isotopes, PCP would result in both enriched $\delta^{18}O$ and $\delta^{13}C$ values (Dreybrodt, 2008; Mühlinghaus et al., 2009; Dreybrodt and Scholz, 2011; Scholz et al., 2009; Deininger et al., 2012).

2.3 Elemental composition of speleothems

Elemental proxies such as magnesium, strontium, barium, phosphorus or uranium have come more and more into the focus of recent research during the last decades (e.g., Roberts et al. (1998); Treble et al. (2003); Borsato et al. (2007); Fairchild and Treble (2009)) and the increase in speleothem studies lead to a deeper understanding of the processes determining the incorporation of (trace) elements in speleothem calcite (Tremaine and Froelich, 2013; Mattey et al., 2010; Regattieri et al., 2014; Tan et al., 2014). Fairchild et al. (2006a) distinguished five types of influences on the geochemistry of speleothems, which apply to trace elements: Atmospheric input, vegetation/soil, karstic aquifer, primary speleothem crystal growth and secondary alteration. This section will give a short overview on the current state of research of the most important elemental proxies in this thesis - magnesium, strontium and phosphorus.

2.3.1 Incorporation of trace elements in calcium carbonate

Most commonly used trace elements in speleothem research are elements (namely Mg, Sr and Ba) which form divalent cations in solution and substitute Ca in the $CaCO_3$ crystal lattice. For such species, a simple distribution or partitioning coefficient can be defined (Morse and Mackenzie, 1990), which relates the composition of solution and mineral components:

$$(\mathrm{T}r/\mathrm{C}a_{\mathrm{C}a\mathrm{CO}_3}) = \mathrm{D}_{\mathrm{T}r} \cdot (\mathrm{T}r/\mathrm{C}a)_{solution} \tag{2.11}$$

where D_{Tr} is the partitioning coefficient and Tr is the trace ion. D_{Tr} can vary more or less significantly with calcite precipitation rate, temperature, crystal morphology or other factors (Fairchild and Treble, 2009). For example, D_{Tr} may be significantly different for aragonite and calcite (McMillan et al., 2005; Wassenburg et al., 2012).

Other elements are incorporated in speleothem carbonate associated with detrital particles of as small-sized colloids (Fairchild and Treble, 2009). Borsato et al. (2007) found a number of trace elements to be enriched synchronously with visible growth layers containing fluorescent humic substances in a stalagmite from Ernesto cave, NE Italy. Some elements such

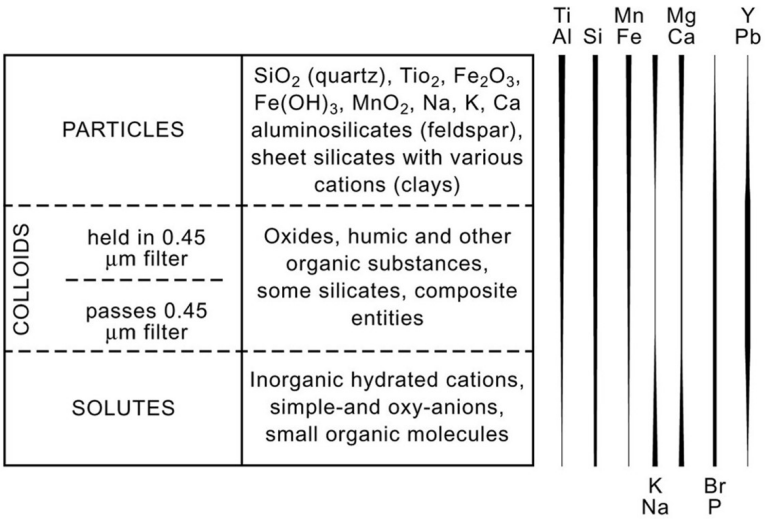

Figure 2.4: *Modes of occurrence of trace elements in karst waters: particle, colloids and solutes (from Fairchild and Treble (2009)). Colloids are defined as entities with at least one dimension in the size range 1 nm to 1 µm (Lead and Wilkinson, 2006). The tendency of selected elements to be transported in a given mode is shown schematically on the right.*

as Na or P (as phosphate ion) tend to be incorporated in defect sites in the crystal lattice, which was found to be promoted by faster growth from more strongly supersaturated solutions (Frisia et al., 2000; Fairchild and Treble, 2009). However, in most cases, it is not known under which chemical and physical conditions and to which species of molecules or particles a trace element is favorably bound. Figure 2.4 gives an overview of the modes of occurrence of trace elements as particles, colloids or solutes as well as the tendency of distinct elements to the transport processes in karstic waters.

2.3.2 Sources of elements, dissolution processes and the karst system

Figure 2.5 summarizes the variety of sources for chemical species including aeolian particles, dry and wet atmospheric deposition, bedrock, superficial sediment deposits and inorganic soil constituents as well as elements recycled via soil biota (Fairchild and Treble, 2009). In contrast to the oxygen isotopic composition in speleothems, the atmosphere is only a subordinate source for trace elements besides for example atmospheric pollutants (Spötl et al., 2005; Tan et al., 2014; Frisia et al., 2005), atmospheric dust deposition or sea spray (Goede et al., 1998; Pett-Ridge, 2009). The primary source of calcium and most trace elements is the host rock and the overlying soil zone. Due to depositional and tectonic processes, each cave site and each drip site itself is characterized by a unique trace element signal of host rock dissolution. For certain elements, it may be small quantities of a minor mineral phase that are the major supply (see section 2.2 in Fairchild and Treble (2009) for more details).

For example, where dolomite and calcite phases in the host rock are reasonable homogeneous and are the main supply for Mg and Sr, their compositions can be used to help

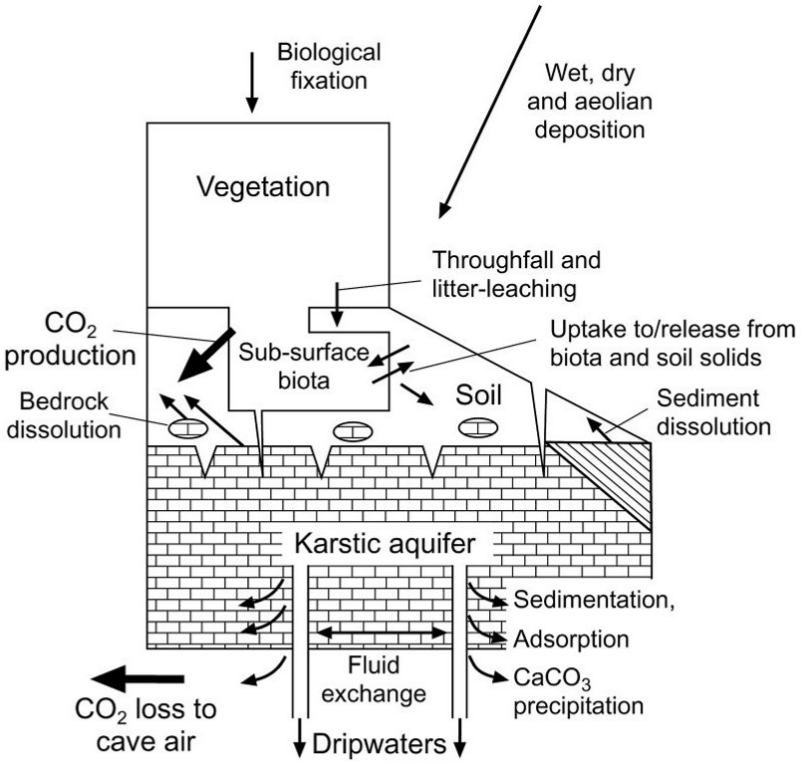

Figure 2.5: *Schematic flow chart indicating sources of elements and processes involved in their transport and deposition in cave systems. Arrows denote element fluxes as particulates, colloids or solutes in aqueous solutions (from Fairchild and Treble (2009))*

understand the ways in which chemical signals are generated and modified in the karstic system (Fairchild and Treble, 2009; Fairchild et al., 2000). One reason is the different dissolution rates of dolomite and calcite, which lead to a significantly lower Mg/Ca ratio in mixed dolomitic-calcitic bedrocks in comparison to that of the mean bedrock composition (Fairchild and Treble, 2009).

A key principle is that dissolution is focused in the zone, where pCO_2 is at a maximum. This can be either within the soil or in the epikarst depending on the distribution of carbonate and of the decomposing organic matter (Atkinson, 1977; Drake, 1983; Fairchild et al., 2000; Fairchild and Treble, 2009). Drip waters may be characteristically enriched in certain trace elements which may be related to dissolution processes and hydrological behavior under both low and high flow conditions (Fairchild and Treble, 2009; Baker et al., 2000; Fairchild et al., 2006a).

2.3.3 Incorporation into carbonate minerals

Much theoretical and experimental work has been done to quantify the partition coefficients for carbonate minerals for different elements. However, many phenomena are still poorly understood, e.g., if the actual sites where the ions are incorporated are considered, the dis-

tribution coefficient approach seems to be inadequate (Fairchild and Treble, 2009), which is especially the case for aragonite. In a recent publication by Wassenburg et al. (2016) it was possible to derive the first quantitative estimates of the distribution coefficients for different elements in speleothem aragonite. In contrast, for many elements the incorporation into speleothem calcite is now reasonable well understood.

Under typical karstic conditions, D_{Mg} seems to be dependent on temperature (Figure 2.7) and a number of earlier studies associated Sr incorporation to be dependent on growth rates (Figure 2.6, and e.g., Gabitov and Watson (2006); Nehrke et al. (2007); Lorens (1981)). However, these relationships seem to be complex due to irregularities in behavior and growth mechanisms (Treble et al., 2005; Borsato et al., 2007; Day and Henderson, 2013). The analysis of various time series from speleothem samples indicate, that the temperature effect on Mg incorporation in speleothem calcite is subordinate from other factors (e.g., Fairchild et al. (2001); Roberts et al. (1998); Fairchild et al. (2006a); Sinclair et al. (2012)). The interpretation of Mg in speleothem studies has thus largely shifted to interpretations in terms of hydrological changes. It was early demonstrated, that speleothem Mg and recorded rainfall are related, e.g., (Tooth and Fairchild, 2003; Karmann et al., 2007; Treble et al., 2003; Sinclair et al., 2012).

Since Mg and Sr are the most commonly used elemental proxies, the various processes influencing its incorporation in speleothem calcite are described in detail in the following section 2.4. For partitioning calculations, the coefficients $D_{Mg} = 0.019$ (for 15°C) and $D_{Mg} = 0.031$ (for 25°C), $D_{Sr} = 0.15$ (all Huang and Fairchild (2001)) and $D_{Ba} = 0.012$ (Tesoriero and Pankow, 1996) are used.

2.4 Magnesium and Strontium systematics in cave environments

Mg and Sr signatures in speleothems are mostly interpreted as hydrologically derived, with changes being linked to rainfall (e.g. Hellstrom and McCulloch (2000); McMillan et al. (2005); Johnson et al. (2006); Cruz et al. (2007); Griffiths et al. (2010); Sinclair et al. (2012)).

However, some difficulties occur in the interpretation of the elemental signals due to the large range of processes that can affect their partitioning into calcite and the fact that many of these apply at a local level in karst systems make it more difficult to interpret records in terms of regional-scale paleo climate (Sinclair et al., 2012). For example, the following processes have all been identified to potentially control Mg and/or Sr incorporation into speleothems: temperature, growth rate, prior calcite precipitation (PCP), dissolution of aragonite or dolomite, incongruent calcite dissolution (ICD), changes in water/rock residence time, changes in karst hydrology, cave atmosphere, marine aerosols, crystal size/geometry, soil zone processes, detrital input, etc. (e.g. Paquette and Reeder (1995); Goede et al. (1998); Fairchild et al. (2000); Hellstrom and McCulloch (2000); Tooth and Fairchild (2003); Treble et al. (2003); McDonald et al. (2004); Desmarchelier et al. (2006); Fairchild et al. (2006b); Johnson et al. (2006); Sinclair (2011); Sinclair et al. (2012)).

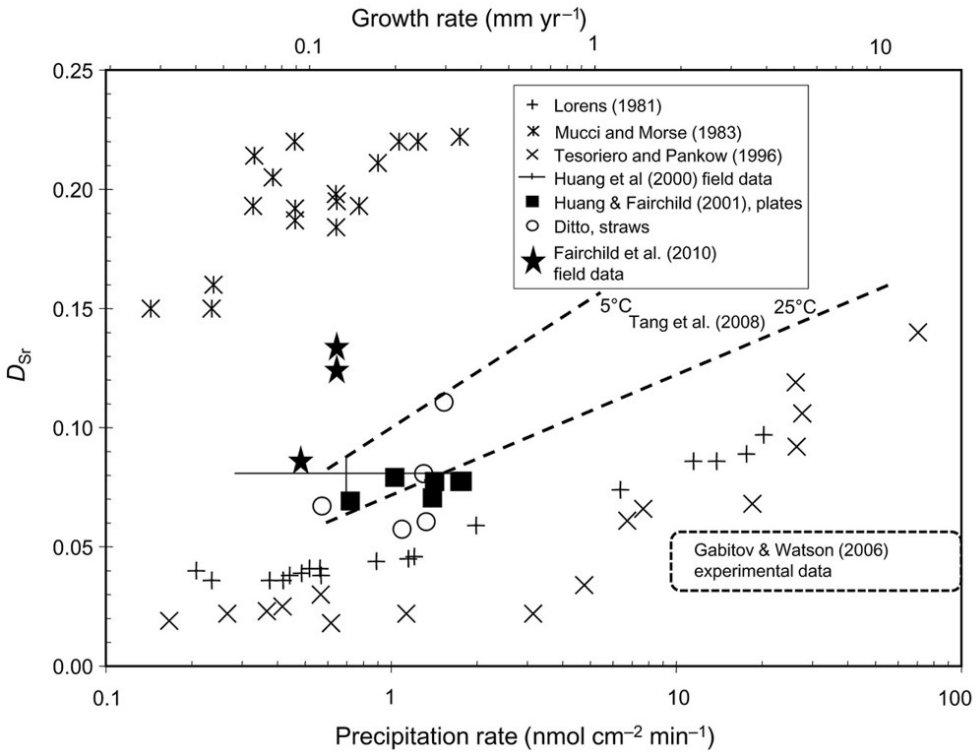

Figure 2.6: *Experimental and field data (mean cave dripwaters compared with speleothem tops) for Sr partitioning replotted from Huang and Fairchild (2001) with additional data. note that most experiments (except Huang and Fairchild (2001)) used high salinity solutions and those of Mucci and Morse (1983) were for marine analogues (Mg-rich). Experimental growth temperatures are mostly 25°C except that some of the experiments of Huang and Fairchild (2001) were conducted at 15°C. Tang et al. (2008) experimental data form good fits to log-linear relationships, which are shown for 5°C and 25°C. the field data from caves are around 6°C. Figure from Fairchild and Baker (2012).*

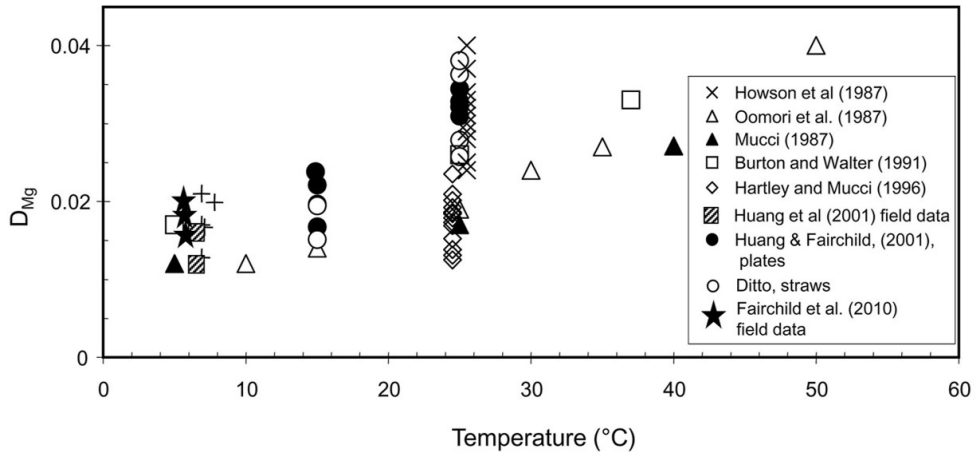

Figure 2.7: *Comparison of experimental and field determinations of D_{Mg} replotted from Huang and Fairchild (2001) with the removal of poorly constrained field data and addition of well-constrained data from three stalagmites at Obir Cave (Fairchild et al., 2010). Figure from Fairchild and Baker (2012).*

A notable feature of many dripwater and speleothem geochemical studies is a positive correlation between Mg and Sr, which is most commonly ascribed to prior calcite precipitation (e.g., Fairchild et al. (2000); Tooth and Fairchild (2003); McDonald et al. (2004); Musgrove and Banner (2004); McMillan et al. (2005); Fairchild et al. (2006a); Johnson et al. (2006); Karmann et al. (2007); Sinclair et al. (2012)).

However, two general mechanisms which might be responsible for co-fractionating the Sr and Mg in the dripwaters can come into consideration. The first is a general modification of dripwaters: karst waters begin with approximately similar Mg and Sr contents (implying host limestones have a broadly similar composition), and the trend observed in the elemental ratios derives from differing degrees of subsequent modification of those karst waters by water-rock interaction upstream of the drip site. The second mechanism is limestone diagenesis: karst waters primarily reflect the composition of their host limestones, and the trend arises because these limestones have systematically evolved different bulk Mg + Sr compositions through different degrees of diagenetic modification (Sinclair et al., 2012). The different mechanisms are described in the next sections following Sinclair et al. (2012).

2.4.1 Modification of dripwaters by calcite water interactions

Prior calcite precipitation

The fundamental process in speleothem formation is the transition of the infiltrating water from a dissolution regime to a precipitation regime (Fairchild et al., 2006a), primarily due to the encountering of a gas phase with lower pCO_2 than they have previously equilibrated. In the following, the waters are supersaturated with respect to $CaCO_3$ and tend to precipitate calcite. In the common case, that dripwaters have already undergone changes as a result of precipitation upflow, this is referred to as prior calcite precipitation (PCP).

Depending on the value of D_{Tr} (equation 2.11), which is typically much less than one, the result of calcite precipitation is a much larger reduction in Ca than of the trace element, and hence an increasing ratio of the trace element to Ca ratio in solution. Thus, where PCP plays an important role, Mg and Sr can be strongly enriched in the speleothem compared to host rock compositions. PCP is enhanced where infiltrating karst waters are able to degas, thus this process is thought to be promoted by drier climatic conditions (Fairchild et al., 2000). The existence of this relationship was also shown by dripwater monitoring at a number of sites (Fairchild et al., 2006a; Karmann et al., 2007; Baldini et al., 2006). Multi-annual dripwater variability at some sites can be used to relate PCP to climate parameters (Baldini et al., 2006).

In an extensive speleothem study with 13 samples, Sinclair et al. (2012) derived a mathematical model in order to formally predict the physical and chemical parameters that affect the Mg and Sr correlations, which is an essential prerequisite for being able to confidently apply correlation analysis as a diagnostic tool in the absence of other field data. The authors show under the assumption, that partition coefficients are constant and that PCP is the only process occurring in a closed water/rock system, that cave waters evolving under PCP, and

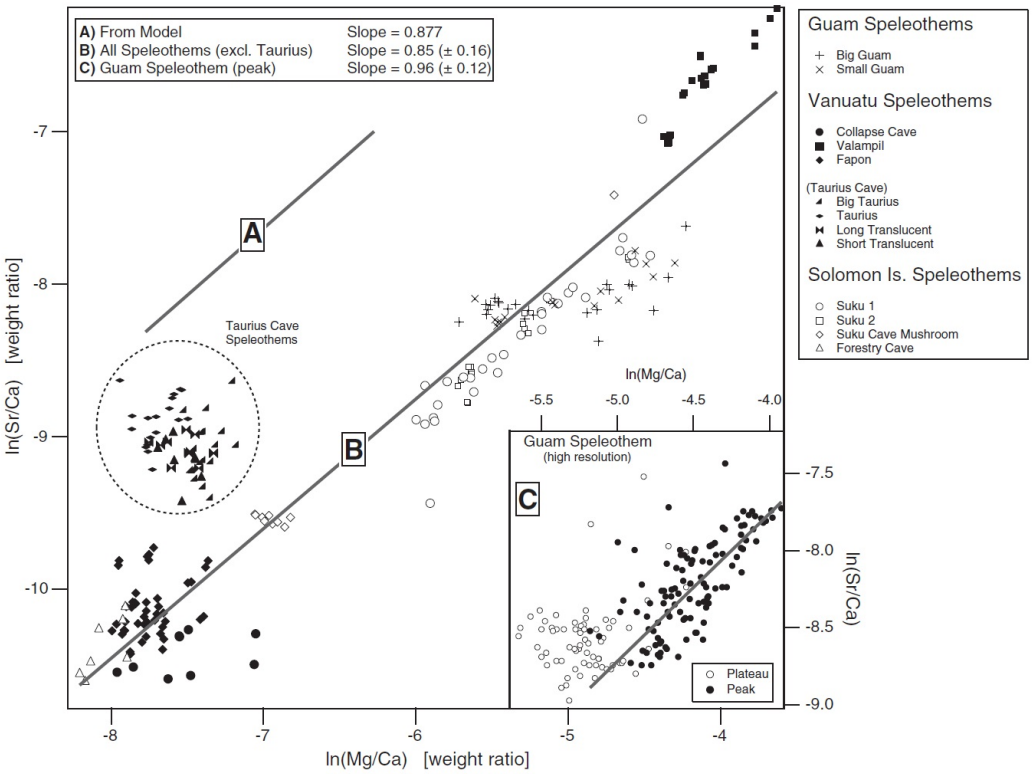

Figure 2.8: *ln(Sr/Ca) vs ln(Mg/Ca) for all speleothems sampled by Sinclair et al. (2012). Line A shows the theoretical slope predicted for PCP and ICD (see text). Line B is the linear fit through all the speleothem data excluding Taurius Cave, where dissolution of aragonite-rich casts elevates Sr values. Graph from Sinclair et al. (2012).*

speleothems forming from them, will display a positive linear correlation between ln(Sr/Ca) vs ln(Mg/Ca), which has a slope given by

$$\frac{D_{Sr} - 1}{D_{Mg} - 1} \tag{2.12}$$

This trend is a universal property of PCP, and is independent of both host-rock and solution composition. For published values of D_{Sr} and D_{Mg}, the slope is ~ 0.88, with minimum values from 0.709 to 1.003 (Sinclair et al., 2012). Because the slope is independent of solution and host-limestone composition, it can be used to diagnose calcite-water interaction in individual cave water studies where host rock composition is unknown, or in speleothems for which no field dripwater data or host-rock geochemistry exists (Sinclair et al., 2012; Sinclair, 2011). Since $D_{Mg} \ll 1$, the predicted PCP slope is highly insensitive to temperature, whereas the growth rate dependence of D_{Sr} would be expected to result in a 3.5 - 7.0% decrease in $\frac{D_{Sr} - 1}{D_{Mg} - 1}$ for an order of magnitude faster growth (Sinclair et al., 2012). A similar equation is derived for incongruent calcite dissolution (ICD) in a companion paper (Sinclair, 2011).

Incongruent calcite dissolution

Incongruent calcite dissolution (ICD) is another potential calcite-water interaction which could fractionate Mg and Sr relative to Ca. Dissolution of calcite - especially from fresh surfaces - is often incongruent, with both Sr and Mg being released in preference to Ca (Land, 1967; Schroeder, 1969; Reeve and Perry, 1994; Fairchild et al., 2000; McGillen and Fairchild, 2005; Sinclair, 2011; Sinclair et al., 2012). Sinclair (2011) developed two mathematical models to study Mg and Sr partitioning during ICD. Both ICD models predict that the slope of a ln(Sr/Ca) vs ln(Mg/Ca) graph varies with time. Under circumstances which might prevail in karst systems, the curves approach linearity with slopes given by $\frac{D_{Sr} - 1}{D_{Mg} - 1}$ (Sinclair, 2011). This is an identical result to the slope predicted for PCP, and just as with PCP, this limiting slope is a constant universal property of the ICD system, independent of host rock or solution composition.

2.4.2 Diagenesis

If the bulk limestone composition imparts a first-order control over dripwater composition, then diagenetic changes to the Mg and Sr content of limestone could account for a covariation of Mg and Sr. Sinclair et al. (2012) do not favor this explanation for their data because they see no correlation between stalagmite Mg and Sr with host limestone age. The authors state that hydrogeochemical processes operating on the scale of individual drips are more significant for setting the bulk Mg + Sr composition of the stalagmites than the composition of the host limestone. However, this does not exclude the possibility that diagenesis along individual drip pathways affects the drips (Sinclair et al., 2012).

Mineral stabilization

Most speleothems sampled by Sinclair et al. (2012) are from young reef limestone host rocks, which are composed primarily of aragonite and high-Mg calcite (Morse and Mackenzie, 1990; Moore, 2001). Their models show, that the slope of ln(Sr/Ca) vs ln(Mg/Ca) is not constant (Figure 2.9 A), which is produced because Mg-calcite dissolves faster than aragonite (Morse and Mackenzie, 1990). The dissolution of aragonite and Mg-calcite would not produce a linear trend like the one seen in equation 2.12. If dolomite was present in the system, then similar arguments apply. Like high-Mg calcite, dolomite is rich in Mg, but depleted in Sr relative to calcite (Fairchild et al., 2000; Finch et al., 2001). Therefore, dissolution of this mineral alone cannot produce a positive correlation in Mg/Ca vs Sr/Ca (Frisia et al., 1997; Fairchild et al., 2000; Sinclair et al., 2012). Although dissolution of high-Mg calcite, aragonite and dolomite are not likely the cause of the correlated Mg and Sr behavior, it may be responsible for second-order deviations from correlated variations arising from another mechanism. For example, Mg input from dolomite dissolution will lower the slope of a ln(Sr/Ca) vs ln(Mg/Ca) plot, while Sr input from aragonite dissolution will steepen the slope (Sinclair et al., 2012).

Calcite recrystallization

As noted in section 2.4.1, Mg and Sr are preferentially partitioned into the solution phase during calcite/water interactions. If the solution is constantly percolating through limestone, dissolving and/or re-precipitating calcite as it goes, the effect will be to progressively leach Sr and Mg from the rock (Sinclair et al., 2012). Sinclair et al. (2012) investigate this leaching using two mathematical models of an open limestone/water system in which karst water reaches equilibrium (determined by the partition coefficients) with the host rock before being removed and replaced by fresh solution (Figure 2.9 B). Both models require some degree of equilibration between limestone and solution. The models are most applicable to cases where there is a low solution volume and a large area of limestone surface. These conditions might be encountered during diagenesis of a very porous limestone and/or vadose diagenesis where solution is a thin film trickling across a large surface area of limestone (Sinclair et al., 2012).

Model 1 begins with a fixed volume of limestone, and tracks its composition as it is progressively dissolved by increments of fresh water which equilibrate with the rock and are

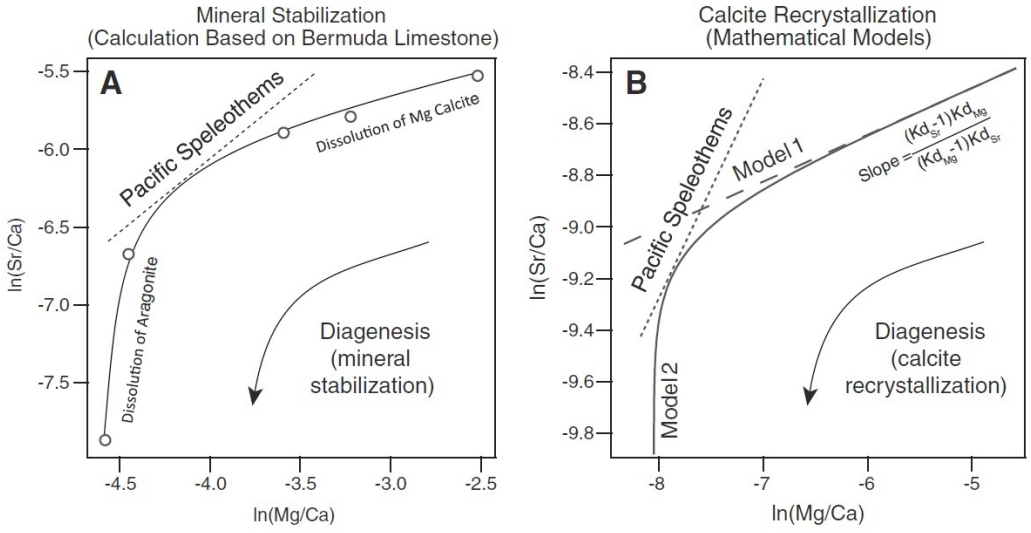

Figure 2.9: *ln(Sr/Ca) vs ln(Mg/Ca) in limestones for diagenesis scenarios (from Sinclair et al. (2012)). A) Calculations for the evolution of limestones as Mg-calcite and aragonite transform to calcite (Sinclair et al., 2012). The dashed straight line indicates the slope of the line observed in Figure 2.9. Diagenesis by mineral stabilization results in progressive depletion of Mg and Sr in the limestone. The trend is highly non-linear: at the early stage of diagenesis, the rapid loss of Mg-calcite results in a rapid decrease in Mg/Ca of the limestone. Once Mg-calcite is depleted, the change in limestone composition is dominated by the loss of aragonite resulting in a rapid decrease in Sr/Ca. B) Mathematical models for the evolution of calcite during open-system recrystallization (Sinclair et al., 2012). The fine dashed straight line indicates the slope of the line observed in Figure 2.8. The heavy dashed straight line is the output of the simplified model 1, while the unbroken line is the output of model 2. The trend of model 2 is highly non-linear, but at early stage of diagenesis it approximates a straight line. The increase in slope results from Mg-depletion in the calcite.*

then removed from the system. This model does not allow for the exposure of new limestone as the initial limestone dissolves, and thus is most applicable at low amounts of partial dissolution where the overall volume of reactive rock has not changed much. The slope for ln(Sr/Ca) vs. ln(Mg/Ca) is then given by

$$\frac{(D_{Sr} - 1)\, D_{Mg}}{(D_{Mg} - 1)\, D_{Sr}} \tag{2.13}$$

which derives values of ~ 0.18 to 0.53.

Model 2 is an extension of model 1, considering the scenario where the thickness of reactive limestone stays constant so that as rock dissolves from the outside surface, the reactive layer migrates into the solid exposing new limestone. Model 2, therefore, provides a more realistic simulation of the system as leaching becomes more pronounced. The model generates a hyperbolic relationship between ln(Sr/Ca) and ln(Mg/Ca) rather than a linear one. However, for partial leaching, the slope of a plot of ln(Sr/Ca) vs ln(Mg/Ca) approaches that derived for Model 1. As more Sr and Mg are removed from the reactive layer, the slope of the function approaches infinity, producing a hyperbolic shape of the function. Although there is a region where the slope will be 0.88, this slope is maintained over only a very narrow range of Mg/Ca and Sr/Ca values, and could not produce the extended straight-line relationship spanning several orders of magnitude, that is observed for PCP and/or ICD.

2.4.3 Other mechanisms

Temperature and growth rate

Since D_{Sr} is not dependent on temperature, it is no likely cause for a covariation of Sr/Ca and Mg/Ca. The same applies to growth rate, which is considered to affect Sr incorporation but not Mg. If temperature or growth rate are responsible for individual peaks in Mg/Ca oder Sr/Ca, respectively, has to be ruled out individually by estimating the potential effects (e.g., in analogous manner like Sinclair et al. (2012)). In most cases, growth rate would have to change by at least an order of magnitude to affect Sr/Ca incorporation significantly. Similarly, a temperature change by 2-3 °C would result in a total change in Mg by at most 15%.

However, it is possible that both effects play a secondary role in fractionating Mg and Sr, respectively. For example, Ku and Li (1998) investigated the use of Mg/Sr ratios as a proxy for temperature, reasoning that if Mg is temperature dependent and Sr is not, then normalizing Mg to Sr could remove the influence of changing dripwater chemistry. Sinclair et al. (2012) find a broad increase in Mg/Sr beginning between 13 and 15 ka, which could plausibly represent post-glacial warming. Even if the Mg/Sr ratio changes by around 100% which is still larger than might be expected based solely on the temperature dependence for D_{Mg}, the authors state that the temperature dependence of this proxy might be larger than implied by inorganic experiments.

Dust and detrital material

Dust has been noted as a significant source of Sr in some speleothems (Goede et al., 1998), and clays can also be enriched in Mg (Spivack et al., 1987; Leeman and Sisson, 1996). Elevated Sr and Mg signals may thus coincide with other signs of detrital contamination, such as elevated porosity, Th, Al, etc. For example, Saharan dust is also known to be a significant source of soil in the Caribbean in general, as evidenced by soil mineralogy, isotopic tracers, trace element ratios and rare earth element patterns (Pett-Ridge, 2009). There is, however, no particular reason why dust input would produce a correlation with the same slope as calcite-water interaction, and it would imply a remarkable coincidence if it were the case (Sinclair et al., 2012).

Soil

Soils play a complex, but potentially important role in setting the Mg and Sr 'starting point' of karst groundwaters (Sinclair et al., 2012). Fairchild and Treble (2009) note that Mg and Sr are normally derived primarily from the carbonate bedrock, with the possible exception where abundant clay minerals are present in the overlying soils. Karmann et al. (2007) show that the Mg and Sr content of drips in the Santana-Pérolas cave system (Brazil) are related to the bulk limestone composition suggesting that the host rock, rather than the soil, plays a dominant role in controlling the overall Mg and Sr composition of groundwaters. However, the authors and Musgrove and Banner (2004) show, that soil waters can acquire a significant fraction of Mg and/or Sr concentrations. Thus it is possible that a Sr/Ca vs Mg/Ca trend derives from a systematic variation in the composition of the soils overlying the different caves (Sinclair et al., 2012). Unfortunately, there is often insufficient information about soil types in remote locations to quantitatively test possible soil-based mechanisms. Given the diversity of factors potentially affecting soil composition and leaching, however, it seems unlikely that this could generate one coherent trend between disparate locations as observed by Sinclair et al. (2012), and highly coincidental that this trend should match that predicted by calcite-water interaction.

Sea spray

In an island karst system, input of seawater to groundwaters through sea spray can be a significant source of ions, especially for Mg and Sr which are both relatively concentrated in seawater (Goede et al., 1998). For example, average Mg and Sr concentrations in seawater are about 1,200 mmol/l and 8 mmol/l, respectively (Stumm and Morgan, 1981), compared to only about 5 mmol/l Mg (Román-Más and Lee, 1987) and 50 nmol/l Sr (Pett-Ridge, 2009) in surface waters in Puerto Rico. For instance, Fairchild et al. (2000) inferred significant seawater input into one of their cave dripwater systems based on concentrations and ion ratios. Mixing between two waters results in a straight-line correlation between Sr/Ca vs Mg/Ca, connecting the two endmembers (Sinclair et al., 2012). The authors state, that the mathematics of sea-

water mixing does not, however, support a straight line in ln(Sr/Ca) vs ln(Mg/Ca) plots, nor does it produce a slope of 0.88. Even if sea spray is not a first order control on Sr and Mg composition, it is possible, that it contributes a second-order effect to the element profiles. For example, an increasing input of seawater (which is very enriched in Mg relative to Sr) may explain the increasing Mg/Sr in a speleothem from Jinapsan Cave (Sinclair et al., 2012).

2.5 Phosphorus in soils and speleothems

The phosphorus content in stalagmites has become a proxy for seasonal hydrological variability and ecosystem processes (Lewis et al., 2011), and is regarded as a key element for marking annual laminae in speleothems (Fairchild et al., 2001; Huang et al., 2001; Baldini et al., 2002; Borsato et al., 2007). However, the sources and sinks of P in the soil and biosphere prior to entering the karst and cave system are manifold, and moreover, there is evidence that the P concentration in percolating waters are subject to calcite-water interactions and microbial activities on top of the speleothem.

2.5.1 Sources and sinks of P above the cave

The P nutrient cycle is a complex system, which is dependent on various parameters, such as for example processes involved in physical, chemical and (micro-biological) soil characteristics, vegetation dynamics and climate conditions (Figure 2.10).

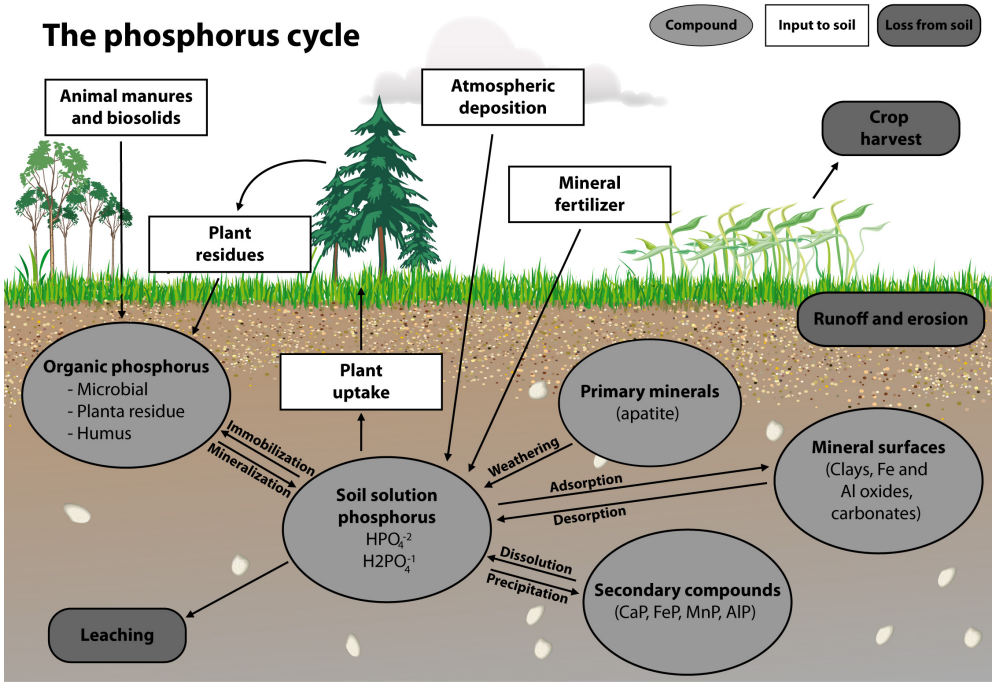

Figure 2.10: *Illustration of the phosphorus cycle. White squares indicate the sources and dark grey rounded squares the sinks of P in the soil zone. The compounds of P are displayed as light grey ellipses.*

The ultimate source of all soil P is primary apatites. As a consequence of weathering, primary phosphates release soluble P which may be leached, be utilized by plants and microorganisms, enter the labile pool, or be transformed into secondary P minerals (Smeck, 1985). In arable land, the application of fertilizers has significantly transformed P budgets (Sharpley and Rekolainen, 1997). Other sources of P into ecosystems may be dry atmospheric deposition. For example, a study from a montane wet tropical forest in the Luquillo Mountains of Puerto Rico constrains that the input of P through mineral aerosol dust deposition may be an important component of nutrient dynamics in tropical forest ecosystems (Pett-Ridge, 2009).

In soils and plants, P is present as phosphate ion (PO_4^{2-}). The total P may be high in most soils but unavailable to the solution due to the pH dependent retention of phosphate in acid and calcareous soils (Bieleski, 1973; Hinsinger, 2001).

There are four different pools of soil P compounds which contribute to soil-solution P (Smeck, 1985; Ashraf, 2015). The first one is the adsorbed P pool. At low pH, phosphate is adsorbed at the surfaces of iron oxides and aluminum oxides. This pool contributes to soil-solution P as the pH of soil increases (Figure 2.11). This process is called desorption. An increase in the concentrations of organic anions in the soil results in P desorption (Hinsinger, 2001; Qayyum et al., 2015).

The second pool of the P compounds in the soil consists of occluded P. Occluded P refers to phosphorus physically encapsulated by minerals which are structurally devoid of phosphorus. Since occluded P is physically sheltered from interaction with more reactive P forms, thus its contribution to the soil-solution P is very small (Walker and Syers, 1976; Wada, 1985).

The third pool is precipitated P. Phosphate ions are precipitated with iron (Fe^{2+} and Fe^{3+}) and aluminum ions (Al^{3+}) at low pH and with calcium ions (Ca^{2+}) at high pH present in the soil solution (Sanchez and Uehara, 1980) (Figure 2.11). These precipitates can be amorphous and

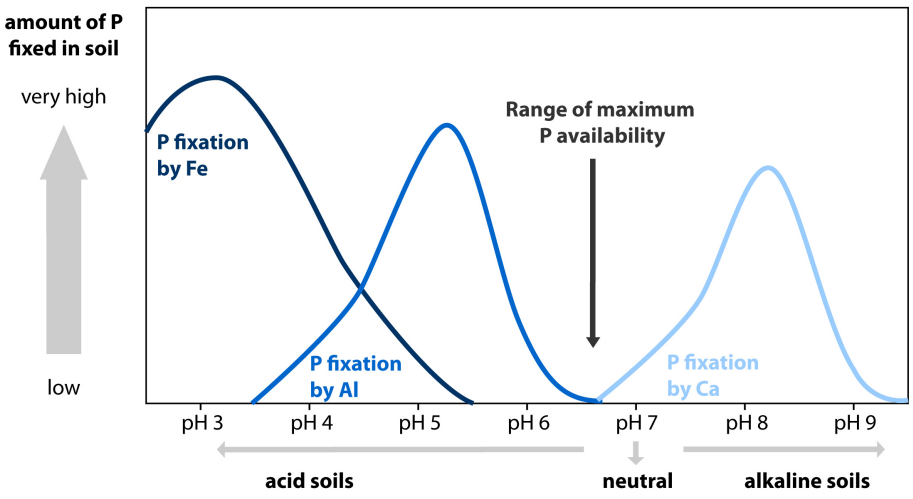

Figure 2.11: *Influence of soil pH on the soil P availability. Maximum P availability is reached in soils with pH values in the neutral or weakly acid range.*

crystalline. The P bound with crystalline forms is also very tightly fixed; hence, P release is very slow. The precipitated P is turned back into the soil solution by dissolution (Smeck, 1985; Hossner et al., 1973; Sims and Pierzynski, 2005). Occluded and precipitated P are summarized as secondary compounds in Figure 2.10.

The fourth soil P pool consists of organic P, coming from dead remains of plants and microbial masses. Organic P is made available to plants by microbial processes and plant roots (Hinsinger, 2001). Organic P may constitute 20-80% of total soil P, which contributes significantly to the soil-solution P (Steffens et al., 2010).

In summary, the main contribution to available P to leaching from the soil is organic P. However, adsorbed and precipitated P may be released to soil solution under certain conditions, which are highly pH dependent (Figure 2.11).

2.5.2 P systematics in speleothems

If the host rock above the cave does not contain a significant amount of apatite, the main source of P in dripwater is the soil solution. Its main compound is organic P, which is thus regarded to exert the main control on dripwater P concentration. Since Phosphate is highly immobile in the soil solution, it is eventually flushed with the soil waters into the karst and cave system. Therefore, P content in speleothems is often found to be associated with hydrological processes (e.g., Huang et al. (2001); Treble et al. (2003); Baldini et al. (2002); Borsato et al. (2007).

In temperate regions, P in speleothem calcite is commonly interpreted to be transported from seasonally decaying vegetation prior to mineralization in the soil (Huang et al., 2001; Fairchild et al., 2001). Borsato et al. (2007) attributed annual P layers to an autumnal flush of organic material from the soil due to the coincidence of vegetation dieback and high infiltration. Where records of phosphorus content extend to inter-annual timescales, patterns of concentration change are suggested to reflect conditions of soil wetness, vegetation productivity, and nutrient desorption and transport according to water availability (Treble et al., 2003; Webb et al., 2014).

Treble et al. (2003) observed a covariation of U and P on annual timescales, which is explained by the formation of phosphate/uranyl complexes. A positive relation of U and P was also reported on longer timescales (Mischel et al., in press; Webb et al., 2014). Both studies interpret higher values in P and U as reflecting more productive vegetation and higher soil moisture, which is supported by an anti-correlation with Mg (Webb et al., 2014) and $\delta^{13}C$ (Mischel et al., in press), respectively. Very low P concentrations in a Belgian cave were interpreted to be the consequence of strong prior calcite precipitation (PCP), which removed nearly all P from the solution (Huang et al., 2001).

The release of phosphorus during vegetation dieback is plausible where climate is seasonal, but in a tropical setting, with a typical tropical rain forest vegetation association, dieback would only occur following severe moisture stress (Frisia et al., 2012). The authors state, that

in the case of Smiths Cave (Christmas Island), P in cave drips is more likely to be sourced from the dissolution of apatite-group minerals present in the epikarst and brecciated rock. This is also supported by the extremely high P concentrations in dripwaters and the analyzed stalagmite SC4 (up to 8000 ppm). In contrast, P concentrations in stalagmites fed by soil P are usually much lower. For instance, speleothem samples from Ernesto Cave (Italy) vary from 10 to 250 ppm P (Huang et al., 2001; Fairchild et al., 2001; Borsato et al., 2007), and Webb et al. (2014) and Mischel et al. (in press) report values mostly far below 1500 ppm.

Moreover, there is some evidence from other studies, that microbial activity may influence calcite precipitation. P is not only present as adsorbed phosphate incorporated into the calcite lattice, but also as crystalline phosphate phases co-precipitated with the calcite (Mason et al., 2007). These P-rich phases were found to be potentially associated with microbially related processes in speleothems from the Grand Cayman (Caribbean) (Jones, 2009). The author thus concluded that speleothem P/Ca ratio might be no reliable paleo climate proxy.

Frisia et al. (2012) tried to elucidate mechanisms of P incorporation into speleothems growing in warm and wet coastal settings. The authors confirm that P concentration variability is a powerful climate proxy, but in their speleothems P peaks appear not to be related to an increase in colloidal transport from the soil, but to complex interactions between hydrological and microbial processes. Frisia et al. (2012) constrain, that there may not be a direct relation between an increase in P concentration and seasonal infiltration as has been found in previous studies, especially if the source of this element is not the labile phosphate released through leaching during seasonal vegetation dieback in temperate climates.

3 Methods

3.1 Dating of speleothems

One of the major advantages of speleothems as paleo climate archive is the relatively strong chronological control, especially for the last 500,000 years, for which the ^{230}Th/U dating (section 3.1.1) is the method of choice (Richards and Dorale, 2003).

A number of other methods than U-series dating can be applied to measure the age of speleothems. Interval (layer) counting (Baker et al., 2008; Tan et al., 2006) and radiocarbon dating (Hua, 2009) are techniques, which are also used in this thesis and will be introduced in the following sections 3.1.2 and 3.1.3. Other studies, e.g. for dating of speleothems older than 500 ka make for example use of the U-Pb method (Woodhead et al., 2006; Rasbury and Cole, 2009). Less commonly applied dating techniques are for example radiometric dating with ^{210}Pb, ^{226}Ra/^{210}Pb or ^{231}Pa, as well as paleo magnetism, tephrochronology and other event markers.

The establishment of a proper age-depth relationship ('age model') is straight forward for continuous interval counting. In the case of other techniques, interpolation between the dated sections of a speleothem is required. This issue is considered in section 3.1.4.

3.1.1 ^{230}Th/U dating

^{230}Th/U dating is considered to be a generally very reliable method and is based on two fundamental assumptions (Ivanovich and Harmon, 1992; Scholz and Hoffmann, 2008). Firstly, only uranium is transported with the karst waters into the cave system and initially incorporated in $CaCO_3$ in contrast to the low-soluble thorium. Secondly, the calcium carbonate remains a closed system, i.e. neither U nor Th is added or removed after precipitation. The basic assumption, that thorium is not present in the groundwater due to its low solubility, enables the reset of the clock of radioactive decay of U to zero. Thus, the amount of daughter products is a direct measure of the time elapsed since the point of incorporation in the speleothem.

The age t of a sample can be calculated iteratively by the following equations for the activity ratios of (^{234}U/^{238}U) and (^{230}Th/^{238}U) (derivation in Ivanovich and Harmon (1992)):

$$\left(\frac{^{234}\mathrm{U}}{^{238}\mathrm{U}}\right)(t) = \left(\left(\frac{^{234}\mathrm{U}}{^{238}\mathrm{U}}\right)_{init} - 1\right) \cdot e^{-\lambda_{234} t} + 1 \tag{3.1}$$

$$\left(\frac{^{230}\mathrm{Th}}{^{238}\mathrm{U}}\right)(t) = \left(1 - e^{-\lambda_{230}t}\right) + \left(\left(\frac{^{234}\mathrm{U}}{^{238}\mathrm{U}}\right)(t) - 1\right) \cdot \frac{\lambda_{230}}{\lambda_{230} - \lambda_{234}} \cdot \left(1 - e^{-(\lambda_{230}-\lambda_{234})}\right) \tag{3.2}$$

with λ denoting the respective decay constants of the nuclides. The evolution of the activity ratios can be illustrated as shown in the figures 3.1 and 3.2.

The main uncertainty of U-Th ages is introduced by the presence of initial Th incorporated in $CaCO_3$. It is transported with the groundwater with organic matter, colloidal material and fine sediments and is typically called 'detrital' Th. Without correction of this initial Th input, the derived ^{230}Th/U ages may be substantially overestimated. The correction for inital radiogenic Th is deduced from the content of the stable ^{232}Th isotope under the assumption that the ratio of the both isotopes in the detrital material is constant and that all the isotopes of the U-series decay chains are in radioactive equilibrium. Most commonly, a bulk earth activity ratio of (^{230}Th/^{232}Th) = 0.8 ± 0.8 is used, assuming a mean mass ratio of ^{232}Th/^{238}U = 3.8 of in the continental crust (Wedepohl, 1995). However, these values vary with host rock and soil characteristics, with a range of activity ratios quoted in the literature from 0.2 (Drysdale et al., 2006) to approximately 18 (Beck et al., 2001). For example Fensterer et al. (2012) argue that the a priori bulk earth ratio for ^{232}Th/^{238}U cannot be used to accurately account for initial ^{230}Th in a stalagmite in Western Cuba and that a ^{232}Th/^{238}U smaller by a factor of 10 is more appropriate. This applies also to the sample studied in section 5. This demonstrates the need for independent determinations of the detrital component, or to focus on 'clean' samples, where the ratio of ^{230}Th/^{232}Th is sufficiently large.

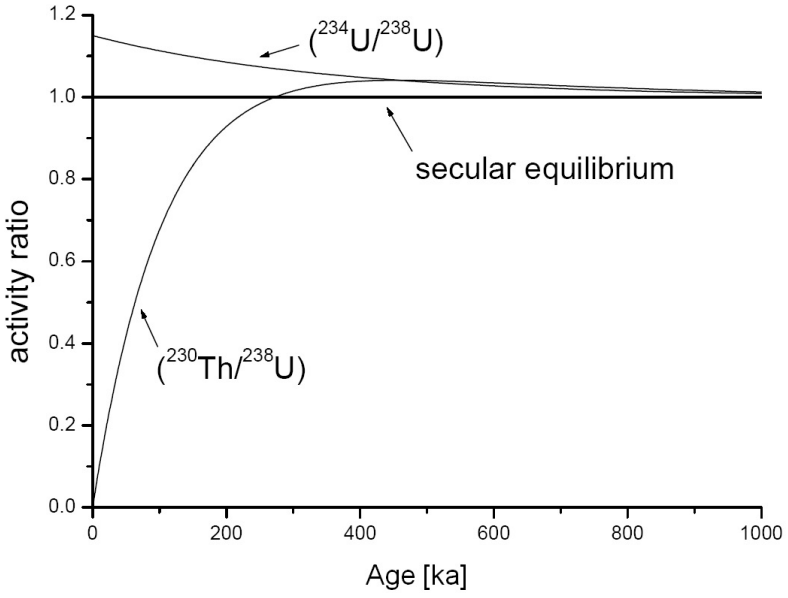

Figure 3.1: *Temporal evolution of the activity ratios (^{234}U/^{238}U) and (^{230}Th/^{238}U). Figure adapted from Neff (2001).*

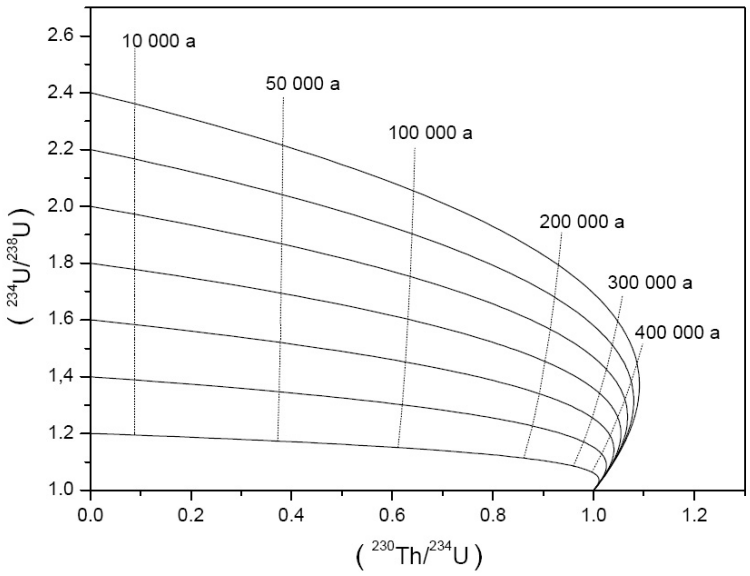

Figure 3.2: *Variation of ($^{234}U/^{238}U$) vs. ($^{230}Th/^{238}U$) with time in a closed system with no inital ^{230}Th. The vertical lines show the isochrones for specific time slices, the near horizontal lines show the return to radioactive equilibrium of the activity ratios with time for different inital $^{234}U/^{238}U$ ratios. Figure adapted from Neff (2001).*

Analytical techniques

In early work in the 1960s, alpha-spectrometry was used to directly measure the emitted alpha-particles in an appropriate detector. However, this method required large sample sizes and low count rates limited the number of analyses. Since the 1990s, the evolution of thermal ionization mass spectrometry (TIMS) finally enabled reliable dating due to the revolutionary improved analytical precision. More recently, multi-collector inductively coupled mass spectrometry (MC-ICPMS) further decreased the needed sample size and simplified preparation chemistry (Hellstrom, 2003; Hoffmann, 2008). Recent state-of-art research works on establishing laser-ablation MC-ICPMS (Hoffmann et al., 2009; Spooner et al., 2016) for in-situ and high-resolution analysis.

The TIMS is a solid source mass spectrometer. Purified U and Th solutions are placed on a rhenium filament, which is placed in the ion source of the mass spectrometer, where the atoms are thermally released by heating the filament. With a total U amount needed for one analysis in the range of a few tens to a hundreds of nanograms a precision of a few permil can be achieved (Scholz and Hoffmann, 2008). In contrast, MC-ICPMS is a plasma source mass spectrometer. Purified dissolved U and Th samples are nebulized and injected with a carrier gas (Ar) into the plasma, where the mixture is ionized. The key difference between the TIMS and the MC-ICPMS technique is the transfer efficiency of the isotopes, which is $\ll 1\,\%$ for TIMS, but ca. 1 % for MC-ICPMS (Scholz and Hoffmann, 2008). This enabled great improvements in dating speleothems with very low uranium contents.

3.1.2 Interval counting

If possible, counting of annual layers provides the most precise chronology for speleothem paleo climate reconstructions. In many cases, speleothems can contain annual variations, for example in trace elements, fluorescent organic matter or in the structure of the crystal lattice (Figures 3.3 and 3.4). Optimum conditions for use apply for sites with seasonal transport of organic matter and/or bedrock-derived trace elements. The reviews of annual laminae in speleothems by Tan et al. (2006) and Baker et al. (2008) focus on the more widely applied fluorescence and petrological laminae rather than trace element laminae.

Annual laminae were first confirmed in hand section by Broecker et al. (1960) and with fluorescence microscopy by Baker et al. (1993) and Shopov et al. (1994). These achievements have led to their use in chronology building and the construction of over 1000yr-long continuous lamina sequences in some samples (e.g. Proctor et al. (2002); Dasgupta et al. (2010)). For trace element laminae, it is needed to confirm the annual signal in the trace element variations.

Manual laminae counting is the typical method, but is very time-consuming. Automated peak counting software was developed for example by Smith et al. (2009) or Meyer et al. (2006). However, any automated approach will benefit from validation against manually counted sequences (Fairchild and Baker, 2012). Cross-validation with absolute dating techniques (^{230}Th/U or ^{14}C dating) further improves laminae counted age-depth chronologies and may confirm the annual nature of the counted laminae.

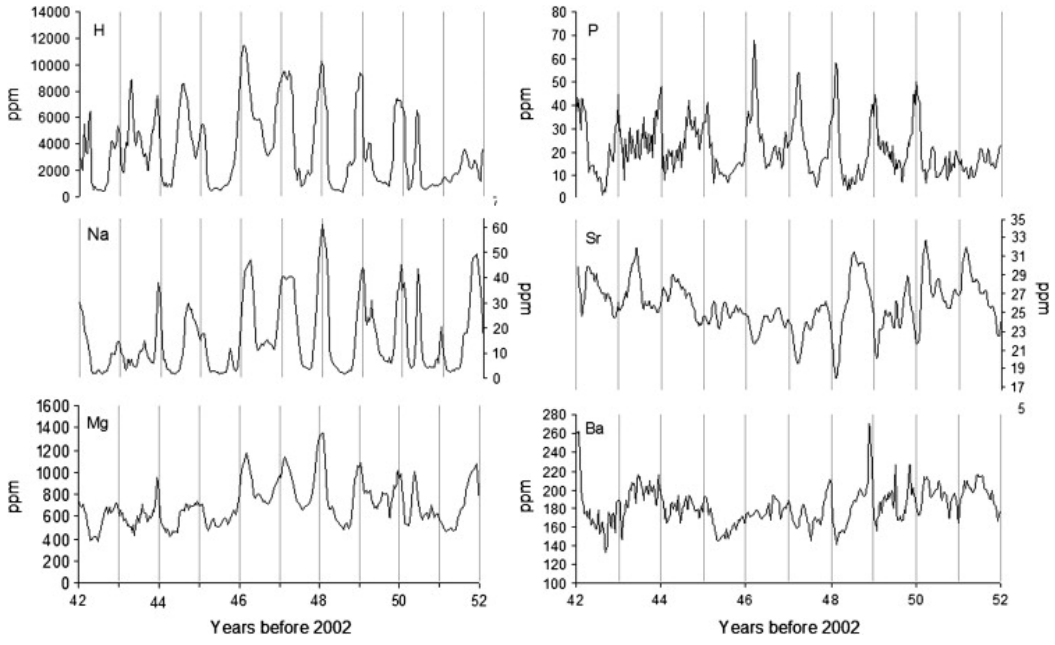

Figure 3.3: *Example for annual trace elemental laminae in speleothem OBI84 from Obir cave (Austria) for the period 1950 - 1960. The vertical lines indicate the locations of the visible laminae. From Smith et al. (2009).*

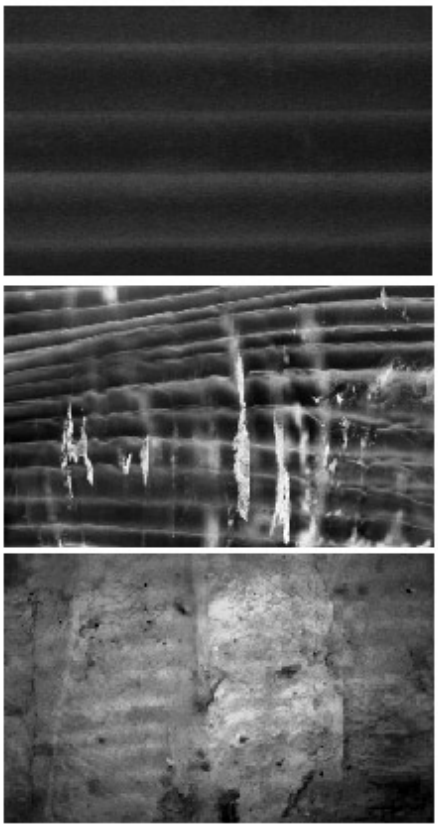

Figure 3.4: *Examples of fluorescent laminae (1) Shihua Cave, Beijing (2) Stalagmite ER-77, Ernesto Cave, Italy. x5 magnification (3) Stalagmite SU-03-2, Uamh an Tartair, Scotland, x10 magnification. From Baker et al. (2008).*

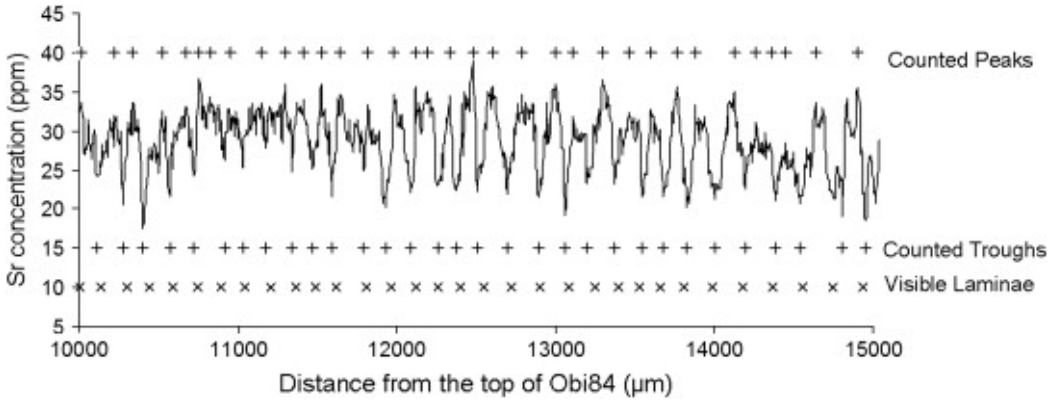

Figure 3.5: *Comparison of chemical laminae in the OBI85 Sr time series counted by an automated peak-counting software (Counted Peaks), the location of the chemical laminae counted by the automated peak-counting software for the inverted Sr series (Counted Troughs) and the location of the visible laminae. From Smith et al. (2009).*

3.1.3 ^{14}C dating

As described in section 2.1, carbon is transferred from the atmosphere through the soil and the hostrock to the speleothem. Natural cosmogenic ^{14}C ('radiocarbon') is produced in the upper atmosphere by cosmic ray action on nitrogen. However, anthropogenic radiocarbon was introduced into the atmosphere by nuclear weapon tests since the 1950s.

^{14}C has a half-life of 5,730 ± 40 years (Godwin, 1962) and was initially attempted to be used for dating speleothems e.g. by Geyh (1970). However, radiocarbon dating of speleothems is problematic, due to the varying dead carbon fraction (dcf). 'Dead carbon' is the fraction of carbon in the sample which is bedrock derived and contains no ^{14}C, because it has long been decayed. Moreover, a substantial portion of 'older' carbon can be introduced to the speleothem by microbial activity in the soil (Noronha et al., 2015; Fohlmeister et al., 2011). Comparison with ^{230}Th/U analyses demonstrated, that the dcf in speleothems exhibits a time-variant, wide range from 5 to 40 % (Genty and Massault, 1999; Genty et al., 1999, 2001). This severely limits the use of ^{14}C as a dating technique for speleothems where both the mean dcf is unknown as well as its variability over time (Fairchild and Baker, 2012). A significant development has been to make use of the additional anthropogenic radiocarbon, the 1960s atmospheric radiocarbon 'bomb peak' (Figure 3.6 and 3.7). This atmospheric ^{14}C spike is transferred and transformed through the vegetation, soil and karst system, leading to a damped and lagged increase of ^{14}C in speleothems (Genty and Massault, 1999; Genty et al., 1999; Noronha et al., 2015). Studies in well ventilated caves demonstrated, that the lag of the atmospheric ^{14}C signal in the speleothem may be very short (Mattey et al., 2008; Smith et al., 2009). The combination and/or cross-validation of different dating techniques such as laminae counting or ^{230}Th/U dating with the demonstration of recent or active calcite deposition by ^{14}C analysis has been increasingly used in the recent years (Mattey et al., 2008; Smith et al., 2009; Rudzka et al., 2012; Sundqvist et al., 2013; Noronha et al., 2015).

3.1.4 Age-depth models

The construction of an age-depth model for the investigated speleothem is of crucial importance in order to infer any time-related interpretation of the proxy time series. For annually laminated samples, chronological errors are mainly caused by counting errors and the age-distance relationships are often very well understood. However, most samples are only discontinuously dated with radiometric ages, limited sections of layer counting or event markers such as the radiocarbon bomb peak. Each of these dates may be associated with uncertainties both in age and distance axes. Moreover, despite stalagmite growth can be described as being autocorrelated to long lag times, sudden nonlinear jumps in growth can occur at irregular levels (Fairchild and Baker, 2012). These jumps even mean a pause in calcite deposition ('hiatus') and might be explained by changes in hydrological routing or the effects of threshold responses (Fairchild and Baker, 2012). A simple approach for constructing age-depth relationships could be simple linear interpolation or spline functions (Richards

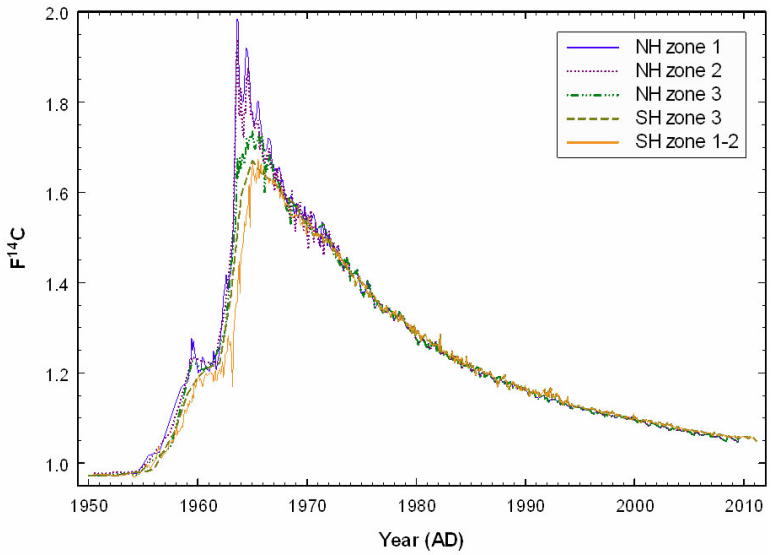

Figure 3.6: *Regional tropospheric ^{14}C curves for the period AD 1955 - 2001 for six different zones (Northern Hemispheric Zones 1-3 and Southern Hemispheric zone 1 - 3). From Hua et al. (2013).*

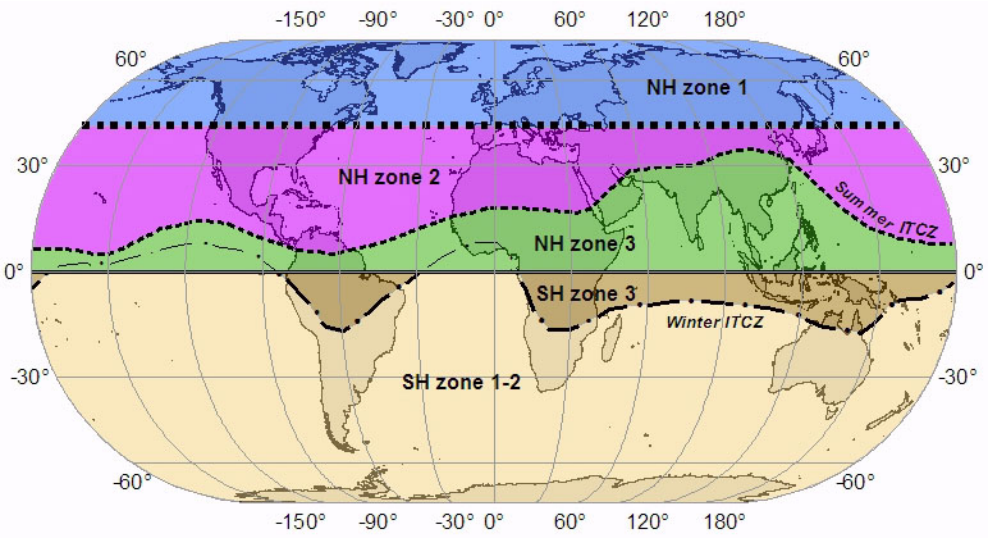

Figure 3.7: *World map showing the four zones into which the tropospheric ^{14}C data have been grouped. From Hua et al. (2013).*

and Dorale, 2003). All these approaches, however, do not really take into consideration the persistence and nonlinearity of speleothem growth. Thus, more sophisticated approaches are useful which take into account the combination of radiometric and interval analyses along with hiatuses. Bayesian and Markov chain Monte Carlo (MCMC) approaches are for example realized in the OxCal tool (https://c14.arch.ox.ac.uk/oxcal.html, Ramsey (1995)) or the Bchron software package implemented in R (Haslett and Parnell, 2008), which was applied in Chapter 7. Scholz and Hoffmann (2011) provide a MCMC R-code for speleothem researchers ('StalAge'), which was used in the Chapters 5 and 6.

3.2 Statistical methods

In this section, the basic principles of statistical methods applied in this thesis are summarized. The reader is referred to special literature and references therein for more details, e.g., Hartung and Elpelt (1992); von Storch and Zwiers (1999) or Papula (2016).

3.2.1 Covariance and correlation

If possible, the aim of climate reconstruction with speleothem proxy time series is to find any relationship or connection between the measured proxy and a climate parameter such as temperature or precipitation. A measure to quantify the dependency of two variables X and Y is the correlation between X and Y. The calculation of the correlation requires a two dimensional sample with n ordered pairs of numbers

$$(x_1 \,:\, y_1), (x_2 \,:\, y_2), ..., (x_n \,:\, y_n) \tag{3.3}$$

with X = $x_1, x_2, ...x_n$ and Y = $y_1, y_2, ...y_n$. The covariance between X and Y is then defined as

$$cov(x, y) = \frac{1}{n-1} \cdot \sum_{i=1}^{n} (x_i - \bar{x})(y_i - \bar{y}) \tag{3.4}$$

with the mean values $\bar{x}$ of X and $\bar{y}$ of Y.

Pearson's product momentum correlation coefficient

The dimensionless correlation coefficient r of the two dimensional sample with variances $\sigma_x^2 \neq 0$ and $\sigma_y^2 \neq 0$ follows by normalization of the covariance $cov(x, y)$

$$r = r_{xy} = \frac{cov(x, y)}{\sigma_x \cdot \sigma_y} \tag{3.5}$$

r is a scale-independent measure for the strength or association of the linear dependency between X and Y. r is always between -1 and +1. For r = 0, X and Y are uncorrelated, whereas for $|r| = 1$ an exact linear dependency exists between the two variables. r is often referred to as

the empirical Pearson's (sample) correlation coefficient. A more convenient way to calculate r may be (Papula, 2016):

$$r = r_{xy} = \frac{\sum x_i y_i - n\bar{x}\bar{y}}{\sqrt{\sum x_i^2 - n\bar{x}^2}\sqrt{\sum y_i^2 - n\bar{y}^2}} \tag{3.6}$$

The quantity

$$r^2 = r_{xy}^2 \tag{3.7}$$

is also called coefficient of determination. It states which proportion of the variance of X is explained by Y and vice versa.

It is to note, that several major factors may influence the magnitude of r apart from the underlying relationship between the two variables. To the extent that a bivariate distribution departs from linearity, r will underestimate that relationship. Also discrepant data points (outliers) can affect the magnitude of r. The nature of the effect depends on where the outlier is located in the scatterplot. Moreover, other things being equal, restricted variation in either X or Y will result in a lower Pearson r than would be obtained were variability greater (Coladarci et al., 2010).

Spearman's rank correlation coefficient

As denoted above, Pearson's r may not be appropriate for non-linear relationships between two variables. In this case, Spearman's rank correlation coefficient ρ or r_s is a nonparametric measure of rank correlation (statistical dependence between the ranking of two variables). It asses how well the association can be described with a monotonic function. If there are no repeated data values, a high Spearman correlation occurs when each of the variables is a monotone function of the other. Spearman's correlation coefficient is defined as Pearson's r between the ranked variables:

$$\rho = r_s = \frac{cov(rg_x, rg_y)}{\sigma_{rg_x}\sigma_{rg_y}} \tag{3.8}$$

3.2.2 Statistical inferences

Empirical correlation coefficients vary from sample to sample because of random sample variation and the reliability of the linear relationship estimated by r_{xy} also depends on the number of data points n in the samples X and Y. The population correlation (or 'true' correlation) is symbolized by the greek ρ. Thus, r is used for making inferences about ρ. The significance of the empirical correlation coefficient r can be evaluated using hypothesis testing and/or interval estimation.

Hypothesis testing

In order to decide, whether the linear relationship in the sample data is strong enough to use to model the relationship in the population, a hypothesis test can be performed to test

the significance of the correlation coefficient. The most common null hypothesis for testing a single correlation coefficient is $H_0 : \rho = 0$. If the hypothesis test concludes, that the correlation coefficient of the population ρ is significantly different from 0, the correlation is regarded as 'significant'. H_0 is tested against the alternative hypothesis H_A: $\rho \neq 0$ (the population correlation coefficient is significantly different from 0) to the significance level α (commonly denominated 'p-value'). For pairs $(x_i : y_i)$ from an uncorrelated bivariate normal distribution the sampling distribution of r_{xy} follows Student's t-distribution with degrees of freedom n - 2:

$$t = \frac{r - \rho_0}{s_r} = \frac{r_{xy}\sqrt{n-2}}{\sqrt{1 - r_{xy}^2}} \tag{3.9}$$

with the standard error s_r of r_{xy}

$$s_r = \sqrt{\frac{1 - r_{xy}^2}{n-2}} \tag{3.10}$$

In a two-tailed test, H_0 is rejected if the absolute calculated t value is above the certain critical t value with a specified α and the number of degrees of freedom n-2:

$$|t| > t_{n-2;1-\alpha/2} \tag{3.11}$$

If logic and theory leads to a directional alternative hypothesis, a one-tailed test may be appropriate. This might be the case when the only reasonable expectation is, if H_0 is false, that spatial reasoning and mathematical ability are positively or negatively related (i.e., $\rho > 0$ or $\rho < 0$)). In this case H_0 is rejected to the level α if

$$t > t_{n-2;1-\alpha} \quad or \quad t < t_{n-2;\alpha} \tag{3.12}$$

The critical t-values for Pearson's correlation coefficients can be also looked up in tables in special literature (e.g. Hartung and Elpelt (1992)). The calculation can also conveniently sidestepped by taking advantage of tables with critical values of r_{xy} - the minimum values of r_{xy} necessary to reject H_0.

Confidence intervals

Rather than (or in addition to) testing the hypothesis H_0 interval estimates of r corresponding to the selected level of confidence can be provided. Since empirical correlation coefficients are not normal distributed, for X and Y from an bivariate normal distribution, the distribution of the empirical correlation coefficient r_{xy} must be corrected with the Fisher-transformation:

$$z := f(r_{xy}) = 0.5 \; ln\left(\frac{1 + r_{xy}}{1 - r_{xy}}\right) = arctanh(r_{xy}) \tag{3.13}$$

z is also for small sample sizes n approximately normal distributed with standard deviation $1/\sqrt{n-3}$ and mean

$$\bar{z} = \frac{1}{2}\, ln\left(\frac{1+\rho}{1-\rho}\right) \tag{3.14}$$

The 1-α confidence interval for z is then given by

$$[z_1, z_2] = \left[f(r_{xy}) - \frac{z_{1-\alpha/2}}{\sqrt{n-3}}\ ,\ f(r_{xy}) + \frac{z_{1-\alpha/2}}{\sqrt{n-3}}\right] \tag{3.15}$$

The confidence interval $[r_1,r_2]$ for ρ is iteratively calculated by re-transforming z_1 and z_1 to the interval limits r_1 and r_2 (compare e.g. Hartung and Elpelt (1992)).

Autocorrelation

Successive values in X or Y may be correlated with one another, which is often the case for climate related time series. This persistence is known as serial correlation (or autocorrelation). It has to be taken into account when testing significance, for example, of the correlation between the two time series. Among other things, serial correlation (and trends) can severely reduce the effective number of degrees of freedom. The sample autocorrelation coefficients r_k give an estimate of the amount of serial correlation for the time lag k = 0, 1, 2,...:

$$r_k = \frac{\frac{1}{n}\sum_{i=k+1}^{n}(x_i - \bar{x})(x_{i-k} - \bar{x})}{\frac{1}{n}\sum_{i=k+1}^{n}(x_i - \bar{x})^2}. \tag{3.16}$$

The autocorrelation coefficients r_k from the autocorrelation function (acf). The lag-1 coefficient may often be an adequate (but rough) indicator of the amount of serial correlation in a time series. A rough estimate of the decorrelation time is given by

$$\tau_0 = -\frac{\tau}{ln(r_1)}. \tag{3.17}$$

The effective number of degrees of freedom is then given by

$$n\tau/\tau_0 = -n\ ln(r_1) \tag{3.18}$$

For more details, see von Storch and Zwiers (1999). For equivalent sample sizes smaller 30 von Storch and Zwiers (1999) recommend the 'Table-look-up'-test (Zwiers and von Storch, 1995) as a small alternative to the conventional t-test that avoids the difficulties of estimating an equivalent sample size. The authors provide tables constructed by means of Monte Carlo simulation with adjusted critical t levels for one- and two sided tests and given sample sizes n with lag-1 autocorrelation coefficient r_1.

4 Study sites

The study sites of this thesis are located in the Caribbean region on the greater Antilles (western Cuba and Puerto Rico, Figure 4.1) and in eastern Europe (SW Romania). Both regions are characterized by a complex interplay between atmospheric teleconnection patterns and competing effects, which will be outlined in the associated publications and following paragraphs, respectively. Since every case study is self-contained and provides the relevant background information, this section rather aims to motivate the selection of the sites and provides an overview of the most important climatological features and recent research.

4.1 Cueva Larga and Santo Tomas

4.1.1 Cueva Larga (Puerto Rico)

Cueva Larga (CL) is located in the north central karst region of Puerto Rico in the northeastern Caribbean (18 °19' N, 66 °48' W, Figure 4.2). CL has a horizontal extension of about 1,440 m (Miller, 2010) and is dominantly a vadose cave with some phreatic features. It is located in the massive dense Oligocene Lares Limestone (Giusti, 1978; Monroe, 1980). In the framework of a collaboration with researchers from the University of Mayagüez, CL is monitored extensively. This collaboration has already been the base for a number of recent publications (Vieten et al. (2016, in press).

Figure 4.1: *Map of Caribbean realm with the location of Cueva Larga in Puerto Rico (blue dot) and the Santo Tomas Cave system in Cuba (red dot)*

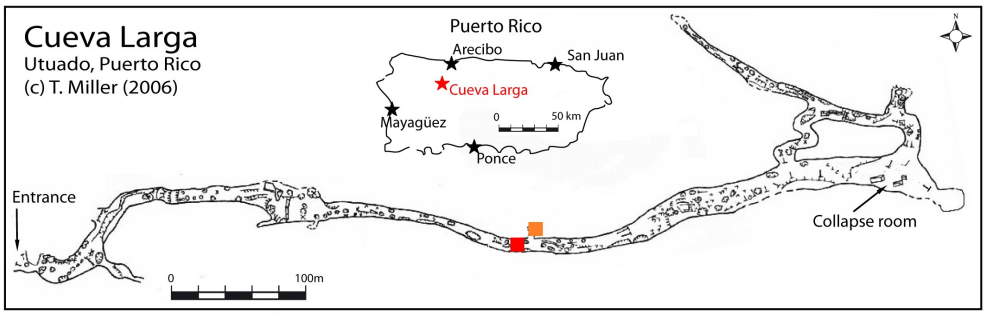

Figure 4.2: *Map of Cueva Larga with the position of sample PR-LA-1 (marked with red square). Insert: Map of Puerto Rico with the location of Cueva Larga (red star). Modified after Miller (2010).*

The focus of the work of Vieten et al. (2016) is the analysis of cave ventilation processes in CL. In CL, pCO_2 varies seasonally between 600 ppm in winter and 1,800 ppm in summer. The seasonal variability in cave pCO_2 permits the estimation of a cave air exchange time of 36 ± 5 days and a winter ventilation rate of $3{,}300 \pm 1{,}000\ m^3$/day for the main cave passage.

Calculations of virtual temperature and differences between cave and surface temperature indicate that the seasonal temperature cycle is the main driver of the alternation between a well-ventilated winter mode and a near-stagnant summer mode (Vieten et al., 2016). Increased cave ventilation leads to lower pCO_2 values in the cave atmosphere and accordingly lower calcium equilibrium concentration which increases carbonate precipitation rates (Baker et al., 2014). Even though it rains more in the summer, speleothems in CL are expected to grow faster during the low pCO_2 winter season. This is important if the drip site has a fast response time to rainfall events above the cave. In the extreme case, speleothems in CL could only grow during the winter and fast responding drip sites will only record a winter

Figure 4.3: *Cone karst formations in western Cuba. Picture provided by J. Pajón.*

environmental signal in the speleothem's carbonate (Vieten et al., 2016).

Preliminary results from rain and dripwater monitoring are presented in Vieten et al. (in press) (Appendix D). It includes monthly analysis of stable isotope ratios of rain and dripwater, trace element ratios of dripwater and cave air parameters. Seasonal rainfall patterns above CL show characteristic stable isotope values. The wet season is characterized by more negative $\delta^{18}O$ and δD values and a maritime deuterium excess (+10 ‰). The dry season has more positive $\delta^{18}O$ and δD values and elevated deuterium excess (>15 ‰).

The seasonal variations in the $\delta^{18}O$ and δD values are smoothed by the soil and karst system which acts as a low-pass filter, indicating that climate proxies derived from speleothems growing in Cueva Larga may only show multi-annual changes. The seepage water reservoir appears to be well-mixed. The transmission time of atmospheric signals into the dripwater is site specific ranging most likely from several months to years (Vieten et al., in press).

4.1.2 Santo Tomas cave system (Cuba)

The Santo Tomas cave system (STC) is located in northwestern Cuba in the Sierra de los Organos in the Province of Pinar del Rio. The karstified area is of Jurassic origin (Figure 4.3) and developed around 170 million of years ago (Pajón et al., 2001). Carbonate dissolution processes lead to the typical cone karst formations, and subsurface water streams eroded the karstified material leading to enormous cave systems. The STC (22 °31'N, 83 °51' W) has a total length of ca. 46 km. In 2008, a cave monitoring program was conducted by Dr. J. Pajón in order to study the hydrological behaviour of the cave system. Measured air temperatures of the STC ranged from 21.6 to 21.9 °C, and relative humidity from 97 to 99 %. A detailed description of the data and results is given in Fensterer (2011).

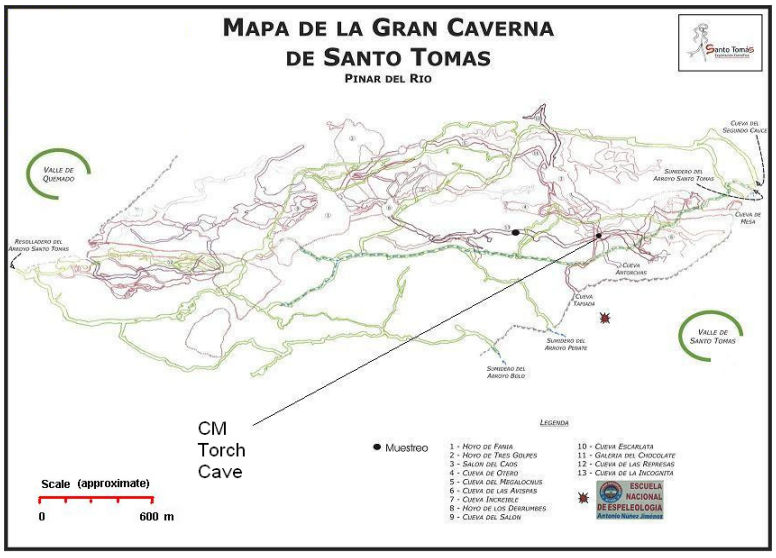

Figure 4.4: *Map of the Santo Tomas cave system. Figure adapted from Parise et al. (2005).*

4.1.3 Climatological framework

The climate of the Caribbean basin can generally be classified as dry-winter tropical climate (Rudloff, 1981). In most parts of the Caribbean, precipitation is bimodal with an initial maximum around May, a relative minimum in June - August, and a second peak in September - October (Rudloff, 1981; Giannini et al., 2000; Chen and Taylor, 2002). This general tendency differs in the southernmost Caribbean (off the Venezuelan coast), which receives less rainfall and has a primary rain season in the winter (November - January; Martis et al. (2002)).

The main driver of the Caribbean rainfall seasons regarding trade winds, the Hadley cell circulation (Figure 4.5 a) and interactions occurring between land surfaces and atmosphere is the Intertropical convergence zone (ITCZ, Poveda et al. (2006)). The ITCZ is a region close to the equator, where trade winds converge, air ascends, low atmospheric pressure occurs together with deep convective clouds and high precipitation (Henderson-Sellers and Robinson, 1986). The ITCZ constitutes, together with the North Atlantic Subtropical High (NASH) and the expansion of the tropical North Atlantic warm pool, the main climatic features influencing the Caribbean climate.

The rainy season occurs (Figure 4.5 b), as easterly trade winds produced by the NASH transport moisture from the Atlantic into the Caribbean Sea, where the flow intensifies forming the Caribbean Low Level Jet (CLLJ, Amador (1998); Amador and Magana (1999); Mestas-Nuñez and Miller (2006); Mestas-Nuñez et al. (2007); Hodell et al. (2008)). During summer in the northern hemisphere, the CLLJ splits in two branches (Figure 4.6). One branch turns northward bringing moisture to the Western Gulf of Mexico and Western Cuba, and the southerly branch of the CLLJ continues westward carrying moisture across the Central American isthmus. During boreal winter, the NASH dominates the intra-American Sea, and moisture transport is shifted south of the Yucatan peninsula (Hodell et al., 2008).

Jury et al. (2007) identified four different clusters of precipitation patterns which differ in length and intensity of the rainfall maxima (Figure 4.7). The annual cycle is more unimodal and largest in the northwest Caribbean (cluster 1) and becomes increasingly bimodal towards lower latitudes (cluster 4) as expected. Cuba is attributed to cluster 1, which is characterized by a relatively higher contribution of May - July rainfall and a relatively lower contribution of the winter rainfall than the other clusters. The seasonal variation in cluster 4, which includes Puerto Rico, is marked by low precipitation amounts through the winter and early spring (January - April), followed by increasing rainfall amounts from May onward with a maximum peak in October (Jury et al., 2007).

For a long time, paleo climate research focused on northern hemisphere high latitude processes, which provided an explanation for the occurrence of Glacial-Interglacial cycles (i.e, the Milankovitch hypothesis) as well as abrupt climate change via changes in the strength of the thermohaline circulation (THC, e.g., Rahmstorf (2003)). The low latitudes represent a very interesting research area, because the tropical hydrological cycle plays a key role in regulating global climate, in particular through the export of heat and moisture to higher lat-

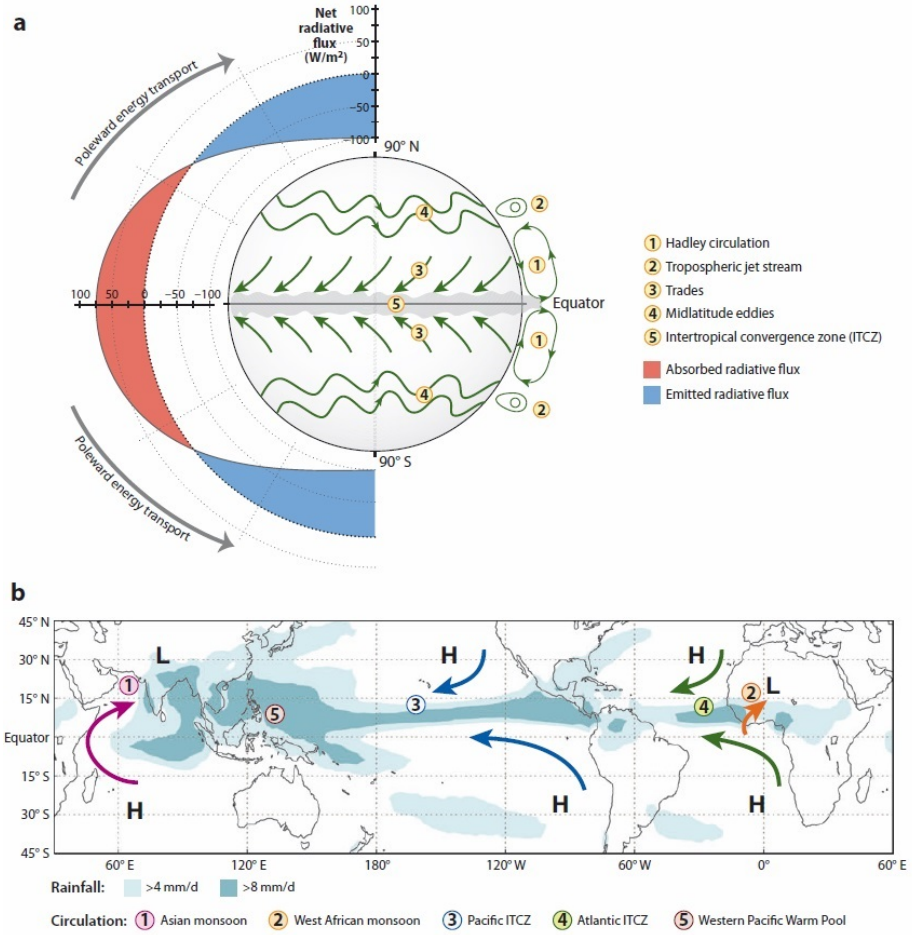

Figure 4.5: *Two views of the tropical climate (from Chiang (2009)): (a) Tropical climate as part of Earth's general circulation. Earth absorbs radiative energy in the Tropics (red portion of the energy flux graph) and emits them in the mid- and high latitudes (blue portions of the energy flux graph). To maintain energy balance, the atmosphere and ocean circulation transports the energy from the Tropics to the mid- and higher latitudes. In the Tropics are the Hadley circulation, with uplift of air by moist convection at the Intertropical Convergence Zone (ITCZ), and subsidence in the subtropics. In the midlatitudes, the circulation is dominated by a strong westerly flow in the upper troposphere - the midlatitude westerlies - in which disturbances known as baroclinic eddies form and develop. (b) Tropical climate from a regional perspective. The figure shows July-August climatological rainfall conditions and surface winds (arrows) depicting circulations associated with the Asian (1) and West African (2) monsoons, as well as the subtropical trades flowing into the ITCZ regions of the Pacific (3) and Atlantic (4). (5) is the convection over the western Pacific warm pool. L and H denote locations of relative surface pressure highs and lows.*

itudes (Lachniet, 2009b). Three major properties of the tropical climate system highlight its importance and impact for global climate change, namely its sensitivity to climate change, its ability to re-organize and to project its influence to the rest of the globe (Chiang, 2009).

The position of the Intertropical Convergence Zone (ITCZ) is extremely sensitive to both local and supra-regional climate conditions, such as spatial gradients in sea surface temperatures (SST, Broccoli et al. (2006)) and large-scale climate patterns like the El Niño Southern Oscillation (ENSO, Alexander and Scott (2002)) and the North Atlantic Oscillation (NAO, Kushnir et al. (2010)). The response of the ITCZ to North Atlantic temperature changes was recorded on different timescales in lacustrine and marine sediments (Haug et al., 2001; Deplazes et al., 2013; Hodell et al., 2008) and speleothems (Fensterer et al., 2012; Winter et al., 2011; Wang et al., 2004; Cruz et al., 2007).

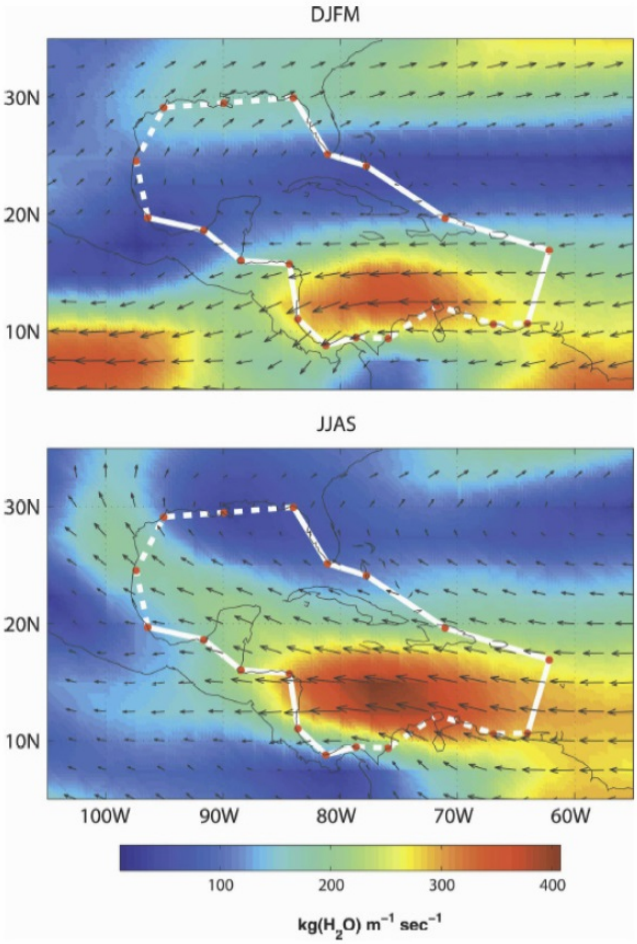

Figure 4.6: *(top) December-March and (bottom) June-September averages of the monthly vertically integrated water vapor flux vectors calculated from the daily 1960-2003 NCEP-NCAR reanalysis (from Mestas-Nuñez et al. (2007)). The magnitudes of the water vapor flux vectors are color contoured. The thick solid (dashed) lines indicate the eastern and western (northern and southern) IAS boundary segments as used by Mestas-Nuñez et al. (2007).*

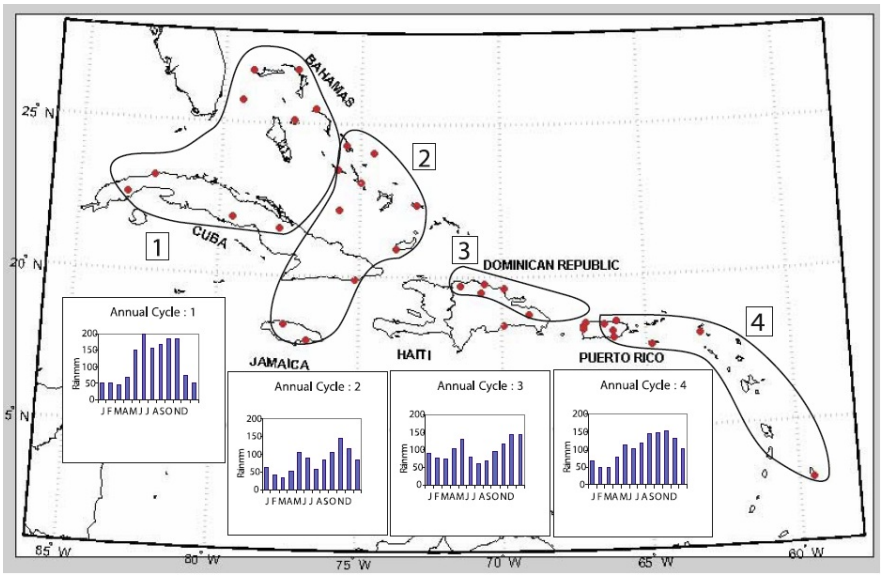

Figure 4.7: *Geographic extent of the four precipitation clusters identified by Jury et al. (2007). Annual cycles left to right for clusters 1 to 4, based on averages over the 31-year period 1951 - 1981. From Jury et al. (2007).*

The Caribbean is located in a region, which is both directly and indirectly influenced by several supra-regional climate patterns, such as the Atlantic Multi-Decadal Oscillation (AMO), ENSO and the NAO, which all operate on different timescales, ranging from several years to multi-decadal. Rainfall variability in the Caribbean and central and northern South America is largely dependent on the position of the ITCZ, which determines the strength and track of the easterly trade winds. When the ITCZ is in a position further north, larger amounts of freshwater are exported towards the Caribbean from the Atlantic basin (Deplazes et al., 2013; Poveda et al., 2006). The meridional oscillation of the ITCZ, in turn, responds to the seasonal insolation cycle, which lags the zenithal position by approximately one month (Poveda et al., 2006). Since the position of the ITCZ is extremely sensitive to inter-hemispheric spatial gradients in SST (Chiang and Koutavas, 2004), climate variability in other regions, such as the NAO and ENSO, which influence the Atlantic SST gradient, may also have a strong impact on Caribbean precipitation (Hurrell et al., 2006). The Atlantic Warm Pool (AWP) exerts a further influence on Caribbean climate, acting as a convective source and adding to the flow of moisture and heat onto land during summer (Correa-Metrio et al., 2012; Wang and Fu, 2007; Wang et al., 2006).

4.1.4 Current state of research

Recent studies have demonstrated a coupling of Caribbean and North Atlantic climate variability during the Holocene. Studies of marine sediments from the Cariaco basin and the Caribbean confirm the prominent role of the position of the ITCZ for Caribbean climate variability e.g. (Deplazes et al., 2013; Haug et al., 2001). In addition, a high resolution $\delta^{18}O$

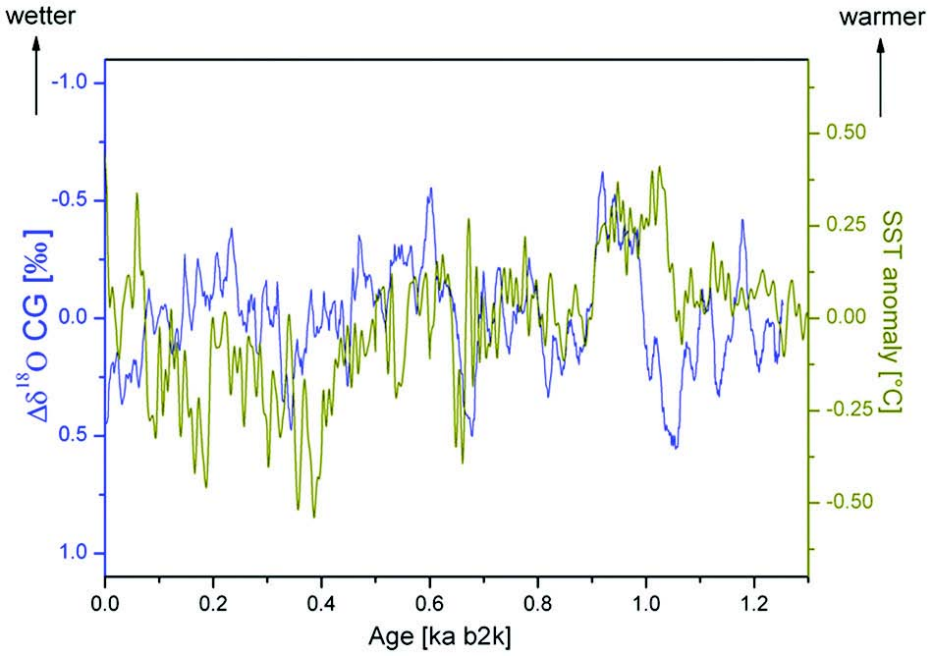

Figure 4.8: *Detrended and smoothed (5 point adjacent average)* $\delta^{18}O$ *values of stalagmite CG (blue) in comparison with the AMO index (green) reconstructed by Mann et al. (2009a). Note that the* $\delta^{18}O$ *axis is inverted. Higher SSTs in the North Atlantic are accompanied by lower* $\delta^{18}O$ *values and, thus, higher precipitation on Cuba. From Fensterer et al. (2012).*

record from a Cuban stalagmite shown in Figure 4.8 exhibits a correlation of precipitation in the northwestern Caribbean with the AMO during the last 1.3 ka (Fensterer et al., 2012, 2013). Drier conditions in the Caribbean area are associated with colder phases in the North Atlantic and vice versa. This suggests that the present-day relationship between Caribbean rainfall intensity and the North Atlantic SST gradient also played an important role during the last millennia. The influence of the AMO on Caribbean climate variability is also evident in a speleothem record from Puerto Rico, which covers the last 800 a (Winter et al. (2011), Figure 4.9). Both Fensterer et al. (2012) and Winter et al. (2011) interpret the $\delta^{18}O$ values of speleothem calcite as a proxy for the amount of summer precipitation with lower $\delta^{18}O$ values corresponding to more rainfall (Figure 4.8).

For the last glacial period, several paleo climate studies from subtropical as well as high northern latitudes have demonstrated a complex relationship between the position of the ITCZ and climate variability, such as changes in ocean circulation (Böhm et al., 2015; Nürnberg et al., 2008) or the tropical hydrological cycle (Kanner et al., 2012; Schmidt and Spero, 2011; Wang et al., 2004). Competing effects between Atlantic and Pacific teleconnection patterns were found to have played an important role during the past glacial cycle (Arellano-Torres et al., 2015; Asmerom et al., 2010; Lachniet, 2009b). In subtropical Brazil, rainfall during the last glacial period appears to be closely related to insolation on precessional timescales (Cruz et al., 2006; Wang et al., 2007). During Heinrich stadials (HS) in the North Atlantic

Ocean, a southward displacement of the ITCZ has been observed resulting in wet periods in the southern Tropics (Jaeschke et al., 2007; Wang et al., 2004). These results have been corroborated by climate modeling studies (Broccoli et al., 2006; Chiang, 2003; Chiang and Bitz, 2005; Zhang and Delworth, 2005), which derive similar results for the impact of the North Atlantic on tropical climate (i.e., a southward displacement of the ITCZ during North Atlantic cold phases and the Last Glacial Maximum (LGM), respectively). Contrary results were found, however, by several studies from Lake Tulane with wetter conditions in Florida (Donders et al., 2011; Grimm et al., 2006). The influence of the movement of the ITCZ was even recorded in the southwestern United States, with a simultaneous movement of the polar jet stream (Asmerom et al., 2010).

Previous work on Holocene Cuban speleothems constrains that $\delta^{18}O$ values in stalagmite calcite reflect past precipitation variability with lower $\delta^{18}O$ values corresponding to higher rainfall due to the amount effect. Fensterer et al. (2012) presented a high resolution record for the last 1.3 ka from Western Cuba, which exhibits a correlation to the AMO (Figure 4.8). A potential mechanism for this relationship may be the strength of the THC. For a weaker THC, lower SSTs in the North Atlantic probably lead to a southward shift of the ITCZ and drier conditions in Cuba. Thus, the Cuban stalagmite record reflects drier conditions during Holocene cold phases in the North Atlantic, such as the Little Ice Age. A second stalagmite

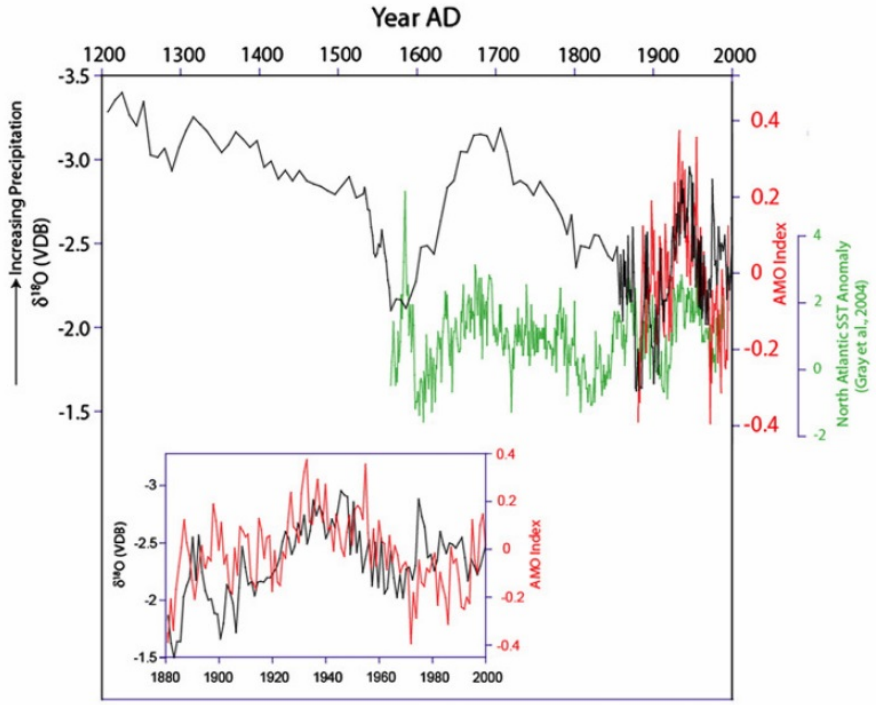

Figure 4.9: *The $\delta^{18}O$ of stalagmite PDR-1 from Puerto Rico spanning the past 8 centuries (black) is shown with annually averaged AMO index (red: Rayner et al. (2006)) and AMO reconstruction (green: Gray et al. (2004)). Inset shows comparison between Puerto Rico stalagmite $\delta^{18}O$ and AMO for the instrumental period. From Winter et al. (2011).*

from Cuba covers the last 12.5 ka (Fensterer et al., 2013). This stalagmite shows a pronounced transition from higher $\delta^{18}O$ values (indicating drier conditions) to more negative $\delta^{18}O$ values (suggesting wetter conditions) between 10 and 6 ka (Figure 4.10). On orbital timescales, the $\delta^{18}O$ value of Caribbean precipitation resembles the $\delta^{18}O$ value of Caribbean surface water. On millennial timescales, the speleothem $\delta^{18}O$ record shows a good agreement with North Atlantic SST as well as a similarity with the Bond events (Bond, 1997; Bond et al., 2001) (Figure 4.10).

In summary, the two Cuban stalagmites confirm the relationship between Caribbean precipitation variability and the position of the ITCZ during the Holocene, which is influenced strongly by the inter-hemispheric SST gradient in the Atlantic (Chiang, 2009).

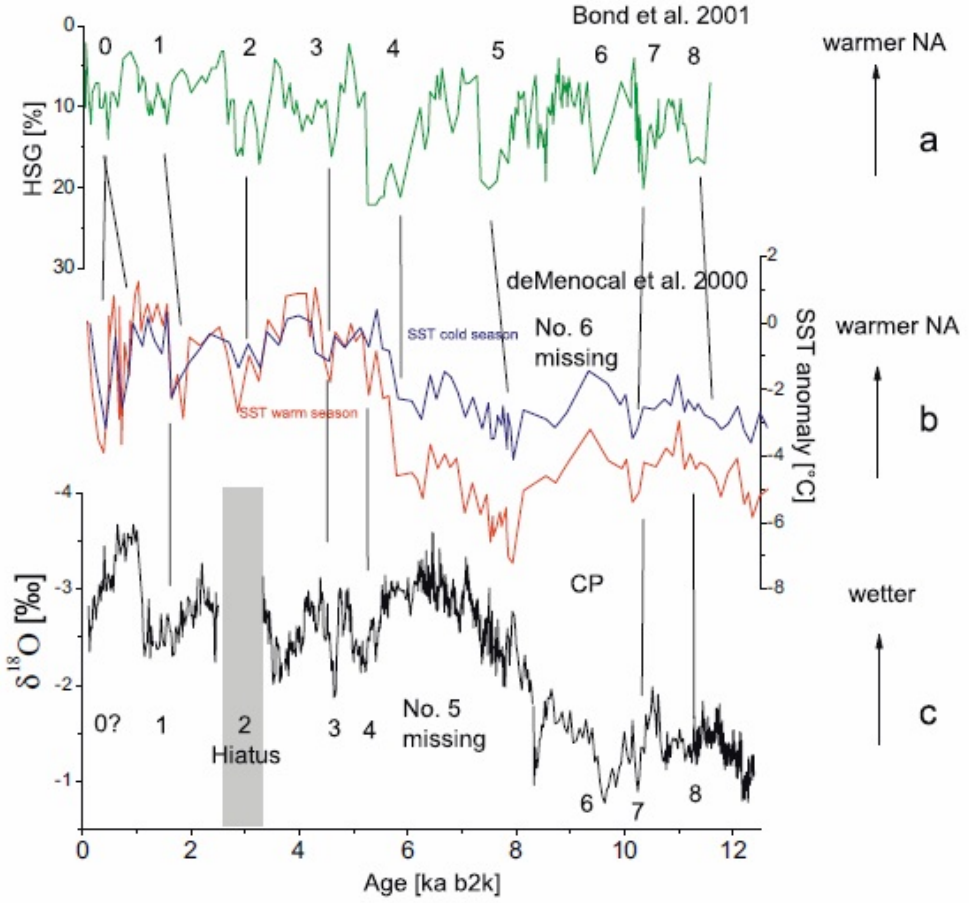

Figure 4.10: *Stalagmite CP $\delta^{18}O$ values (c) in comparison with the percentage of hematite-stained grains (HSG) in sub-polar North Atlantic deep-sea sediments (a), which record the Bond events (Bond, 1997; Bond et al., 2001). (b) Two SST records off West Africa (red: reconstructed temperature during warm season, blue: cold season) (deMenocal et al., 2000). The numbers identify the different Bond events, which are linked to cold SSTs in West Africa (deMenocal et al., 2000). During most Bond events, the stalagmite record suggests drier conditions on Cuba. From Fensterer et al. (2013).*

4.2 Cloşani Cave

4.2.1 Site description

Cloşani Cave (45.07 °N, 22.80 °E) is located in southwestern Romania at the southern slope of the Carpathians (Figure 4.11). It is developed in massive Upper Jurassic limestone mainly consisting of calcite (93 %) with minor occurrence of dolomite (7 %) (Constantin, 2003).

Drip water and cave air parameters were monitored from 2010 to 2015 (Constantin et al., unpublished data). The deeper sectors of both main passages (Figure 4.12) are characterized by a stable cave climate. Cave temperature shows a mean value of 11.3 °C with inter-annual variations of ± 0.5 °C (Diaconu, 1990). Relative humidity is mostly close to 100 %. The pCO_2 of the cave shows a strong annual variability with maximum values of up to 8800 ppm in late

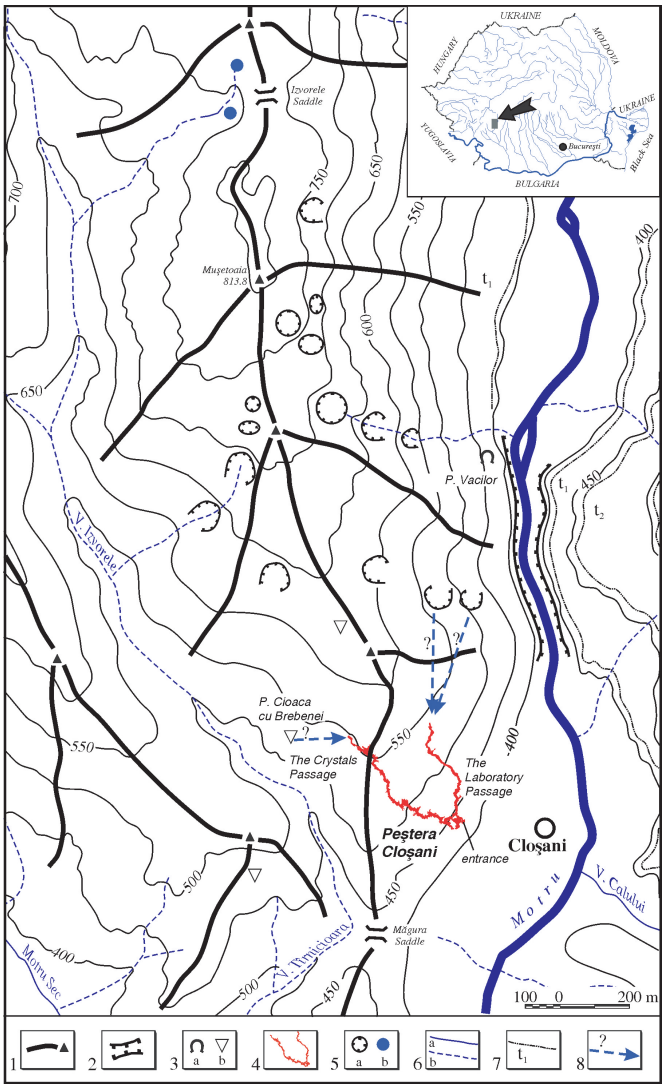

Figure 4.11: *Location of Cloşani Cave in Romania (inset) and regional setting of the cave. The cave is located at the southern slope of the Carpathian mountains. Map from Constantin (2003).*

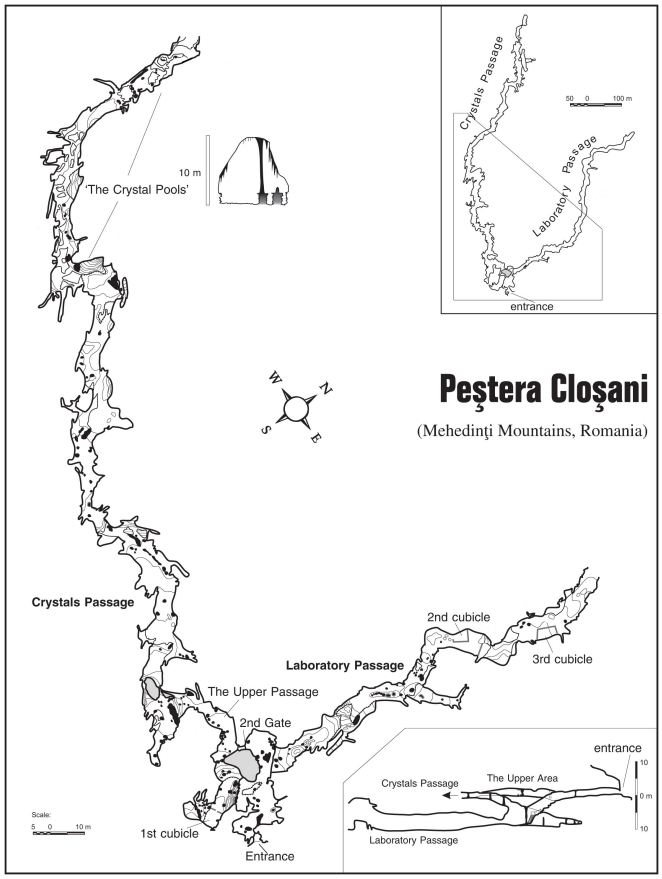

Figure 4.12: *Internal structure of Cloşani Cave. The cave consists of two main passages, the Crystals Gallery and the Laboratory Gallery. Map from Constantin (2003).*

summer and minimum values in winter and spring (1500 ppm). The high pCO_2 during summer leads to very different conditions for speleothem growth between the seasons, favouring calcite precipitation during winter (Chapter 7).

4.2.2 Climatological framework

The regional climate of the Romanian Carpathians realm is characterized by westerly circulation and the influence of the mountain chain topography (Busuioc et al., 2014; Ionita et al., 2014; Micu et al., 2015). By their geographical position within the continent, the Romanian Carpathians lie in an area of interference between five major pressure centers operating over Europe e.g., the Azores Anticyclone, East-European Anticyclone, Mediterranean Cyclones, Icelandic Cyclone and Scandinavian Anticyclone (Micu et al., 2015).

The influence of the Southern Carpathians divides Romania into two major regions of different climatic characteristics by blocking the northerly polar or arctic airflows in winter, as well as of the southerly (tropical) ones. This results in a wetter and colder northern part and drier and warmer conditions in the south. Micu et al. (2015) give a very detailed picture of the air flows and resulting climate patterns in SW Romania.

Annual precipitation in the region of the cave shows two maxima, one from April to June, which is mainly caused by North Atlantic cyclones, and a smaller one between October and December, generated by cyclones originating from the western and central Mediterranean Basin. The winter continental airflows, usually dry and cold, originate in the Arctic Ocean, whereas continental air masses from eastern Eurasia and north Africa or southwest Asia frequently influence the summer precipitation regime with usually very warm and dry spells (Micu et al., 2015). In the region of Cloşani cave, snow fall accounts to about 10 % of total annual precipitation amount, however in the Southern Carpathians frequent snowfalls only occur in areas higher than 1,000 - 1,100 m (Micu et al., 2015).

Large-scale teleconnection patterns

The North Atlantic Oscillation (NAO) - which affects the strength of westerly flow and weather patterns in Europe (e.g. Wanner et al. (2001); Hurrell et al. (2003)) was found to have a strong relationship with winter climate in Romania (Micu et al., 2015). The NAO is the leading mode of climate variability in the North Atlantic region and is characterized by a meridional see-saw in the atmospheric pressure between the Icelandic Low and the Azores High (Wanner et al., 2001). During periods characterized by a positive NAO index westerly flow is enhanced across the North Atlantic and the European region. As a consequence, this phase is associated with stronger-than-average winds across the mid-latitudes of the Atlantic onto Europe and anomalously northerly flows in the Mediterranean region. For example, snow variability in SW Romania is tightly connected with the NAO (Micu et al., 2015). Moreover, positive thermal anomalies and negative precipitation anomalies in the Romanian area are associated with a high NAO index (Bojariu and Gimeno, 2003; Bojariu and Paliu, 2001).

Another prominent teleconnection pattern over the North Atlantic region is the East Atlantic - West Russia pattern (EAWR, Barnston and Livezey (1987)), which has a strong influence on European climate, especially in the southern and eastern sector. The EAWR was found to have a strong influence over the precipitation in the Mediterranean region (Krichak et al., 2002; Krichak and Alpert, 2005). Extreme wet (dry) winter months are characterized by anomaly patterns which project onto the negative (positive) phase of the EAWR. A strong relationship between the EAWR and the temperature variability inside a cave from the north-western part of Romania has also been found with high (low) temperatures associated with an atmospheric circulation that resembles the center of action of the EAWR pattern (Rimbu et al., 2012). Nissen et al. (2010) found that both NAO as well as EAWR play a significant role on the variability of cyclones and wind activity over the Mediterranean region. The authors state, that during the positive phase of the EAWR, the storm numbers over the central Mediterranean region are decreasing and the number of strong wind events over the eastern Mediterranean region is increasing. Although the EAWR is one of the dominant modes of variability over the North Atlantic-Eurasian region, less attention has been paid to the role of the EAWR pattern on the European climate (Ionita, 2014). The authors investigated the relationship between the EAWR teleconnection pattern and the hydroclimatology of the

European region. The main conclusions of Ionita (2014) are that the EAWR has a strong impact on the coupling between the sub-tropical Atlantic Jet and the African Jet, which in turn affects the climate variability over Europe, and that the strongest impact of the EAWR on precipitation in the central and eastern part of Europe is in mid-winter and early spring. Additionally, the link between EAWR and European temperature persists from mid-winter to late spring. In general, the link between mid-winter EAWR and European precipitation and temperature was found to be stable in time, however for southwestern Romania, this only applies for winter temperatures and spring precipitation (SPI3, 3-month standardized precipitation index).

Moreover, Comas-Bru and McDermott (2014) concluded, that the relationship between North Atlantic Oscillation (NAO) and winter climate over the North Atlantic - European sector can be linked to the combined effects of the NAO and either the East Atlantic pattern (EA) or the Scandinavian pattern (SCA). In terms of $\delta^{18}O$ of precipitation, the results of Comas-Bru et al. (2016) show, that although the East Atlantic (EA) pattern is generally uncorrelated to $\delta^{18}O_p$ during the instrumental period, its polarity affects the $\delta^{18}O_p$ - NAO relationship. In the case of SW Romania, the authors conclude that $\delta^{18}O$ may not be a robust proxy to reconstruct any relationship of the NAO with air temperature or precipitation.

4.2.3 Current state of research

From the southern Carpathian realm, few terrestrial climate records exist despite its important geographical position as a transitional climatic zone between central Europe and the Mediterranean e.g., Constantin et al. (2007); Feurdean et al. (2008); Onac et al. (2014); Rudzka et al. (2012). Reconstructions based on tree-ring data provide valuable information for the past several hundred years (Levanič et al., 2012; Popa and Kern, 2008), but are limited to the warm season. More recently, guano-derived $\delta^{13}C$-based paleo hydroclimate records made it possible to characterize hydroclimate regimes in Romania during the late Holocene (Onac et al., 2014, 2015; Forray et al., 2015). Low-resolution (i.e. centennial to millennial timescales) stalagmite records, which mainly reflect past variability of winter climate, suggest that the climate in the Carpathian-Balkan region is linked to the North Atlantic region on different time scales (Constantin et al., 2007; Drăguşin et al., 2014; Onac et al., 2002).

Part II

Publications

5 Paper I: Cueva Larga

Millennial scale climate variability on Puerto Rico reconstructed from a multi-proxy speleothem record spanning 46 - 15 ka BP

Sophie F. Warken[1,2*], Denis Scholz[1], Rolf Vieten[3], Christoph Spötl[4], Klaus P. Jochum[5], Thomas E. Miller[6], Amos Winter[3,7], Andrea Schröder-Ritzrau[2] and Augusto Mangini[2]

[1] Institute for Geosciences, University of Mainz, Germany

[2] Institute of Environmental Physics, University of Heidelberg, Germany

[3] Marine Science, University of Puerto Rico, Mayagüez, Puerto Rico

[4] Institute of Geology, University of Innsbruck, Austria

[5] Climate Geochemistry Department, Max Planck Institute for Chemistry, Mainz, Germany

[6] Department of Geology, University of Puerto Rico, Mayagüez, Puerto Rico

[7] Earth and Environmental Systems Department, Indiana State University, Terre Haute, Indiana, USA

Abstract We present geochemical data from a speleothem from Cueva Larga, Puerto Rico, covering 15 to 46 ka. The chronology is based on precise ^{230}Th/U dating. High resolution $\delta^{18}O$ values reflect changes in rainfall amount, temperature variability and disequilibrium fractionation effects. The anti-correlation of P/Ca and $\delta^{13}C$ values highlights the influence of vegetation and soil productivity on both proxies. In contrast, Mg/Ca, Sr/Ca and Ba/Ca ratios show little variability and are subject to various second order effects. The average $\delta^{18}O$ composition suggests that climate on Puerto Rico during the last Glacial was generally cooler by ~2 - 4 °C and drier than today. Warm Dansgaard/Oeschger interstadials were characterized by relatively warm and humid conditions. $\delta^{18}O$ values during D/O's 7 and 11 even show comparable conditions to modern climate. In contrast, temperature drops by about 3 - 5 °C and increased aridity are recorded during cold Heinrich stadials, which were partly accompanied by a decline in vegetation and soil productivity. HS 1 was found to be the coolest and driest of all recorded Heinrich stadials. These observations are in agreement with recent research and are ascribed to the southerly movement of the ITCZ and the variable strength of the AMOC.

Our record is the one of the first from this region which clearly shows the impact of both stadials and interstadials on Caribbean climate variability over a relatively long time period. It allows an approximate quantification of last glacial climate conditions.

5.1 Introduction

The reconstruction of tropical hydroclimates has shifted more and more into the focus of paleo climate research (Haug et al., 2001; Cruz et al., 2007; Hodell et al., 2008; Chiang, 2009; Lachniet et al., 2009). Several studies reveal a strong variability in the tropical hydrological cycle during the last glacial period closely related to North Atlantic climate variability (Peterson, 2000; Wang et al., 2001; Cruz et al., 2007; Wang et al., 2017).

Ice core and deep sea sediment records of the last 45,000 years show a series of millennial scale climate events known as Heinrich stadials (HS) and Dansgaard/Oeschger (D/O) cycles (Dansgaard et al., 1984). Dansgaard/Oeschger events are millennial scale alternations between warm (interstadial) and cold (stadial) periods. The typical cycle has a sawtooth pattern, with a very rapid warming event (occurring in a few decades), a slow cooling trend, and then a final fast cooling (Bond, 1997; Wolff et al., 2010).

The so-called Heinrich events are recognized in North Atlantic marine sediments as ice rafted debris (IRD) deposited by icebergs upon melting (Bond, 1997; Heinrich, 1988; Hemming, 2004). This freshwater input promoted a slowdown of the Atlantic meridional overturning circulation (AMOC) and an interhemispheric climate response (McManus et al., 2004; Wolff et al., 2010; Böhm et al., 2015). Heinrich stadials subsequent to Heinrich events were associated with a reduction in sea surface temperatures (SSTs) in the North Atlantic (Sachs and Lehman, 1999; Hagen and Keigwin, 2002) which was also predicted by model studies (Zhang and Delworth, 2005). This cooling is thought to be caused by reduced northward heat transport, driven by the slowdown of the AMOC (McManus et al., 2004; Clement and Peterson, 2008; Böhm et al., 2015), or as suggested by Chiang and Bitz (2005), the increase in sea/land ice. Reduced Northern Hemisphere SSTs led to the southward shift in the Intertropical Convergence Zone (ITCZ) and drier conditions in the tropical Northern Hemisphere (Chiang and Bitz, 2005; Zarriess et al., 2011; Stager et al., 2011). Recent studies have also demonstrated the impact of varying height of the Laurentide ice sheet as a climate forcing during Heinrich stadial events (Roberts et al., 2014).

During interstadial periods (i.e. D/O cycles), the inverse occurs with a poleward shift of the Northern Hemisphere summer ITCZ and the jet streams (Asmerom et al., 2010). However, the exact mechanisms driving these events are still not well understood (Clement and Peterson, 2008). The global, abrupt response to Dansgaard/Oeschger interstadials and Heinrich stadials is recorded in various types of climate archives. For example, the paleo climate records suggest that the global signature of Heinrich stadials includes: a drier Europe (Genty et al., 2003), weaker Asian monsoon (Wang et al., 2001), wetter southwestern North America (Asmerom et al., 2010; McGee et al., 2012), drier northern South America (Peterson, 2000), wetter southern South America (Kanner et al., 2012), an overall drier tropical Asia and Africa (Stager et al., 2011; Deplazes et al., 2014) and a gradually warming Antarctica (Wolff et al., 2010).

While a comprehensive picture of climate responses during North Atlantic Heinrich sta-

dials exists from both hemispheres, few studies have been conducted in the (sub-)tropical western Atlantic (Sachs and Lehman, 1999; Grimm et al., 2006; Ziegler et al., 2008; Lachniet et al., 2013; Arienzo et al., 2015; Grauel et al., 2016). Most of these studies either cover only a relatively short time period or show only a selective response to stadials and/or interstadials.

For the northern Caribbean, it is still debated whether the region experienced substantially wetter or drier conditions during Heinrich stadials. Evidence from lacustrine and marine sediments from Florida and the Gulf of Mexico suggests, that the northern Caribbean experienced warm and wet conditions (Grimm et al., 2006; Donders et al., 2011; Ziegler et al., 2008), in contrast to the southern and southwestern part of the Caribbean basin (Correa-Metrio et al., 2012; Escobar et al., 2012; Lachniet et al., 2013; Deplazes et al., 2013; Grauel et al., 2016). Moreover, a speleothem record from the Bahamas is interpreted to show cooler temperatures rather than hydrological changes during Heinrich stadials 1, 2 and 3 (Arienzo et al., 2015).

This debate accounts to difficulties in the comparability of the various records, largely because some sites are located in regions which are strongly influenced by multiple effects (e.g., Lachniet et al. (2009)) or because the climate archives reflect different seasonal signals. In addition, uncertainties in chronology and differences in temporal resolution may constitute further complications.

The value of speleothems for paleo climate reconstructions is commonly recognized (e.g., Wang et al. (2001); Fairchild et al. (2006a); Cruz et al. (2007)). Stable isotopes of oxygen and carbon are the most commonly used proxies for speleothem studies (Lachniet, 2009a). In tropical locations, the $\delta^{18}O$ values of speleothem calcite is typically interpreted to reflect changes in rainfall amount and/or the temperature of the cave (Kanner et al., 2012; van Breukelen et al., 2008).

In Puerto Rico and through-out the Caribbean and south Florida, there is an inverse relationship between the amount of rainfall and the $\delta^{18}O$ value of the rainwater (van Breukelen et al., 2008; Scholl et al., 2009) and therefore the amount effect is considered to constitute the main control on the $\delta^{18}O$ composition of the rainfall precipitation (Dansgaard, 1964; Lachniet, 2009a). Also the cave site of this study, monitoring of rain and dripwater over several years confirms that this relationship is also valid for speleothems from this location (Vieten et al., in press).

Consequently, several studies from the Caribbean presented $\delta^{18}O$ speleothem records associated with past precipitation variability on various timescales (Lachniet et al., 2009; Winter et al., 2011; Fensterer et al., 2012, 2013; Lachniet et al., 2013). For instance, Winter et al. (2011) related Puerto Rican rainfall with the variability of the Atlantic Multidecadal Oscillation (AMO), as evident from a speleothem $\delta^{18}O$ record covering the last 800 a.

Using trace elements as climate proxies is more and more routine in speleothem research. Elements such as Mg or Sr are well-established as hydrological tracers under certain circumstances (Cruz et al., 2007; Fairchild and Treble, 2009). Sinclair et al. (2012) developed a model which allows to investigate the most commonly used interpretation of changes in Mg and Sr as being linked to rainfall as a result of calcite-water interactions such as prior calcite

precipitation (PCP).

In this study, geochemical data are presented which are obtained from a speleothem from Cueva Larga, Puerto Rico, spanning the last 46 to 15 ka. Paleo climate reconstruction reveals substantial changes in the hydrological regime in Puerto Rico associated with Heinrich stadials 1 to 5 and Dansgaard/Oeschger cycles 1 to 12.

5.2 Material and methods

5.2.1 Study location

Stalagmite PR-LA-1 was collected from Cueva Larga which is located about 350m above sea level (asl) in the north central karst region of Puerto Rico in the northeastern Caribbean (18°19'N 66°48'W, Figure 5.1 and 5.2). The limestone overburden is between 30 and 100 m thick and the area above the cave is covered by thick tropical forest with thin soil cover that is nearly absent on the higher elevated and exposed locations. The area receives a total annual rainfall amount of more than 2,100 mm per year and a mean annual temperature of 22.5 °C (Vieten et al., in press). The dominant control on the air flow are the trade winds (85 %).

Cueva Larga is mainly a vadose cave with some phreatic features. It is located in the massive dense Oligocene Lares Limestone (Monroe, 1980) with a horizontal extent of about 1,440 m (Miller, 2010).

Cave air and drip sites are monitored since 2012. Temperature and relative humidity are very constant in the main passage with 22.5 ± 0.2°C and RH close to 100%. Cave air pCO_2

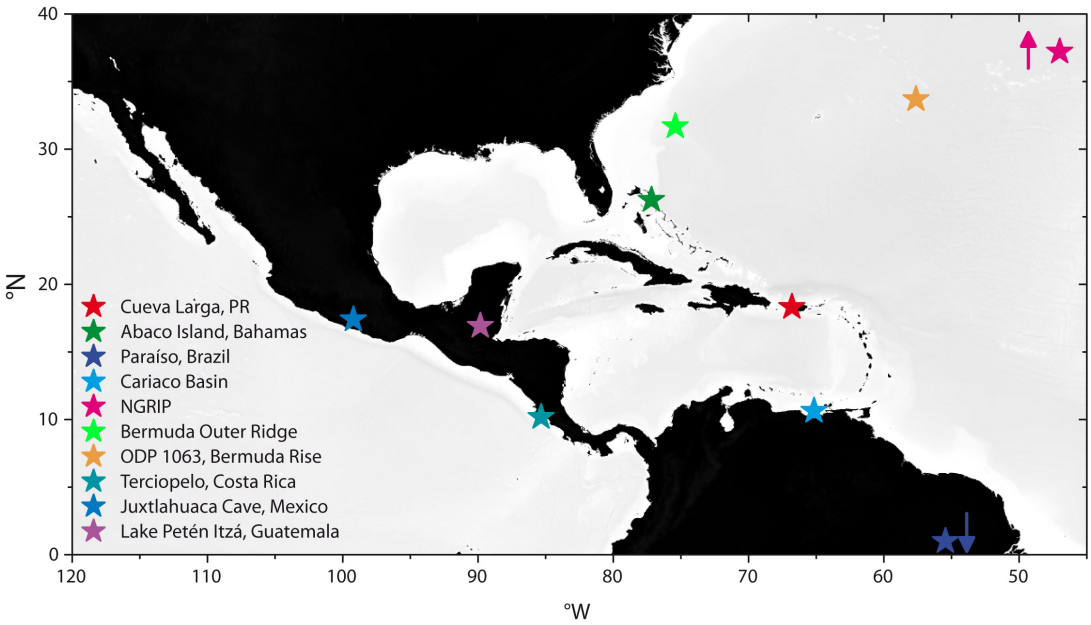

Figure 5.1: *Map showing the locations of Cueva Larga, Puerto Rico, and paleo climate reconstruction sites discussed in this study.*

in the main passage varies seasonally, between 600 ppm in winter and 1,800 ppm in summer (Vieten et al., 2016). The seasonal variability in cave pCO_2 permits the estimation of a cave air exchange time of 36 ± 5 days and a winter ventilation rate of 3,300 ± 1,000 m^3/day for the main cave passage (Vieten et al., 2016).

Despite its tropical location, calculations of virtual temperature and differences between cave and surface temperature indicate that the seasonal temperature cycle is the main driver of the alternation between a well-ventilated winter mode and a near-stagnant summer mode (Vieten et al., 2016). The winter mode is characterized by a positive buoyancy contrast at night leading to maximal cave ventilation, while cave ventilation is at a minimum during summer.

Seasonal rainfall patterns above Cueva Larga show characteristic stable isotope values with more negative $\delta^{18}O$ and δD values during the wet season and more positive $\delta^{18}O$ and δD values in dry season (Vieten et al., in press). The seasonal variations in the $\delta^{18}O$ and δD values are smoothed by the soil and karst system which acts as a low-pass filter, resulting in a well-mixed seepage water reservoir (Vieten et al., in press). The transmission time of atmospheric signals into the dripwater is site specific ranging most likely from several months to years (Vieten et al., in press).

Monitoring of dripwaters indicates that the wet season rainfall contributes proportionally more to the dripwater than the rainfall during the dry season (Vieten et al., in press). However, despite the strong seasonality in rain water $\delta^{18}O$ values, isotopic dripwater signature does not reflect the surface pattern with a mean composition of -2.7 ± 0.2‰ at the drip site SW2 near PR-LA-1 (Vieten et al., in press). The $\delta^{18}O$ signature of recently precipitated calcite at drip sites near PR-LA-1 is in the range of -3.1 ± 0.1‰. Similar to the stable isotope values, elemental composition shows no seasonal variations in dripwaters.

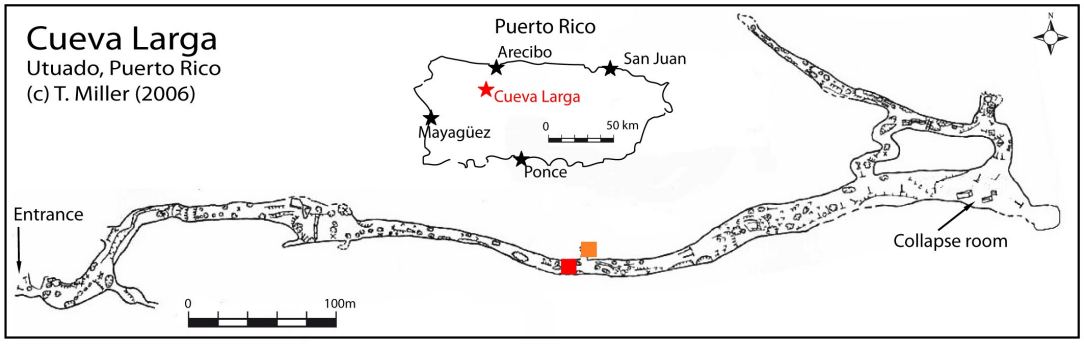

Figure 5.2: *Map of Cueva Larga with the position of PR-LA-1 (marked with red square) and drip site SW2 (orange square). Insert: Map of Puerto Rico with the location of Cueva Larga (red star). Modified after Miller (2010).*

5.2.2 Sample description

PR-LA-1 has a total length of about 2 m and was found lying on the cave floor in the main passage of Cueva Larga (Figure 5.2 and Figure 5.3), where the rock overburden is approximately 40 - 80 m thick. It is suspected, that the stalagmite fell due to the unstable ground conditions, which consists of deep (> 10 m) stream sediments (Miller, 2010).

For the recovery of the sample, it was cut into five pieces (L1A to L1E) of lengths between 25 and 55 cm (and about 40 to 50 kg each), which were removed in several field trips between 2011 and 2013. The subsamples were cut in two halves along their main growth axes (Figure 5.3 B). A slab was prepared from one half, which was subsequently cut into two further halves along the main growth axis, respectively. One half was used for ^{230}Th/U-dating, the opposite half for stable isotope and trace element measurements.

In order to measure the elemental composition of the host rock, samples were taken at four locations in and outside the cave: HR1 (base weather station), HR2 (weather station), HR3 (Cueva Larga entrance) and HR4 (Cueva Larga SW1). The weather station is located directly above Cueva Larga (Vieten et al., in press).

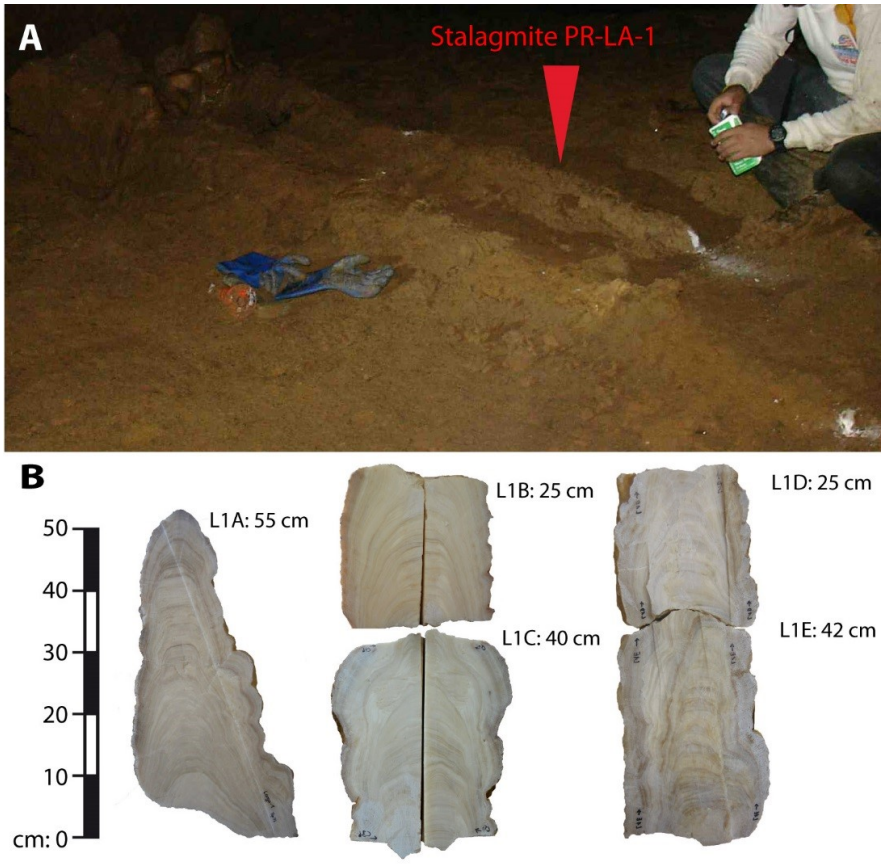

Figure 5.3: *(A) Pan view on stalagmite PR-LA-1 before cutting and removal from Cueva Larga. PR-LA-1 was found lying on the cave floor. (B) Sample slabs L1A, L1B, L1C, L1D and L1E cut from top to bottom of PR-LA-1. Approximate lengths of the slabs are given in the figure.*

5.2.3 Methods

^{230}Th/U-dating was conducted using multi-collector inductively coupled plasma mass spectrometry (MC-ICPMS) at the Max Planck Institute for Chemistry (MPIC), Mainz. Th and U activity ratios were corrected for detrital contamination assuming a ^{232}Th/^{238}U weight ratio of 0.14 ± 0.11 and ^{230}Th, ^{234}U and ^{238}U in secular equilibrium (compare discussion 5.4.1).

Speleothem calcite proxies were analyzed along the growth axes of L1A to L1E. Stable carbon and oxygen isotope measurements were performed using an on-line, automated carbonate preparation system linked to a triple collector gas source mass spectrometer at the University of Innsbruck. Samples were drilled with a spatial resolution of 1 mm. The concentrations of Mg, Al, P, Sr, Y, Ba, Th, U, Pb, Cd, La and Ce of the speleothem and host rock samples were measured by LA-ICP-MS at the MPIC, Mainz.

Correlation analysis was performed with a test statistic based on Pearson's product moment correlation coefficient r (x,y) and follows a t-distribution with length(x)-2 degrees of freedom. Asymptotic confidence intervals are given based on Fisher's Z transform. The given Pearson's correlation coefficients are all significant to at the 0.05 level.

Further details about materials and methods are given in the supplementary material (Appendix A.1).

5.3 Results

5.3.1 ^{230}Th/U dating and age models

In total, 74 ^{230}Th/U-ages were performed from PR-LA-1, from which 24 are from L1A, 10 for L1B, 17 for L1C, 8 for L1D and 15 for L1E. The relevant results for all samples are given in the supplementary material A.2. ^{230}Th/U-ages are shown in Figure 5.4. U content of the samples is relatively low with 0.1 - 0.3 µg/g. In most samples, detrital ^{232}Th content is low but significant already in small concentrations (see further discussion in section 5.4.1).

All ages from L1A, L1B and L1C are in chronological order covering the period from 15 to 35 ka. In the sections L1D and L1E, samples with relatively high detrital Th and/or comparably low U content exhibit significant deviations from the 'clean' samples. These suspicious samples are marked with red symbols in Figure 5.4 and were excluded before calculating the age models (see further discussion in section 5.4.1).

Chronologies were modeled using the algorithm 'StalAge' (Scholz and Hoffmann, 2011) for each section L1A to L1E individually. The age models reveal, that stalagmite PR-LA-1 covers the period from 15 to 46 ka with a hiatus between 35 and 41 ka.

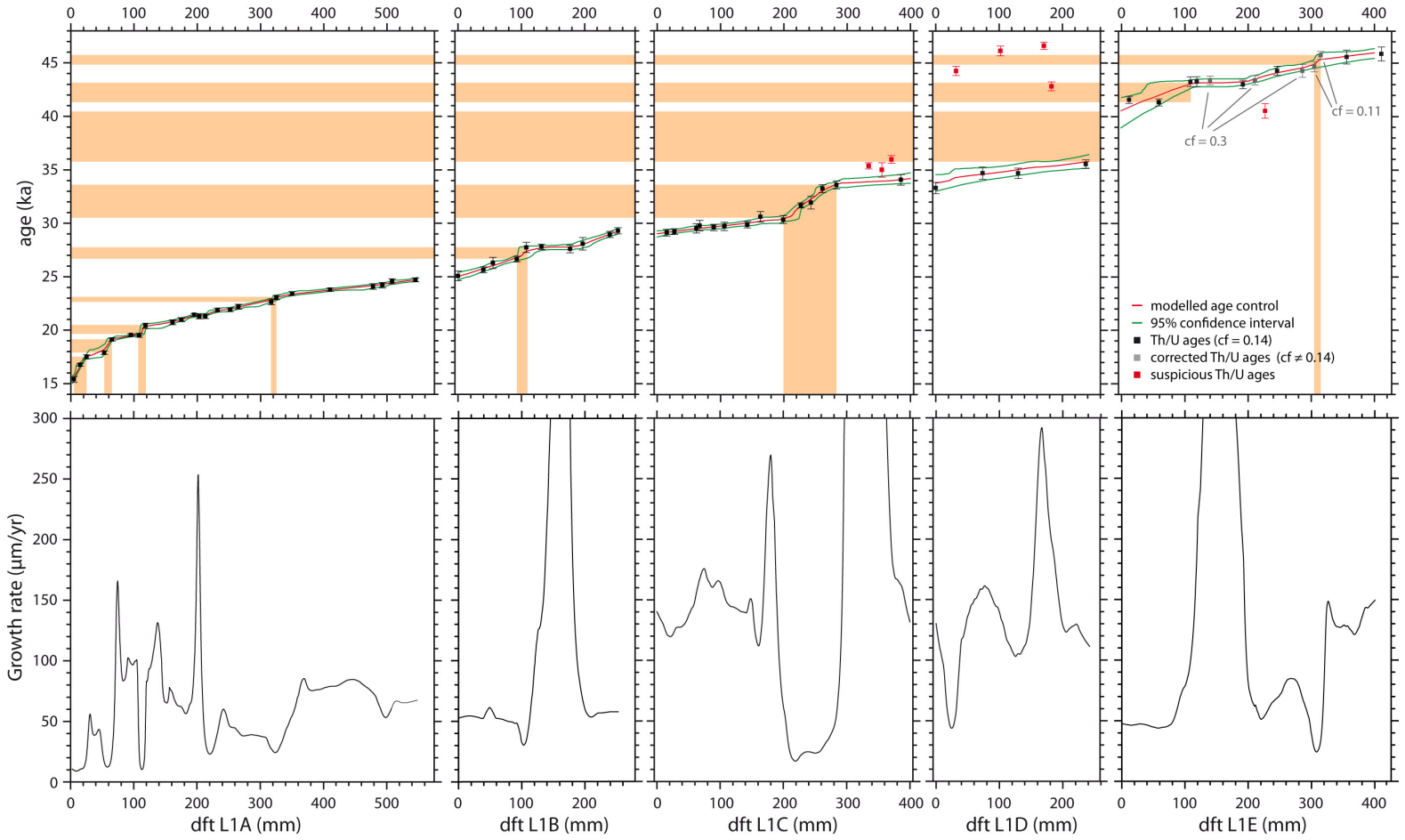

Figure 5.4: *Upper panels (from left to right): ^{230}Th/U-ages measured for PR-LA-1 for the sections L1A to L1E. ^{230}Th/U ages marked with red squares were not considered in the age models (more details in sections 5.3.1 and 5.4.1). ^{230}Th/U marked with grey squares were calculated with the detrital weight ratio different from 0.14 ± 0.11 indicated next to the ages, respectively (compare results tables in appendix A.2). Age models were calculated using 'StalAge' (Scholz and Hoffmann, 2011). Orange bars indicate intervals of slow growth or hiatuses (compare section 5.3.1). Lower panels (from left to right): growth rates calculated for PR-LA-1 for the sections L1A to L1E as 50 point smoothed first derivatives from the age models presented in the upper panels.*

Since the age model is very tight, growth rate variability was estimated by calculating the first derivatives from the age models, which were subsequently smoothed with a 50-point running mean (Figure 5.4). On average, PR-LA-1 grew relatively fast with growth rates of around 50 to 150 µm/yr. Several sections with comparably slow and fast growth can be identified. Low growth rates down to 10 to 30 µm/yr are detected in L1A from 15.4 - 17.5 ka, 17.9 - 19.1 ka, 19.5 - 20.4 ka and 22.6 - 23.1 ka. In L1B and L1C growth speed decreased between 26.6 - 27.6 ka, 30.3 - 33.6 ka. At the transition of L1D to L1E, a hiatus might be located between 35.6 - 40.8 ka. From 40.8 to 43.2 ka, the uncertainties of the age model are relatively large. Another section with low growth rates might be located between 41.4 and 43.3 ka, as well as from 44.7 - 45.7 ka. The mentioned sections are marked with orange bars in Figure 5.4. In contrast, very fast growth is detected around 27.6 - 27.7 ka, 33.6 - 34.1 ka, 43.3 - 43.5 ka and 45.6 - 45.9 ka. The period around 43.3 - 43.5 ka could be also a section with very high growth rates.

5.3.2 Proxy analysis

The records of $\delta^{18}O$ and $\delta^{13}C$ values of L1A to L1E are shown in Figures A.1 and A.2 in the supplementary material. The transitions of the single records between the different parts of the stalagmite fit well for the chosen age models (section 5.3.1 and Figure A.2 (c)). Thus, the five records are combined to a composite record for PR-LA-1, which is displayed in Figure 5.5. $\delta^{18}O$ values vary around 0 ± 2 ‰, with highest values between 1 and 2 ‰ from 17 - 15 ka. $\delta^{13}C$ values are around -9 ± 3 ‰ and share a similar pattern with $\delta^{18}O$ values.

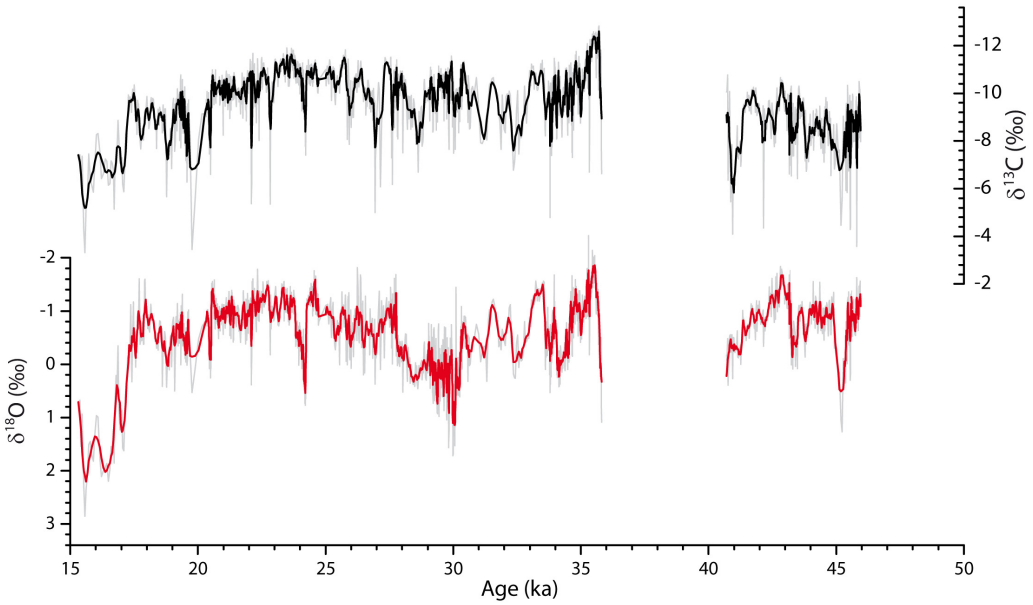

Figure 5.5: *Stacked stable isotope record of PR-LA-1 combined from the single records of L1A to L1E from 15 to 46 ka. Raw records are shown in light grey, 5p running mean of $\delta^{18}O$ values in red and 5p running mean of $\delta^{13}C$ values in black.*

The single records of all measured trace elements of the parts L1A to L1E are attached to the supplementary material A.3. Concentrations of Y, Cd, Pb, La and Ce were mostly near their individual detection limit and showed no pronounced variability.

Figure 5.6 shows the complete record of PR-LA-1 of the elements Mg, Ba, Sr, U, P and Al. U/Ca varies throughout the record around 0.1 µmol/mol. P/Ca ratios are around 1 mmol/mol from 46 to 17 ka, and decline to 0.3 mmol/mol until the end of the record. Mg/Ca, Sr/Ca and Ba/Ca show an inverse pattern with the highest values between 17 and 15 ka. In the earlier part of the record, the three elements show little variability with Mg/Ca around a baseline of 1 mmol/mol, and Sr/Ca (Ba/Ca) values being at a level of 0.06 mmol/mol (0.07 µmol/mol), respectively.

Analysis of elemental composition of the host rock at Cueva Larga reveals a minor occurrence of Mg of about 1 %, with the other elements only being present in minimal traces (Figure A.10).

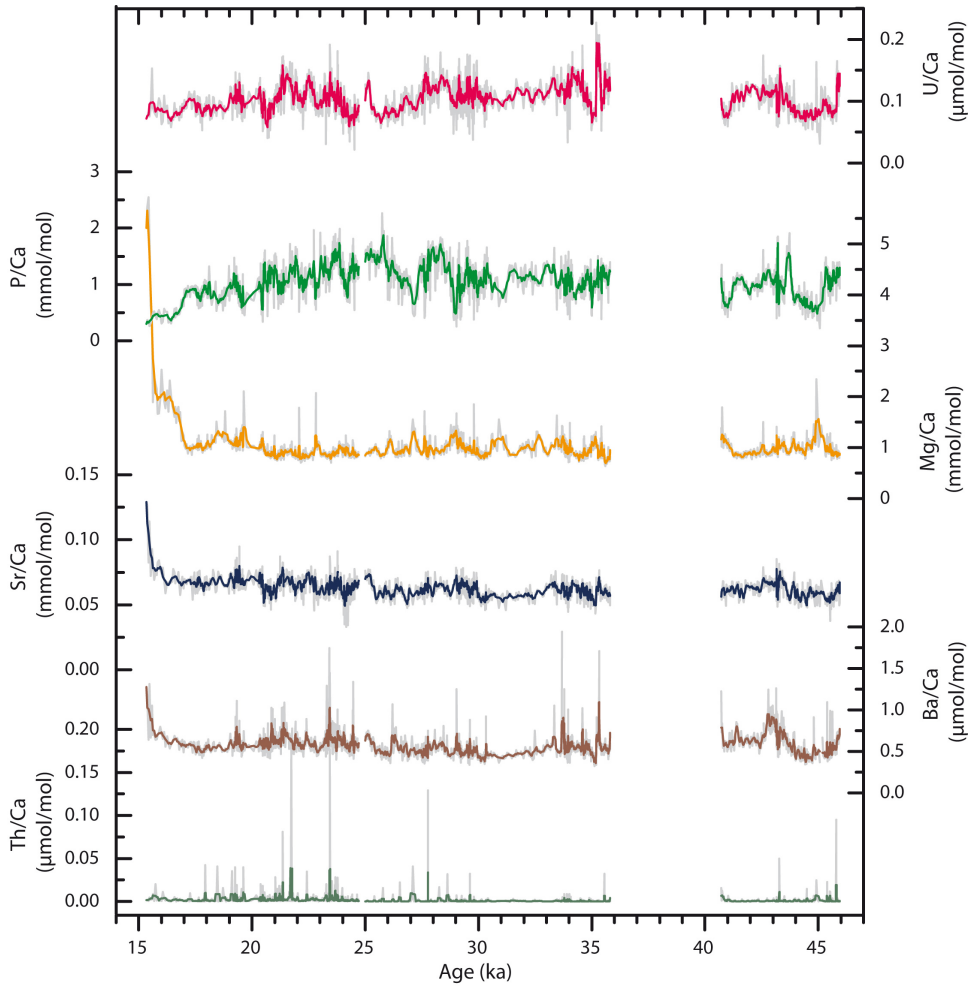

Figure 5.6: *Stacked molar ratios of U/Ca, P/Ca, Mg/Ca, Sr/Ca, Ba/Ca and Al/Ca measured in PR-LA-1 from 15 to 46 ka. Light grey: Resolution 1 mm, colored lines: 5p running means.*

5.3.3 Correlation analysis

Element to Ca ratios are reduced to the resolution of the stable isotope records in order to derive correlation coefficients between the individual records. Regarding the whole record from 15 to 46 ka, $\delta^{18}O$ and $\delta^{13}C$ values share the strongest correlation with $r_{\delta^{13}C/\delta^{18}O} = 0.51$ and Ba/Ca with Al/Ca ($r_{Ba/Al} = 0.60$). Slightly smaller correlation coefficients are found for $\delta^{13}C$ values vs. P/Ca with $r_{\delta^{13}C/P} = -0.45$, as well as for U/Ca vs. P/Ca ($r_{U/P} = 0.41$).

Moderately strong correlations exist between Sr/Ca vs. Ba/Ca ($r_{Sr/Ba} = 0.39$) and Mg/Ca with Sr/Ca ($r_{Sr/Mg} = 0.36$), P/Ca ($r_{Mg/P} = -0.35$), $\delta^{18}O$ ($r_{\delta^{18}O/Mg} = 0.38$) and $\delta^{13}C$ values ($r_{\delta^{13}C/Mg} = 0.36$). Figure 5.7 illustrates the correlation coefficients between all measured proxies in a heat map.

For the 5-point running means of the record, the correlations change (Figure 5.7 b). Whereas $r_{(\delta^{13}C/\delta^{18}O)_{sm}} = 0.48$ and $r_{(U/P)_{sm}} = 0.28$ decrease, all other coefficients mentioned in the previous paragraph increase from $r_{(\delta^{18}O/Mg)_{sm}} = 0.45$ to $r_{(\delta^{13}C/P)_{sm}} = -0.62$.

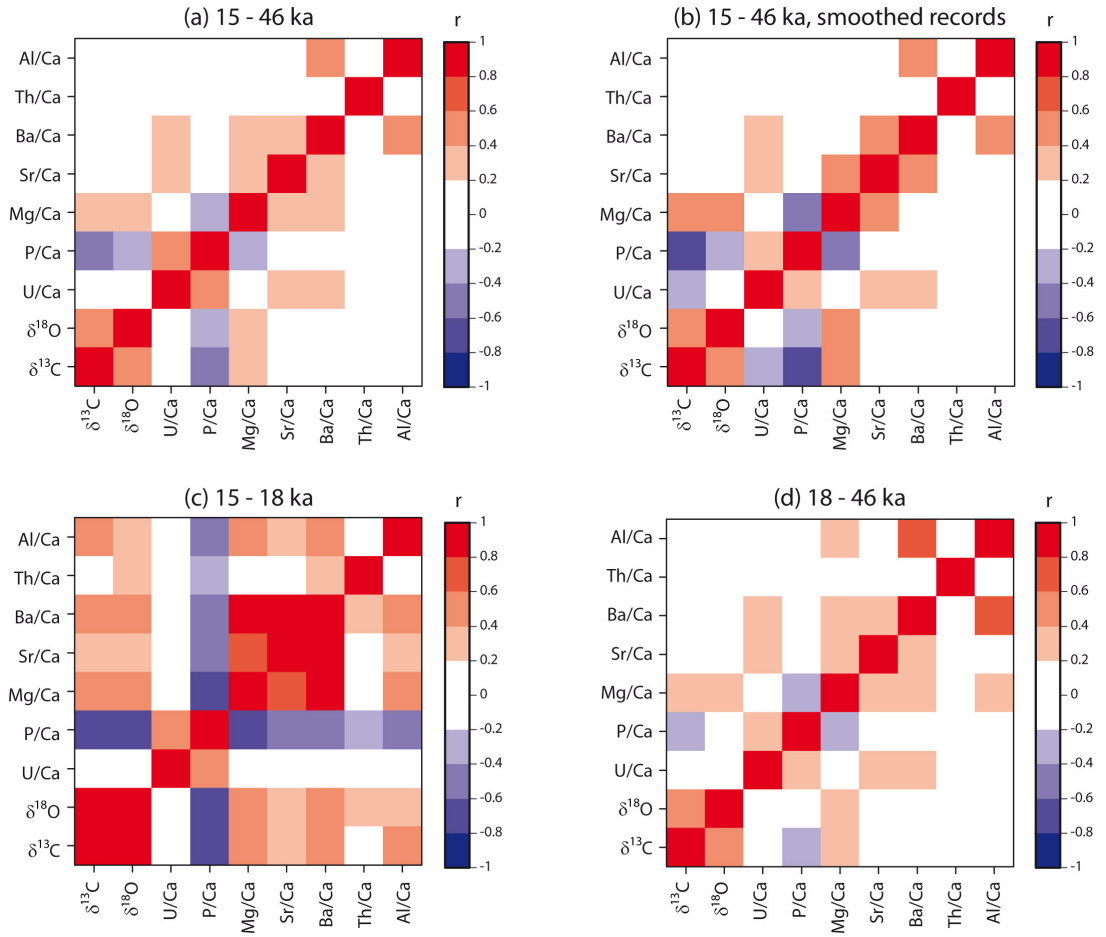

Figure 5.7: *Heat maps of correlation coefficients derived for the proxies measured between 15 and 46 ka (a) and the smoothed (5 point running means) records (b). The bottom row shows the correlations for the split record, with the period between 15 and 18 ka on the left (c) and 18 - 46 ka on the right (d).*

In the following, the records are split into distinct time frames (Figure 5.7 c and d). Between 15 and 18 ka, $r_{\delta^{13}C/\delta^{18}O}$ strongly increases to 0.86, together with $r_{Sr/Mg} = 0.78$, $r_{Sr/Ba} = 0.91$ and $r_{Mg/Ba} = 0.80$. Omitting these first 3 ka from the whole record, it becomes obvious that this period is responsible for most of the overall co-variations The only correlations persisting when leaving this phase out are $r_{\delta^{13}C/\delta^{18}O} = 0.43$, $r_{Mg/P} = -0.31$, $r_{Sr/Ba} = 0.39$, $r_{\delta^{13}C/P} = -0.40$ and $r_{\delta^{13}C/Mg} = 0.33$. The correlations between Mg/Ca and Sr/Ca and $\delta^{18}O$ values decrease to $r_{\delta^{18}O/Mg} = 0.25$ and $r_{Sr/Mg} = 0.25$.

5.4 Discussion

5.4.1 Age model and correction for detrital contamination

The major source of uncertainty of $^{230}Th/U$ dating is the range of values of detrital radiogenic to stable Th, $^{230}Th/^{232}Th$, which varies with host rock and soil characteristics (Fairchild and Baker, 2012). Most commonly, a bulk earth activity ratio of $(^{230}Th/^{232}Th) = 0.8 \pm 0.8$ is used, assuming a mean mass ratio of $^{232}Th/^{238}U = 3.8$ of in the continental crust.

However, comparison of the samples with elevated ^{232}Th with the 'clean' samples reveals that the a priori bulk earth ratios for $(^{232}Th/^{238}U)$ cannot be used to account for initial ^{230}Th in stalagmite PR-LA-1. Thus, we follow an approach similar to Fensterer et al. (2010) to estimate a more appropriate $(^{230}Th/^{232}Th)$ ratio. Hence, most $^{230}Th/U$ ages of PR-LA-1 are calculated using a detrital $^{232}Th/^{238}U$ mass ratio of 0.14 ± 0.1, resulting in a detrital activity ratio $(^{230}Th/^{232}Th)$ of 22 ± 18, bringing nearly all samples from L1A to L1E in chronological order.

The composition of the detrital phase can be very different from the a-priori assumed bulk earth value, e.g., due to partial leaching effects, Th adsorption, alpha recoil or non silicate origin of the detrital phase prior to deposition (Hellstrom, 2006). Hence, $^{230}Th/^{232}Th$ activity ratios higher than 0.8 are typical for tropical limestones, as for example used for different samples from the Bahamas, with values between 2.2 to 18.7 (Beck et al., 2001; Hoffmann et al., 2010; Arienzo et al., 2015) or 6.1 to 9.6 on Cuba (Fensterer et al., 2010, 2012).

However, some samples are still not in chronological order. The samples which were found to fit in the chronology with a slightly different correction factor are marked in Table A.5 with '†' and '‡' and are also highlighted in Figure 5.4. These ages are corrected with a detrital weight ratio of 0.30 ± 0.24 ($(^{230}Th/^{232}Th) = 11 \pm 8$) and 0.11 ± 0.09 (29 ± 22), respectively. It is to note, that all applied correction factors agree within their uncertainty range since a significant temporal change in the composition of $(^{238}U/^{232}Th)$ is unlikely. All other samples which could not be corrected within a reasonable range with the bulk samples are omitted for calculating the age models. All excluded ages are characterized by relatively high ^{232}Th-content and ^{238}U-content, respectively.

Diagenetic alteration can be another source for $^{230}Th/U$ age inversions. Post-depositional U loss leads to increasing $(^{230}Th/^{238}U)$ activity ratios and, thus, apparently older ages. In contrast, post-depositional addition of U results in decreased $(^{230}Th/^{238}U)$ activity ratios and

(a) *L1A (6 - 13 cm dft)* ***(b)*** *L1B (4 - 15 cm dft)* ***(c)*** *L1C (21 - 32 cm dft)*

Figure 5.8: *Macroscopic view on visible lamination of the sections L1A (a), L1B (b) and L1C (c). In L1A and L1B, lamination shows the typical convex shape. In L1C, lamination is irregular with a concave shape in the middle of the stalagmite.*

apparently younger ages (Scholz et al., 2014). In PR-LA-1, the sections with age inversions show macroscopic hints for diagenetic alteration. For example, the concave shape of the lamina in the bottom part of L1C (Figure 5.8c) is a sign of dissolution effects during or after deposition. In this case, the more soluble U ions are removed from speleothem calcite leading to older ages, as observed in the samples from this part. In contrast, the visible lamination in L1A or L1B shows a typical convex shape (Figures 5.8a and 5.8b). For a detailed and more profound analysis, thin section of the suspicious sections should be analyzed in order to identify alterations of the crystal fabrics. For example, Scholz et al. (2014) found that the occurrence of mosaic fabric was a clear indication for diagenetic alteration in their investigated sample.

5.4.2 Environmental controls on speleothem proxies

Trace element variability

The trace elements Mg/Ca, Sr/Ca and Ba/Ca in PR-LA-1 generally show little variability throughout the record but a positive covariation among each other (Figure 5.7 b). A pronounced feature are the elevated values of Mg/Ca, Sr/Ca and Ba/Ca from 17 to 15 ka. In this period, the correlation coefficient between the three proxies strongly increase (Figure 5.7 c).

The co-variability of Sr/Ca, Ba/Ca and Mg/Ca ratios is tested applying the model of Sinclair et al. (2012). Figure 5.9 shows the plots of ln(element/Ca) for the section L1A. The corresponding plots for the sections L1B to L1E are attached to the supplementary material (Figures A.8 and A.9. The slopes $\frac{D_i-1}{D_j-1}$ (i,j = Mg, Sr, Ba) were calculated using the partition coefficients D_{Mg} = 0.031 (for 25°C), D_{Sr} = 0.15 (both Huang and Fairchild, 2001) and D_{Ba} = 0.012 (Tesoriero and Pankow, 1996). The only part of the whole record showing a variability which follows the theoretically expected slopes for the presence of prior calcite precipitation (PCP) and/or incongruent calcite dissolution (ICD) is the time period between 15 and 16.5 ka.

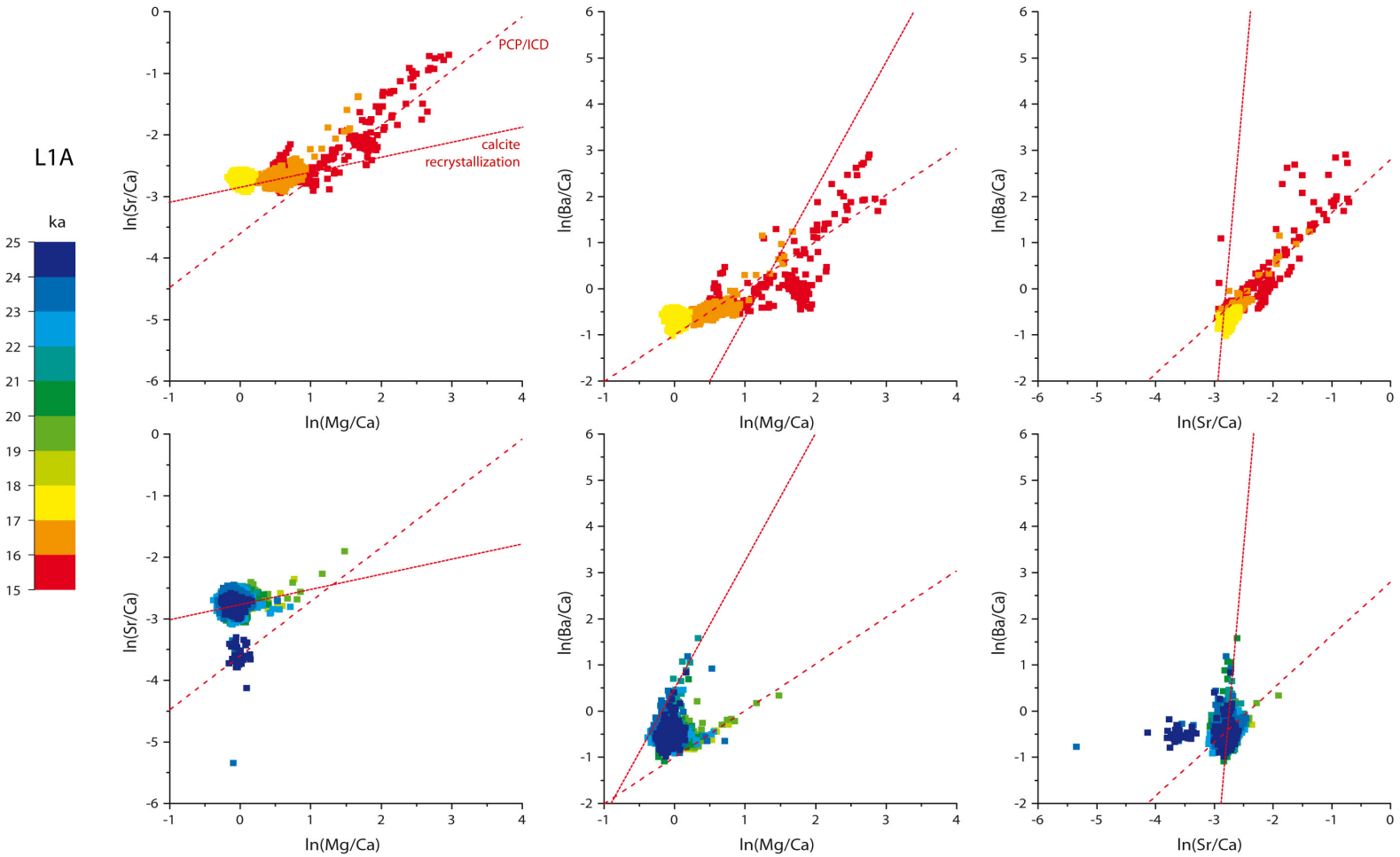

Figure 5.9: *Cross plots of element to calcium ratios (in mmol/mol) in speleothem calcite of section L1A displayed as ln(Sr/Ca) vs. ln(Mg/Ca) (left), ln(Ba/Ca) vs. ln(Mg/Ca) (middle) and ln(Ba/Ca) vs. ln(Sr/Ca) (right). The dashed red lines indicate the theoretically expected slopes for PCP and/or ICD after Sinclair et al. (2012). The dotted lines show the same for the case of calcite recrystallization (Sinclair et al., 2012). For more details see section 5.4.2. The upper panel row indicates the time frame between 15 and 18 ka, the bottom panels cover 18 - 25 ka.*

Diagenetic effects along the drip pathways are potential other controls which could account for a covariation of Mg and Sr and provide a hydrological interpretation of the observed variability. Sinclair et al. (2012) discuss the potential effects of stabilization of mineral assemblages and calcite recrystallization. The authors state, that the dissolution of dolomite or Mg-calcite alone cannot produce a positive correlation in Mg/Ca vs. Sr/Ca, however, it may be responsible for second-order deviations from correlated variations arising from other mechanisms. At Cueva Larga, analysis of host rock samples indicates only a minor proportion of Mg and Sr in the limestone overburden (section 5.3.2), which is reflected by the comparably low Mg and Sr content in speleothem calcite and the dripwater (Vieten et al., in press). Speleothems sampled from dolomitic or high-Mg calcite host rocks are usually characterized by higher Mg contents. For example, the speleothems sampled by Sinclair et al. (2012) incorporated up to 30 mmol/mol Mg/Ca and 10 mmol/mol Sr/Ca.

Calcite recrystallization might also induce a correlation between Sr and Mg. After Sinclair et al. (2012), the slopes in Figures 5.9, A.8 and A.9 would then be significantly different than for PCP/ICD. Therefore, the theoretically predicted slopes for this case $\frac{(D_i-1)D_j}{(D_j-1)D_i}$ (i,j = Mg, Sr, Ba) are also indicated in the corresponding figures. The graphs suggest that some values of trace element ratios might indeed be affected by calcite recrystallization, however the majority of points do not follow any linear function.

Sinclair et al. (2012) note, that their models of calcite recrystallization require some degree of equilibration between limestone and solution and that the models are most applicable to cases where there is a low solution volume and a large area of limestone surface. These conditions might be encountered during diagenesis of a very porous limestone and/or vadose diagenesis where solution is a thin film trickling across a large surface area of limestone.

Thus, Mg/Ca, Sr/Ca, and Ba/Ca ratios suggest that the influence of calcite water interactions before 17 ka was comparably small. This is also reflected by the decreased correlation coefficient between 46 and 17 ka (Figure 5.7) and the relatively small internal variability of the trace elemental signatures. Modern dripwater monitoring also suggests, that PCP is not a dominant process in Cueva Larga (Vieten et al., in press).

Other factors besides hydrological processes determining the Mg/Ca or Sr/Ca ratio in speleothems are for example temperature (in the case of Mg) or growth rate, which was found to determine Sr fractionation. D_{Mg} is dependent on temperature, however, a temperature change by 2-3°C would result in a total change in Mg by at most 15% (Huang and Fairchild, 2001). Between 46 and 17 ka, Mg/Ca varies between approximately 0.8 and 1.2 mmol/mol. This variability is small but still larger than expected if temperature would be the only factor controlling Mg incorporation. Moreover, Ku and Li (1998) and Sinclair et al. (2012) state, that the temperature dependency of this proxy might be larger than implied by inorganic experiments. Thus, temperature potentially plays a secondary role in fractionating Mg.

In contrast, Sr/Ca incorporation may depend on the calcite precipitation rate (Lorens, 1981; Huang and Fairchild, 2001; Gabitov and Watson, 2006; Nehrke et al., 2007). Growth rate varies in PR-LA-1 by at least an order of magnitude from less than 10 to more than 300 µm/year (Fig-

ure 5.4, periods of low growth rates are indicated with vertical bars). This variability would be enough to affect Sr/Ca incorporation significantly. Figure 5.10 shows the Sr/Ca ratio and the growth rate variability in PR-LA-1, with intervals of slow growth indicated with orange bars. During some of these phases with relatively low growth rates Sr/Ca does show comparably low values with regard to the variability of the other proxies such as Mg/Ca or $\delta^{18}O$ and $\delta^{13}C$ values, which exhibit systematic higher values. This implies, that growth rate effects may indeed influence the incorporation of Sr in PR-LA-1 and superpose the hydrological controls.

Other effects on Mg/Ca or Sr/Ca might be incorporation of dust/detrital material, changes in the soil zone or sea spray. In an island karst system, input of seawater to groundwaters can be a significant source of ions, especially for Mg and Sr which are both relatively concentrated in seawater (Goede et al., 1998). For example, average Mg and Sr concentrations in seawater are about 1,200 mmol/l and 8 mmol/l, respectively (Stumm and Morgan, 1981), compared to only about 5 mmol/l Mg (Román-Más and Lee, 1987) and 50 nmol/l Sr (Pett-Ridge, 2009) in surface waters in Puerto Rico. A potential source of sea spray might be tropical cyclones, which today affect the site on a regular basis. Thus it is possible, that sea spray contributes a second-order effect to the element profiles. Saharan dust is also known to be a significant source of soil in the Caribbean in general and also Puerto Rico, as evidenced by soil mineralogy, isotopic tracers, trace element ratios and rare earth element patterns (Pett-Ridge, 2009).

Input of detrital material is not regarded to have a major influence on the trace element variability in PR-LA-1 which is indicated by the generally very low Al/Ca and Th/Ca ratios, which are proxies for the contamination with clay minerals and other detritus (Fairchild and Treble, 2009). However, the correlation coefficients with Mg/Ca and Ba/Ca suggest, that detrital contamination might have a small effect on these elemental signatures (Figure 5.7 c and d).

Besides Mg/Ca and Sr/Ca, also P/Ca and U/Ca exhibit a moderate variability in PR-LA-1. Both ratios are generally positively correlated. A covariation of U and P on annual timescales was observed by Treble et al. (2003), who interpreted P to be transported from seasonally decaying vegetation prior to mineralization in the soil. Borsato et al. (2007) attributed annual P layers to an autumnal flush of organic material from the soil due to the coincidence of vegetation dieback and high infiltration. A covariation of U and P was also reported on longer timescales by Mischel et al. (in press) and Webb et al. (2014). Both studies interpret higher values in P and U as reflecting more productive vegetation and higher soil moisture, which is supported by an anti-correlation with Mg (Webb et al., 2014) and $\delta^{13}C$ values (Mischel et al., in press), respectively.

In PR-LA-1, P/Ca ratios are both anti-correlated with Mg/Ca values, as well as $\delta^{13}C$ and Sr/Ca (Figure 5.7 b). This is also visible in the records in Figure 5.10, with relatively low P/Ca ratios during periods of slow growth rates and higher Mg/Ca, $\delta^{18}O$ and $\delta^{13}C$ values. This indicates, that P/Ca could be interpreted in the same way as stated above. The anti-correlation with P/Ca values generally favors the interpretation of Mg/Ca as proxy for hydrological pro-

cesses rather than a dominance of the temperature dependency. Since wetter conditions in the tropics are usually accompanied by higher temperatures, the temperature effect would cause a correlation rather than an anti-correlation of Mg/Ca with P/Ca.

In summary, the phase between 17 and 15 ka shows a strong characteristic imprint of PCP and/or ICD in Mg/Ca, Sr/Ca and Ba/Ca. Before 17 ka, the variability due to calcite water interactions is substantially lower compared to the phase afterwards. Hydrologically affected calcite water interactions such as PCP, ICD or calcite recrystallization might have had influence on Mg/Ca and Sr/Ca during some short term phases as indicated by Figures 5.9, A.8 and A.9.

$\delta^{18}O$ and $\delta^{13}C$ values

The $\delta^{13}C$ of speleothem calcite is dependent on the type and amount of vegetation above the cave, root respiration, organic material decomposition and the amount of calcite water

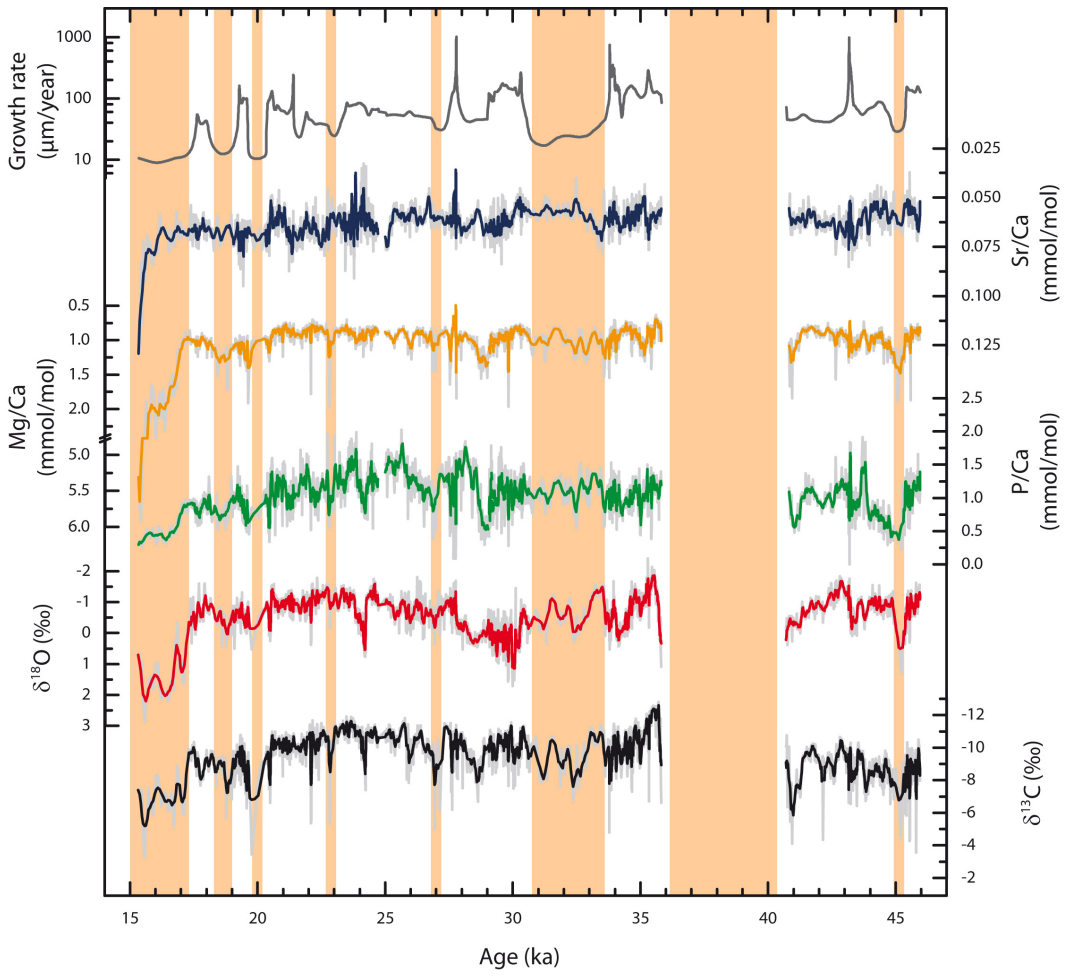

Figure 5.10: *Selected speleothem proxy records of PR-LA-1 from 15 to 46 ka. The orange bars indicate intervals of low growth rates or hiatuses.*

interactions (Fairchild et al., 2006a). Variations in the biogenic CO_2 component of the carbon are in turn influenced by precipitation amount and temperature (Genty et al., 2003). Generally the pCO_2 is expected to show an inverse correlation with $\delta^{13}C$ values in the soil horizon. Changes in the amount of rainfall or temperature could also alter the ratio of C3 and C4 plants, causing further isotopic changes, particularly over longer timescales (Fairchild et al., 2006a).

In the tropics, speleothem $\delta^{18}O$ values are often interpreted to reflect rainfall amount (Vuille, 2003; Lachniet, 2009a; Winter et al., 2015). This is also observed at Cueva Larga, with more negative rain water $\delta^{18}O$ values correlating with increasing amount of rainfall. A decrease of 1 ‰ in $\delta^{18}O$ values corresponds to a rainfall increase of about 250 mm/month (Vieten et al., in press), which is in agreement with the trend observed in rainfall collected at the GNIP weather station in San Juan between 1968 and 1973 (location indicated in Figure 5.2, weather data downloaded from: https://nucleus.iaea.org/wiser).

However, comparing the annual averages of $\delta^{18}O$ and rainfall amount in San Juan instead of monthly values indicates a smaller slope of approximately 100 mm/month (1200 mm/year) for the period 1968 to 1973. A 1 ‰ decrease in $\delta^{18}O$ values thus corresponds roughly to a 50% increase in rainfall amount compared to the modern annual rainfall sum at Cueva Larga (2100 mm/year) and 100% at San Juan (1350 mm/year). As a comparison, the variability at weather station San Juan was between 60 and 200% of the mean annual precipitation amount during the period 1963 to 1983.

At the location of PR-LA-1, temperature was found to be nearly constant over time with 22.5 ± 0.2°C and reflects the mean annual temperature (MAT) outside the cave (Vieten et al., in press). Long-term changes in MAT are thus expected to influence speleothem isotopic composition (Lachniet, 2009a).

Modern dripwater composition at various drip sites near PR-LA-1 is about -2.6 ± 0.2 ‰ (VSMOW, Vieten et al. (in press) and Vieten et al., unpublished data). For the cave temperature of 22.5 °C, the theoretical expected value of precipitated calcite under equilibrium conditions is -3.1 ± 0.2‰ (VPDB) (Tremaine et al., 2011). Recently precipitated calcite is at a value of -3.2 ± 0.2 ‰ (VPDB, Vieten et al, unpublished data), indicating that calcite precipitates near equilibrium conditions. Calculating the fractionation after Kim and O'Neil (1997) suggests a disequilibrium fractionation effect of about 1.5 ± 0.2‰. However, we use the equation after Tremaine et al. (2011) which was developed under field conditions and is in better agreement with field data and other studies (e.g., Coplen (2007)).

Nevertheless, both $\delta^{18}O$ and $\delta^{13}C$ values are subject to disequilibrium fractionation effects occurring inside the cave (Mickler et al., 2004; Dreybrodt and Scholz, 2011; Deininger et al., 2012; Meyer et al., 2014). $\delta^{18}O$ and $\delta^{13}C$ values in PR-LA-1 are positively correlated throughout the record, which documents the influence of cave-internal effects on both proxies in the past. Speleothem $\delta^{18}O$ and $\delta^{13}C$ values are affected by fractionation effects due to variations of temperature, drip interval (or drip rate), evaporation and pCO_2.

Cave air pCO_2 measurements revealed, that Cueva Larga is affected by seasonal ventila-

tion effects with low pCO_2 values in winter (Vieten et al., 2016). This might bias speleothem climate records towards the winter season due to increased calcite precipitation rates. Enhanced kinetic fractionation due to stronger ventilation and thus, possibly more evaporation, has a significant effect on $\delta^{18}O$ and $\delta^{13}C$ values of the calcite (Deininger et al., 2012). This so called 'kinetic' fractionation results in higher $\delta^{18}O$ and $\delta^{13}C$ values than expected under conditions of stable isotope equilibrium (e.g., Boch et al. (2011); Frisia et al. (2011); Mattey et al. (2010); Scholz et al. (2012); Tremaine et al. (2011)).

Drip rates varied site-specifically and showed seepage flow behaviour (Vieten et al., in press). Decreasing drip rates result in higher (enriched) values of $\delta^{13}C$ and $\delta^{18}O$ (Mühlinghaus et al., 2009). Recent laboratory experiments under conditions similar to those in natural cave systems confirmed the importance of drip rate variability on the stable isotope composition in speleothem calcite (Hansen et al., 2013).

All these cave-internal processes may be attached to climatic changes, e.g. generally drier conditions may be accompanied by lower drip rates. In tropical locations, these effects - including temperature variability - would amplify the negative relationship between rainfall amount and speleothem $\delta^{18}O$. This interpretation is supported by the comparison of $\delta^{18}O$ and $\delta^{13}C$ variability with growth rate (Figure 5.10), where the stable isotope records show systematically higher values during periods of decreased calcite precipitation indicative for slower drip rates. $\delta^{18}O$ signatures in PR-LA-1 are thus interpreted as reflecting precipitation amount above the cave.

5.4.3 Climate variability in Puerto Rico during the last Glacial

Dansgaard-Oeschger interstadials

Most of the Dansgaard/Oeschger warm interstadials (D/O) are recorded in PR-LA-1 as more negative peaks in $\delta^{18}O$ values and relatively low Mg/Ca values indicating generally warm and humid conditions on Puerto Rico (Figure 5.11). The timing of the D/O cycles corresponds well with other precisely dated records, such as the recent publication from the Amazonian basin by Wang et al. (2017) or the reflectance record from the Cariaco basin (Deplazes et al., 2013), which reflects the position of the ITCZ during the last Glacial. The similarity of the $\delta^{18}O$ signature of PR-LA-1 to these both records (Figure 5.11) indicates a connection between rainfall variability on Puerto Rico with the latitudinal shift of the ITCZ associated with North Atlantic temperature variability (NGRIP members, 2004).

D/O interstadials 7 (~35 ka) and 11 (~43 ka) reach the most negative values with approximately -1.8 ‰. Interstadials 2, 3, 5, 6, 12 and 13 are characterized by $\delta^{18}O$ values of about -1.2 to -1.5 ‰, whereas during D/O's 4 and 4.1, the values are below 1 ‰.

Comparing glacial with modern oxygen isotopic signatures in Cueva Larga reveals that climate conditions on Puerto Rico during interstadials 7 and 11 were most comparable to modern conditions. During the other interstadials, oxygen isotope values indicate only slightly cooler and/or drier conditions. Under glacial boundary conditions, we assume a 1.1 ‰ change

as a result of global ice volume and only minor local salinity changes in the subtropical Atlantic surface waters during the Last Glacial Maximum (LGM, Shackleton (1974); Hagen and Keigwin (2002); Schrag et al. (2002)), whereas the difference at ~35 ka and ~43 ka was only about 0.5 ‰. Assuming in a first approximation that all other parameters stay constant and fractionation processes in the cave remain comparable to modern conditions (-3.2 ± 0.2 ‰), this yields a value for precipitated calcite corrected for the composition of the sea surface waters of about -2.2 to -2.7 ‰ for the LGM and MIS 3, respectively.

Suggesting generally cooler and/or drier conditions during the last glacial period, $\delta^{18}O$ values are shifted towards higher values, which are reached during the other interstadials. SST reconstructions suggest a shift of 2 - 4 °C between Holocene and peak glacial conditions in the Caribbean basin and the Gulf of Mexico (e.g., Lea et al. (2003); Schmidt et al. (2004);

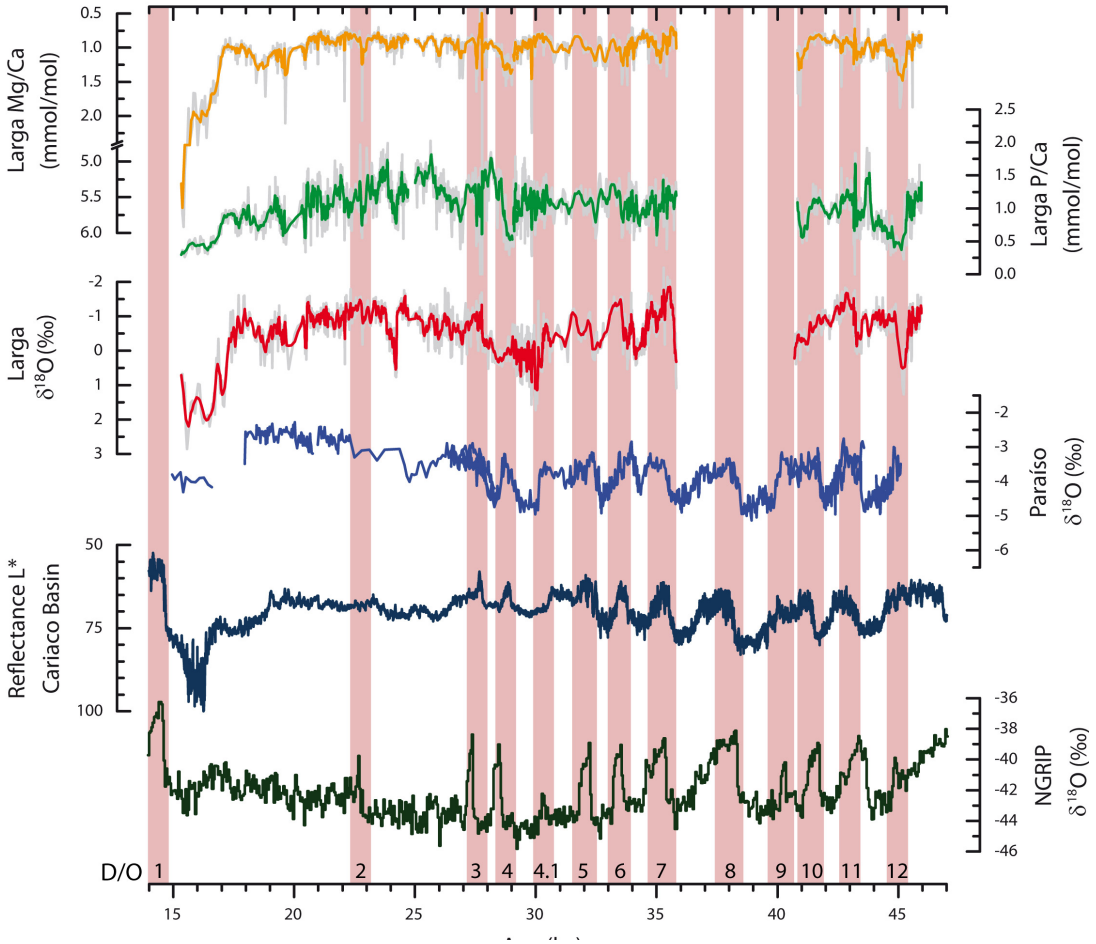

Figure 5.11: *Proxy records (Mg/Ca (orange), P/Ca (green), $\delta^{18}O$ (red)) from PR-LA-1 between 15 and 46 ka in comparison with the speleothem $\delta^{18}O$ record from Paraíso Cave from the Amazonian basin, Brazil (blue, note the inverted axis, Wang et al. (2017)), the reflectance record from the Cariaco basin off the Venezuelan coast (dark blue, Deplazes et al. (2013)), and the NGRIP ice core record (dark green, NGRIP members (2004)). Dansgaard-Oeschger Interstadials are highlighted with light red bars and the corresponding numbers.*

Ziegler et al. (2008)), whereas lacustrine sediments in Guatemala even suggest a cooling of 5 - 10 °C (Grauel et al., 2016). During Greenland interstadials, Correa-Metrio et al. (2012) and marine records (Shackleton, 1974; Hagen and Keigwin, 2002; Schmidt et al., 2004) suggest a 0.5 - 1 °C warming compared to average glacial conditions. A temperature decrease of 2 - 4 °C yields temperature fractionation corrected $\delta^{18}O$ values of speleothem calcite of about -1.6 ± 0.3 ‰ for the LGM. This is in the range of the peak values of most D/O interstadials measured in PR-LA-1 and about 1 ‰ lower than the baseline of about 0 to -1‰ between 45 and 18 ka. For MIS 3 (1 - 3 °C temperature decrease) a value of -2.3 ± 0.3 ‰ is calculated.

An additional decrease in rainfall amount of roughly 50% compared to modern values would explain a further increase of 1 ‰ in $\delta^{18}O$ values (compare section 5.4.2). Since disequilibrium effects may change the isotopic composition of a stalagmite significantly, this value of 50% decrease in rainfall amount is regarded as an upper limit. Most likely, the additional increase in $\delta^{18}O$ values is a combination of less rainfall and associated disequilibrium effects.

Assuming no change in rainfall amount and/or disequilibrium effects, a value of about -0.5‰ is reached with a temperature decrease of more than 8 °C. However, with respect to the observations of other paleo climate reconstructions and model studies from the Caribbean realm (e.g., Schmidt et al. (2004); Zhang and Delworth (2005); Murphy et al. (2014); Arienzo et al. (2015)), this scenario is regarded to be not realistic for Puerto Rico.

Heinrich stadials

Analogous to the warm D/O interstadials, Heinrich stadials HS1 (17.2 - 15.5 ka), HS2 (24.3 - 23.8 ka) and HS5 (45.4 - 44.8 ka) are clearly pronounced with elevated $\delta^{18}O$ values and a relatively low P/Ca signature (Figure 5.12). HS1 and HS5 are also characterized by significantly higher Mg/Ca ratios and low growth rates (Figures 5.10 and 5.12). The exact timing of HS3 in the $\delta^{18}O$ record is not clear, but similar conditions to the other HS are observed between 30.2 and 28.9 ka. HS4 is not recorded in PR-LA-1. The proxies indicate that Heinrich stadials in Puerto Rico were characterized by cooler/drier conditions and a decline of vegetation and soil productivity. The timing of HS1 to HS5 is in agreement with other paleo climate reconstructions from the subtropical and tropical Atlantic realm (Escobar et al., 2012; Deplazes et al., 2013; Lachniet et al., 2013; Arienzo et al., 2015) and other northern hemispheric records (Wang et al., 2001).

The observations in PR-LA-1 are in concert with other proxies from the subtropical/tropical western Atlantic which support the overall drying and/or similar cooling associated with Heinrich stadials (Peterson, 2000; Escobar et al., 2012; Lachniet et al., 2013; Arienzo et al., 2015; Grauel et al., 2016). Decreasing SSTs by ~ 3 - 5 °C across Heinrich stadials were detected at the Bermuda rise (Sachs and Lehman, 1999; Keigwin and Boyle, 1999; Hagen and Keigwin, 2002). A similar cooling by ~ 4 °C during Heinrich stadials 1 to 3 is observed in the Bahamian speleothem record (Arienzo et al., 2015). Lacustrine sediments from Guatemala shows increased aridity and a 6 - 10 °C cooling associated with Heinrich stadial 1 (Hodell et al., 2008;

Escobar et al., 2012; Correa-Metrio et al., 2012; Grauel et al., 2016) and a speleothem record from southwestern Mexico demonstrates a reduction of the North American Monsoon (Lachniet et al., 2013).

In Puerto Rico, the increase in $\delta^{18}O$ values during HS 2, 3 and 5 is about 2 ‰ and for HS1 even 3 ‰. However, this difference cannot solely be explained by the above reported temperature decrease compared to glacial boundary conditions. A total drop of about 10 °C compared to modern temperatures would only result in a $\delta^{18}O$ signature of ~0 ‰. Also Arienzo et al. (2015) only observe an $\delta^{18}O$ increase of about 1 - 1.5 ‰ in speleothem calcite. The decreased

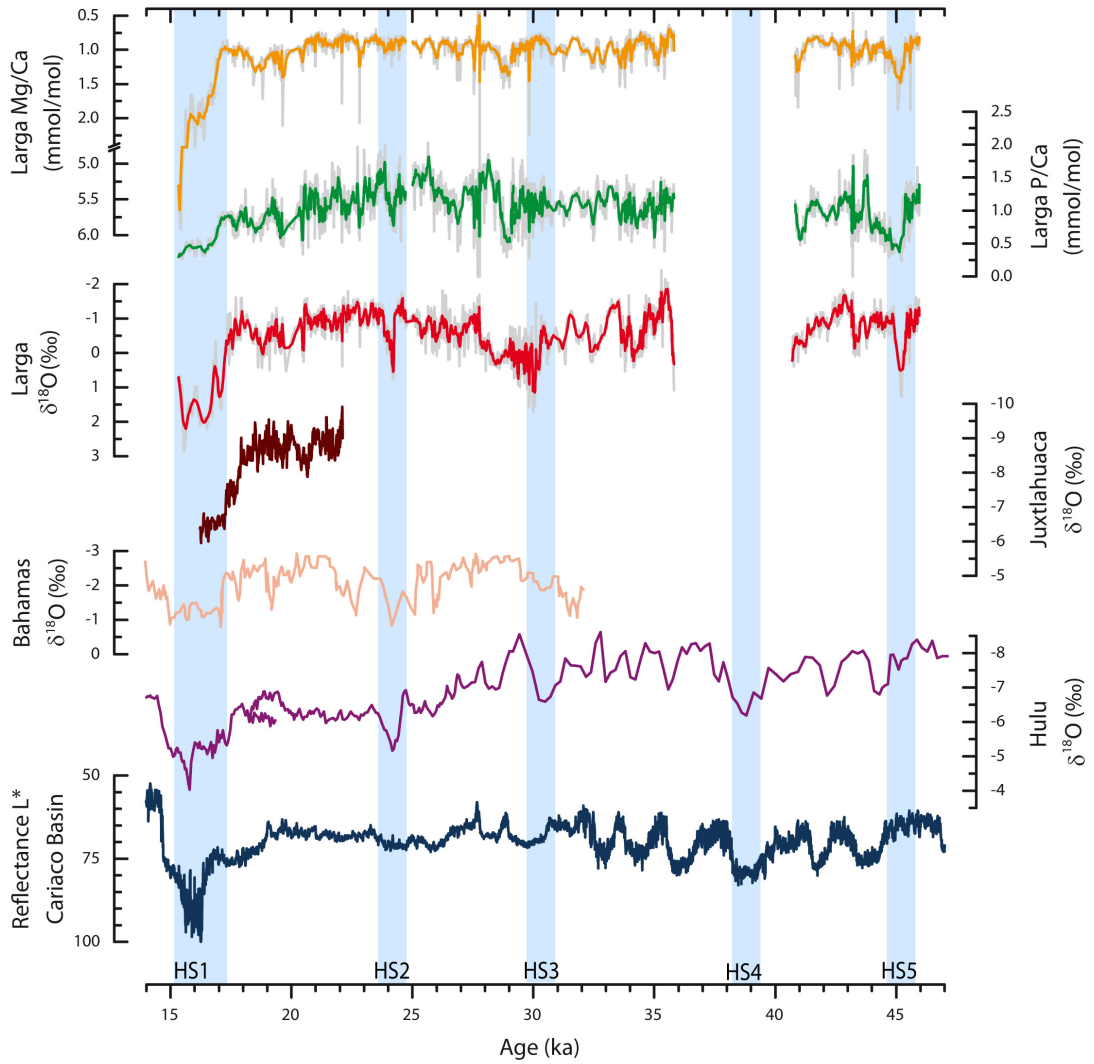

Figure 5.12: *Proxy records (Mg/Ca (orange), P/Ca (green), $\delta^{18}O$ (red)) from PR-LA-1 between 15 and 46 ka in comparison with speleothem $\delta^{18}O$ records from Juxtlahuaca Cave, Mexico (dark red, Lachniet et al. (2013)), from Abaco Island, Bahamas (light red, Arienzo et al. (2015)) and from Hulu Cave, China (purple, Wang et al. (2001)). The marine sediment reflectance record from the Cariaco basin off Venezuela is shown in dark blue (Deplazes et al., 2013). The timing of the Heinrich stadials is indicated with light blue bars.*

temperatures for the tropical Northern Hemisphere coincident with Heinrich stadials are in principle also supported by model studies. However, the modeled temperature changes are much less (Zhang and Delworth, 2005; Murphy et al., 2014), and for the location of Puerto Rico, Murphy et al. (2014) even report no significant change in surface temperatures.

Moreover, comparing the Mexican speleothem record from Juxtlahuaca Cave (Lachniet et al., 2013) with the PR-LA-1 $\delta^{18}O$ signature (Figure 5.12) reveals that the timing and magnitude in the increase of the $\delta^{18}O$ values during HS1 is nearly synchronous. This supports the significance of the supra-regional control of rainfall changes in the subtropical Caribbean driven by the southerly shifted ITCZ and reduced AMOC (Lachniet et al., 2013). The major contribution to the HS-signatures observed in PR-LA-1 $\delta^{18}O$ values is thus expected to originate from a further decrease in rainfall amount compared to glacial boundary conditions and potentially associated drip-rate modulated disequilibrium fractionation effects.

Comparing the recorded Heinrich stadials in PR-LA-1 with each other, HS1 (17.2 - 15.5 ka) appears to be accompanied by the most extreme conditions in Puerto Rico. This is a common observation, since most records declare HS1 the severest Heinrich stadial (Escobar et al., 2012; Arienzo et al., 2015), accompanied by e.g., a near shut down of the AMOC (Böhm et al., 2015).

During HS1, paleo climate proxy reconstructions in the Caribbean realm report an warm and wet interruption at about of the cold and dry period. This interruption occurs in lacustrine sediments in Guatemala (Escobar et al., 2012) at about ~17 ka, and in the Bahamian speleothem from 17.5 to 17.1 ka (Arienzo et al., 2015). In Puerto Rico, HS1 starts at about 17.2 ka with a gradual increase in Mg/Ca and $\delta^{18}O$ values indicating a decrease of rainfall amount and temperature. The intermediate phase can be associated with a short-term $\delta^{18}O$ excursion to slightly more negative values at around 16.8 ka succeeded by relatively stable Mg/Ca values indicating a rather constant precipitation regime until 15.9 ka. The proxies in PR-LA-1 suggest, that the following period until 15.4 ka was the driest and coolest phase of the whole record. P/Ca and $\delta^{13}C$ values also suggest that the decrease in rainfall and temperature was accompanied by a decline of soil productivity.

In contrast, even though HS2 is associated with a similar decrease of the strength of the AMOC as HS1 (Böhm et al., 2015), the climate response in Puerto Rico was apparently not the same. During HS2 (24.3 - 23.8 ka), $\delta^{18}O$ values increased by about 2 ‰, accompanied by a relative decrease in P/Ca. Mg/Ca ratios, in contrast, only shows a minor increase. A similar pattern is observed during HS3. HS5 again exhibits again a clear increase of $\delta^{18}O$ and Mg/Ca values accompanied by a decline in P/Ca, however not as pronounced as reported for HS1. Nevertheless, the big picture of all proxies together indicate, that all Heinrich stadials recorded in PR-LA-1 were characterized by drier and/or cooler climate conditions.

5.5 Conclusions

Precise ^{230}Th/U dating shows, that PR-LA-1 grew from 15 to 46 ka with a hiatus between 35 and 41 ka and covers several millennial scale events during the last Glacial such as Dansgaard/Oescher interstadials 1 - 12 and Heinrich stadial 1 - 5. Contamination with detrital Th was found to be generally low, but has significant influence on the calculation of the ^{230}Th/U ages.

The comparison of the PR-LA-1 proxy records with climate records sensitive for global and regional climate change (Figure 5.12 and 5.11) reveals, that most of the prominent climate events during the last glacial period - the Heinrich stadials and Dansgaard/Oeschger cycles - also had an impact on local climate on Puerto Rico.

Our observations are in concert with model studies and other climate proxy reconstructions (e.g., Schmidt et al. (2004); Zhang and Delworth (2005); Murphy et al. (2014); Arienzo et al. (2015)) where most of them found generally drier and cooler conditions in the Caribbean realm during the last Glacial. The average oxygen isotopic composition of speleothem calcite between 46 and 18 ka suggests in agreement with other records, that climate on Puerto Rico was generally cooler by ~2 - 4 °C and also drier than today.

Warm North Atlantic Dansgaard/Oeschger interstadials as observed in Greenland ice cores (Figure 5.11) are also recorded in Puerto Rico and were found to be characterized by relatively warm and humid conditions. δ^{18}O values during single D/O peaks 7 and 11 are even interpreted to show comparable climate conditions to the modern environment. In contrast, cold Heinrich stadials are recorded as relatively cold and dry periods, which were additionally accompanied by a decline in vegetation and soil productivity. The variability of δ^{18}O values during Heinrich stadials is in agreement with other records (e.g., Escobar et al. (2012); Arienzo et al. (2015)), indicating temperature drops by about 3 - 5 °C and associated decreased rainfall amounts.

These climatic changes are ascribed to the southerly movement of the ITCZ and the variable strength of the AMOC. Our record is the first from this region which clearly shows the impact of both stadials and interstadials on western Caribbean climate variability over a relatively long time period and allows an approximate quantification of last glacial climate conditions.

Acknowledgements

Special thanks go to Juan Estrella, Flora Sperberg and Jose Santiago from the University of Puerto Rico (Mayagüez) and Julie Dutil, Jeff Kruse, Tim Rowe, Anthony Castro and Jo Scheer for their great help and exceptional physical support in the field.

S.W. and D.S. are thankful to the Deutsche Forschungsgemeinschaft (DFG) for funding (SCHO 1274/6-1).

T. Kluge and A. Schröder-Ritzrau are thanked for valuable input that improved this version of the manuscript.

6 Paper II: Santo Tomas Cave

Variability of the tropical hydrological cycle during the last Glacial deduced from a multi-proxy speleothem record from western Cuba

Sophie F. Warken[1,2*], Denis Scholz[1], Christoph Spötl[3], Klaus P. Jochum[4], Jesús M. Pajón[5] and Augusto Mangini[2]

[1] Institute for Geosciences, University of Mainz, Germany

[2] Institute of Environmental Physics, University of Heidelberg, Germany

[3] Institute of Geology, University of Innsbruck, Austria

[4] Climate Geochemistry Department, Max Planck Institute for Chemistry, Mainz, Germany

[5] Department of Paleogeography and Paleobiology, National Museum of Natural History, La Habana, Cuba

Abstract We present a precisely dated speleothem stable isotope and trace element record from Cuba (96-7 ka), showing pronounced hydrological variability throughout the last Glacial. During the Last Glacial Maximum, increasing P/Ca and U/Ca ratios as well as $\delta^{13}C$ values indicate a decline of vegetation and soil activity. The inverse relationship of P/Ca compared to the conventional interpretation in temperate regions is suspected to originate from site-specific soil characteristics. Mg/Ca, Sr/Ca and Ba/Ca were found to be mainly controlled by calcite-water interactions such as PCP/ICD and calcite recrystallization. However, there is also evidence for several second order effects obscuring the hydrological controls. In contrast, $\delta^{18}O$ values are regarded as robust proxy for precipitation amount on Cuban speleothems. During the transition into the Holocene, the record shows a gradual change to generally warmer and wetter conditions. Across the last Glacial, we observe a similar relationship. During North Atlantic cold events (e.g., Heinrich stadials and the Younger Dryas), climatic conditions on Cuba were comparably cool and/or dry. This is in agreement with previous evidence for the Holocene, when North Atlantic cold events coincided with drier conditions on Cuba (Fensterer et al., 2013). In contrast, warm Dansgaard/Oeschger cycles were accompanied by more humid conditions. These observations are in concert with previous studies, especially from the Central American realm. Rainfall variability on Cuba was found to be mainly connected to insolation and the strength of the AMOC. The associated variability in Caribbean SSTs and the shift of the ITCZ led to partially severe changes of the hydrological cycle in the Northwestern Caribbean realm.

6.1 Introduction

Recent research suggests major changes in the tropical hydrological cycle during the last glacial period coinciding with North Atlantic (NA) climate variability due to changes in the position of the Intertropical Convergence Zone (ITCZ) and the linked wind and pressure systems (e.g., Deplazes et al. (2013); Lachniet et al. (2009); Schmidt et al. (2006)). The migration of the ITCZ has been associated with the changes in insolation as well as the strength of the Atlantic Meridional Overturning Circulation (AMOC) and its associated inter-hemispheric heat flow (Broccoli et al., 2006; McGee et al., 2014; Schmidt and Spero, 2011; Strikis et al., 2011; Lachniet et al., 2013).

However, the nature of these changes and details of their spatial and temporal evolution are still under debate. For instance, it has been suggested that the inter-hemispheric temperature gradient during the late Quaternary affected the mean position and the intra-annual migration of the ITCZ, which subsequently moved southward during NA cold phases (Chiang, 2003; Schmidt and Spero, 2011; Correa-Metrio et al., 2012; Arbuszewski et al., 2013). In contrast, other studies suggested that the ITCZ contracted near its present position (Collins et al., 2011).

Most climate records from the Caribbean covering the last 100 ka are based on marine and lacustrine sediments (Grimm et al., 2006; Schmidt et al., 2006; Donders et al., 2011; Escobar et al., 2012; Correa-Metrio et al., 2012; Deplazes et al., 2013; Grauel et al., 2016).

From the tropical and subtropical Americas, several speleothem and lacustrine climate records spanning glacial-interglacial time scales are available. These are mainly centered in northeastern Brazil or Central America (CA) and document a relationship with NA climate variability (Cruz et al., 2007; Wang et al., 2007; Lachniet et al., 2009; Correa-Metrio et al., 2012; Lachniet et al., 2013; Roy et al., 2013). For instance, a speleothem record (100 - 24 ka) from Costa Rica shows a controversial response to North Atlantic cold events (Lachniet et al., 2009). Lachniet et al. (2009) thus concluded that past rainfall variability in CA rather depends on spatial gradients in sea-surface temperature (SST) and sea-surface salinity (SSS) between the Atlantic and the Pacific Ocean than on NA climate variability.

Recent research on a Bahamian speleothem reveals a temperature decrease associated with Heinrich Stadials (HS) rather than a change in rainfall amount (Arienzo et al., 2015), whereas pollen-inferred climate reconstructions from Lake Tulane (Florida) indicate wetter summer and warmer winter conditions during HS and the Younger Dryas (YD) (Grimm et al., 2006; Donders et al., 2011). Marine sediments from the Cariaco Basin suggest a response of the ITCZ and the associated rainfall patterns to NA climate change, such as the Dansgaard/Oeschger (D/O) warm events (Deplazes et al., 2013). In summary, a clear response of Caribbean terrestrial climate records to both glacial NA cold (HS) and warm (D/O) events has not been established yet, and the available records only provide a fragmentary picture of climate change in the Caribbean region during the last glacial period.

For the Holocene, several speleothem records from the central Caribbean are available. The

majority of these records are based on $\delta^{18}O$ values (Winter et al., 2011; Fensterer et al., 2012, 2013; Winter et al., 2015; Medina-Elizalde et al., 2016), which are interpreted to be dominated by the amount effect (Vuille, 2003; Lachniet et al., 2009; Strikis et al., 2011; Fensterer et al., 2012). Only a limited number of studies from the tropics have made use of trace elements to support the interpretation of the stable isotope records in terms of climate variability (Cruz et al., 2007; Griffiths et al., 2010; Sinclair et al., 2012). Trace elements such as Mg or Sr are well-established proxies of past hydrological variability under certain circumstances (Fairchild and Treble, 2009; Fairchild et al., 2006a), and many studies have documented trace element variations on annual, decadal, millennial and glacial-interglacial timescales (Huang et al., 2001; Treble et al., 2003; Borsato et al., 2007; Cruz et al., 2007; Griffiths et al., 2010; Regattieri et al., 2014; Tan et al., 2014). Speleothem trace element records from the central Caribbean are not available yet.

Here we present a stable isotopes and trace element speleothem record from Cuba covering the period from 96 to 7 ka, which provides an important step towards a better understanding of the spatial and temporal response of the tropical climate system to abrupt NA climate variability.

6.2 Material and methods

Stalagmite Cuba Medio (CM) was collected from the Santo Tomás cave system (22.52°N, -83.85°E, Figure 6.1) in the cone (mogote) karst region of the Sierra de Quemados in western Cuba. The cave system has a total length of 46 km and shows several stages of development eroded by subsurface water streams and fluvial processes (Pajón et al., 2001; Parise et al., 2005). The cave system is developed in stratified micritic limestones of late Jurassic age, including minor dolomite and chert (Parise et al., 2005). Soil and vegetation characteristics are typical for the mogote karst region of the Greater Antilles with a dense mixture of trees, palms and ferns and a thin, but generally very productive soil layer.

CM was collected in Torch cave in a gallery 170 m above sea level (35 m above valley level), overlain by approximately 60 m of rock. The speleothem has a total length of 520 mm and is divided into two main growth parts separated by a 1 mm-thin detrital layer associated with a hiatus at 23 mm distance from top (dft, Figure 6.2). The uppermost part (0 - 23 mm dft) covering the early Holocene was already included in the study of Fensterer et al. (2013). Next to the growth axis of the stalagmite, two smaller stalagmites formed, which were also analyzed (Figure 6.2). The stalagmite was not active at the time of collection.

^{230}Th/U-dating was performed using thermal ionization mass spectrometry (TIMS) at the Heidelberg Academy of Sciences and multi-collector inductively coupled plasma mass spectrometry (MC-ICPMS) at the Max Planck Institute for Chemistry (MPIC), Mainz. Stable carbon and oxygen isotope analysis was performed at a resolution of 0.10-0.33 mm along the growth axis of CM, CMa and CMb using an on-line, automated carbonate preparation system linked to a triple collector gas source mass spectrometer at the University of Innsbruck.

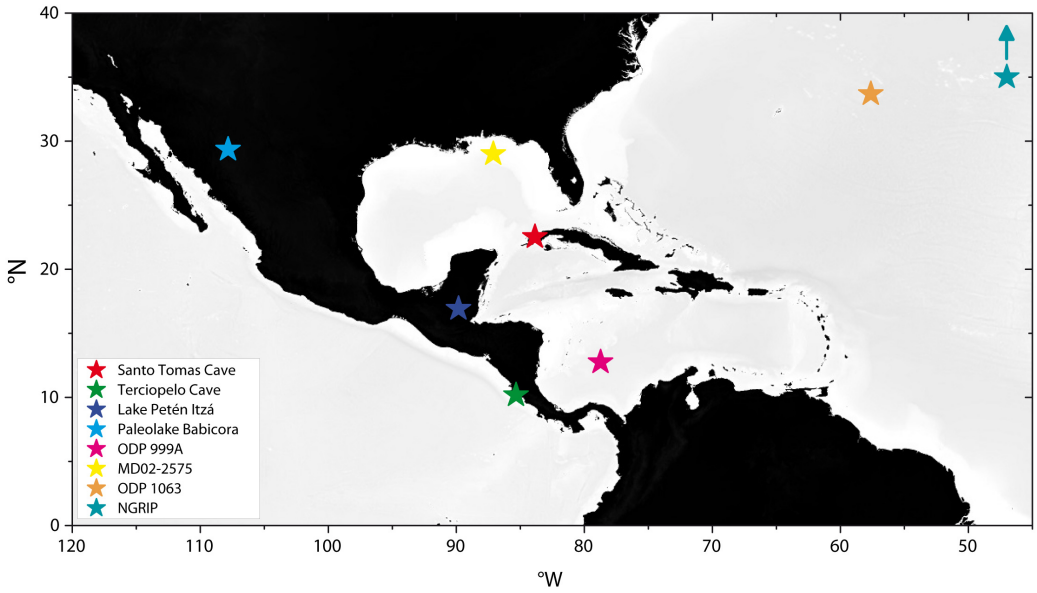

Figure 6.1: *Map indicating the locations of Santo Tomas Cave (western Cuba) and the most relevant studies discussed in this manuscript: Terciopelo Cave, Costa Rica (Lachniet et al., 2009); Lake Petén Itzá, Guatemala (Hodell et al., 2008; Correa-Metrio et al., 2012; Escobar et al., 2012); paleo lake Babicora, Mexico (Roy et al., 2013); sediment cores ODP 999A, Caribbean sea (Schmidt et al., 2004); sediment core MD02-2575, Gulf of Mexico (Ziegler et al., 2008); sediment core ODP 1063, Bermuda rise (McManus et al., 2004; Channell et al., 2012; Böhm et al., 2015) and Greenland ice core NGRIP (NGRIP members, 2004).*

Line scans of the concentrations of Mg, Al, P, Sr, Y, Ba, La, Ce, Pb, Th and U were measured along the major growth axis of CM by laser ablation ICPMS at the MPIC, Mainz with a spot size of 110 µm and a scan speed of 10 µm/s. The raw time series were outlier corrected with a 5-point running median and subsequently reduced to an equidistant record, corresponding to a 5 point smoothing. Figure B.3 in the supplementary material shows the molar ratios of all measured elements.

Correlation analysis was performed with a test statistic based on Pearson's product moment correlation coefficient r (x,y) and follows a t-distribution with length(x)-2 degrees of freedom. Asymptotic confidence intervals are given based on Fisher's Z transform. The given Pearson's correlation coefficients are all significant at the 0.05 level. Further details about materials and methods are given in the supplementary material (Appendix B).

6.3 Results

6.3.1 ^{230}Th/U dating

On the main growth axis CM, in total 34 TIMS (Tables B.1 and B.2) and 40 MC-ICPMS (Table B.3) ^{230}Th/U ages were performed (Figure B.1). For each of the small stalagmites CMa and CMb, three MC-ICPMS ages each were determined (Tables B.4 and B.5).

U content is generally low with 0.06 - 0.2 µg/g. In most samples, detrital ^{232}Th content is smaller 0.2 ng/g. For stalagmites from the same host rock, an activity ratio of (^{230}Th/^{232}Th) of 8 ± 4 was found to be appropriate for correction of detrital contamination (Fensterer et al., 2010, 2012), resulting from a detrital weight ratio of ^{232}Th/^{238}U = 0.38 ± 0.30. Hence, the correction for detrital Th is significant already for small concentrations.

In addition, many TIMS ages have relatively large errors and are systematically 'older' than the MC-ICPMS data. This can be ascribed to the lower transmission efficiency of the TIMS technique (Scholz and Hoffmann, 2008). The MC-ICPMS technique enables a higher precision of ^{230}Th/U dating for samples with low U contents, thus it is regarded the more reliable method here.

Therefore, the age control is focused on the MC-ICPMS data and all TIMS ages which are not in chronological order with the MC-ICPMS chronology are omitted. In total, 14 TIMS ^{230}Th/U ages are used for constructing the age model of CM in addition to the 40 MC-ICPMS ages (Figure 6.2).

6.3.2 Age model and growth rate

The growth axis CM spans from 82 ka (MIS 5a) to the early Holocene (7 ka) indicating nearly continuous growth with the exception of the hiatus from 13 to 10 ka (Figure 6.2). CMa (76 to 70 ka) replicates the MIS 5a growth phase of CM, whereas CMb grew between 97 and 93 ka (MIS 5b/c).

However, the chronology and petrography as well as the trace element and stable isotope record of CM show indication for several phases of very slow growth in CM, which could also be related to more growth stops. These sections are indicated with grey bars in the Figures 6.2 and B.4. In order to correctly account for potential hiatuses in the age model, the records are carefully revisited in order to find additional evidence for growth stops. Very high concentrations of trace elements indicate high detrital contamination, which is typical for hiatuses. For this purpose, Al/Ca which is included with clay minerals in speleothem calcite was used as indicator (Fairchild and Baker, 2012). Two growth stops are identified at 408 mm dft (69.4 - 66.9 ka) and 439 mm (73.6 - 72.7 ka). Further evidence for very short hiatuses lasting only a few hundred years was found at 62.5 mm dft (16.5 - 17 ka) and 356 mm (64.6 - 64.3 ka).

The age models (Figure 6.2) were subsequently constructed for each stalagmite individually. For CM and CMb, we used the algorithm StalAge (Scholz and Hoffmann, 2011) between the identified hiatuses, respectively. For CMa, the age model was tuned to the parallel axis CM taking into account the measured ^{230}Th/U-ages on both axes as well as the best correlation between the two stable isotope records.

Growth rate varies over an order of magnitude, with values of 2-3 µm/a up to 20-60 µm/a and average values of 7-10 µm/a. Lowest values apart from the mentioned growth stops (highlighted with vertical grey bars in Figure 6.2 and 6.3) are observed between 62.5 and 77 mm dft (24 - 17 ka), 121 - 131 mm (34 - 30.5 ka), 166 - 173 mm (42 - 37 ka), 245 - 250 mm (59 - 52 ka).

6.3.3 Proxy variability

The results of the element to calcium ratios along growth axis CM versus dft and age, are shown in the supplementary material (Figures B.4 and B.5). La/Ca, Ce/Ca, Y/Ca and Pb/Ca show a very noisy signal with values close to the detection limit and are not considered in the following discussion. Al/Ca ratios share a similar pattern with frequent peaks of more than 2 mmol/mol, which was used for the identification of potential hiatuses (section 6.3.2).

Figure 6.3 shows the stable isotope record and the molar element to calcium ratios of U/Ca, P/Ca, Sr/Ca and Mg/Ca with intervals of low growth rates highlighted by grey vertical bars. U/Ca and P/Ca ratios range from 0.01 to 0.3 µmol/mol and 0.1 to 2.5 mmol/mol, respectively. Extraordinarily high contents of both elements are observed between 25 - 17 ka, and at 32.5 - 28.5, 36 - 34, 62.5 and 59 as well as 89 - 75 ka. High U/Ca and P/Ca values also have a tendency to be accompanied by relatively high $\delta^{13}C$ values (Figure 6.3). The Mg/Ca ratio of CM is

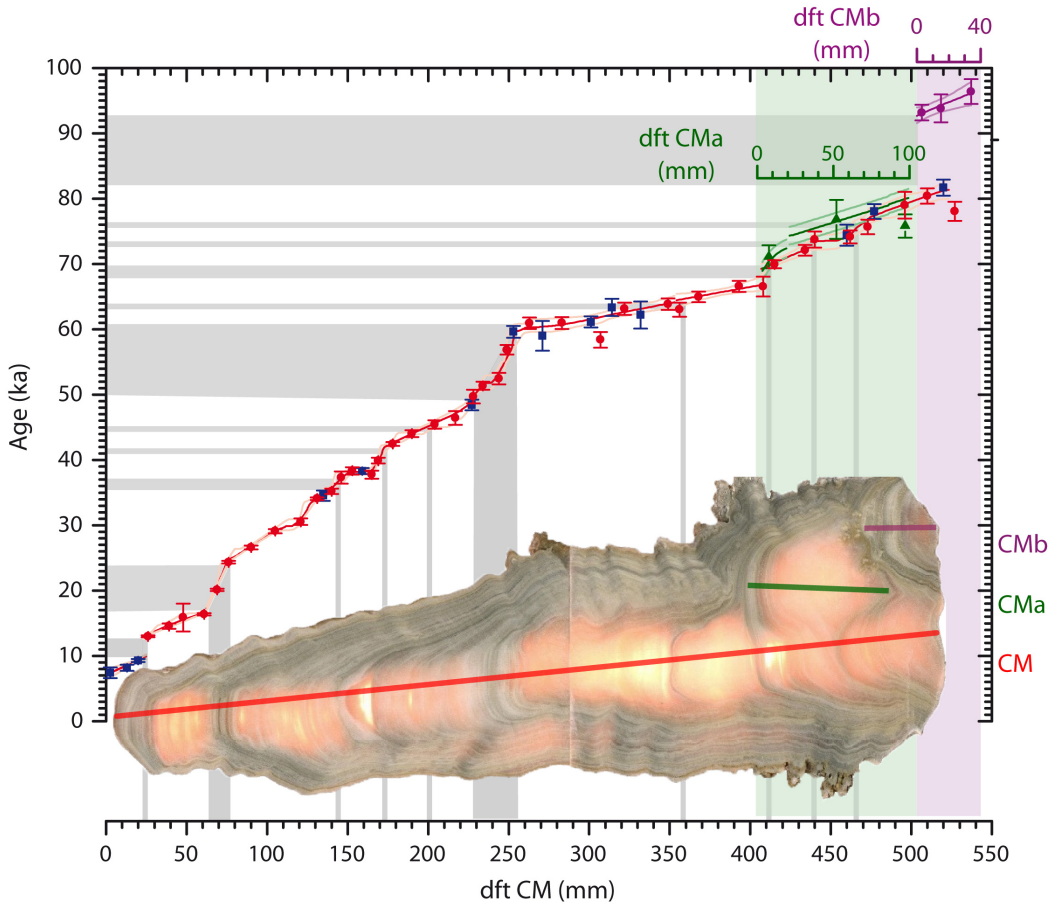

Figure 6.2: *^{230}Th/U-ages measured along the growth axes CM, CMa (green) and CMb (violet). Blue squares indicate the TIMS data which are used for constructing the age model. Red dots show the MC-ICPMS data from CM. The growth axes are indicated on the scan of sample Cuba medio. The age models are indicated with colored lines, respectively.*

generally high with an average value of 20 mmol/mol and shows a large variability. Sr/Ca ratios are characterized by a similar structure with large, abrupt changes and values between 0.02 and 0.06 mmol/mol.

Figure B.2 in supplementary material shows the individual records of $\delta^{18}O$ and $\delta^{13}C$ values of CM, CMa and CMb. The three records are combined to a composite record CM, which

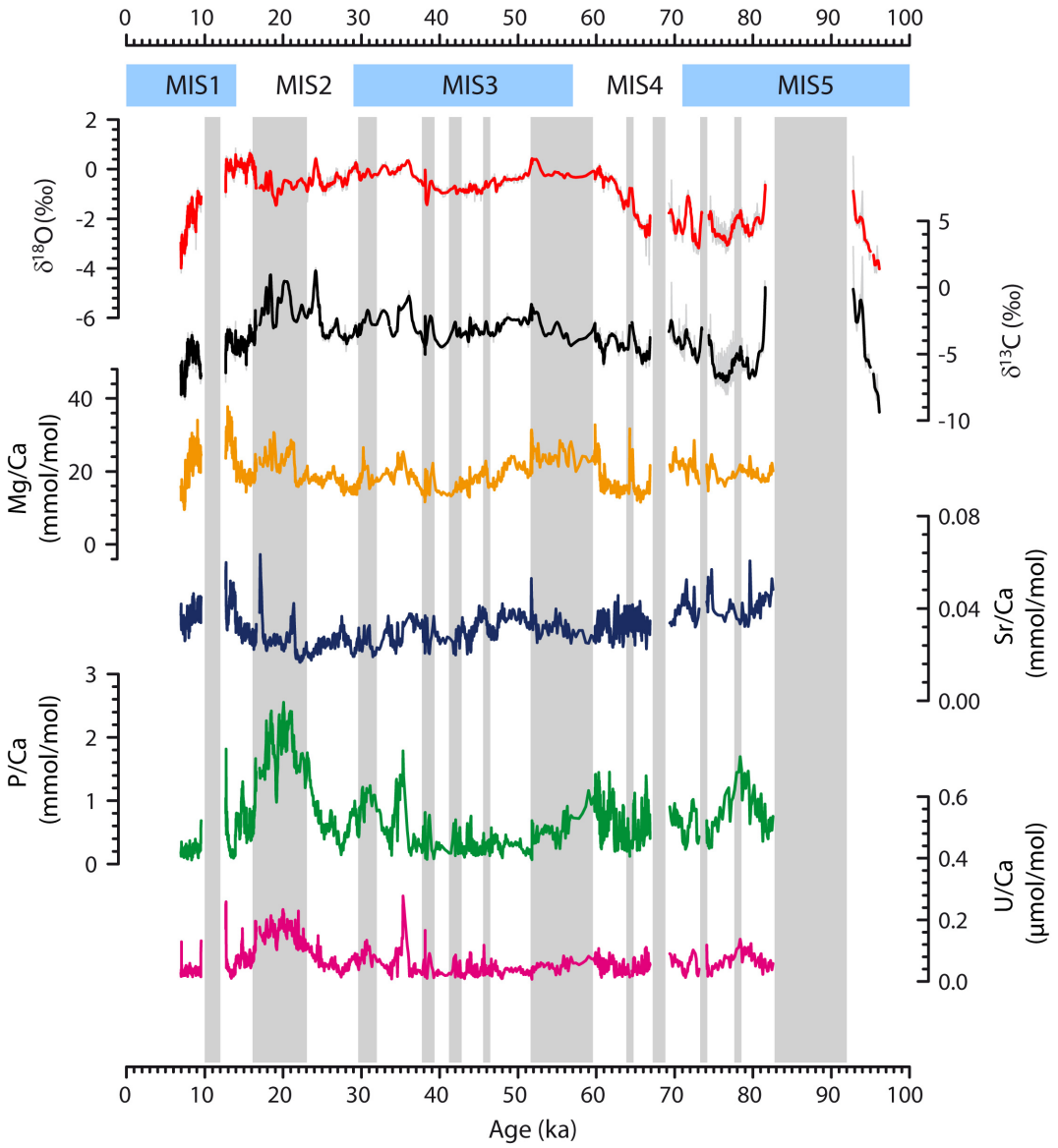

Figure 6.3: *Temporal evolution of the stable isotope ratios and element to Ca ratios in stalagmite Cuba Medio. Proxy records from top to bottom: Composite $\delta^{18}O$ record (CM, CMa, CMb, light grey line), 5 point running mean (5pRM, red); stacked $\delta^{13}C$ record (CM, CMa, CMb, light grey line) and 5pRM (black). The following panels show the molar element to Ca ratios reduced to the spatial resoluton of the stable isotope records. Light grey vertical bars indicate periods of slow growth discussed in section 6.3.2. Unsmoothed data and the records of Ba, Ce, La, Pb and Th are shown in the supplementary material B.3.*

is shown in Figure 6.3. $\delta^{18}O$ values in CM vary between -4 and +1 ‰. The lowest values are observed during MIS 5 and the early Holocene. The last glacial period (i.e., between early MIS 4 (65 ka) and the start of the transition to the Holocene (15 ka)) is characterized by relatively high values ranging from 0 to -1.5‰. $\delta^{13}C$ values range from -10 to +1 ‰. As for the $\delta^{18}O$ values, minima are observed during the early Holocene and MIS 5, whereas maximum $\delta^{13}C$ values occur during the LGM (25 - 17 ka)

6.3.4 Correlation analysis

The variability of element to calcium ratios and stable isotope records is further assessed by calculating Pearson's correlation coefficients between the individual records. In order to investigate temporal changes in the correlation of the different proxies, the record was split into seperate sections (Figure 6.4). Correlations were calculated for the whole record and the five marine isotope stages covered by CM: MIS 1 (Holocene, 10 - 7 ka), MIS 2 (29 - 12 ka, LGM and deglaciation), MIS 3 (57 - 29 ka), MIS 4 (71 - 57,ka) and MIS 5a (82 - 71 ka). Significant positive correlations are shown in red colors, negative correlations are shown in blue. The lighter the color, the less pronounced is the correlation.

One group of element ratios found in CM consists of U/Ca and P/Ca being highly correlated with $r_{U/P} = 0.89$. Both are inversely connected with Sr/Ca and Ba/Ca ($r_{Sr/P} = -0.45$,

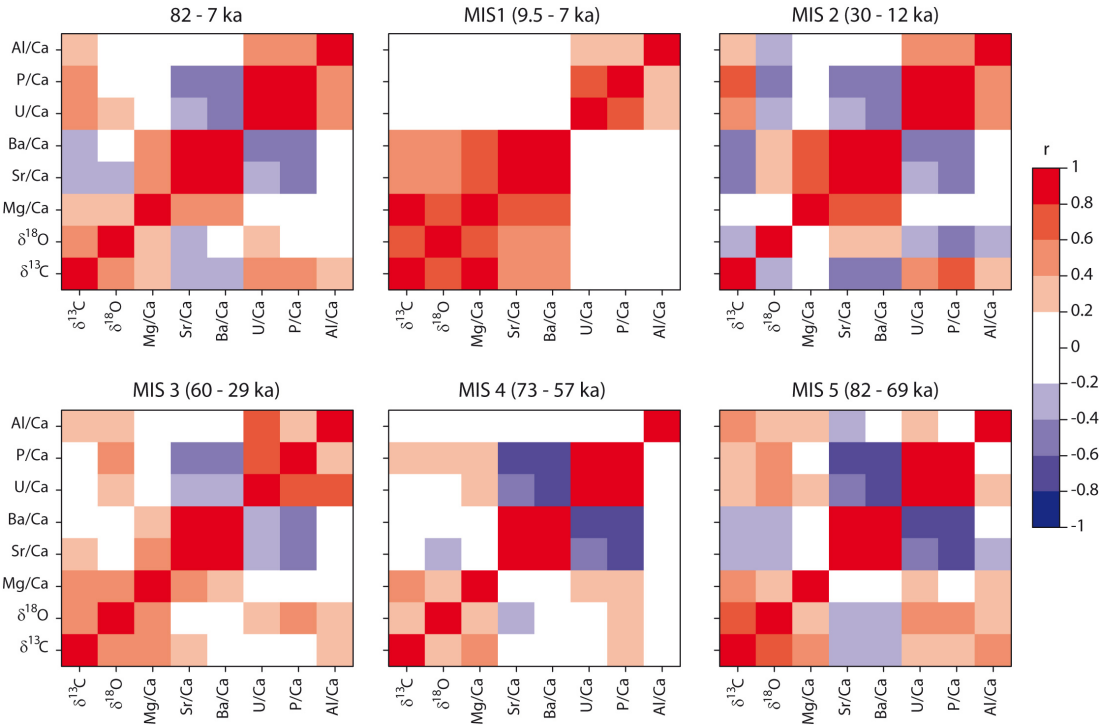

Figure 6.4: *Visualization of Pearson's correlation coefficients of Al/Ca, P/Ca, U/Ca, Ba/Ca, Sr/Ca, Mg/Ca, $\delta^{18}O$ and $\delta^{13}C$ values for the whole record (upper left panel) and MIS 1 to MIS 5a of stalagmite CM. Only significant correlations (p = 0.05) are shown.*

$r_{Ba/P}$ = -0.53, $r_{Ba/U}$ = -0.43, $r_{Sr/U}$ = -0.37). Mg/Ca, Sr/Ca and Ba/Ca are all positively correlated in the whole record with $r_{Mg/Ba}$ = 0.46, $r_{Mg/Sr}$ = 0.43 and $r_{Sr/Ba}$ = 0.87. The correlations of Sr/Ca and Ba/Ca as well as P/Ca and U/Ca persist across all analysed sections. Al/Ca shows weak correlations with U/Ca, P/Ca and $\delta^{13}C$ values during some sections.

While $\delta^{18}O$ and $\delta^{13}C$ values are positively correlated throughout the record ($r_{\delta^{18}O/\delta^{13}C}$ = 0.53), the relationship with the previously mentioned element ratio groups is controversial. During the Holocene, $\delta^{18}O$ and $\delta^{13}C$ values are highly correlated with Sr/Ca, Ba/Ca and Mg/Ca (Figure 6.4). The correlation with Mg/Ca weakly persists during MIS3 through MIS5a, whereas the covariation of Mg/Ca with Sr/Ca and Ba/Ca decreases during MIS 3 and is not significant in MIS 4 and 5. The relationship of Sr/Ca and Ba/Ca to the stable isotope signals is, however, not consistent. In contrast, both element ratios keep the strong anti-correlation with U/Ca and P/Ca through MIS 2 to MIS 5. The correlation of $\delta^{18}O$ and $\delta^{13}C$ values is most pronounced during the early Holocene and MIS 5a. The correlation is lowest in MIS 3 and 4 and even weakly negative during MIS 2 (glacial to full glacial conditions).

The covariation of Mg/Ca, Sr/Ca and Ba/Ca is further analyzed applying the models developed by Sinclair et al. (2012) to the element data in CM. Figure 6.5 shows the cross plots of ln(Sr/Ca) vs. ln(Mg/Ca), ln(Ba/Ca) vs. ln(Mg/Ca) and ln(Ba/Ca) vs. ln(Sr/Ca) for the whole record from 82 to 7 ka. The corresponding plots for the individual time slices MIS 1, MIS 2, MIS 3, MIS 4 and MIS 5 are attached to the supplementary material (Figures B.6, B.7 and B.8). The slopes $\frac{D_i-1}{D_j-1}$ (prior calcite precipitation (PCP) or incongruent calcite dissolution (ICD)) and $\frac{(D_i-1)D_j}{(D_j-1)D_i}$ (calcite recrystallization) with i,j = Mg, Sr, Ba were calculated using the partition coefficients D_{Mg} = 0.031 (for 25°C), D_{Sr} = 0.15 (both Huang and Fairchild, 2001) and D_{Ba} = 0.012 (Tesoriero and Pankow, 1996).

For all time slices, only the ln(Ba/Ca) vs. ln(Sr/Ca) data points follow the theoretically expected slope for PCP/ICD. The ln(Sr/Ca) vs. ln(Mg/Ca) and ln(Ba/Ca) vs. ln(Mg/Ca) slope only fits with the PCP/ICD model during the deglaciation (17 - 12 ka, Figure B.6 bottom panel). During the early Holocene, MIS 2 and MIS 3 the actual slopes are lower than expected for PCP/ICD (Figure B.6 upper panel) and vary between 0.23 and 0.42 for ln(Sr/Ca) vs. ln(Mg/Ca) and between 0.31 and 0.48 for ln(Ba/Ca) vs. ln(Mg/Ca). For MIS 4 and MIS 5, the cross plots for ln(Sr/Ca) vs. ln(Mg/Ca) and ln(Ba/Ca) vs. ln(Mg/Ca) have no explanatory power, since no significant correlation exists between Mg/Ca with Sr/Ca and Ba/Ca. In general, it seems that the ln(Sr/Ca) vs. ln(Mg/Ca) plots follow the slope derived by Sinclair et al. (2012) for calcite recrystallization. However, the ln(Ba/Ca) vs. ln(Mg/Ca) plots do not confirm this pattern.

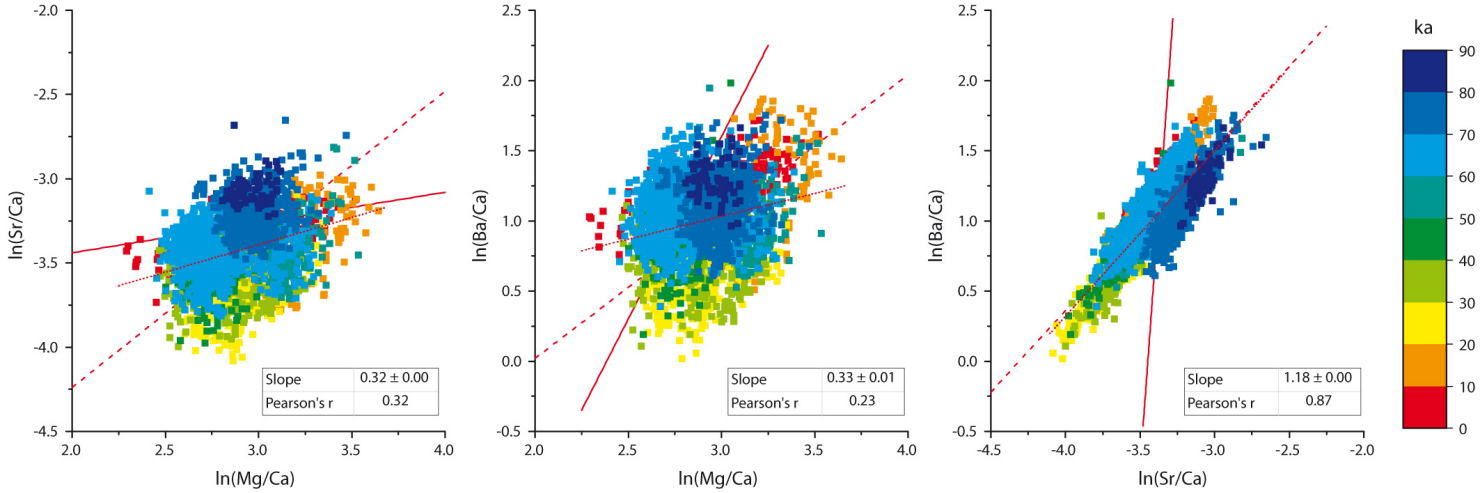

Figure 6.5: *Cross plots of element to calcium ratios in speleothem calcite of CM shown as ln(Sr/Ca) vs. ln(Mg/Ca) (left), ln(Ba/Ca) vs. ln(Mg/Ca) (middle) and ln(Ba/Ca) vs. ln(Sr/Ca) (right) for the whole record (82 - 7 ka). The red lines indicate the theoretically expected slopes for PCP and/or ICD after Sinclair et al. (2012) calculated with the corresponding partition coefficients. The dashed lines show the same for the case of calcite recrystallization (Sinclair et al., 2012). The dotted lines show the fitted slope of the data points. The plots for the individual time slices MIS 1, MIS 2, MIS 3, MIS 4 and MIS 5 are attached to the supplementary material (Figures B.6, B.7 and B.8)*

6.4 Discussion

6.4.1 Trace elements

The trace elements in CM can be assigned to three major environmental patterns reflecting (1) detrital contamination, (2) vegetation and soil dynamics and (3) hydrological variability (calcite-water interactions). Al/Ca and Th/Ca are interpreted to reflect the incorporation of detrital material. High Al content indicates the presence of clay minerals, which adsorb a range of trace elements (Dorale et al., 2004; Fairchild and Treble, 2009; Wassenburg et al., 2012). In CM, weak correlations are observed with P/Ca, U/Ca and $\delta^{13}C$ values, which may obscure their potential climate signal. For instance, a high concentration of detrital material in CM is observed at the hiatus that marks the Younger Dryas (YD, 13 - 10 ka) and during the late Last Glacial Maximum (LGM, 24-17 ka) (Figure B.5).

Environmental controls on P/Ca and U/Ca

A second major group of trace element ratios, which is most prominent on glacial-interglacial timescales, is formed by P/Ca and U/Ca (Figure 6.3). P in speleothem calcite may be interpreted to be transported from seasonally decaying vegetation prior to mineralization in the soil (Huang et al., 2001; Fairchild et al., 2001). Treble et al. (2003) observed a covariation of U and P on annual timescales, which is explained by the formation of phosphate/uranyl complexes. Borsato et al. (2007) attributed annual P layers to an autumnal flush of organic material from the soil due to the coincidence of vegetation dieback and high infiltration. A covariation of U and P was also reported on longer timescales (Mischel et al., in press; Webb et al., 2014). Both studies interpret higher values in P and U as reflecting more productive vegetation and higher soil moisture, which is supported by an anti-correlation with Mg (Webb et al., 2014) and $\delta^{13}C$ (Mischel et al., in press), respectively.

In stalagmite CM, high values of P and U tend to coincide with elevated $\delta^{13}C$ and Mg/Ca values suggesting a different relationship. Higher $\delta^{13}C$ values are usually interpreted to reflect a less productive vegetation and reduced soil activity above the cave (Genty et al., 2003; McDermott, 2004; Meyer et al., 2014). The (positive) covariation of $\delta^{13}C$ with U/Ca and P/Ca in CM thus suggests a connection of the three proxies to long-term vegetation and soil dynamics with higher P/Ca values indicating a decline in vegetation and soil activity in contrast to the common interpretation.

At tropical sites, vegetation dieback is not so seasonally pronounced and litter fall may occur throughout the year. This suggests a different pattern of infiltration of P-bearing waters than in temperate locations with pronounced seasonality. A general decline of vegetation might have the same effect also in tropical locations over several years, however, this process might not be persistent over several millennia. Based on monitoring data from a tropical cave, Frisia et al. (2012) infer, there may not be a direct relation between an increase in P concentration and seasonal infiltration, especially if the source of this element is not the

labile phosphate released through leaching during seasonal vegetation dieback in temperate climates. The authors found that incorporation of P into speleothems may be complex and showed that co-precipitation of P-rich phases may occur during intervals of reduced drip rates, which may indicate dry spells. This observation may support our interpretation.

We suggest, that the observed inverse connection of P/Ca with vegetation variability may be also the result of different soil types compared to the Australian caves. In their study, Treble et al. (2003) argue with the low P retention capacity of the sandy southwestern Australia soils, which might explain why a strong seasonal P signal associated with seasonal flush of organic-rich complexes is seen in speleothems from this region. In contrast, subtropical and tropical soils are often characterized by a high P retention capacity (Sanchez and Uehara, 1980; Daroub et al., 2003), which means that phosphate is bound much tighter to the non-soluble phase. In principle, P retention in soils is pH dependent. At low soil pH, P is fixed into slightly soluble forms by precipitation and sorption reactions with Fe and Al compounds as well as crystalline and amorphous colloids (Sanchez and Uehara, 1980). At the cave site in western Cuba, the dominant soil types are Luvisols, Cambisols and Gleysols (Gardi et al., 2014). A survey shows, that Luvisols as well as Gleysols in most cases show serious to very serious phosphorus deficiencies, and Cambisols average phosphorus deficiency (Roche et al., 1978), with Luvisols being neutral and Cambisols rather acid (Schulte and Ruhiyat, 1998). A decline in vegetation productivity may result in a lower soil pCO_2, which in turn elevates soil pH. Under certain circumstances a threshold soil pH might be reached, which facilitate the release of previously adsorbed phosphate to the soil solution and thus increases the flush of P-rich complexes.

Recently it was also shown that with increased aridity the P cycle may become decoupled from the N cycle with increased P concentrations in the soil (Delgado-Baquerizo et al., 2013). Although this study rather applies to dry sub-humid to arid ecosystems, it may be of some significance for the tropical glacial environments, which experienced presumably much drier conditions than today (Escobar et al., 2012; Correa-Metrio et al., 2012).

Thus, the positive correlation of U and P with $\delta^{13}C$ in stalagmite CM suggests a connection to vegetation and soil dynamics on longer timescales, rather than a direct response of these proxies to infiltration.

Environmental controls on Mg/Ca, Sr/Ca and Ba/Ca

Sr/Ca, Ba/Ca and Mg/Ca form the third major group of trace element ratios. A positive correlation between these element ratios is often interpreted to reflect hydrological variability due to PCP and/or changes in the residence time of the recharge water (Roberts et al., 1998; McMillan et al., 2005; Cruz et al., 2007; Fairchild and Treble, 2009; Fairchild and Baker, 2012; Sinclair et al., 2012). However, such a covariation may also be caused by other processes and is thus further tested by applying the model of Sinclair et al. (2012).

The resulting plots of the whole record (82 - 7 ka, Figure 6.5) are exemplary for the general conclusion. The ln(Ba/Ca) vs. ln(Sr/Ca) plot matches with the theoretically calculated slope

of Sinclair et al. (2012) for prior calcite precipitation (PCP) and/or incongruent calcite dissolution (ICD) suggesting a hydrological control on these proxies. In contrast, the slopes of the ln(Sr/Ca) vs. ln(Mg/Ca) and ln(Ba/Ca) vs. ln(Mg/Ca) plots are systematically lower than expected for PCP/ICD and do also not correspond systematically with the model developed for calcite recrystallization. The deviation of the slope in the ln(Mg/Ca) plots is suggested to results from additional Mg input from dissolution of dolomite or high Mg-calcite in the host rock (Sinclair et al., 2012). Relatively high Mg/Ca ratios in CM support the existence of an additional Mg source along the water pathway feeding stalagmite CM.

Calcite recrystallization might also induce a correlation between Sr and Mg. The graphs ln(Sr/Ca) vs ln(Mg/Ca) and ln(Ba/Ca) vs ln(Mg/Ca) in the Figures B.6, B.7 and B.8 suggest that the trace element signatures might indeed be affected by calcite recrystallization, which in general is a high non-linear process (Sinclair et al., 2012). Sinclair et al. (2012) note, that their models of calcite recrystallization require some degree of equilibration between limestone and solution and that the models are most applicable to cases where there is a low solution volume and a large area of limestone surface. These conditions might be encountered during diagenesis of a very porous limestone and/or vadose diagenesis where solution is a thin film trickling across a large surface area of limestone.

Other processes may also exert a second-order effect on the incorporation of Mg, Sr and Ba. D_{Mg} is dependent on temperature, however, a temperature change by 2 - 3 °C would result in a total change in Mg by at most 15% (Huang and Fairchild, 2001). The variability of Mg/Ca in CM is much greater with peaks from about 20 up to 30 mmol/mol, so temperature effects are regarded to play only a minor role. In contrast, changes in calcite precipitation rate affect the incorporation of Sr in speleothem calcite but have no effect on Mg (Gabitov and Watson, 2006; Nehrke et al., 2007). A change in growth rates by more than an order of magnitude is expected to notably affect Sr incorporation in speleothem calcite and may thus obscure the covariation with Mg/Ca. High growth rates would lead to higher Sr/Ca ratios in the speleothem and vice versa, whereas the potential hydrological controls such as PCP/ICD or calcite recrystallization would have the opposite effect on Mg/Ca as well as Sr/Ca. More humid conditions may permit higher growth rates due to higher drip rates (Kaufmann, 2003), so these constitute competing effects concerning the incorporation of Sr in speleothem calcite.

This effect is for example visible in the CM record before 50 ka, when the correlation of Mg/Ca with Sr/Ca and Ba/Ca diminishes. This section is characterized by relatively strong changes in speleothem growth rates. Between 63 and 59 ka, the highest growth rates of the whole record with more than 20 µm/yr are observed, accompanied by relatively low Mg/Ca compared to the period with low growth rates down to 2 - 3 µm/yr afterwards (59 - 52 ka). The growth rate dependency of Sr/Ca obviously rules out the hydrological influence, because the absolute Sr/Ca level shows no comparable change across the discussed sections. For interpreting the Sr/Ca (and Ba/Ca) variability in CM in terms of climatic changes, both effects have thus to be taken carefully into account.

Sr/Ca and Ba/Ca are generally negatively correlated with P/Ca and U/Ca which seem to be connected with soil dynamics (section 6.4.1). This observation is in concert with the interpretation of both element groups. According to section 6.4.1, low soil pCO_2 might explain higher P and U complexes in the percolating water. On the other hand, it also induces less dissolution in the host rock and thus lower precipitation rates.

Other effects on Mg/Ca or Sr/Ca might be incorporation of dust/detrital material or sea spray. In an island karst system, input of seawater to groundwaters can be a significant source of ions, especially for Mg and Sr which are both relatively concentrated in seawater (Goede et al., 1998). A potential source of sea spray might be tropical cyclones, which today affect the site on a regular basis. Thus it is possible, that sea spray contributes a second-order effect to the element profiles. Input of detrital material is not regarded to have a major influence on the Mg/Ca, Sr/Ca and Ba/Ca variability in CM which is indicated by the generally very low Al/Ca and Th/Ca ratios and the non-significant correlation coefficients (section 6.3.4).

High values of Mg/Ca thus most likely reflect a higher degree of calcite-water interactions through PCP/ICD and/or calcite recrystallization and thus generally drier conditions in western Cuba. This is also consistent with the generally positive correlation with $\delta^{18}O$ and $\delta^{13}C$ values and the previously discussed variability of P/Ca and U/Ca. It is to note that, since especially calcite recrystallization is a highly non-linear process, the inferences from the Mg/Ca signal in terms of rainfall changes can only remain highly qualitative.

6.4.2 Stable isotopes

Environmental controls on $\delta^{13}C$ values

Since speleothem $\delta^{13}C$ values are influenced by a variety of processes, they may be used to disentangle the interpretation of speleothem climate records (McDermott, 2004; Dreybrodt and Scholz, 2011; Meyer et al., 2014). A positive relationship between Mg/Ca ratios and $\delta^{13}C$ values may indicate that both proxies are driven by calcite-water interactions such as PCP/ICD due to varying residence time (Cruz et al., 2007; Johnson et al., 2006), drip-rate modulated stable isotope fractionation under disequilibrium conditions (Deininger et al., 2012; Scholz et al., 2009) or that the variations originate in the soil zone.

Varying $\delta^{13}C$ values have commonly been interpreted to reflect changes in vegetation and soil activity above the cave (Fohlmeister et al., 2011; McDermott, 2004; Meyer et al., 2014; Mischel et al., in press). The positive covariation of $\delta^{13}C$ with U and P supports the interpretation that these three proxies record long-term vegetation and soil dynamics. Higher $\delta^{13}C$ values are thus interpreted to reflect generally drier conditions as a mixed signal of long-term decline in vegetation density and reduced soil activity as well as enhanced calcite water-interactions (PCP/ICD) due to longer residence time. Stronger disequilibrium stable isotope fractionation occurring inside the cave during very dry intervals would have the same effect.

In stalagmite CM, Mg/Ca and $\delta^{13}C$ show a number of synchronous positive peaks (around

13, 18-19, 20-21, 23-24, 30-31, 34.5-35.5 and 38-39, 45-46, 51-52, 59-60 and 64-65 ka, Figure 6.3), which may thus be interpreted as dry events. Some of these dry events coincide with prominent North Atlantic cold events (Heinrich stadials, see the later discussion in section 6.4.3).

Environmental controls on $\delta^{18}O$ values

The amount effect has been suggested as one of the most important drivers of the $\delta^{18}O$ value of low-latitude precipitation (Vuille, 2003; Lachniet and Patterson, 2006; Lachniet, 2009a). Thus, $\delta^{18}O$ values of tropical speleothems are usually interpreted to reflect changes in rainfall amount (Cruz et al., 2009; Lachniet et al., 2009; Winter et al., 2011), what also applies to the Holocene part of stalagmite CM and other speleothems from the same cave system (Fensterer et al., 2012, 2013). This interpretation of the Holocene $\delta^{18}O$ values is further supported by the strong positive correlation of $\delta^{18}O$ with our Mg/Ca, Sr/Ca and Ba/Ca record in CM between 10 and 7 ka (Figure 6.4). This strong covariation of the elemental ratios during the Holocene was found to be most likely caused by calcite/water interactions (PCP/ICD, sections 6.3.4 and 6.4.1), demonstrating that the major factor influencing these proxies during the Holocene was indeed rainfall amount. The positive covariation of $\delta^{18}O$ values with Mg/Ca weakens across the earlier part of the record and is even partly opposite with Sr/Ca and Ba/Ca, possibly due to the additional processes modulating the trace element signatures in CM (section 6.4.1). During MIS 2, also $\delta^{13}C$ values are decoupled from the $\delta^{18}O$ signal, which may be explained by the enhanced influence of soil dynamics during the LGM on the carbon composition of the speleothem (section 6.4.3).

In order to further elucidate the environmental controls on $\delta^{18}O$ values in Cuba, the record is compared (Figure 6.6) to a number of sea surface temperature (SST) and planktonic $\delta^{18}O$ records representing potential sources of rainwater from the Caribbean (Schmidt et al., 2004), the Gulf of Mexico (Ziegler et al., 2008) and the western subtropical Atlantic (Channell et al., 2012). On glacial-interglacial timescales, the CM $\delta^{18}O$ record resembles the SST and $\delta^{18}O$ patterns of the three marine records. The variability of the $\delta^{18}O$ values of surface water in the tropical Atlantic is about 2 ‰ on glacial-interglacial timescales, the global increase of $\delta^{18}O$ values in seawater during the LGM was ca. 1‰ (Schrag et al., 2002). In contrast, the difference between the Holocene and Glacial $\delta^{18}O$ values of stalagmite CM is about 4 to 5 ‰, thus only 2 - 3 ‰ of the variability are not caused by changes of the source waters. This difference of the $\delta^{18}O$ values of CM between the Holocene and the Glacial may be explained by a combination of temperature differences and a decrease in rainfall amount as stated in previous studies (e.g., Schmidt et al. (2004); Ziegler et al. (2008); Hodell et al. (2008); Lachniet et al. (2009); Correa-Metrio et al. (2012); Arienzo et al. (2013); Grauel et al. (2016)). Assuming a cooling of ca. 5 °C during the Last Glacial Maximum (LGM) relative to the late Holocene would have had a temperature-induced increase in carbonate-water isotopic fractionation (relative to modern cave air temperatures) during the LGM of ~1‰ (Kim and O'Neil, 1997; Tremaine et al., 2011). Thus about another ~1 - 2‰ may be attributed to a reduction in precipitation

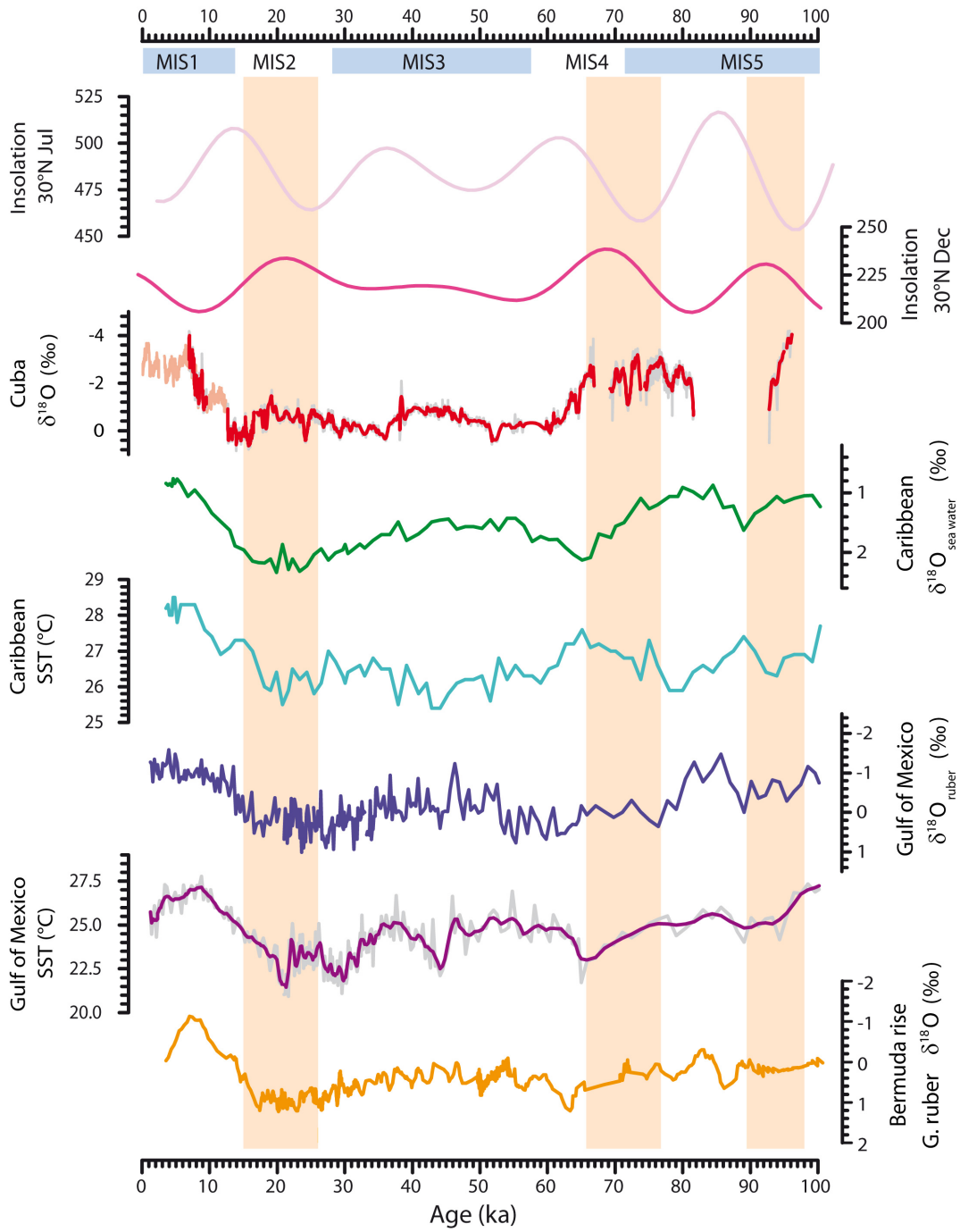

Figure 6.6: *Speleothem CM $\delta^{18}O$ values (raw composite record: light grey, 5p RM: red line, this study) together with the Holocene speleothem $\delta^{18}O$ record from Fensterer et al. (2013) (light red). The records are compared with insolation during July (light pink) and December (pink) at 30°N, as well as SST and $\delta^{18}O$ records obtained from planktonic foraminifera from the Caribbean (green: $\delta^{18}O$, cyan: SST, ODP 999A, Schmidt et al. (2004)), the Gulf of Mexico (violet: $\delta^{18}O$, purple: SST, Ziegler et al. (2008)) and the Bermuda rise (orange, Channell et al. (2012)). Vertical bars indicate periods with relatively high (winter) insolation which are accompanied by high $\delta^{18}O$ values in CM indicating wetter and warmer conditions on Cuba.*

amount, together with potentially linked disequilibrium fractionation effects inside the cave driven by ventilation or drip rate variability, which would further enrich the $\delta^{18}O$ signature (Lachniet, 2009a; Deininger et al., 2012).

The variability of the tropical hydrological cycle has been closely related to variations in insolation, since the position of the Intertropical Convergence Zone (ITCZ), which determines the trade wind season on Cuba, is highly sensitive to solar insolation on seasonal and longer timescales (Poveda et al., 2006). Previous studies have documented a clear link between summer insolation, which is dominated by precession in the tropics, and rainfall proxy records from speleothems (Cruz et al., 2005a; Wang et al., 2007) and lake sediments (Baker et al., 2001). Interestingly, on glacial-interglacial timescales, the $\delta^{18}O$ values of CM show a close relationship rather to winter insolation, in particular from MIS 4 to 2 (Figure 6.6), which is opposite to that expected based on a direct insolation-monsoon strength mechanism.

Forcings on the Caribbean hydrological cycle

A connection of speleothem $\delta^{18}O$ values to northern hemisphere winter insolation was also observed by Lachniet et al. (2009) in a record from Costa Rica, Central America (CA), which is shown in Figure 6.7.

Lachniet et al. (2009) consider two possibilities for a direct and indirect control of winter insolation to Caribbean rainfall, respectively. First, it is possible that high winter insolation warms tropical North Atlantic and Caribbean SSTs, which contributes to a longer wet season the following summer. This is supported by evidence that warmer SSTs in the Caribbean promote decreased tropospheric stability and a higher rainfall probability over Central America and by the strong connection of rainfall anomalies in CA with SST anomalies in the Caribbean Sea (Enfield and Alfaro, 1999; Lachniet et al., 2009). When the Caribbean is warm, the rainy season starts early and ends late which would be associated with low $\delta^{18}O$ values in the stalagmite records. This direct forcing would suggest that antecedent conditions in tropical SST are important for the following wet season rainfall. The second suggestion by Lachniet et al. (2009) is, that high winter insolation may also drive an enhanced SST gradient across the isthmus, which in turn would not directly influence the rainfall variability on Cuba.

Both the Cuban and the Costa Rican speleothem records share a similar pattern and show similarities with the SST's in the Caribbean basin (Schmidt et al., 2004; Lachniet et al., 2009), suggesting that higher rainfall on Cuba and in CA is associated with periods of a warm tropical North Atlantic Ocean. This relationship is consistent with data that suggests that the Caribbean exerts a stronger control than the Pacific on Central American and Northwestern Caribbean rainfall, because positive SST anomalies result in a longer wet season (Enfield and Alfaro, 1999). For example, a relatively dry interval is recorded in Cuba as well as in Central America between ca 60 and 45 ka, which is associated with decreasing or relatively low Caribbean SSTs (Figure 6.6). This close connection between Cuba and CA originates in the North Atlantic Subtropical High (NASH) which produces the easterly trade winds. The flow intensifies in the Caribbean Sea forming the Caribbean Low Level Jet (CLLJ), which

splits into two branches during boreal summer (Amador, 1998; Amador and Magana, 1999; Mestas-Nuñez and Miller, 2006; Mestas-Nuñez et al., 2007; Hodell et al., 2008). One branch turns northward bringing moisture to the western Gulf of Mexico, and the southerly branch of the CLLJ continues westward carrying moisture across the CA isthmus to the Pacific.

A central observation of Lachniet et al. (2009) is, that higher rainfall in Costa Rica is also connected with large SST gradients between the Atlantic and Pacific Oceans (Lachniet et al., 2009), and little correlation was found with $\delta^{18}O$ values in the subtropical North Atlantic Ocean. In contrast, rainfall in Cuba was found to be closely connected with North Atlantic SSTs and the strength of the AMOC (Fensterer et al. (2012, 2013) and section 6.4.3). These different modulations of rainfall variability might explain the differences on millennial scale to the Costa Rican record, which exhibits a much higher internal variability than the Cuban $\delta^{18}O$ signal.

6.4.3 Implications for climate variability on Cuba during the last Glacial

Impact of North Atlantic millennial scale events

Previous work on Cuban speleothems suggest a close link to North Atlantic climate variability (Fensterer et al., 2012, 2013). In Central America, lacustrine sediment cores provide evidence for a close link of precipitation changes also during the last glacial period in the northern hemisphere neotropics with fresh-water forcing to the high-latitude North Atlantic (Hodell et al., 2008; Correa-Metrio et al., 2012; Escobar et al., 2012; Roy et al., 2013; Grauel et al., 2016). A series of studies from Lake Petén Itzá, Guatemala, showed that cooler and more arid climate dominated the Central American lowlands during North Atlantic stadials (e.g., Heinrich events). In contrast, Greenland warm phases were associated with warm and relatively wet conditions (Correa-Metrio et al., 2012; Escobar et al., 2012). Similar observations with a stronger North American monsoon during warm interstadials were made by Roy et al. (2013) for the drylands of northern Mexico at 29 °N (Figure 6.7).

Figure 6.7 presents the Cuban $\delta^{18}O$, Mg/Ca and P/Ca record together with the Greenland ice core $\delta^{18}O$ chronology NGRIP members (2004), the $\delta^{18}O$ speleothem record from Terciopelo Cave, Costa Rica (Lachniet et al. (2009) and lacustrine sediment climate reconstructions from Mexico (Roy et al., 2013) and Guatemala (Correa-Metrio et al., 2012) representing the impact of NA millennial scale climate changes in Central America. The comparison shows, that most NA cold events associated with freshwater input into the North Atlantic (so called Heinrich stadials (Heinrich, 1988; Hemming, 2004)) were characterized by cooler and/or drier conditions on Cuba. During the Younger Dryas (YD, 13 - 10 ka), HS 1 (17 - 15 ka), H7 a/b (~ 73 and ~ 76 ka) and HS 8/9 (between 93 and 84 ka) actual growth stops were identified in stalagmite CM, and HS 2 (~ 22-24 ka), HS 3 (~ 30 ka), HS 4 (~ 38 ka) and HS 6 (~ 63 ka) were all associated with comparably slow speleothem growth rates. HS 5 might be linked with a thin detrital layer around ~ 45 ka. This is supported by lower $\delta^{18}O$ and relatively high Mg/Ca values during most Heinrich stadials. HS 1 seems to be split into to consecutive cold/dry spells, with

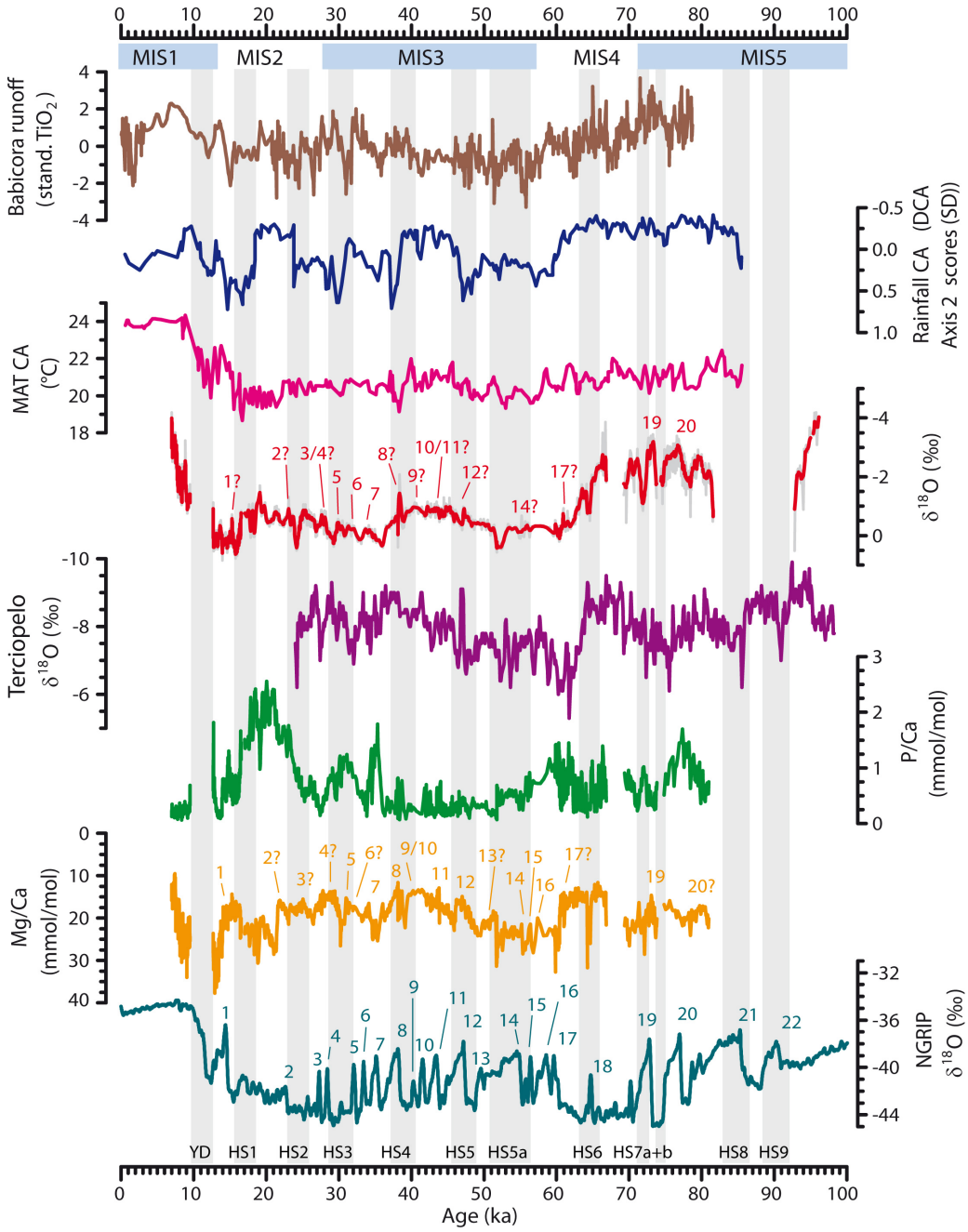

Figure 6.7: *Comparison of proxy records of CM with previous studies: In red: speleothem CM* $\delta^{18}O$ *values (raw composite record: light grey, 5p RM: red line, this study) together with the Holocene speleothem* $\delta^{18}O$ *record from Fensterer et al. (2013) (light red); orange: Mg/Ca and green: P/Ca records of CM. Brown: lacustrine sediment record from paleo lake Babicora (northern Mexico) representing runoff variability (Roy et al. (2013)); Blue and pink: rainfall and temperature reconstructions from Lake Petén Itzá, Guatemala deduced from pollen assemblages, both Correa-Metrio et al. (2012)); Purple: speleothem* $\delta^{18}O$ *values from Terciopelo Cave, Costa Rica (Lachniet et al. (2009)); Cyan: NGRIP* $\delta^{18}O$ *ice core record (cyan, NGRIP members (2004)). Vertical grey bars indicate the approximate timing of North Atlantic cold events (Younger Dryas (YD) and Heinrich stadials (HS)). Numbers indicate the Dansgaard/Oeschger warm interstadials in Greenland, which are partially recorded in the CM* $\delta^{18}O$ *and Mg/Ca record.*

$\delta^{18}O$ values increasing by about 0.5 - 1 ‰ between 18.4 - 17.8 ka, followed by an additional increase to values around 0 ‰ from 16.5 - 15.7 ka after a short intermediate recovery. Simultaneously, HS 1 is characterized by the highest $\delta^{18}O$ values of the whole record indicating that this period was the coolest and driest interval. Both observation were also made in other records from the tropical latitudes, such as e.g. Stager et al. (2011); Escobar et al. (2012) or Arienzo et al. (2015). The two periods of maximum cold and/or arid conditions coincide approximately with two pulses of ice-rafted debris (IRD) recorded off southern Portugal (Bard et al., 2000). McManus et al. (2004) and Böhm et al. (2015) report, that HS 1 was characterized by a near shut down of the Atlantic meridional overturning circulation (AMOC) which might explain the severe changes in the hydrological regime.

In contrast, warm Greenland interstadials (Dansgaard/Oeschger stadials) are only partly pronounced in the Cuban speleothem record (Figure 6.7). The early D/O cycles 19 and 20 between 82 and 69 ka are clearly visible in the $\delta^{18}O$ record and characterized by large variations of about 2 ‰. The $\delta^{18}O$ signature nearly reaches values comparable to Holocene conditions of around 3 ‰ during warm interstadials. Wetter conditions with relatively high pluvial discharge between 80 and 58 ka was also found in paleo lake Babicora (Northern Mexico, Roy et al. (2013)) as well as in Guatemala (Correa-Metrio et al., 2012). The increase of $\delta^{18}O$ values begins in CM about 65 ka and reaches its glacial level around 0 ‰ at 60 ka. A similar, much sharper change was found in a Costa Rican speleothem (Lachniet et al., 2009)), whereas the decrease in runoff in Northern Mexico is smoother (Roy et al., 2013). Drier conditions between 60 and 48 ka are also consistent with the pollen derived record of Correa-Metrio et al. (2012) (Figure 6.7)

During MIS 3, the variability of $\delta^{18}O$ values in CM is comparably low, and only major D/O cycles may be linked with small negative excursions of the $\delta^{18}O$ and Mg/Ca record (Figure 6.7). Similar observations were made at Lake Petén Itzá, Guatemala, with fairly constant ostracod $\delta^{18}O$ values during MIS 3 with the exceptions of the Heinrich stadials (Escobar et al., 2012).

Last Glacial Maximum

During the Last Glacial Maximum (LGM, 24 - 19 ka), our record shows an apparently controversial pattern. From 24 to 21 ka, Mg/Ca ratios are relatively low, which might denote comparably moist conditions. A sharp increase after 21 ka suggests a shift to relatively drier climate, whereas considerably higher P/Ca ratios indicate a gradual change in vegetation and soil dynamics between 25 - 16 ka with highest values from 21 - 18 ka, coinciding with the high Mg/Ca values. Even though Mg/Ca ratios in CM may not be a reliable precipitation proxy (section 6.4.1), growth rates were generally low during the whole MIS2 (24 - 16 ka), supporting the interpretation of generally drier and/or cooler conditions. In contrast, relatively stable $\delta^{18}O$ values around -0.5 ‰ show no evidence for a severe temperature and/or rainfall decrease as suggested by the signal of the other proxies.

For the LGM, temperature reconstructions from the Northern Caribbean realm estimate

a cooling of up to 6 - 10 °C (Hodell et al., 2008; Correa-Metrio et al., 2012; Arienzo et al., 2013; Grauel et al., 2016). We speculate that during the LGM, long-lasting relatively low temperatures might have triggered the unfavorable conditions for the existing biosphere and caused a gradual change in soil constitution which is displayed in the P/Ca ratio. A similar threshold might have been reached during HS 3 and HS 4 as well as around 80 and 60 ka, which mark also sections with relatively high P/Ca ratios.

Concerning the hydrological regime, climate reconstructions are not consistent. Whereas Roy et al. (2013) state below average runoff for the LGM in Northern Mexico, higher lake levels and relatively moister climate were suggested for Guatemala (Hodell et al., 2008; Escobar et al., 2012). Pollen analysis from the same lake indicate moist conditions but air temperatures at least 4.0 - 6.0 °C cooler than today (Bush et al., 2009), which is consistent with recent temperature estimates for the LGM in CA (Correa-Metrio et al., 2012; Grauel et al., 2016). The competing influence of cooler and comparably humid conditions might explain the relatively stable $\delta^{18}O$ values in CM during the LGM.

A wetter LGM in the Northern Caribbean might be explained by greater summer precipitation caused by a more northerly position of the ITCZ (Escobar et al., 2012). McManus et al. (2004) and Böhm et al. (2015) inferred, that the strength of the AMOC during the LGM was similar to the strength during the Bolling-Allerod-period, a time for which there is evidence of a northerly ITCZ position (Peterson, 2000). Alternatively, a relatively high winter insolation may have prolonged the wet season (compare section 6.4.2). Hodell et al. (2008) and Escobar et al. (2012) also speculate, that greater winter precipitation from increased intensity and frequency from the North may also account for wetter LGM conditions.

6.5 Conclusions

The here presented trace element and stable isotope record from western Cuba provides evidence for a pronounced variability of the tropical hydrological cycle across the last glacial cycle into the early Holocene (96 - 7 ka).

Based on precise MC-ICPMS $^{230}Th/U$ dating, a tight age model could be established for the proxy records. High resolution trace element records were found to be controlled by three different processes, detrital contamination, soil/vegetation dynamics and calcite-water interactions.

In particular, P/Ca and U/Ca were found to be associated with soil dynamic processes, deduced from a positive covariation with Mg/Ca and $\delta^{13}C$ values. This is one of the first records showing that high P/Ca ratios may be also connected with a decline of the vegetation system above the cave. We speculate, that this inverse interpretation compared to previous work, such as by Treble et al. (2003), may be related to different soil characteristics which enable under certain environmental conditions a triggering in soil pH, which subsequently releases adsorbed phosphate to the soil solution.

Mg/Ca, Sr/Ca and Ba/Ca were found to be mainly controlled by calcite-water interactions

such as PCP/ICD and calcite recrystallization. However, there is also evidence for several second order effects particularly on Sr/Ca and Ba/Ca which obscure the interpretation as pure hydrological proxies. In contrast, $\delta^{18}O$ values are regarded as relatively robust proxy for precipitation amount on Cuban speleothems.

In concert with previous work from the Caribbean realm, especially from Central America, rainfall variability on Cuba is connected to insolation and tropical North Atlantic and Caribbean SSTs, as well as to the strength of the AMOC and high-latitude temperature variability.

Our record shows, that North Atlantic cold events, in particular Heinrich stadials, were associated with relatively cold and dry conditions on Cuba. In particular, HS 1 was the driest and coolest interval of the whole record. Several other cold events, such as the YD were even accompanied by growth stops. In contrast, Greenland warm interstadials especially during MIS 5 were characterized by relatively warm and wet conditions, whereas the response to high latitude temperatures during MIS3 to MIS4 in the Cuban record was much smaller.

During the LGM, climate on Cuba was relatively cool, but not especially dry. Nevertheless, environmental conditions were sufficiently unfavorable for the existing biosphere, resulting in a decline in vegetation and soil dynamics.

Acknowledgements

S.W., D.S. and A.M. acknowledge funding by DFG grants MA 821/37-2 and SCHO 1274/6-1.

The authors thank R. Eichstädter (Heidelberg), B. Stoll, U. Weis, B. Schwager (all MPIC Mainz), M. Wimmer (Innsbruck) and M. Weber (Mainz) for assistance in the laboratory.

N. Frank and A. Schröder-Ritzrau are thanked for useful comments that helped to improve this version of the manuscript.

7 Paper III: Cloşani Cave

Hydroclimate variability in SW Romania during the last 3.6 ka reconstructed from a high-resolution speleothem multi-proxy record

Sophie F. Warken[1,2*], Andrea Schröder-Ritzrau[2], Jens Fohlmeister[2], Jennifer Arps[2], Silviu Constantin[3], Mihai Terente[3], Christoph Spötl[4], Axel Gerdes[5], Jan Esper[6], Norbert Frank[2], Augusto Mangini[2] and Denis Scholz[1]

[1] Institute for Geosciences, University of Mainz, Germany

[2] Institute of Environmental Physics, University of Heidelberg, Germany

[3] "Emil Racovita" Institute of Speleology, Bucharest, Romania

[4] Institute of Geology, University of Innsbruck, Austria

[5] Institute of Geosciences, University of Frankfurt, Germany

[6] Department of Geography, University of Mainz, Germany

Abstract Here we present a combined high-resolution trace element and stable isotope record from a speleothem from SW Romania, covering the last 3.6 ka. Age control is based on three independent methods providing a precise age model, in particular for the last 250 years. Correlation analysis of proxy records against instrumental climate data revealed a significant anti-correlation ($r = -0.66$, $p < 0.01$) of speleothem Mg/Ca ratios with regional winter precipitation. This association was used to develop a quantitative reconstruction of winter precipitation for SW Romania. The agreement with other regional rainfall reconstructions during the last three centuries confirms our interpretation and supports the expansion of the precipitation estimates over the last 3.7 ka. Speleothem $\delta^{18}O$ values represent a mixed signal of competing influence of Mediterranean and continental moisture sources, changes in seasonality and temperature variability. $\delta^{13}C$ values are interpreted to reflect variable effects of isotope fractionation under conditions of disequilibrium due to degassing of CO2 and prior calcite precipitation. This record provides a robust qualitative and quantitative climate reconstruction for the realm of SW Romania. The Medieval Climate Anomaly (AD 900 to 1200) was generally more humid than average. The Little Ice Age (AD 1400 and 1700) started with a cool and dry interval from AD 1380 to 1430, followed by wet and probably warmer decades. Subsequently, winter precipitation in SW Romania gradually decreased and reached a minimum at the beginning of the 18th century.

7.1 Introduction

Speleothems are widely used in reconstructing past climate variability on various timescales up to sub-annual resolution (e.g., Wang et al., 2001; Mattey et al., 2008; Fleitmann et al., 2009; Orland et al., 2014; Baker et al., 2015). Speleothem $\delta^{18}O$ values are considered as reliable recorders of the $\delta^{18}O$ values of precipitation and air temperature (see reviews of Fairchild et al., 2006a; Lachniet and Patterson, 2009), but recent research also focuses on the use of elemental proxies (e.g., Treble et al., 2003; Johnson et al., 2006; Fairchild and Treble, 2009; Griffiths et al., 2010; Sinclair et al., 2012; Tan et al., 2014). In some cases, speleothem proxy time series have been successfully calibrated against instrumental data, thus permitting quantitative reconstructions of climate parameters (Proctor et al., 2002; Jex et al., 2011; Tan et al., 2013). However, the relation between climate at the surface and speleothem proxy signals requires a rigorous understanding of the processes involved in the proxy signal transport from the surface into the cave as well as in-cave processes (Mattey et al., 2010; Dreybrodt and Scholz, 2011; Meyer et al., 2014; Casteel and Banner, 2015).

Fast growing laminated stalagmites may provide annual to sub-annual proxy records, which are suitable for calibration and high-resolution climate reconstructions (Johnson et al., 2006; Mattey et al., 2008; Tan et al., 2013; Baker et al., 2015). However, such climate reconstructions are only available from a limited number of locations. In such studies, layer counting has to be cross-validated with absolute dating methods, such as the $^{230}Th/U$-method, to account for missing or double-counted years and hiatuses (Smith et al., 2009; Comboul et al., 2014). The top section of recently growing and active speleothems can also be dated by identifying the mid-20th century radiocarbon bomb peak (e.g., Fohlmeister et al. (2011); Mattey et al. (2008); Rudzka-Phillips et al. (2013); Sundqvist et al. (2013)).

Stable isotopes of oxygen and carbon are the most commonly used proxies in paleo climate reconstructions from speleothems (Lachniet, 2009a). However, trace elements are more and more established climate proxies. Elements such as Mg or Sr are well-understood as hydrological tracers under certain circumstances (Cruz et al., 2007; Fairchild and Treble, 2009). For example, Sinclair et al. (2012) developed a model which allows to investigate the most commonly used interpretation of changes in Mg and Sr as being linked to rainfall as a result of calcite-water interactions such as prior calcite precipitation (PCP).

From the Carpathian realm, few terrestrial Holocene climate records exist despite its important geographical position as a transitional climatic zone between central Europe and the Mediterranean (e.g., Constantin et al., 2007; Feurdean et al., 2008; Rudzka et al., 2012; Onac et al., 2014). Reconstructions based on tree-ring data provide valuable information for the past several hundred years (Popa and Kern, 2008; Levanič et al., 2012), but are limited to the growth season. More recently, guano-derived $\delta^{13}C$-based paleo hydroclimate records made it possible to characterize hydroclimate regimes in south western Romania (Onac et al., 2014, 2015) for the Medieval Climate Anomaly (MCA). The existing stalagmite records mainly reflect past variability of winter climate and suggest that the climate in the Carpathian-

Balkan realm is linked to the North Atlantic region (Onac et al., 2002; Constantin et al., 2007; Drăguşin et al., 2014).

Here we present a high-resolution multi-proxy record based on trace elements and stable isotopes from a laminated stalagmite from southwestern Romania covering the last 3.6 ka. For the past 250 years, the chronology is constructed combining elemental layer counting with ^{230}Th/U-dating and the detection of the radiocarbon bomb peak constituting a solid base for both qualitative and quantitative climate reconstruction.

7.2 Material and methods

7.2.1 Study location

Cloşani Cave (45.07 °N, 22.80 °E) is located in southwestern Romania at the southern slope of the Carpathians at 433 m above sea level (a.s.l., Figure 7.1 A and B). The regional climate is characterized by westerly circulation and the influence of the Carpathian mountain topography (Busuioc et al., 2014; Ionita et al., 2014; Micu et al., 2015). Annual precipitation shows two maxima, one from April to June, which is mainly caused by North Atlantic cyclones, and a smaller one between October and December, generated by cyclones originating from the

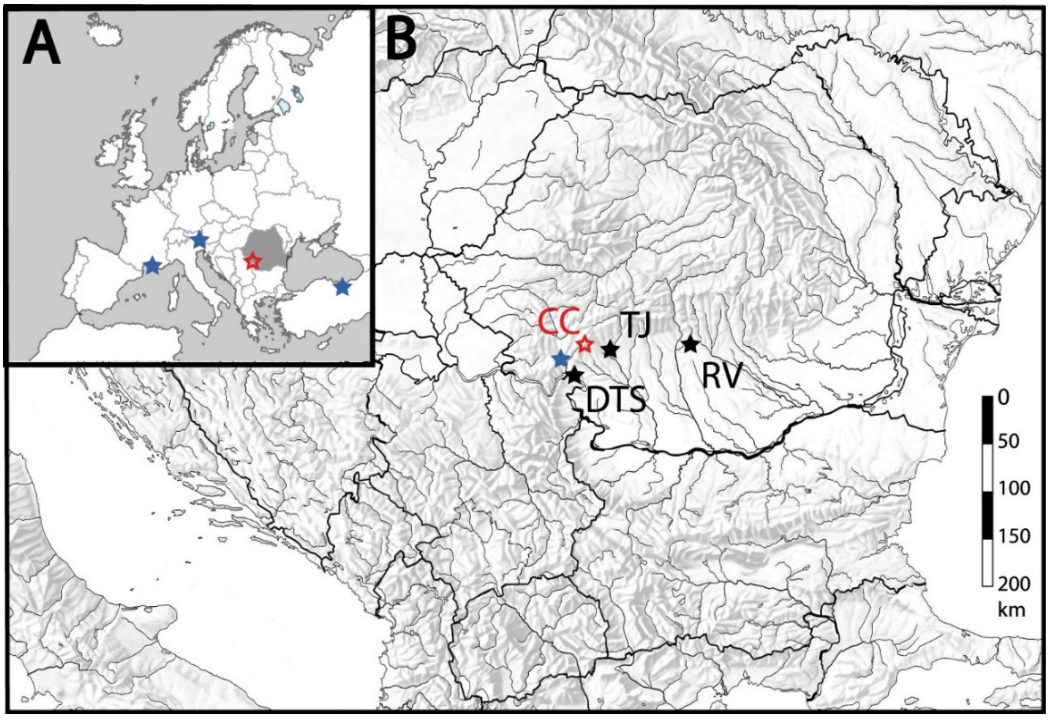

Figure 7.1: *Location of Cloşani Cave (CC, red star). Blue stars indicate other relevant records: (A) Gümüşhane, NE Turkey (Jex et al., 2011), Spannagel cave, Austria (Fohlmeister et al., 2013); marine sediment core PB-09, Gulf of Lions (Sabatier et al., 2012). (B) Blue star: Băile Herculane (Levanič et al., 2012). Black stars: Weather stations Targu Jiu (TJ) and Drobeta/Tr. Severin (DTS) and GNIP station Râmnicu Vâlcea (RV).*

western and central Mediterranean Basin. The winter continental air flows, usually dry and cold, originate in the Arctic Ocean, whereas continental air masses from eastern Eurasia and north Africa or southwest Asia frequently influence the summer precipitation regime with usually very warm and dry spells (Micu et al., 2015). Cloşani Cave is developed in massive Upper Jurassic limestone mainly consisting of calcite (93 %) with minor occurrence of dolomite (7 %) (Diaconu, 1990; Constantin, 2003). The cave consists of two main passages with a total length of 1,458 m (Figure 7.2 A). At the position of the stalagmite the hostrock overburden is approx. 80 - 100 m (Diaconu, 1990; Constantin and Lauritzen, 1998) and overlain by a soil layer of up to 1.5 m thickness. The area is densely covered by vegetation consisting of grasses, shrubs and trees.

7.2.2 Sample description

Stalagmite C09-2 was fed by dripwater at the time of removal in 2009. The specimen (Figure 7.2 B) has a total length of 70 cm and a diameter of 7-8 cm. The stalagmite was cut in two halves along its growth axis, and a slab was prepared. One half of the slab was used to sample for ^{230}Th/U-dating and ^{14}C-analyses, whereas sampling for stable isotopes and trace element measurements was performed on the opposite half. The focus of this study is on the upper 46 cm, which are composed of clean, translucent calcite. This section exhibits frequent, both macroscopically (Figure 7.2 C) and microscopically (Figure 7.2 D) visible lamination with alternating translucent and whitish layers. Stalagmite C09-2 was collected beneath drip site CC2 (Figure 7.2 A) about 160 m from the cave entrance in the deeper part of the cave, which is characterized by a stable cave environment.

7.2.3 Methods

^{230}Th/U-analysis was performed using multi-collector inductively coupled mass spectrometry (MC-ICPMS) at the Institute of Environmental Physics, Heidelberg. Samples for radiocarbon dating were analysed with the MICADAS facility (Synal et al., 2007) operated at the Klaus-Tschira-Facility (Mannheim, Germany). Stable carbon and oxygen isotope analysis was performed using an on-line, automated carbonate preparation system linked to a triple collector gas source mass spectrometer at the University of Innsbruck. Concentrations of trace elements were measured along the major growth axis of C09-2 by laser ablation MC-ICPMS at Goethe University Frankfurt, Germany.

Drip water and cave air parameters are monitored in Cloşani Cave since 2010 (Constantin et al., unpublished data). Instrumental data (data downloaded from www.ecad.eu, Klein Tank et al. (2002)) were taken from the weather stations Targu Jiu (TJ, 203 m a.s.l., mean annual temperature MAT: 10.6 °C, mean annual total precipitation MTP: 786 mm (1961 - 1990)) and Drobeta/Turnu Severin (DTS, 77 m a.s.l., MAT: 11.6 °C, MTP: 686 mm), located about 50 km from Cloşani Cave (Figure 7.1 B). TJ provides a long-term record of monthly mean precipitation P (1918 - 2000) and monthly mean temperature T (1900 - 1993), whereas DTS covers

P from 1925 - 2015 and T from 2006 - 2015. $\delta^{18}O$ values of meteoric precipitation ($\delta^{18}O_p$) are available for the years 2012 - 2014 from the GNIP station Râmnicu Vâlcea (RV, 237 m a.s.l., MAT 10.3 °C, MTP 699 mm, Global Network of Isotopes in Precipitation, accessible at: http://www.iaea.org/water). The climate diagrams of the weather stations are summarized in Figure 7.3.

Correlation analysis was performed with a statistic test based on Pearson's product moment correlation coefficient r (x,y) and follows a t-distribution with length (x-2) degrees of freedom. Asymptotic confidence intervals are given based on Fisher's Z transform. If necessary, p-values are adjusted for autocorrelation following Zwiers and von Storch (1995). The statistics of the given correlation coefficients is shown in the supplemental material. For further correlations tests (section 7.3.4), we also used the software 'PearsonT3' (Ólafsdóttir and Mudelsee, 2014) to calculate correlation coefficients and corresponding bootstrap confidence intervals that are also valid in the presence of autocorrelation.

Detailed information about cave monitoring, sample preparation, analytical procedures and data reduction is given in the supplementary material (Appendix C).

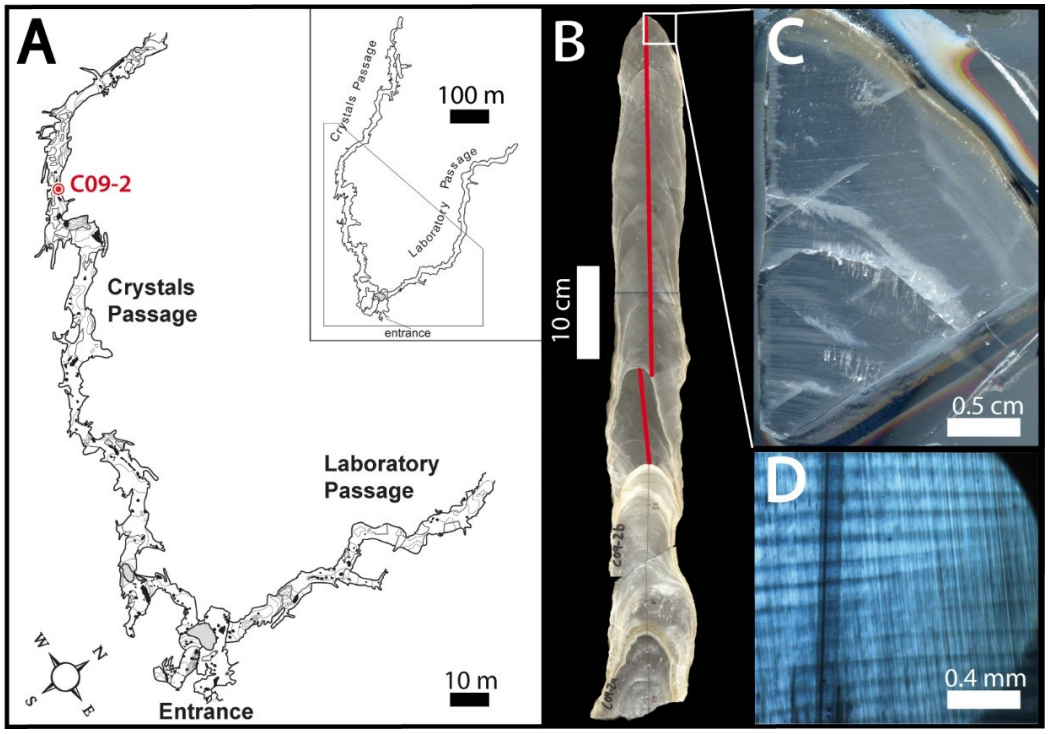

Figure 7.2: *(A) Location of stalagmite C09-2 in Cloşani Cave prior to removal in 2009. The cave map has been modified after Constantin (2003). (B) Scan of stalagmite C09-2. This study focuses on the upper 46 cm of the sample (track of proxy analyses indicated with red line). (C) Example of a slab used for LA-ICPMS measurements. (D) Microscopic view of the lamination of C09-2*

7.3 Results

7.3.1 Radiometric dating

Eleven ^{230}Th/U ages were determined in the upper 46 cm of the stalagmite, which formed during the last 3.7 ka (Figure 7.6 A and Table 7.2). The ^{238}U content of the stalagmite is generally low (on average about 40-50 ng/g), and ^{232}Th is below 50 pg/g in most samples. Relative errors of the final ages range from 1.5 to 3 % for the ages older than 600 years. The uncertainties of the younger samples are between 3 and 5 % due to the extremely low ^{230}Th content which is in the order of 5-10 fg/g.

^{14}C measurements reveal a strong increase in radiocarbon in the uppermost 5 mm dft (Table 7.1 and Figure 7.4). The rise of the ^{14}C activity is interpreted as the start of the mid-20th century atmospheric bomb peak recorded by the stalagmite. All published radiocarbon bomb spikes in speleothems show that the response of speleothem ^{14}C activity to the increase in atmospheric radiocarbon activity occurs nearly simultaneously (Fohlmeister et al., 2011; Mattey et al., 2008; Rudzka-Phillips et al., 2013; Sundqvist et al., 2013). Therefore, the timing was established by identifying the last sample corresponding to the radiocarbon plateau of the early 20th century (sample I in Figure 7.4). This sets the reference point for all other measurements to the year 1955 AD at 3.2 mm dft.

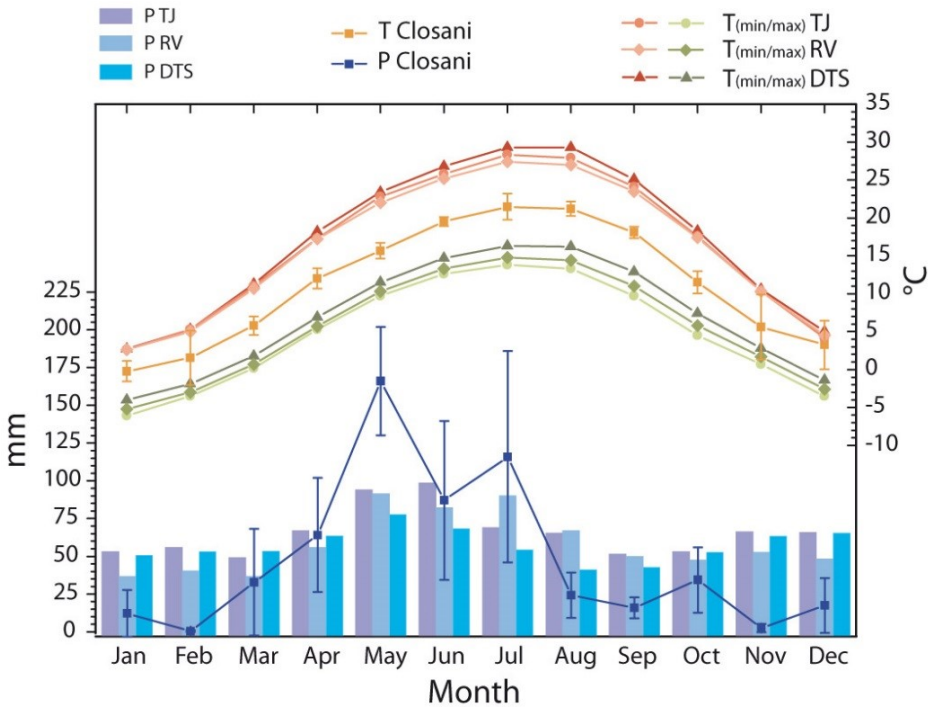

Figure 7.3: *Comparison of monthly means of precipitation amount P and temperature T: Instrumental precipitation data (blue bars) and monthly mean minimum/maximum T (green/red lines) from the stations DTS, TJ and RV displayed as mean values (1961 - 1990). Data from Cloşani Cave (Constantin et al., unpublished data) are summarized from the years 2011 - 2016.*

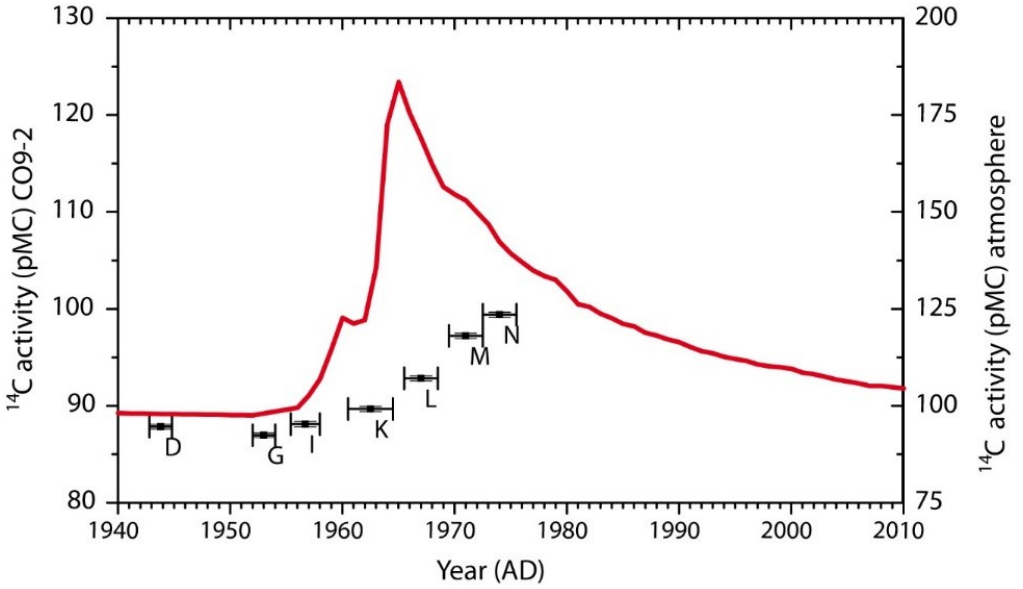

Figure 7.4: *^{14}C activity measured in C09-2 calcite (black points) and atmospheric radiocarbon bomb peak (Levin et al., 2010). Note the different scales of the two vertical axes.*

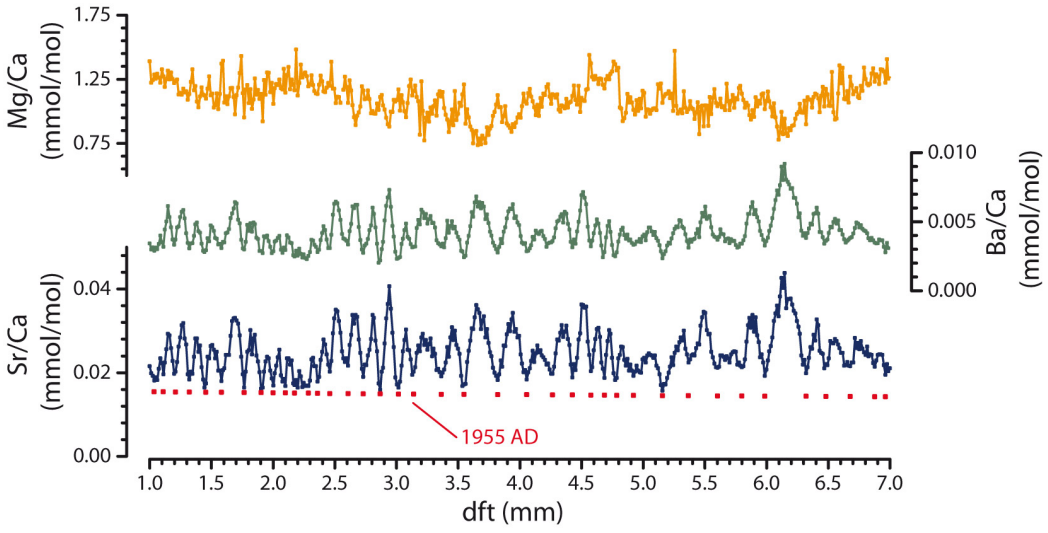

Figure 7.5: *Top segment (1 to 7 mm dft) of the raw trace element ratios of C09-2, with Sr/Ca_c (blue), Ba/Ca_c (green) and Mg/Ca_c (orange) ratios. Red points: minima allocated to summer conditions. The reference point (AD 1955) is indicated at 3.2 mm dft.*

7.3.2 Layer counting and age model

On annual to sub-annual scale, $Sr/Ca_{c(alcite)}$ and Ba/Ca_c ratios show alternating minima and maxima, which are pronounced nearly throughout the record (Figure 7.5). A periodic signal is continuously visible in Sr/Ca_c and Ba/Ca_c, whereas Mg/Ca_c only shows partly anti-phased extreme values compared to the other element to Ca ratios (e.g. between 3.2 and 4.5 mm dft). Minima are characterized by sharp peaks, whereas maxima have a variable but generally wider width. Monitoring of the drip site and cave air parameters suggests, that the observed cycles in Sr and Ba are the result of seasonal variability in calcite precipitation rates and represent annual layers (section 7.3.3, discussion 7.4.1 and supplementary material). Thus, we use the sharp minima in Sr/Ca_c to define annual elemental layers which were manually counted. This routine was repeated independently and yielded n = 10 time series. Each series was anchored to the reference point of the year 1955 AD at 3.2 mm dft. The distribution of the resulting chronologies enables the estimation of the uncertainties of layer counting and the calculation of the most probable age model (Figure 7.6 A). For the upper 47 mm dft, the uncertainty of all chronologies is very small (216 ± 3 counted minima). For the 20th century, the uncertainty of the layer counting is about ± 1 year. Thus, the total uncertainties of this part amount to ± 3 years, taking into account the error of allocating the start of the ^{14}C increase in the stalagmite (± 2 years). The combination of layer counting and radiocarbon dating yields a precise age model for the period from 1759 to 1973 AD, which is in good agreement with the uppermost $^{230}Th/U$-age (1836 ± 20 AD at 35 mm) (Figure 7.6 A). The final age model (Figure 7.6 B) is divided into two parts, with the layer counted part representing the upper 47 mm. Below, the age model is constructed with the $^{230}Th/U$-ages using the R-package 'Bchron' (Haslett and Parnell, 2008).

Table 7.1: *Results of radiocarbon measurements. Errors are given as 1σ range. Absolute age errors are estimated to ± 2 years mainly due to uncertainties in the allocation of the exact depth of the start of the ^{14}C increase in the stalagmite.*

Lab. No.	Label	dft (mm)	a^{14}C (pmC)	error (pmC)	age (AD)
MAMS 11688	C09-2 N	1.2	99.39	0.27	1972
MAMS 11687	C09-2 M	1.6	97.21	0.25	1969
MAMS 11686	C09-2 L	2	92.83	0.25	1965
MAMS 11685	C09-2 K	2.4	89.67	0.25	1961
MAMS 11669	C09-2 I	3.2	88.11	0.28	1955
MAMS 11682	C09-2 G	4	86.96	0.24	1951
MAMS 11668	C09-2 D	5.2	87.84	0.27	1942

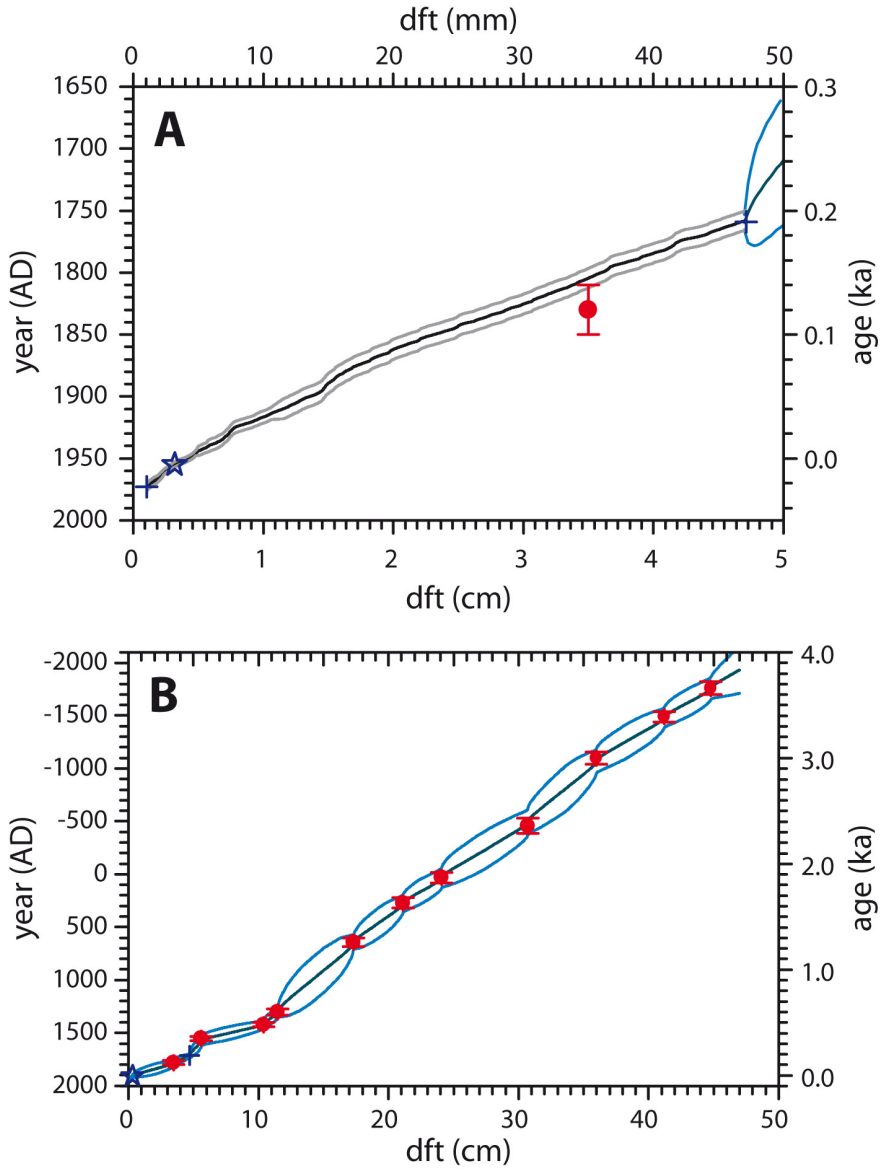

Figure 7.6: *Age model of C09-2. (A) Age models for the top 50 mm. Black: age model obtained from layer counting (grey: 2σ SD including the ±2 years uncertainty of the radiocarbon dating); cyan: age model obtained from Bchron (Haslett and Parnell, 2008) (light blue: 2σ SD). (B) Age model and 2σ SD obtained with Bchron for C09-2. Symbols in (A) and (B): blue star: position of the reference point (3.2 mm, AD 1955); blue crosses: positions of the start and end points of the layer counting; red points:* ^{230}*Th/U ages.*

Table 7.2: *Activity ratios and ^{230}Th/U-ages for stalagmite C09-2. Uncertainties are given as 2σ range. Ages are quoted relative to AD 1950.*

Lab. No.	Sample ID	dft (cm)	^{238}U (ng/g)	^{232}Th (ng/g)	^{230}Th/^{238}U Act.ratio	^{230}Th/^{232}Th Act.ratio	^{234}U/^{238}U Act.ratio	Age (uncorr.) (ka)	Age (corr.) (ka)
7686	C09-2-3.5	3.5	42.098 ± 0.005	0.0273 ± 0.0001	0.0026 ± 0.0002	12.31 ± 0.91	1.448 ± 0.001	0.13 ± 0.01	0.12 ± 0.02
7687	C09-2-5.6	5.6	45.524 ± 0.008	0.0188 ± 0.0001	0.0056 ± 0.0003	41.86 ± 2.38	1.445 ± 0.002	0.36 ± 0.02	0.35 ± 0.02
7688	C09-2-10.4	10.4	57.975 ± 0.007	0.0287 ± 0.0001	0.0072 ± 0.0003	44.20 ± 1.52	1.416 ± 0.001	0.49 ± 0.02	0.48 ± 0.02
7689	C09-2-11.5	11.5	52.899 ± 0.006	0.0470 ± 0.0002	0.0090 ± 0.0003	30.90 ± 1.04	1.428 ± 0.002	0.62 ± 0.02	0.60 ± 0.03
7690	C09-2-17.3	17.3	44.216 ± 0.010	0.0212 ± 0.0001	0.0174 ± 0.0005	111.2 ± 3.1	1.431 ± 0.002	1.27 ± 0.04	1.26 ± 0.04
7691	C09-2-21.1	21.1	49.798 ± 0.015	0.0800 ± 0.0003	0.0226 ± 0.0006	43.05 ± 1.09	1.434 ± 0.002	1.66 ± 0.04	1.63 ± 0.05
7692	C09-2-24.1	24.1	49.132 ± 0.017	0.0138 ± 0.0001	0.0256 ± 0.0007	280.0 ± 7.8	1.451 ± 0.003	1.88 ± 0.05	1.87 ± 0.05
7693	C09-2-30.7	30.7	51.666 ± 0.018	n.d.	0.0315 ± 0.0009	n.d.	1.429 ± 0.002	2.36 ± 0.07	2.36 ± 0.07
7694	C09-2-36.0	36.0	54.847 ± 0.015	n.d.	0.0400 ± 0.0008	n.d.	1.439 ± 0.002	3.00 ± 0.06	3.00 ± 0.06
7695	C09-2-41.2	41.2	48.417 ± 0.009	0.0495 ± 0.0001	0.0446 ± 0.0007	134.0 ± 2.0	1.423 ± 0.001	3.41 ± 0.05	3.39 ± 0.05
7696	C09-2-44.8	44.8	44.231 ± 0.010	n.d.	0.0471 ± 0.0007	n.d.	1.401 ± 0.002	3.66 ± 0.06	3.66 ± 0.06

7.3.3 Data

Climate parameter

The weather stations TJ and DTS were chosen, because both are located at the southern slope of the Carpathian mountain chain and are thus the closest stations with the longest overlap with the speleothem proxy data. The comparison of MATs with mean cave temperature (11.4 ± 0.5 °C) show that the weather station data are representative for the cave site. Figure 7.3 shows the measured outside air temperature and precipitation at the cave site in comparison with the instrumental data from the weather stations TJ, DTS and RV, averaged for the period 1961 - 1990. Measured temperatures at the cave site are well between the averaged mean monthly minimum and maximum temperatures of all stations. Winter temperatures at Cloşani tend to slightly higher values than observed at the other stations. Due to infrequent system malfunctions of weather monitoring equipment at Cloşani Cave, precipitation could not be recorded continuously, so interpretation of this time series is limited, which is visible in the large error bars. The seasonal cycle follows the observed pattern in the long-term record of the weather stations. Annual (570 ± 310 mm) and monthly totals are in agreement with the station data with respect to the large error bars.

Since weather data are only sparsely available for the cave site and no $\delta^{18}O_p$ values of meteoric precipitation were analyzed, the dripwater data are compared to the available data sets from the weather stations. Potential evapotranspiration (PET) was calculated by applying the formula of Thornthwaite (1948) to the station data in order to estimate monthly infiltration. The estimation of PET reveals, that during the summer months infiltration may only amount to about 0 to 25% of precipitation, whereas winter precipitation contributes to 75 to 100 % to the infiltrating water mass.

$\delta^{18}O_p$ values of meteoric precipitation from 2012 to 2014 (RV) range from -16 ‰ in winter to -3 ‰ in summer. The correlation between temperature on monthly scale and $\delta^{18}O_p$ at RV is very high ($r_{T/\delta^{18}O_p} = 0.86$, 0 = 32, $p < 0.1$ (adjusted)). Drip water $\delta^{18}O$ values at Cloşani Cave do not exhibit a clear seasonal pattern with a mean value of -9.81 ± 0.37 ‰ (min. -9.35 ‰, max. -10.03 ‰, Figure 7.7).

However, the estimated infiltration-weighted annual mean in precipitation at RV calculated following Wackerbarth et al. (2010), $\delta^{18}O_{inf} = -10.9 \pm 1.6$ ‰, is in the range of the mean dripwater $\delta^{18}O$ value. The difference of the two values could be explained by the different mean annual temperatures of the cave site and station RV ($\Delta T = 1.1$ °C). Calculation of the slope $d(\delta^{18}O_p)/dT$ at station RV yields a value of 0.45 ‰°C^{-1}, resulting in $\Delta(\delta^{18}O_p) = 0.5$‰ and shifting $\delta^{18}O_{inf}$ towards higher values.

Cave and drip characteristics

Cave temperature shows a mean value of 11.4 °C with inter-annual variations of ±0.5 °C. Relative humidity is close to 100 %. Figure 7.7 shows the monitored long-term cave air and dripwater parameters at drip site CC2, corresponding to stalagmite C09-2. The pCO_2 of the

cave air shows a strong annual variability with maximum values of up to 8800 ppm in late summer and minimum values in winter and spring (1000 ppm) following the seasonal outside temperature cycle. The pH values of the dripwater and the calculated saturation indices also share this seasonal signal with highest values during the cold season, showing that calcite precipitation is favored in winter (Figure 7.7). Ca-content of the dripwater varies around 2.2 mmol/l and exhibits a less pronounced seasonal signal, as well as the Sr/Ca_w and Mg/Ca_w ratios of the dripwater.

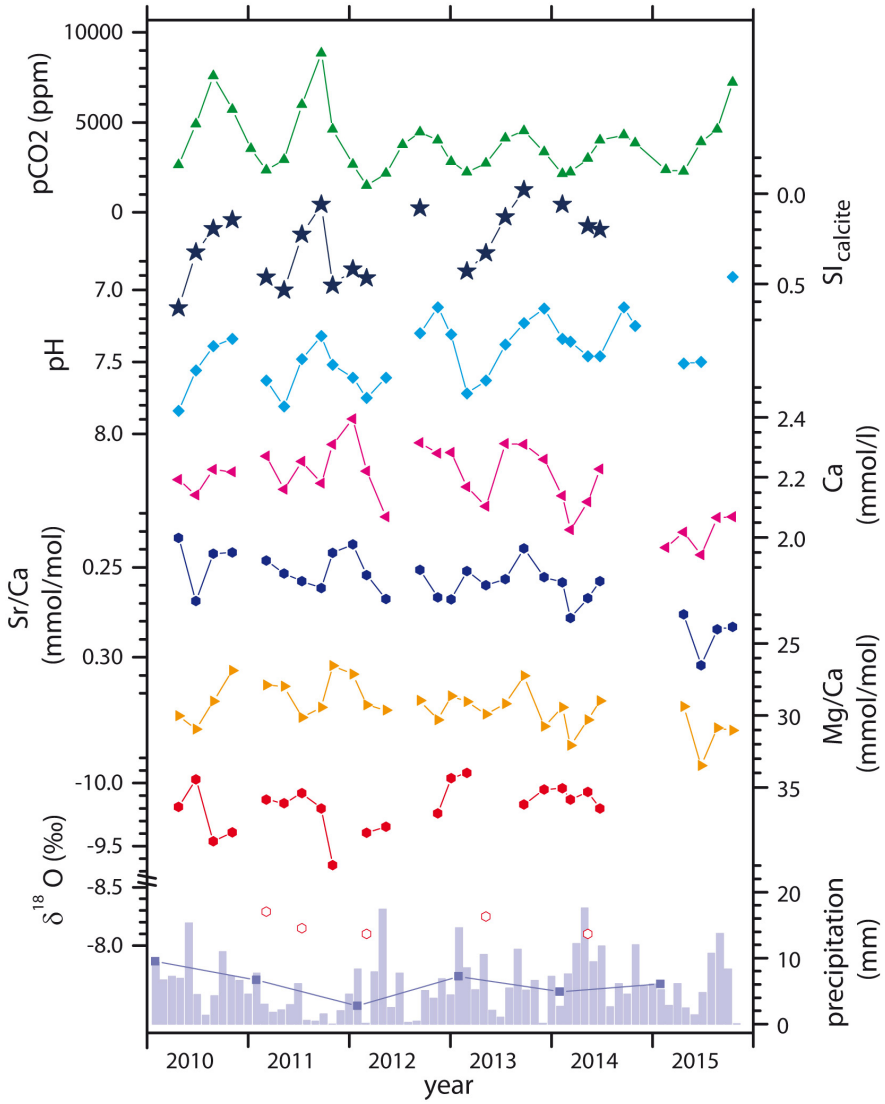

Figure 7.7: *Cave air and dripwater monitoring in Cloşani Cave for drip site CC2 for the years 2010 to 2015 (Constantin et al., unpublished data). pCO_2 (green), SI (dark blue stars) and pH (light blue) show a pronounced seasonal signal, which is reflected in Ca content (magenta) and also weakly visible in Sr/Ca_w (dark blue dots), Mg/Ca_w (orange) and $\delta^{18}O_{dripwater}$ (red filled symbols, axis inverted). The variability in $\delta^{18}O_{dripwater}$ is strongly muted in $\delta^{18}O_{calcite}$ (red open symbols). Light blue bars indicate monthly precipitation at Cloşani Cave, dark blue squares the mean value of the months October to March.*

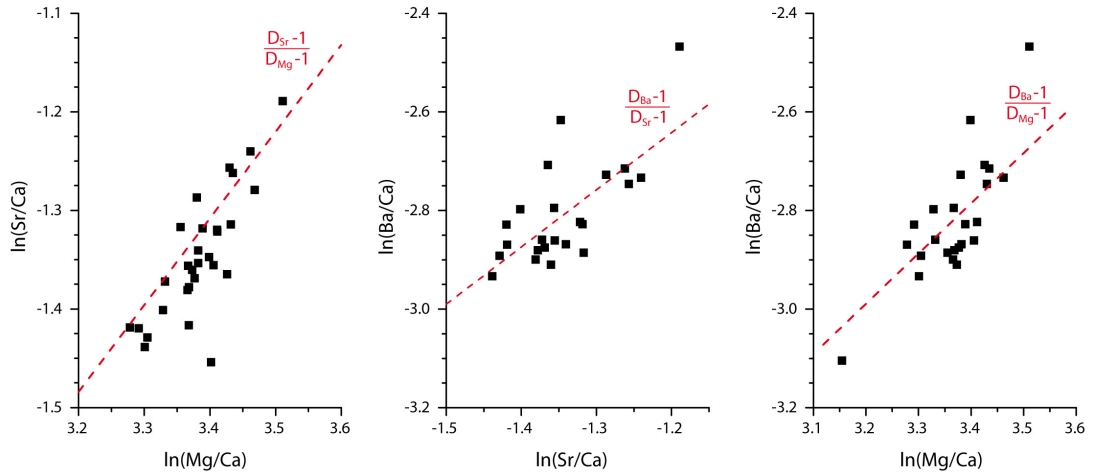

Figure 7.8: *Cross plots of dripwater ratios of ln(Sr/Ca$_w$) vs. ln(Mg/Ca$_w$) (left), ln(Ba/Ca$_w$) vs. ln(Sr/Ca$_w$) (middle) and ln(Ba/Ca$_w$) vs. ln(Mg/Ca$_w$) (right). The red lines indicate the theoretically expected slopes for PCP and/or ICD after Sinclair et al. (2012) calculated with the corresponding partition coefficients.*

The drip rate at site CC2 was constant throughout the monitoring period (0.5 drips/min). The drip is fed by a stalactite and during the monitoring period only little calcite precipitation was observed - much less than expected from the observed growth rates in C09-2. Mg/Ca$_{dripwater}$, Sr/Ca$_{dripwater}$ and Ba/Ca$_{dripwater}$ (the latter not shown in Figure 7.7) exhibit only small variations. However, the cross-plots of the logarithmic trace element to calcium ratios after Sinclair et al. 2012 (Figure 7.8) show, that the values in the dripwater follow the theoretically expected slopes for the presence of prior calcite precipitation (PCP) and/or incongruent calcite dissolution (ICD). The slopes were calculated using the partition coefficients D_{Mg} = 0.019, D_{Sr} = 0.15 (both Huang and Fairchild, 2001) and D_{Ba} = 0.012 (Tesoriero and Pankow, 1996).

In general, dripwater and cave air parameters show no direct connection with monthly precipitation amount (light blue bars). However, the long-term trend in mean winter precipitation (ONDJFM) is similar to the (inverted) long-term variability of Sr/Ca, Mg/Ca and $\delta^{18}O$ (Figure 7.7).

Speleothem proxy variability

From 1700 BC to ~ 1400 AD, $\delta^{18}O$ values vary around a mean value of about -8 ‰ (Figure 7.9). Afterwards, the signal decreases by about -0.5 ‰ and remains at its modern level of about -8.5 ‰. $\delta^{13}C$ values show a different pattern, with a distinct feature being the interval between 1300 AD and 1650 AD, where the $\delta^{13}C$ signal rises by about 0.5 to 1 ‰ to values of -10.5 to -10 ‰. Regarding the whole record, $\delta^{18}O$ and $\delta^{13}C$ values exhibit a weak negative correlation ($r_{\delta^{13}C/\delta^{18}O}$ = -0.31).

Superposed on the annual variability, the element to Ca ratios show a generally stable signal with mean values of about 1.2 mmol/mol for Mg/Ca$_c$, 0.025 mmol/mol for Sr/Ca$_c$ and

0.005 mmol/mol of Ba/Ca_c. Sr/Ca_c and Ba/Ca_c ratios share a similar long-term pattern ($r_{Sr/Ba}$ = 0.96, statistics of correlation coefficients given in this section are summarized in Table C.1 in supplementary material) whereas Mg/Ca_c ratios follow a different pattern with negative correlation to Sr and Ba ($r_{Mg/Sr}$ = -0.45 and $r_{Mg/Ba}$ = -0.46) (Figure 7.10) .

Between 1700 BC to 1400 AD C09-2 grew with a mean rate of about 100 µm/yr, with several short excursions of apparently slow growth of about 1 mm length, indicated by poor lamination, low Sr/Ca_c, high Mg/Ca_c and partially low $\delta^{13}C$ values (sections indicated in Figure 7.9). Taken as a whole, the centuries after 1400 AD until ~ 1680 AD are characterized by faster growth of about 200 µm/yr with one distinct period of poor lamination (slow growth) around 1600 AD. The same is visible between 1680 and 1760 AD, which deposited in only 5 mm total distance, indicating growth rates of about only 50 µm/yr. For the period from 1759 to 1973 AD, the distance between the counted Sr/Ca_c minima is defined as total layer width (equatable to mean annual mean growth rate). It varies between 50 and 600 µm with a mean value of 210 µm (Figure 7.10). Since the elemental layers are not continuously developed in C09-2, continuous layer counting is not possible beyond 1759 AD. Between AD 1759 and 1974, annual mean growth rate shows a strong correlation to the annual mean element to Ca ratios ($r_{gr/Mg}$ = -0.67, $r_{gr/Sr}$ = 0.57 and $r_{gr/Ba}$ = 0.61). In this part, the correlation of Sr and Ba persists,

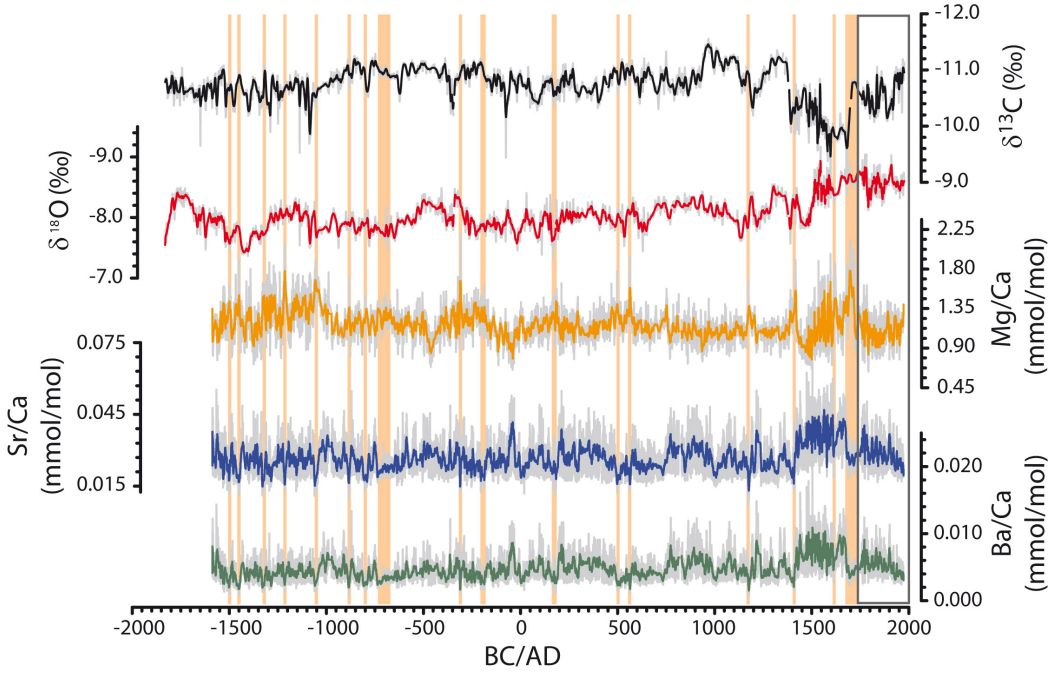

Figure 7.9: *C09-2 proxy records, with Ba/Ca_c (green), Sr/Ca_c (blue) and Mg/Ca_c (orange) ratios and stable carbon (black) and oxygen (red) values (note the inverted axes of the stable isotopes). Total record from 2000 yrs BC with the raw time series (light grey lines) and 10p-running means (RM, colored lines) of the stable isotope values. Element to Ca ratios are displayed as 5p RM (light grey lines) and 50p RM (colored lines). Short-term sections of poor lamination, low Sr/Ca_c, high Mg/Ca_c and partially low $\delta^{13}C$ values which indicate slow speleothem growth are highlighted with light orange vertical bars.*

whereas it is weaker for Mg to Sr and Ba ($r_{Sr/Ba}$ = 0.95, $r_{Mg/Ba}$ = -0.32 and $r_{Mg/Sr}$ = -0.32, outlier corrected raw data).

Whereas growth rate, Sr/Ca_c and Ba/Ca_c ratios are positively connected to $\delta^{13}C$ values ($r_{gr/\delta^{13}C}$ = 0.31, $r_{\delta^{13}C/Sr}$ = 0.33, $r_{\delta^{13}C/Ba}$ = 0.33), the relationship of the elemental proxies to the $\delta^{18}O$ record is negative ($r_{\delta^{18}O/Sr}$ = -0.29, $r_{\delta^{18}O/Ba}$ = -0.32). All correlation coefficients are significant to the 95 % interval.

7.3.4 Correlation analysis with instrumental data

The overlap between the stalagmite proxy records and the instrumental records of precipitation (1918 to 1973, n = 55) and temperature (1901 to 1973, n = 69) was used to infer potential connections between the climate parameters and the speleothem proxies. Due to the main contribution of winter precipitation to infiltration (section 7.3.3), the winter months October to March were chosen for further analysis and in the following labeled as the winter precipitation and temperature time series P_w and T_w. Similar to Jex et al. (2011), the precipitation time series P_w were smoothed with a 5-point linear weighted running mean to account for the mixing of the precipitation information of the previous years in the host rock (P_{lin}).

Due to the lower temporal resolution of the $\delta^{13}C$ and $\delta^{18}O$ values of up to 3 years per sample point, the overlapping period with instrumental data is too short to compute reliable

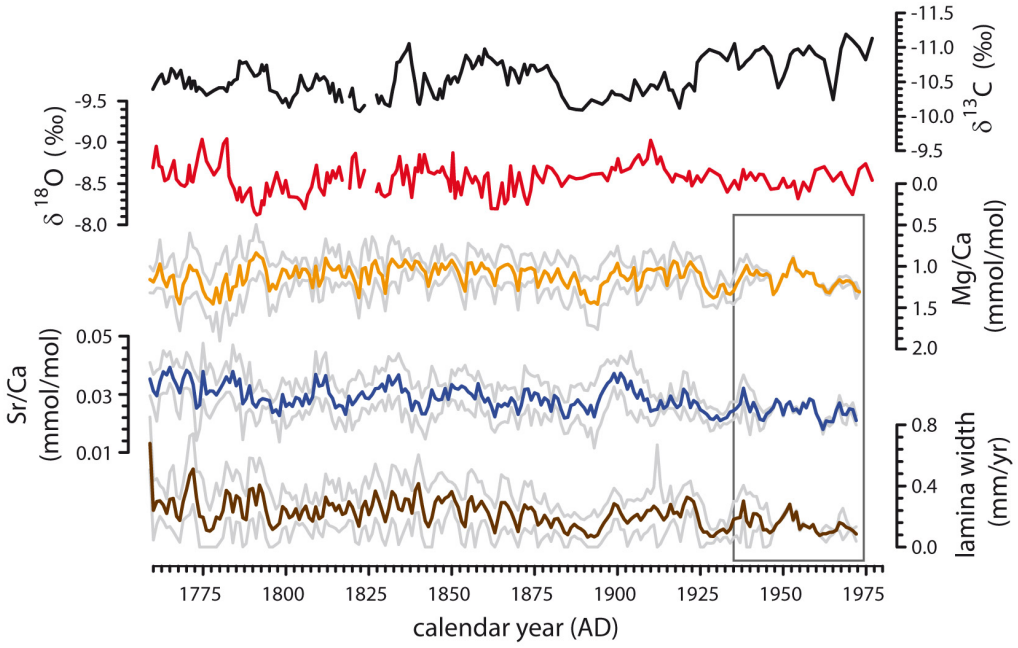

Figure 7.10: *Uppermost section of C09-2 proxy records, based on layer counted age control (AD 1759 to 1974). Stable carbon (black) and oxygen (red) values are displayed with inverted axes. Mg/Ca_c (orange, axis inverted), Sr/Ca_c ratios (blue) and lamina width (brown) are shown as annual mean values with the grey lines indicating the 95 % confidence bands due to the variance of the layer counting (section 7.3.2). The grey rectangle shows the section which is shown in Figure 7.5.*

quantitative correlations. Thus, the comparison remains qualitative. The multi-annual $\delta^{18}O$ variability seems to be mainly related to T_w (Figure 7.11) with a minor dependence on P_w. In contrast, the $\delta^{13}C$ values only show weak relationships with T_w and P_w.

In order to account for autocorrelation which origins from the smoothing of the climate signal in the karst aquifer, the following correlation coefficients are computed with PearsonT3 (Ólafsdóttir and Mudelsee, 2014). The best correlation was found for Mg/Ca_c ratios, revealing a high anti-correlation with winter precipitation P_w (October to March) with $r_{Mg/P} = -0.42$ [-0.61, -0.19]. This correlation increases to $r_{Mg/P\_lin} = -0.58$ [-0.85, -0.08] for the 5-point linear weighted running mean $P_{w,lin}$ (Figure 7.12). Detrending of both time series increases the

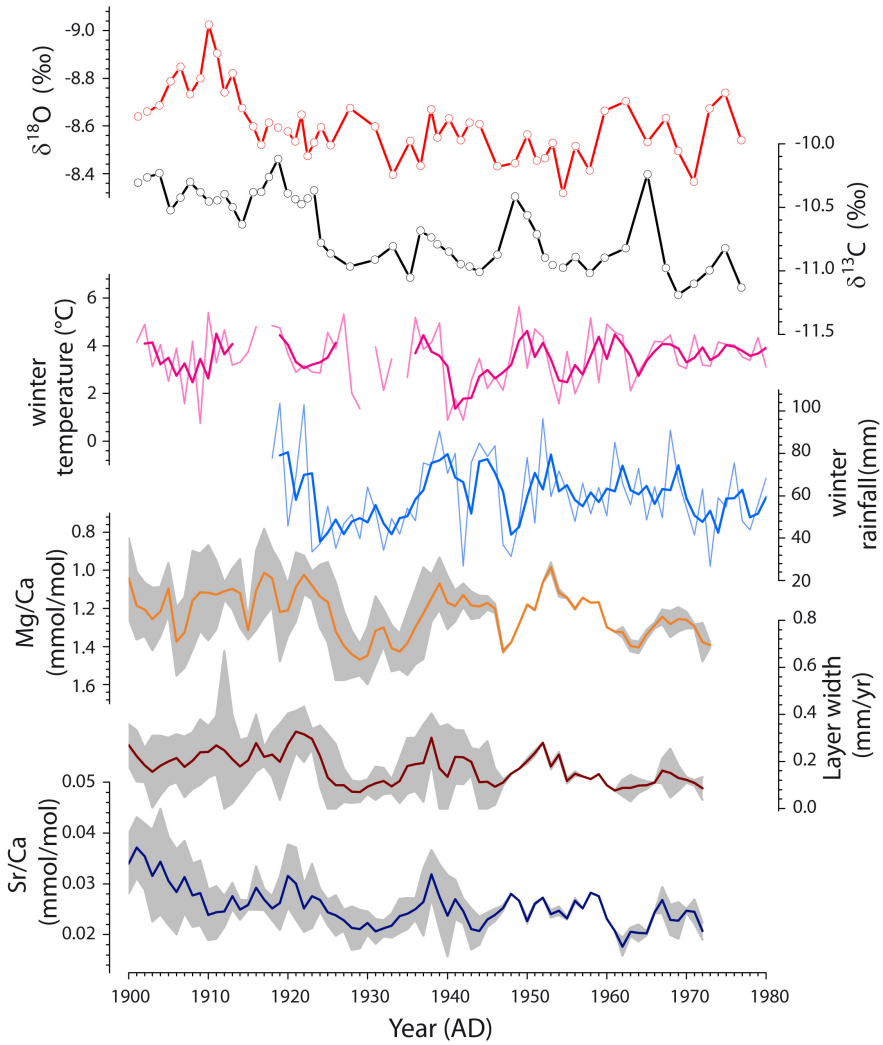

Figure 7.11: *Instrumental and proxy data for the 20th century. From bottom to top: Annual mean Sr/Ca ratio (dark blue, grey shading: 2 SD uncertainty due to layer counting); annual mean layer width (brown); annual mean Mg/Ca (orange); winter precipitation P_w (light blue, linear 5pRM P_{lin} thick blue line); winter temperature T_w(light purple) and 5p RM (purple); $\delta^{13}C$ values (black) and $\delta^{18}O$ values (red). Note the inverted axis for Mg/Ca ratios.*

correlation slightly to r_{Mg/P_lin} = -0.61 [-0.86, -0.12] (Figure 7.12). Mean annual growth rates are also connected with winter precipitation variability (r_{gr/P_lin} = 0.37 [0.01, 0.64]). The confidence intervals of all other cross-correlations are too large to infer significant correlations (Table C.2 in supplementary material).

Regarding the age uncertainties, the significance of $r_{Mg/P}$ is further tested. Taking into account the uncertainty of the layer counting and the allocation of the reference years the uncertainty of age control accounts to ± 3 years (section 7.3.2). Therefore, a Monte Carlo (MC) routine is applied which simulates 1000 cross-correlations $r_{Mg/P}$ by shifting every layer counted age model (n = 10, section 7.3.2) within the age uncertainties and calculating the corresponding correlation coefficient. The routine was repeated 1000 times to get a robust result. The calculation of the mean of the simulated correlation coefficients $r_{Mg/P}$ is based on Fisher's Z transform. The MC ensemble of Mg/Ca time series was also used to calculate the uncertainty of Mg/Ca due to age uncertainties, which is displayed as orange bands in Figure 7.12. This approach was developed similar to the model of Dee et al. (2015), who incorporate age uncertainties in the proxy signal by means of ensemble-based age models.

It is to note, that the probabilities of the directions of the shift are not equal. A shift by -3 years changes the reference point to AD 1952, which would imply that the speleothem would have reacted unusually fast. The allocation of radiocarbon sample 'K' (Figure 7.4), which clearly shows a rise in ^{14}C activity in speleothem calcite, to the year AD 1958 would result in a response time of the speleothem to the atmospheric rise in ^{14}C activity of less than 2 years, as the first year of significant atmospheric increase is AD 1956. Thus, the probability distribution of the shift is not symmetric (Figure C.1). The calculated overall mean value is $r_{Mg/P}$ = -0.46 ± 0.14, which is still significant at an p-value of 0.1 (corrected for autocorrelation).

7.3.5 Regression analysis

In order to get a quantitative estimate of past winter precipitation, the robust correlation with Mg/Ca_c provides the basis for a regression analysis. The reconstruction is performed fitting a linear regression model $P_{rec} = a \cdot Mg/Ca_c + c$ to the 5-yr linear weighted running mean to predict precipitation from the $Mg/Ca_{Mg/Ca}$ value in the speleothem. The resulting regression equation is

$$P_{rec} = (-62 \pm 12) \cdot Mg/Ca_c + (130 \pm 14) \tag{7.1}$$

The uncertainties $\Delta(P_{rec})$ of the reconstructed estimate P_{rec} are based on the calculated prediction intervals of the regression $\Delta(P_{rec})_{pred}$. However, the uncertainty of the age control of the Mg/Ca_c ratio also has to be taken into account. Therefore, the ensemble-based age uncertainty of Mg/Ca_c is taken into account with

$$\Delta(P_{rec})_{age} = \frac{\partial P_{rec}}{\partial(Mg/Ca_c)} \Delta(Mg/Ca_c) = (62 \pm 12) \cdot \Delta(Mg/Ca_c) \tag{7.2}$$

These uncertainties are then added to the prediction intervals from the regression analysis:

$$\Delta(P_{rec}) = \Delta(P_{rec})_{pred} + \Delta(P_{rec})_{age} \tag{7.3}$$

Figure 7.13 shows, that these uncertainties do not substantially increase the error band for the common period, however, they may become significant for the older parts with higher age errors. The reconstructed precipitation amount P_{rec} explains 34 % of the variance of P_{lin} ($r^2 = 0.34$). The original values of P_w and P_{lin} are well within the estimated uncertainty bands (Figure 7.13).

The validity of the winter precipitation reconstruction was further assessed by applying a split calibration/verification approach on the instrumental and proxy data (Fritts, 1976). For the split approach, a random set of entries of the precipitation time series is omitted. This procedure is repeated n times. A separate regression model is derived for each of the n new time series in which the precipitation observations and corresponding Mg/Ca_c values for the chosen years are omitted. The five years preceding every omitted year are also omitted in order to remove all information that is used to derive the linear weighted running mean of the precipitation time series. The result is n independently derived estimates of winter precipitation that constitute a validation series. The validation series is compared to the instrumental precipitation time series. A moderately strong correlation was found between the precipitation estimates and the annual time series P_w ($r = 0.43$, $p = 0.05$). The standard deviation of the precipitation estimates is 6.9 mm.

We conclude, that the performance of the regression is sufficiently strong to merit further application. The regression model was applied to the Mg/Ca_c data of older stalagmite sections to produce the precipitation estimates of the amount of winter precipitation

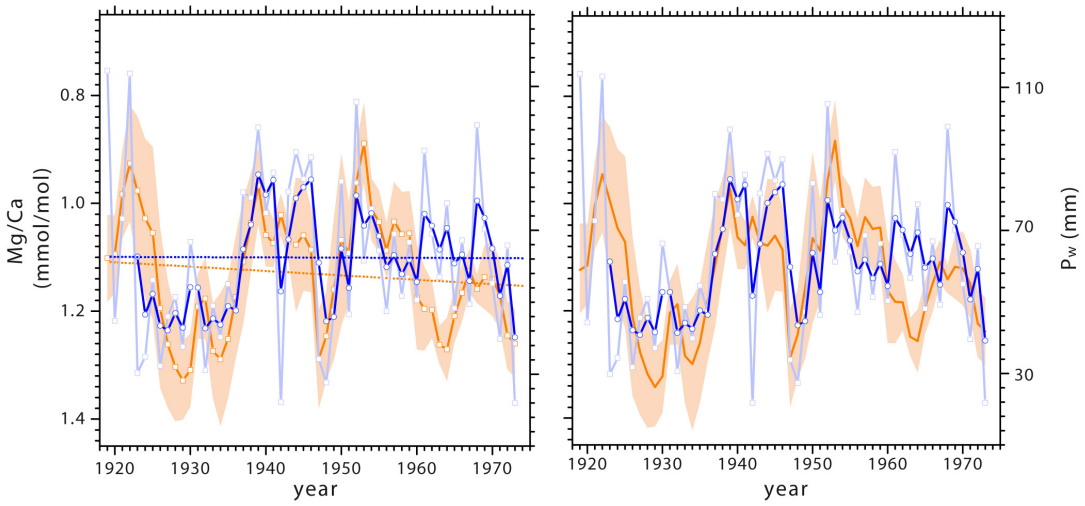

Figure 7.12: *Left: Mg/Ca_c ratio (orange) in speleothem C09-2 vs. winter precipitation P_w (light blue) and the 5p linear weighted running mean P_{lin} (dark blue). Orange shaded bands indicate the ensemble based uncertainty of Mg/Ca_c due to the error of the age control (see text for more details). Dotted lines indicate the trend lines of the time series, respectively. Right: Detrended time series of Mg/Ca_c, P_w and P_{lin}.*

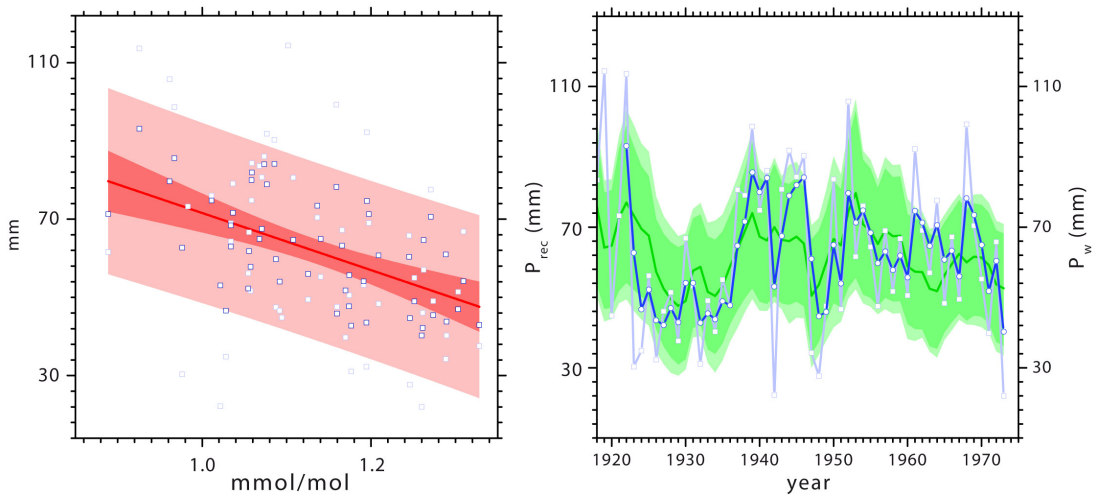

Figure 7.13: *Results of regression analysis. left: Regression model (red) applied to winter precipitation (mm) versus Mg/Ca$_c$ ratio (mmol/mol). Light open symbols indicate ONDJFM values between 1919 and 1973, whereas dark open symbols show the 5p linear weighted RM values. The shaded bands are the 95% confidence (dark red) and 95% prediction (light red) bands. Right: Reconstructed precipitation time series P$_{rec}$ (green) with prediction intervals (dark green shaded band) and final uncertainty bands including the error from the age control (light green bands). Scattered lines indicate P$_w$ (light blue) and P$_{lin}$ (dark blue).*

(mm/month) from 1759 to 1973 AD. The model was also applied to the Mg/Ca$_c$ record from 1700 BC to 1759 AD in order to derive an estimate of past winter precipitation which can be qualitatively explored.

7.4 Discussion

7.4.1 Trace element variability

Seasonal cyclicity

Trace element analyses reveal a pronounced variability in Mg/Ca$_c$, Sr/Ca$_c$ and Ba/Ca$_c$, as well on seasonal scale, but also superposed by decadal to centennial changes. Cave monitoring results suggest, that growth rate variability and calcite water interactions are the most important processes determining trace element composition of speleothem calcite.

On seasonal scale, Ba/Ca$_c$ and Sr/Ca$_c$ exhibit a strong positive correlation, while both are negatively correlated with Mg/Ca$_c$ (Figure 7.9, 7.10 and Table C.1). However, this anti-cyclicity is not as strong as the correlation of Sr/Ca$_c$ and Ba/Ca$_c$ and is only prominent in limited sections of the record. Roberts et al. (1998) interpreted an anti-correlation of Sr/Ca (and Ba/Ca) with Mg/Ca as seasonal variations in water residence time in the unsaturated zone. A similar interpretation was favored by Treble et al. (2003), who argued that the dependence of Sr and Ba concentrations on growth rate may lead to an anti-correlation with Mg/Ca. We match with this interpretation and suggest, that growth rate variability causes

the observed seasonal Sr/Ca_c and Ba/Ca_c variability rather than calcite-water interactions such as PCP, ICD or residence time changes.

Monitoring of cave air and dripwater parameters revealed a strong seasonality in Cloşani Cave. pCO_2 shows a pronounced seasonal cycle with very high values of up to 8800 ppm in summer and minimum values (1000 ppm) in winter (section 7.3.3 and Figure 7.7). Calculation of calcite saturation indices (SI) and pH values show, that during summer, only little calcite precipitation is expected, and the main season of carbonate precipitation is winter (section 7.3.3). Thus, the pronounced seasonal cave air pCO_2 cycle leads to seasonally different stalagmite growth rates. This in turn influences Sr (and Ba) incorporation into the speleothem calcite due to the dependency of the partitioning coefficient D_{Sr} (and D_{Ba}) on calcite precipitation rate (Huang and Fairchild, 2001; Nehrke et al., 2007; Fairchild and Treble, 2009).

Annual mean growth rates of C09-2 determined by measuring the total width of the Sr/Ca_c cycles are between 50 and 600 µm/year (section 7.3.3). Taking these extreme values, minimum growth rates for summer can be assumed to be about 1 - 10 µm/month. This yields values of up to more than 100 µm/month for winter months. For this range in growth rate, D_{Sr} varies by at least an order of magnitude between ca. 0.02 for slow growth and >0.15 for fast growth (Huang and Fairchild, 2001; Nehrke et al., 2007; Fairchild and Treble, 2009). Gabitov and Watson (2006) showed in laboratory experiments that growth rate effects on Sr in calcite become significant at a growth rate >500 µm/year, which is exceeded in C09-2 during the winter season. Calculating theoretical dripwater Sr/Ca_w ratios using the measured maximum and minimum values of Sr/Ca_c and the estimated values for D_{Sr} is in good agreement with the dripwater data (Sr/Ca_w = 0.27 mmol/mol).

In contrast, Mg/Ca incorporation in speleothem calcite is not dependent on growth rate. D_{Mg} was found to be related with temperature (Huang and Fairchild, 2001; Gascoyne, 1983), however this process is regarded to be subordinate since temperature in the cave is very constant. In contrast Mg/Ca_c was not found to be correlated with outside surface air temperature (section 7.3.3). Thus, the Mg/Ca_ccomposition reflects processes determining dripwater variability. In some years, Mg/Ca_c shows seasonal variability with higher values during summer and lower in winter (Figure 7.10). This pattern is also observed in the dripwater, with only small variations of $(Sr/Ca)_w$ and $(Mg/Ca)_w$ on seasonal timescales coinciding with the pCO_2, SI and pH seasonal cycle (Figure 7.7). Such patterns in Mg/Ca are commonly interpreted to reflect a higher amount of prior calcite precipitation (PCP) in the season with low infiltration (summer) and less PCP in high infiltration seasons (winter) (Cruz et al., 2007; Fairchild and Baker, 2012). Cruz et al. (2007) interpret higher (lower) Mg/Ca and Sr/Ca values associated with lower (higher) levels of recharge into the karstic aquifer, as a result of the increase (decrease) in the volume of calcite precipitated in the unsaturated zone above the cave during dry (wet) climate periods.

Sinclair et al. (2012) developed a theoretical model which predicts that the slope of a graph of ln(Sr/Ca) and ln(Mg/Ca) (measured in dripwaters or speleothem calcite) in the presence of PCP or incongruent calcite dissolution (ICD) is independent of solution and host-limestone

composition and is given by $\frac{D_{Sr}-1}{D_{Mg}-1}$. Figure 7.8 shows, that according to this model, Sr/Ca, Mg/Ca and Ba/Ca composition of the dripwater can be ascribed to PCP or ICD. The covariation with $\delta^{13}C$ values in the dripwater also supports the presence of PCP (Cruz et al., 2007; Sinclair et al., 2012). Residence time variability (Fairchild and Treble, 2009) or ICD (Sinclair, 2011) influence the Mg/Ca ratio in the speleothem in the same direction, however all of those processes reflect calcite water interactions and can be traced back to the amount of infiltrating meteoric precipitation.

Though, we suggest that the seasonal variability in Mg/Ca, if present, is caused by calcite - water interactions related to the seasonal cycle in water supply with low infiltration in summer and high infiltration in winter (section 7.3.3). These processes might also contribute to the observed annual Sr/Ca and Ba/Ca cycle. However, the strong growth rate effect dominates the incorporation of both elements in speleothem calcite.

Mg/Ca - a proxy for winter precipitation

The high correlation of Mg/Ca_c with winter precipitation variability (section 7.3.4) strongly indicates that precipitation-forced processes influence Mg/Ca composition of the speleothem also on multi-annual timescales. From the mentioned processes in the previous section, the presence of calcite - water interactions are the most likely processes explaining this connection. Unfortunately, due to the decoupling of Sr/Ca_c (Ba/Ca_c) and Mg/Ca_c, the model of Sinclair et al. (2012) is not applicable to the trace element composition in the speleothem. Sinclair et al. (2012) discuss other processes such as diagenetic effects which could influence the trace element composition. Thinkable scenarios could be for example Mg input from dolomite dissolution, calcite recrystallization or soil processes. Another process influencing elemental and stable isotopic composition of the dripwater could be degassing effects due to seasonal ventilation (Johnson et al., 2006; Deininger et al., 2012). However, all these processes are all not necessarily related with recharge. Thus, the correlation of Mg/Ca_c with precipitation indicates that it is unlikely, that other processes than calcite - water interactions determine the incorporation of Mg/Ca_c on multi-annual timescales. However, this does not exclude, that the other mentioned processes contribute a second-order effect to the element profiles. The relation of lamina width with precipitation (section 7.3.4) also supports this interpretation. Low growth rates are accompanied by high Mg/Ca_c ratios and less winter precipitation which may be caused by enhanced PCP leading to lower supersaturation and thus less precipitation of calcite on the stalagmite's surface. This also supports the long - term persistent anti-correlation of Sr/Ca_c (Ba/Ca_c) and Mg/Ca_c.

The estimation of PET (section 7.3.3) also suggests that most of the summer precipitation is lost to the annual infiltrating water budget and that mainly winter precipitation contributes to the infiltrating water feeding the karst reservoir. This explains the relation of Mg/Ca_c to winter precipitation. The highest correlation was found for the smoothed time series over the 5 previous years. This is related to the karst system, which acts as a low pass filter. This is taken into account with the calculation of a linear weighted 5-point running mean

of the precipitation time series (comparable to Jex et al. (2011); Mischel et al. (2015)). This filter considers the potentially stronger influence of the more recent years in comparison to the previous years. An alternative mixing model, which simulates a mixture of fracture and storage flow, as proposed in Fairchild and Baker (2012) (based on the work of Baker et al. (2007), Baker and Bradley (2010) and Jex et al. (2010)) did not significantly improve the correlation, suggesting a simple reservoir with an overflow feeding stalagmite C09-2. Smoothing always reduces the degrees of freedom of a time series, but still the calculated correlation coefficient between Mg/Ca and winter precipitation has proved to be significant (section 7.3.4) even when taking into account the auto-correlation and age uncertainties. In conclusion, the presented results suggest that Mg/Ca is a proxy for past winter precipitation variability and can be used for qualitative and quantitative reconstruction.

Limitations of the precipitation estimates

This reconstruction was performed using a linear regression model (section 7.3.5), which explains about 34% of the variance of the winter precipitation time series. For the last 250 years, the reconstructed precipitation amount is based on a tight age control, providing a solid basis for further interpretation. Furthermore, the mean values and variances of the Mg/Ca_c time series between 1919 - 1974 (1.13 ± 0.11 mmol/mol) and 1756 - 1918 (1.08 ± 0.13 mmol/mol) indicate no substantial difference during both periods. However, in the older sections, the reliability of the transfer from Mg/Ca values to absolute precipitation estimates underlies several uncertainties. On the one hand, the age uncertainties become larger which increases the uncertainties of the reconstruction. On the other hand, the calibration period is very short with respect to the reconstruction period and it is difficult to proof to what extent the correlation persists throughout the record.

For example, from the previously mentioned potential second-order effects enhanced degassing of CO_2 due to slow drip rates may lead to changes in $\delta^{13}C$ values as well as in trace element to Ca ratios in speleothems (Fairchild and Treble, 2009; Johnson et al., 2006). This may be the case in sections with poor or absent lamination in C09-2. These intervals are characterized by low Sr/Ca_c as well as Ba/Ca_c ratios and high Mg/Ca_c and $\delta^{13}C$ values, indicating very low growth rates.

Periods with extreme snow cover events could be one explanation for this effect. During the last century, the effect of snow cover in winter generally played a minor role because the fraction of snow is only about 10 % of total annual precipitation. However, extreme events may have a significant influence on the record. A very high fraction of snow in winter precipitation and severe winters may cause less infiltration during the main season of calcite precipitation. This may be reflected in higher Mg/Ca_c ratios even though the total amount of precipitation is high. Periods of extremely low reconstructed precipitation may thus also be the consequence of extreme events during severe winters. For example, this might be the case for the period of extraordinarily low precipitation between about AD 1630 and 1750 during the Little Ice Age. During these periods (highlighted in Figure 7.9), the reconstructed precipitation

amount potentially underestimates the actual value and is thus to be interpreted with care.

7.4.2 $\delta^{18}O$ and $\delta^{13}C$ values

The $\delta^{18}O$ value of the precipitation, $\delta^{18}O_p$, falling in the region of the cave site seems to be related to temperature as indicated by the high correlation coefficient ($R = 0.86$, $p < 0.001$) between the monthly means of temperature and $\delta^{18}O_p$ at the GNIP station at Râmnicu Vâlcea (RV). The correlation between precipitation amount and $\delta^{18}O_p$ at RV, in contrast, is not significant. The mean $\delta^{18}O$ value of the dripwater reflects the evapotranspiration-weighted mean annual $\delta^{18}O$ value of precipitation (section 7.3.3). In general, the most important effects on precipitation $\delta^{18}O$ values are the temperature effect, the continental effect, the source effect, changes in seasonality and the amount effect (Lachniet and Patterson, 2009).

According to Micu et al. (2015), annual precipitation is mainly characterized by a mixture of Mediterranean and Atlantic air masses, dominating summer and winter precipitation maxima, respectively. Due to the different trajectories and moisture sources, the $\delta^{18}O$ values of the air masses is expected to be different. Mediterranean surface waters are generally warmer than those of the Atlantic, which results in higher $\delta^{18}O$ values. The Atlantic air masses in turn are potentially more depleted when they reach Romania since the trajectories over the continent are longer. Thus, changes in the seasonal precipitation pattern has an effect on the annual weighted mean $\delta^{18}O$ value. Higher $\delta^{18}O$ values in the stalagmite could thus be interpreted to reflect a higher proportion of warmer Mediterranean moisture and vice versa. A similar situation of competing air masses was described for stalagmite ER76 from Grotta di Ernesto in northern Italy (Scholz et al., 2012), confirming the complexity of the interpretation of $\delta^{18}O$ values in stalagmites, in particular for geographically complex locations, as it is also the case in SW Romania.

At Râmnicu Vâlcea, the amount effect appears to be not important. However, dripwater $\delta^{18}O$ values at Closani Cave may suggest a connection to precipitation variability (Figure 7.7) with lower $\delta^{18}O$ values coinciding with more humid phases and vice versa. Since the Mediterranean water masses contribute the largest amount of annual precipitation (section 7.3.3), higher $\delta^{18}O$ values could also reflect more humid conditions due to enhanced summer rainfall. Due to both competing processes, it is difficult to draw a direct connection between $\delta^{18}O$ values and precipitation amount. The comparison with other precipitation records in Figure 7.15 does also not permit a simple interpretation for the $\delta^{18}O$ values.

Drăguşin et al. (2014) presented a novel approach to discriminate temperature and hydrologic effects on $\delta^{18}O$ values of speleothems in Romania over the middle Holocene. The authors constrain, that $\delta^{18}O$ values of speleothems from the western Mediterranean appear to be mainly controlled by temperature changes, whereas samples from the eastern Mediterranean, including southwestern Romania, recorded a similar isotopic enrichment due to changing hydrology.

The C09-2 $\delta^{18}O$ values are also compared to the record of Sabatier et al. (2012), who recon-

structed storm activity in the western Mediterranean using the smectite/(illite+chlorite) ratio of a sediment core from the Gulf of Lions in order to assess the influence of Mediterranean cyclones on speleothem stable isotope signals. Striking features in the record of Sabatier et al. (2012) are the pronounced low storm activity from approximately 600 to 100 BC and from 900 to 1200 AD. These phases are accompanied by comparably low $\delta^{18}O$ values in C09-2, indicating less influence of Mediterranean moisture. The same pattern is observed for other shorter intervals in the middle of the 14th and 15th century (Figure 7.14). The southwesterly and southerly air masses, originating from the western and central parts of the Mediterranean Basin are responsible for causing warmer weather and shorter cold seasons (Micu et al., 2015). Thus, we also compare our record to the COMNISPAII record (Figure 7.14) from Spannagel Cave (Fohlmeister et al. (2013) and references). Several studies have shown that this record

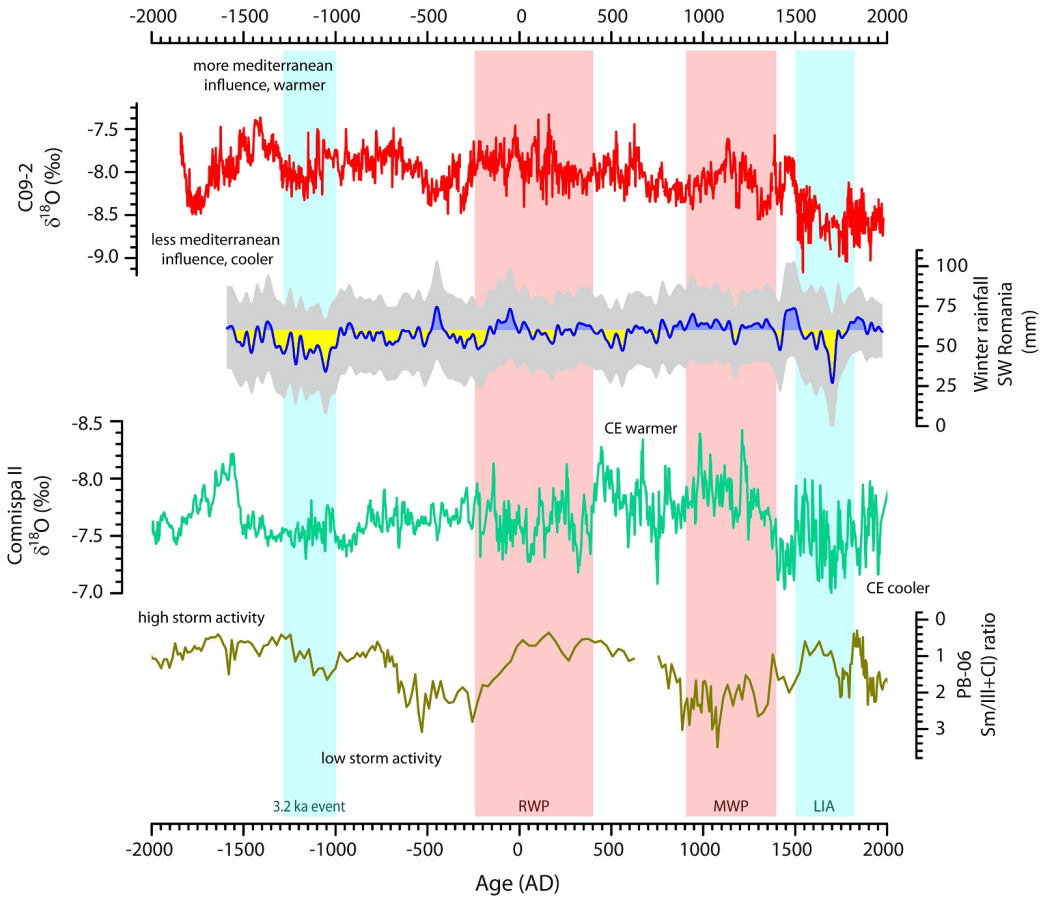

Figure 7.14: *C09-2 $\delta^{18}O$ values (red) and reconstructed winter precipitation from Mg/Ca ratio (blue) in comparison with the COMNISPA II $\delta^{18}O$ record in turquoise (Fohlmeister et al., 2013). Note inverted axis, lower values indicating warmer temperatures in central Europe (CE) and vice versa. Light green: storm activity in the Gulf of Lions (NW Mediterranean Sea, Sabatier et al. (2012)). Low values of smectite/(illite+chlorite) ratio correspond to periods of high storm activity. Grey bands indicate the uncertainties of reconstructed rainfall, blue (yellow) shading indicates wetter (drier) than average conditions in SW Romania. Vertical bars indicate the timing of prominent climate events during the late Holocene in Europe.*

is not only representative of local climate in the Alps, but its signal tracks large-scale climate variations (Fohlmeister et al., 2013). Mangini et al. (2005) showed that for Spannagel cave higher speleothem $\delta^{18}O$ values represent colder conditions and vice versa. On centennial to millennial timescales, $\delta^{18}O$ values in C09-2 and the COMNISPA II appear to be anti-correlated, especially during the last 2000 years. The comparison to the both records strengthens our assumption that $\delta^{18}O$ values in precipitation in SW Romania are connected to Mediterranean cyclone activity and, on millennial scale, to temperature variability.

The $\delta^{13}C$ signal recorded in speleothems depends on environmental as well as isotope fractionation processes occurring at the surface, in the soil, the epikarst, the cave and on the stalagmite surface (Dreybrodt and Scholz, 2011). Climate variability directly or indirectly influences these processes, and their interactions renders the interpretation of speleothem $\delta^{13}C$ values non-trivial. Whereas the $\delta^{13}C$ signal is dominated by soil processes on millennial time-scales, short-term variability is influenced by isotope fractionation under conditions of disequilibrium controlled by inter-annual differences in degassing of CO_2 related to drip rate variability (Frisia et al., 2011; Johnson et al., 2006). We therefore expect that processes at the surface and in the soil zone play only a minor role in controlling the $\delta^{13}C$ values over the last ~4ka. The $\delta^{13}C$ values of stalagmite C09-2 are thus interpreted to primarily reflect effects of disequilibrium fractionation occurring inside the cave and on the stalagmite surface (Deininger et al., 2012; Scholz et al., 2009) and to lesser extent changes in soil activity and vegetation.

7.4.3 Late Holocene climate variability

For the last 250 years, we compare our precipitation estimates to the summer drought reconstruction based on tree rings from Băile Herculane, located only a few km south-west of Cloşani Cave (Levanič et al., 2012) (Figure 7.15). The combination of the C09-2 P_w reconstruction and the summer drought record provides a comprehensive picture of past precipitation variability in SW Romania.

A second record is a reconstruction based on speleothems from northern Turkey (Jex et al., 2011). The authors found that autumn/winter precipitation in Gümüşhane is influenced by pressure fields over the Caspian Sea/Western Russia. These patterns, the North Sea Caspian Pattern (NCP) and East Atlantic/West Russia pattern (EAWR), may also affect winter climate in SW Romania by influencing northerly circulation and the influence of the North Atlantic Oscillation (NAO)(Comas-Bru et al., 2016).

During the 20^{th} century, all three records are precisely dated based on annual layer counting. Even though the August standardised precipitation index (SPI) record of Levanič et al. (2012) is a summer drought record and the speleothem records reflect winter conditions, all reconstructions show relatively dry periods during the late 1900s, the late 1920s and early 1930s, around 1945, during the early 1960s and after 1975 (indicated with orange bars in Figure 7.15). Before AD 1900, a possible shift in the age control of the record of Jex et al. (2011)

might be the reason for the lower covariation of the records from SW Romania and northern Turkey. During the late 18th century, relatively dry periods in SW Romania prevailed in summer (Levanič et al., 2012) as well as winter, whereas the period between 1800 and 1900 was relatively humid (Figure 7.15). A similar pattern was also observed by Feurdean et al. (2015) deduced from a peat profile in the northern Carpathians.

Figure 7.14 shows the $\delta^{18}O$ record of C09-2 and the reconstructed winter precipitation in SW Romania for the last 3700 years. The most prominent climate anomalies during the last 1500 years were - besides the Industrial Era - the Medieval Climate Anomaly (MCA) between ca. 900 and 1400 AD and the Little Ice Age (LIA) between ca. 1500 and 1800 AD. In our precipitation record from SW Romania, the beginning of the MCA was more humid than average, whereas during the second half conditions were slightly drier. This pattern was also observed by Onac et al. (2015) deduced from a cave guano sequence from a cave in SW Romania. A similar pattern appears during the Roman Warm Period (RWP, 250 BC to 400 AD), which was characterized by generally warmer and humid conditions in SW Romania, with a drier pe-

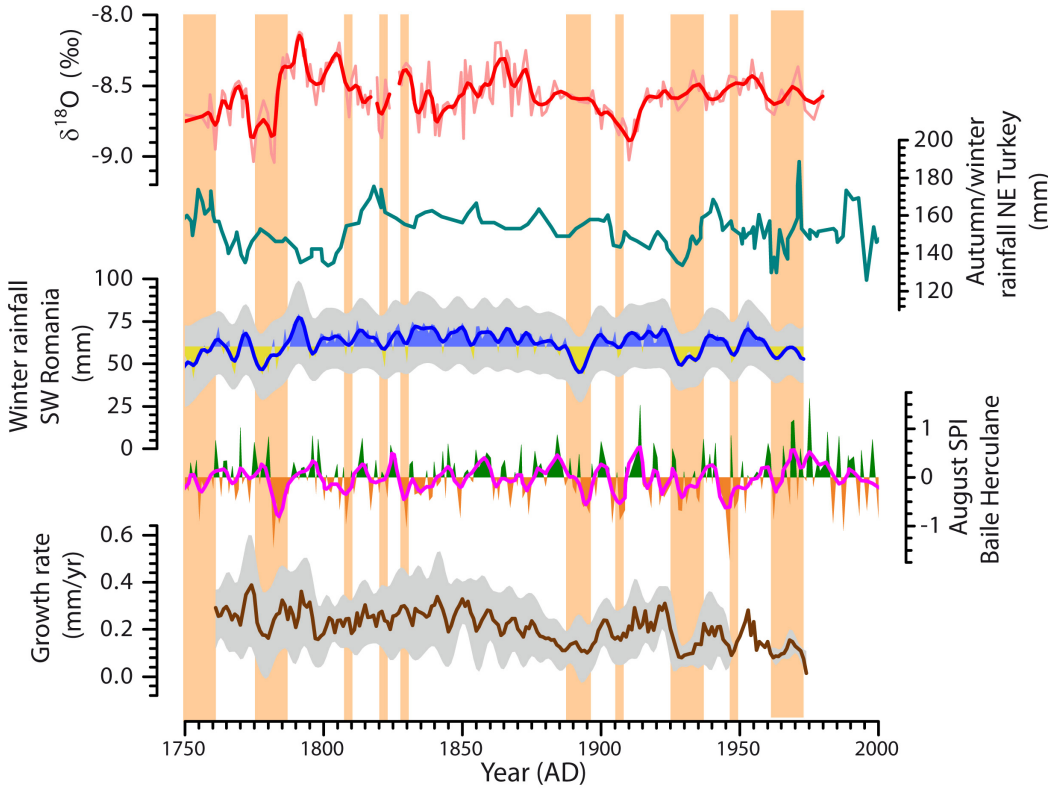

Figure 7.15: *C09-2 $\delta^{18}O$ values (red), growth rate (brown) and reconstructed winter precipitation from Mg/Ca ratio (blue) in comparison with the autumn/winter rainfall reconstruction of Jex et al. (2011) and the summer drought record from SW Romania by Levanič et al. (2012). Grey bands indicate the uncertainties of reconstructed rainfall and growth rate. Blue (yellow) shading indicates wetter (drier) years than the mean values of the common period (1919 - 1973). Vertical orange bars indicate relatively dry periods in SW Romania.*

riod from 0 to 200 AD. This phase is accompanied by high storm activity in the Gulf of Lions (Sabatier et al., 2012) and lower $\delta^{18}O$ values in C09-2, indicating an enhanced influence of Mediterranean moisture sources. Other humid phases in SW Romania are observed around 500 BC and between 1400 and 1500 AD.

The LIA is a very pronounced period in the C09-2 record with a strong decrease in precipitation and $\delta^{18}O$ values. This phase is known as a very cold phase in Europe (Mann et al., 2009b). In C09-2, this phase is characterized by very low growth rates, with the most extreme values between 1680 and 1760 AD. This indicates, that the very low reconstructed precipitation amounts in SW Romania during this phase potentially underestimate the actual values, probably due to more severe winter conditions (compare section 7.4.1).

Another dry phase in the C09-2 record is recorded at the end of the late Bronze Age from around 1300 to 1000 BC (Figure 7.14). This interval is documented in both archaeological and paleo climate records around the eastern Mediterranean and referred to as the '3.2 ka event' (Drake, 2012; Drăguşin et al., 2014). Drăguşin et al. (2014) report a change in temperature and climate-hydrology during this period in southern Romania, whereas Aegean Sea winter surface temperatures were found to be lower (Rohling et al., 2002). A dry phase is recorded as well in northern Romania (Schnitchen et al., 2006) as in the eastern Mediterranean realm (Kaniewski et al., 2010, 2013).

7.5 Conclusions

We present a multi-proxy record from a speleothem in SW Romania, which covers the last 3.6 ka. The age control of the youngest section is based on three independent methods, which provide an internally consistent, precise age model for the instrumental period. This enables to calibrate the proxy data with meteorological data. Based on the high anti-correlation between Mg/Ca in speleothem calcite and regional winter precipitation, we were able to reconstruct winter precipitation variability during the last 3.6 ka in SW Romania. Sr/Ca and Ba/Ca ratios are dominated by the seasonal cycle in cave pCO_2. $\delta^{18}O$ values appear to be connected to varying influence of Mediterranean and Atlantic moisture sources, temperature variability and changes in seasonality, which makes the interpretation in terms of climate variability complex. The comparison with other precipitation reconstructions shows that particularly dry periods in the speleothem record are also visible in a tree ring-based summer drought reconstruction in close vicinity to Closani cave (Levanič et al., 2012). A reconstruction of winter precipitation from Turkey using speleothem proxies (Jex et al., 2011) shows a good agreement during the last 100 years, where both records are based on a precise age control. This record is the first of its kind in SE Europe. However, due to a lack of other (supra-) regional precipitation records, it is currently not clear whether the reconstructed precipitation data reflect a local or a regional signal. Nevertheless, the multi-decadal variability is likely representative for SE Europe because prominent northern hemispheric periods, such as the LIA or the MCA, are recorded.

Acknowledgments

This project was funded by the German Science Foundation (DFG grant SCHO 1274/6-1) and the DFG Research Group 668 (DAPHNE) and also benefited from the support of MC-ICPMS infra-structure DFG-NVST 1143.

The authors are grateful to René Eichstädter, Manuela Wimmer, Sylvia Riechelmann, Anne Marie Wefing, Hanna Rosendahl and Arno Hartmann for assistance in the laboratory and with data acquisition. Dana Riechelmann and Michael Deininger are thanked for their support and helpful discussions.

We acknowledge the data providers in the ECA&D project (Klein Tank et al., 2002). Data and metadata available at http://www.ecad.eu.

Part III

Discussion

8 Consequences for the interpretation of speleothem derived proxies for climate reconstruction

In this summary, the results of the previous chapters are presented and assessed in the context of current research. The contribution of this thesis to improving the application and interpretation of multi-proxy approaches in climate reconstruction with speleothems are elaborated.

The analyzed proxies could be associated to certain general environmental patterns in all presented case studies. First, this comprises detrital contamination, which was found to be mainly related with the element ratios Al/Ca and Th/Ca. The second major pattern refers to vegetation and soil dynamics, and is mainly attributed to the elemental ratios P/Ca and U/Ca, as well as $\delta^{13}C$ values. The third main group is associated with hydrological variability in general and consists of Mg/Ca, Sr/Ca and Ba/Ca, as well as the stable isotope $\delta^{18}O$ (and $\delta^{13}C$) values.

In this chapter, the inferred interpretations of the most relevant proxies and the consequences for their application are elucidated. This comprises the most commonly used $\delta^{18}O$ values (section 8.1) as well as the elemental proxies Mg/Ca and Sr/Ca, which are often regarded as tracers of hydrological variability (section 8.2). Additionally, the apparent controversial interpretations of the P/Ca ratio in the presented speleothem studies are summarized and compared (section 8.3).

8.1 $\delta^{18}O$ - the proxy of first choice?

Stable isotope $\delta^{18}O$ values are routinely measured in environmental archives such as ice cores, foraminifera, corals or speleothems in order to make inferences on the water cycle (Dansgaard, 1964; Swart et al., 1993). In speleothems, the oxygen isotopic signature is commonly analyzed simultaneously with $\delta^{13}C$ values, which helps tracing the isotopic composition of all components of the carbonate. These proxies provide the main basis for reconstructing the temperature or precipitation history of a site from speleothems (Bradley, 2015).

As outlined in section 2.2, oxygen isotopic variations in the speleothem calcite ($\delta^{18}O_c$) should in theory provide a proxy of temperature variations through time, since the fractionation of oxygen isotopes is dependent on the temperature of deposition (O'Neil et al., 1969). However, $\delta^{18}O$ and $\delta^{13}C$ values in speleothems are subject to a variety of processes outside

and inside the cave environment (Mickler et al., 2004). Nevertheless, both are still the proxies of choice. This section summarizes the use of $\delta^{18}O$ values in speleothem research deduced from the conclusions drawn from the presented case studies in this thesis.

8.1.1 Speleothem $\delta^{18}O$ in the tropics

In concert with previous research (van Breukelen et al., 2008; Scholl et al., 2009), an inverse relationship of $\delta^{18}O$ values in rain water with precipitation amount was inferred for the location of Cueva Larga in Puerto Rico (Vieten et al., in press). Monitoring of dripwaters suggests that this relationship is also valid for speleothems from this cave and Vieten et al. (in press) were even able to estimate a quantitative relation between changes in rainfall amount and $\delta^{18}O$ values.

Furthermore, in Chapter 5 of this thesis it was found that the relationship between temperature in Cueva Larga, which reflects the mean annual surface temperature, and $\delta^{18}O$ values of dripwaters and recent calcite is well described by the fractionation equation derived by Tremaine et al. (2011) (section 5.4.2). These relations formed the basis of interpreting the $\delta^{18}O_c$ in stalagmite PR-LA-1 and allowed qualitative and quantitative inferences of past temperature and precipitation variability in Puerto Rico during the last Glacial (section 5.4.3).

In Santo Tomas Cave, Cuba, (Chapter 6), some samples of drip and pool waters have been analyzed in the past (Fensterer, 2011). However, the monitoring program was less comprehensive than at the location of Cueva Larga. Nevertheless, Fensterer et al. (2012) and Fensterer et al. (2013) were able to relate the changes in $\delta^{18}O_c$ of Holocene stalagmites from the same cave system with Caribbean rainfall variability. This was possible due to the fact that in tropical cave environments, $\delta^{18}O$ values of dripwaters and speleothems are regularly found to be determined by the amount effect (van Breukelen et al., 2008; Kanner et al., 2012). This originates in the opposed seasonal cycles of temperature and $\delta^{18}O$ composition of precipitation in low latitudes, with high (low) temperatures coinciding with more depleted (enriched) $\delta^{18}O$ values. Thus high temperatures and rainy season tend to coincide (Vuille, 2003), and as a consequence, all potential effects such as additional drip rate and ventilation driven disequilibrium fractionation (section 2.2) should influence the oxygen isotope signature in the same direction.

However, $\delta^{18}O$ values in speleothem carbonate are affected by two processes that have nothing to do with changes in precipitation amount - the influence of temperature on carbonate - water isotopic fractionation in the cave and the influence of changing $\delta^{18}O$ of seawater. Quantitatively accounting for both 'artifacts' can significantly alter the interpretations of speleothem records (Baker and Fritz, 2015). These corrections may have grave implications for the interpretation of tropical Northern Hemisphere speleothem records where the combined adjustments tend to decrease or even eliminate the 'true' signal amplitude (Baker and Fritz, 2015).

For example, assuming a cooling of ca. 5 °C during the Last Glacial Maximum (LGM)

relative to the late Holocene would have had a temperature-induced increase (relative to modern cave air temperatures) during the LGM of ~1‰ (Kim and O'Neil, 1997; Tremaine et al., 2011). The global increase of $\delta^{18}O$ values in seawater during the LGM was ca. 1‰ (Schrag et al., 2002). All other considerations aside, this would have led to a 1‰ increase in the $\delta^{18}O$ of water vapor, precipitation, groundwater, and speleothem carbonate (Baker and Fritz, 2015). Thus, an amount of ~2‰ should be subtracted from the $\delta^{18}O$ value of LGM speleothem calcite to account for both effects. As a consequence, the largest corrections (to more negative values) accumulate during glacial maxima and the smallest corrections during interglacials (when temperature and $\delta^{18}O$ of seawater were near present-day values).

8.1.2 Speleothem $\delta^{18}O$ in temperate regions

A more complex situation is encountered in temperate regions, such as Cloşani Cave, Romania (Chapter 7). Due to a long-term monitoring program the cave-internal processes determining the composition of dripwater are relatively well understood.

In the mid-latitudes, the rainfall season may be independent of the annual temperature cycle, which decouples the temperature- from the amount effect on $\delta^{18}O$ values of precipitation. In the case of Romania, annual rainfall has two maxima, which are mainly generated by mediterranean and continental air masses, respectively (section 4.2 and Micu et al. (2015)). Due to their origin, these air masses have different isotopic signatures, which raises the 'problem' of interpreting the $\delta^{18}O$ values in speleothems from this region to the level of the interplay of atmospheric teleconnections influencing seasonality in rainfall at the site.

In general, winter climate and associated $\delta^{18}O$ values of precipitation in Central Europe were found to be connected with the variability of the North Atlantic Oscillation (Wanner et al., 2001). The strong influence of the NAO on precipitation and temperature patterns was in principle also found for Romania (Bojariu and Paliu, 2001; Bojariu and Gimeno, 2003; Tomozeiu et al., 2005; Micu et al., 2015) and the existing speleothem $\delta^{18}O$ records from the Carpathian realm have all been related with North Atlantic climate variability (Onac et al., 2002; Constantin et al., 2007; Tămaş et al., 2010).

However, a recent model study by Comas-Bru et al. (2016) shows, that $\delta^{18}O$ values of precipitation may not be a robust proxy to reconstruct any relationship of the NAO with air temperature and precipitation due to the complex interferences of the NAO with other large-scale circulation patterns such as the Scandinavian pattern (SCA) or the East Atlantic pattern (EA).

In order to discriminate between the effects of temperature and hydrology on speleothem $\delta^{18}O$ values from Romania, Drăguşin et al. (2014) take advantage of a novel approach. The authors use pollen-based temperature reconstructions to constrain temperature-driven isotopic changes of speleothem calcite. Drăguşin et al. (2014) infer, that in the Atlantic-dominated western Romania, changes in $\delta^{18}O_c$ values largely reflect temperature variations. However they note a significant deviation of the measured data to the calculated temperature-driven

isotopic changes which is ascribed to additional 'climate-hydrology' factors.

Also for stalagmite C09-2, which is presented in Chapter 7, changes in temperature or precipitation could not be clearly distinguished in the $\delta^{18}O_c$ variability, despite the existence of a long-term cave monitoring, and the possibility of linking speleothem time-series with instrumental data. In this particular case, the Mg/Ca ratio was found to constitute a more reliable tracer, due to the strong and significant correlation with winter precipitation which even enabled the quantitative reconstruction of winter rainfall during the last 4 ka.

This demonstrates, that the discrimination of temperature- and precipitation driven controls on $\delta^{18}O_c$ values in the Carpathian-Balkan region is complex and that the amendment of further evidence and independent proxies is desirable for speleothem studies from this area.

8.1.3 Additional information

Monitoring of rain and dripwaters in the cave strongly facilitates the quantification of many relevant processes, such as disequilibrium fractionation effects or the influence of ventilation as it was possible for Cueva Larga (Vieten et al., 2016, in press) or also Cloşani Cave. Meanwhile, cave monitoring studies constitute a new standard for the interpretation of speleothem proxies and characterising the relationship between water isotopes of precipitation and cave dripwater is becoming routine in caves worldwide (Cruz et al., 2005a; Mattey et al., 2010; Riechelmann et al., 2011; Genty et al., 2014).

Supplemental information, such as climate reconstructions from other archives may represent essential parts of the puzzle of the multiple effects on speleothem $\delta^{18}O$ values. A useful archive are instrumental or historical data providing a direct measure of the climate parameter which can be directly correlated with the proxy time-series. Here, the fundamental prerequisite is establishing a precise age model, and the proper evaluation of its uncertainties as demonstrated in Chapter 7. However, this is only possible for speleothem time series covering the instrumental era (i.e. approximately the last 150 years). For older samples, calibrated quantitative climate reconstructions such as tree-ring derived temperature or drought records may be useful (e.g., (Popa and Kern, 2008; Levanič et al., 2012)).

Independently analyzed tracers in the speleothem are a measure which should be considered in any case. The benefit of certain elemental proxies in speleothem research such as Mg/Ca, Sr/Ca as hydrological proxies or P/Ca as tracer of soil and vegetation dynamics is discussed in the following sections.

A comparison of multiple proxies (Meckler et al., 2015) shows the potential of speleothems for absolute paleo temperature reconstructions by comparing the results of four different 'paleo thermometers' that are (i) speleothem fluid inclusions (Dublyansky and Spötl, 2009; Affolter et al., 2014), (ii) liquid-vapour homogenization of fluid inclusions (Krüger et al., 2011), (iii) noble gases concentration in stalagmite water (Kluge et al., 2008; Vogel et al., 2013) and (iv) clumped isotopes (Ghosh et al., 2006; Eiler, 2007; Meckler et al., 2014).

Independent of the underlying technique, the analysis of stable isotopes in fluid inclusions

in speleothem calcite may provide valuable information about past dripwater composition and temperature estimates (Schwarcz et al., 1976; Fleitmann et al., 2003; van Breukelen et al., 2008; Kluge et al., 2008; Affolter et al., 2015; Labuhn et al., 2015). The analysis of the temperature dependent preference for heavy nuclides to bond to each other, rather than to a lighter isotope is referred to as clumped isotope geochemistry (Ghosh et al., 2006; Eiler, 2007) is a promising technique, despite some complications of applying the system to speleothems (Affek et al., 2008; Daëron et al., 2011; Wainer et al., 2011; Kluge and Affek, 2012; Kluge et al., 2013).

8.1.4 Conclusions

In summary, the use of speleothem $\delta^{18}O$ values in terms of paleo climate reconstruction is unchallenged. The fundamental problem of interpreting speleothem $\delta^{18}O$ values is the discrimination of temperature and precipitation effects. In most cases, the analysis of $\delta^{18}O$ and $\delta^{13}C$ alone is not enough to derive satisfying results in terms of climate reconstruction.

In particular in tropical regions which are dominated by the amount effect, the oxygen isotopic signature is regarded a reliable proxy of past hydrological variability, when taking into account second order effects, that may change the interpretation of $\delta^{18}O_c$ significantly, e.g. on glacial-interglacial timescales. However, this also presumes the knowledge of a quantitive estimate past temperature changes.

In the mid-latitudes, a deep understanding of the climatological framework is indispensable, but still the controls of speleothem $\delta^{18}O$ values may remain obscure, because a variety of effects may compete each other. Independent information from 'paleo thermometers' or hydrologically forced proxies constitute valuable opportunities to disentangle the climate information of the stable isotopic composition of the speleothem.

8.2 Magnesium and Strontium - tracers of hydrological processes?

Magnesium and strontium are amongst the most commonly used elemental proxies in speleothem research. Despite the existence of a number of processes influencing the incorporation of Mg and Sr (section 2.4), most published records are interpreted to be linked with rainfall variability when Mg/Ca and Sr/Ca covary (Hellstrom and McCulloch, 2000; McMillan et al., 2005; Cruz et al., 2007). However, two general mechanisms - limestone diagenesis and water-rock interactions - might be responsible for co-fractionating Sr and Mg in the dripwaters. In this thesis, the model of Sinclair et al. (2012) was used to make inferences about the processes governing apparent co-variations in Mg/Ca and Sr/Ca.

8.2.1 Results of the case studies

In Chapter 5, Mg/Ca and Sr/Ca ratios were found to be generally positively correlated in speleothem PR-LA-1, however, little variability is observed throughout the record. Monitoring of dripwaters in Cueva Larga did not provide evidence for the existence of strong prior calcite precipitation (PCP) (Vieten et al., in press).

Applying the model of Sinclair et al. (2012) to the elemental ratios of speleothem calcite confirms, that the influence of calcite-water interactions such as PCP or ICD was comparably small in the main part of the record. Temperature as well as growth rate variability were also found to be potential drivers of second order-effects in Mg/Ca and Sr/Ca, respectively, as well as the influence of sea spray or detrital contamination could not be excluded. The only interval showing a notable signature of prior calcite precipitation (PCP) and/or (ICD) and being thus mainly controlled by calcite-water interactions is the last section between 15 and 16.5 ka indicating drier conditions during Heinrich stadial 1. For the earlier part of the record, additional evidence from other trace elements, such as P/Ca, or stable isotope $\delta^{18}O$ and $\delta^{13}C$ values, was necessary to reconstruct climate conditions at the surface above the cave.

A similar picture is observed in stalagmite CM (Chapter 6). With 82 - 7 ka, the record spans a longer time frame than PR-LA-1 (Chapter 5). Mg/Ca and Sr/Ca are generally positively correlated, however, the slopes of the ln(Sr/Ca) vs ln(Mg/Ca) plots are systematically lower than expected for PCP/ICD. This is interpreted to be caused by an additional Mg source along the pathway of the dripwater through the host rock, e.g. high Mg-calcite or dolomite (section 6.4.1). However, the partly very variable slopes of the logarithmic plots could also be caused by calcite recrystallization, which is in general a highly non-linear process (Sinclair et al., 2012). Despite this is still a process determined by the amount of water percolating through the host rock, it is therefore not possible to make inferences from the absolute variations to the actual amount of rainfall above the cave.

Moreover, in CM, the incorporation of Sr and Mg in speleothem calcite may also be obscured by temperature and growth rate effects, variable soil leaching or sea spray (section 6.4.1). However, the generally positive correlation of Mg/Ca with $\delta^{18}O$ and $\delta^{13}C$ values suggests that high Mg/Ca values in CM most likely reflect a higher degree of calcite-water interactions through PCP, ICD and/or calcite recrystallization and thus generally drier conditions.

In stalagmite C09-2 from southwestern Romania (Chapter 7), a different pattern in Mg/Ca and Sr/Ca systematics is noted. Both elements are correlated in the dripwater, but anti-correlated within speleothem calcite (section 7.4.1). The anti-correlation is based on the decoupling of Mg and Sr signals due to seasonal growth rate effects. Thus, the model of Sinclair et al. (2012) is not applicable to the Sr and Mg values in the stalagmite. However, in the dripwater, the slopes of the logarithmic plots between both elements follows the theoretically derived values by Sinclair et al. (2012), indicating that PCP and/or ICD exerts a first order control prior to calcite precipitation on the stalagmite. This signal is subsequently modulated by the growth-rate dependency of the incorporation of Sr.

The control on Mg/Ca as tracer for rainfall variability is further constrained by a strong correlation of annual mean Mg/Ca in the speleothem with winter precipitation in southwestern Romania through the 20th century. This correlation has proven to be robust against age uncertainties and autocorrelation effects and could even be used to deduce a quantitative reconstruction of precipitation estimates for the last ~4000 years.

Conclusions

In summary, Mg/Ca and Sr/Ca have shown to be mainly controlled by hydrological processes in all records. For Cloşani, a direct link of Mg/Ca in stalagmite C09-2 with rainfall was found. The interpretation of the Romanian record clearly benefits from the direct comparison with instrumental data, which is not possible for the other studies. Here, the case is not that clear and the hydrological control on the Mg/Ca ratio remains ambiguous. Reconstruction of past hydrological conditions thus has to rely on the combination of several proxies such as $\delta^{18}O$ values (section 8.1) to derive concrete conclusions.

However, care must be taken when interpreting trace element signals from samples which exhibit a variable calcite precipitation rate. If growth rate varies over more than an order of magnitude, it may significantly affect the Sr/Ca ratio of speleothems, which was shown to apply for all samples in this thesis to a greater or lesser extent. Also temperature variability may exert a non-negligible second-order effect on Mg/Ca. The same may apply at some locations to detrital contamination, the effect of soil processes and sea spray as well as limestone diagenesis. These aspects have to be properly assessed and evaluated and, if quantitative estimation of the processes is possible, compared to the present variability in the trace element signal.

The model of Sinclair et al. (2012) provides a helpful tool to reach a better understanding of the processes which may be responsible for the observed trace element variability in speleothem records. In remote cave locations, it is often not possible to establish a cave monitoring program, or the results may not be transferable to the analyzed sample. It clearly shows, that a correlation of Mg/Ca with Sr/Ca may not be necessarily linked with hydrological processes, and if so, they may not underly a linear relationship.

8.3 Phosphorus - a proxy for vegetation and soil dynamics?

P/Ca was analyzed and interpreted in speleothem PR-LA-1 and CM. In stalagmite C09-2, the measured P concentration was in the range of the detection limit, and was thus not interpreted in Chapter 7. However, the raw intensities appear to confirm the expected pattern for temperate climates, with a positive correlation of the P and U signal and the P content being related with annual laminae (section 2.5.1).

The P content in C09-2 seems to exhibit a seasonal cyclicity which is anti-correlated to Sr/Ca and Ba/Ca (Figure 8.1). High Sr/Ca values in C09-2 were attributed to the winter sea-

son and vice versa. Thus, the peak value of the P/Ca cycles seems to occur during the summer. Thus, P input in the speleothem appears to be highest during the warm season, when vegetation activity is high. However, infiltration and calcite precipitation during the summer is regarded to be very low in Cloşani Cave, so the high peak in P content potentially marks the onset of calcite precipitation after the summer season, when infiltration increases and soil P is flushed into the cave. The P peak in C09-2 is rather sharp, which may be associated to the still relatively low calcite precipitation rates during late summer and autumn compared to winter/spring months, where pCO_2 in cave air reaches its minimum and speleothem growth is at a maximum.

This explanation agrees with the common interpretation of the P content in speleothems. Borsato et al. (2007) attributed annual P layers to an autumnal flush of organic material from the soil due to the coincidence of vegetation dieback and high infiltration, similar to Treble et al. (2003), who argue that P from seasonal vegetation decay is transported to the speleothem before it is mineralized in the soil.

The correlation of U and P is observed in all three samples included in this thesis (sections 5.4.2 and 6.4.1). This is explained by the formation of phosphate/uranyl complexes, which was first described by Treble et al. (2003).

In the Puerto Rican speleothem, P/Ca ratios are anti-correlated with both Mg/Ca and $\delta^{13}C$ values (section 5.4.2). Similar patterns are previously observed by Webb et al. (2014) and Mischel et al. (in press), respectively. As a consequence, both studies interpret higher values in

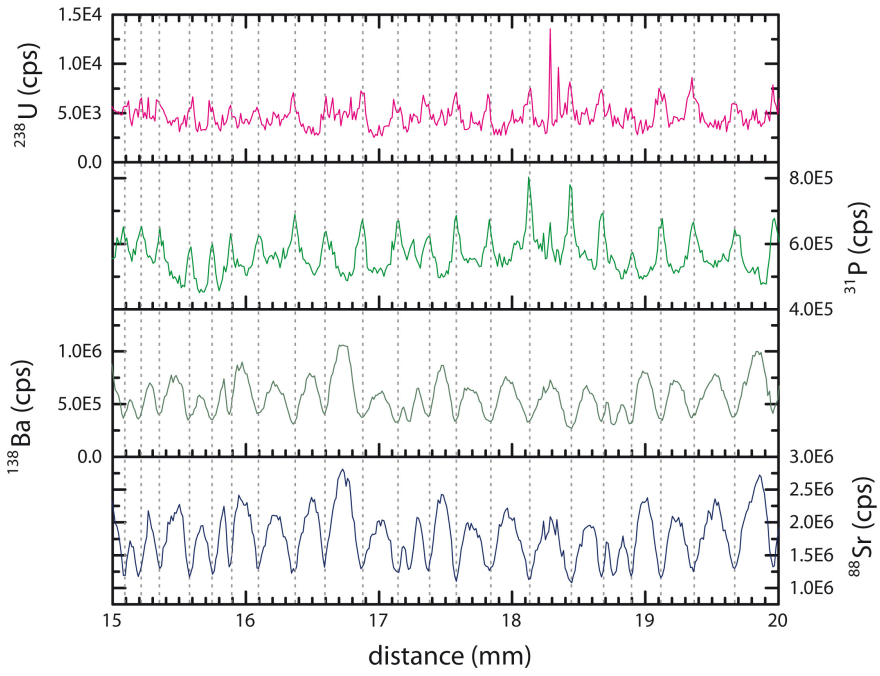

Figure 8.1: *Raw intensities of a section of a laser ablation line scan from C09-2. In this section, the cyclicities of the Sr, Ba, P and U signals are well prounounced. The P content of the speleothem is characterized by distinct peaks, which are anti-sorrelated to Sr and Ba maxima.*

P and U as reflecting more productive vegetation and higher soil moisture. This interpretation is regarded to explain P/Ca variability in PR-LA-1.

8.3.1 Non-conventional P/Ca systematics in CM

In contrast, stalagmite CM exhibits an inverse relationship with Mg/Ca and $\delta^{13}C$ values (section 6.4.1). So far, such a pattern has not been described in speleothem records before. Since no extensive monitoring of dripwaters or analyses of soil characteristics exist for the location of the cave, the interpretation of this signal has to rely on some assumptions.

The most prominent interval of the record is the Last Glacial Maximum (LGM). Several proxies and other studies indicate that this period is characterized by lower temperatures and rainfall compared to the Holocene (section 6.4.3). Low growth rates, high Mg/Ca and $\delta^{13}C$ values confirm, that the LGM experienced a deterioration of climate conditions in Cuba. In this period, P/Ca and U/Ca exhibit a broad maximum with values up to 3 mmol/mol (3000 ppm). Such high values are usually not observed in speleothems, whose P content is only fed by soil P interpreted to be mainly dominated by organic P (compare section 2.5.1).

In a tropical speleothem from Christmas Island, Frisia et al. (2012) report values of up to 8000 ppm, and state that the high P values are likely to be sourced from the dissolution of apatite-group minerals present in the epikarst and brecciated rock. Apatite inclusions are not reported for the host rock at the location of CM, however, this does not generally exclude this source. However, this source is not regarded as the main driver of high P/Ca values in CM. More dissolution of apatite minerals is more likely to occur during more humid intervals, which is also observed by Frisia et al. (2012), where periods of high P concentration generally reflect effective recharge of the aquifer in the rainy season.

In another speleothem 645-FS04 from southern Australia, Frisia et al. (2012) report distinct P concentration peaks associated with 'stromatolite-like' layers which mark periods of reduced drip rate and thus potentially indicative of dry phases of unknown duration within the otherwise wet climate regime of the Early Pliocene. These laminae are characterized by micrometer-scale micritic structures which are suspected to be caused by microbial processes which may have been involved in the P incorporation in the speleothems.

Although petrographic analyses are not available for CM to compare the crystal structures to the observations by Frisia et al. (2012), it is unlikely that the proposed processes also caused high P/Ca values during dry intervals in CM. Firstly, the elemental patterns within these 'stromatolite-like' layers are not consistent with correlations of P/Ca with Mg/Ca observed in CM. Moreover, the P-rich interval in CM is stretched over several mm to cm, whereas the P concentration peaks in the Australian sample are concentrated on mm-thin layers (Frisia et al., 2012).

Thus, in Chapter 6 another interpretation for the high P/Ca ratios during intervals with apparently drier and cooler conditions is suggested. Organic P may not be the only main source of P in the soil solution during the LGM indicated by the high concentrations and the

apparently cool and dry climate. Since P fixation in soils is pH dependent, it is suspected, that the observed inverse connection of P/Ca with vegetation variability may be the result by changing soil characteristics due to pH shifts. Treble et al. (2003) argue with the low P retention capacity of the sandy southwestern Australia soils, which might explain why a strong seasonal P signal associated with seasonal flush of organic-rich complexes is seen in speleothems from this region. In contrast, subtropical and tropical soils are often characterized by a high P retention capacity (Sanchez and Uehara, 1980; Daroub et al., 2003), which means that phosphate is bound much tighter to the non-soluble phase. A decline in vegetation productivity on long timescales may result in a lower soil pCO_2, which in turn increases soil pH. P availability in soils has a maximum at neutral or weakly acid soil pH (Figure 2.11). It may be possible, that certain circumstances of climate and soil conditions might have shifted the P cycle to this maximum, releasing previously adsorbed phosphates to the soil solution and thus increasing the flush of P-rich complexes.

8.3.2 Conclusions

The compilation of the P cycle in section 2.5.1 shows, that the processes governing the P concentration leached from the soil solution into cave dripwaters may be very diverse and site-specific, depending on physical and chemical soil and host rock characteristics, microbial activity, vegetation dynamics and the climatic boundary conditions.

However, it can be summarized that, P in speleothems is most commonly related to vegetation and soil dynamics, associated with hydrological variability, as observed in many previous studies and also in stalagmites C09-2 and PR-LA-1 (Chapters 5 and 7). However, the results from Chapter 6 and published by Frisia et al. (2012) show, that other processes may significantly change the hydrological interpretation of P. The P cycle is a complex system and many processes involving microbial activities as well as site-specific soil characteristics were found to have a strong effect under certain circumstances.

Information about physical, chemical and biological soil characteristics should be considered to complement the interpretation of P in speleothems, especially where elemental patterns appear to be controversial. Moreover, Frisia et al. (2012) claim, that the use of P to refine paleo climate information from speleothems should be underpinned by petrographic and elemental mapping, along with the chemical and textural characterization of the karst host rocks.

9 Climatological inferences in the framework of recent research

This part comprises the climatological aspects of this thesis, which covers the last glacial period (section 9.1) and the associated long-term and millennial scale climate fluctuations, as well as the late Holocene (section 9.2) with its extensively studied prominent climate anomalies. The most relevant results of the corresponding studies are revisited and important intervals of the climate records discussed.

9.1 Spatio-temporal imprints in the tropical hydrological cycle

Climatic fluctuations on different timescales may be brought by internal or external mechanisms. Solar insolation is considered a main driver of the climate system, and its influence during Earth's past due to orbital variations mainly caused the ice age cycles (Milankovitch, 1941; Imbrie and Imbrie, 1986; Paillard, 2001). The influence of various internal parameters such as ice sheet dynamics, atmospheric CO_2 concentration, global deep-ocean circulation, and others lead to a variable climate during the glacial cycles marked by long-term variations, the marine isotope stages, MIS, (Emiliani, 1955) as well as abrupt temperature oscillations.

During the last two decades, ice core records and marine sediment cores from the North Atlantic region revealed that the last glacial period was characterized by abrupt climate changes that recurred on millennial time scales (Clement and Peterson, 2008). The most recent and perhaps best studied of these events is the Younger Dryas (YD), an abrupt return to near-glacial temperatures in the high-latitude North Atlantic lasting roughly a millennium during the last deglaciation (Alley et al., 1993; Clement and Peterson, 2008).

Rapid temperature excursions, named the Dansgaard/Oeschger cycles (D/O) were a characteristic feature of Greenland climate during the last glacial period recurring roughly every 1500 years as abrupt warmings over Greenland of as much as 10°C followed by a more gradual return to cold glacial conditions, and were showed to closely match sea surface temperature (SST) changes recorded in high-accumulation rate sediments in the North Atlantic (Bond et al., 1993).

Additionally, discrete layers of ice-rafted debris (IRD) were found in sub-polar North Atlantic sediments (Heinrich, 1988; Bond et al., 1992), named the Heinrich events. The IRD was deposited periodically during the coldest phases of the D/O cycles and were attributed to originate from icebergs that came out of the Hudson Strait (Hemming, 2004). This freshwater

input promoted a slowdown of the Atlantic meridional overturning circulation (AMOC) and an inter-hemispheric climate response (McManus et al., 2004; Wolff et al., 2010; Böhm et al., 2015). Heinrich stadials subsequent to Heinrich events were associated with a reduction in sea surface temperatures (SSTs) in the North Atlantic (Sachs and Lehman, 1999; Hagen and Keigwin, 2002). Reduced Northern Hemisphere SSTs led to the southward shift in the ITCZ and drier conditions in the tropical Northern Hemisphere (Chiang and Bitz, 2005; Zarriess et al., 2011; Stager et al., 2011).

In the Chapters 5 and 6, two speleothem records are presented from the Caribbean realm covering long intervals during the last Glacial period. Both records provide new insights into the variability of the tropical hydrological cycle on different timescales (Figure 9.1). The $\delta^{18}O$ record from stalagmite PR-LA-1 (Chapter 5) documents the clear imprint of prominent abrupt millennial-scale climate oscillations during the last Glacial. It is the first speleothem derived long-term reconstruction of rainfall variability from the western tropical Atlantic realm which records both the Heinrich stadials as well as the Dansgaard/Oeschger cycles. In contrast, the $\delta^{18}O$ signal from western Cuba deduced from speleothem CM (Chapter 6) exhibits a much lower internal variability. However, geochemical evidence from the stable isotope and trace element signatures yield a comprehensive picture of past environmental variability over a long time interval. This record is one of the longest speleothem records from the Caribbean region.

The discussion of the effects of last Glacial climate variations on the tropical hydrological cycle was extensively elaborated in both Chapters, so this section rather depicts a summary and comparison of the results from both studies. In the first part, the variations and forcings of both records on longer timescales are compared (section 9.1.1). Section 9.1.2 focuses on the abrupt fluctuations on millennial scale.

9.1.1 Long term variability on glacial / interglacial timescales

The Cuban record covers most of the last glacial cycle from the late stages of MIS5 (MIS5c, 96-87 ka, MIS5b, 87-82 ka and MIS5a, 82-71 ka) until the middle of MIS1 (14 ka today), whereas PR-LA-1 grew during MIS3 (57-29 ka) and MIS2 (29-14 ka). The deduced climate reconstruction showed, that rainfall variability on Cuba and Puerto Rico is connected to insolation and tropical North Atlantic and Caribbean SSTs, as well as to the strength of the AMOC and high-latitude temperature variability. The comparison in Figure 9.1 shows, that both records are on the same level of $\delta^{18}O$ values during MIS2 and MIS3, which supports the common, supra-regional controls of Caribbean rainfall. In contrast, the speleothem record from Costa Rica (Lachniet et al. (2009), Figure 9.1) is characterized by much lower $\delta^{18}O$ values, reflecting the more remote position from the moisture source - which are mainly the western tropical Atlantic and the Caribbean Sea - close to the Pacific coast across the isthmus.

The position of the Intertropical Convergence Zone (ITCZ) and associated changes in tropical rainfall has been closely related to variations in summer insolation (Baker et al., 2001;

Cruz et al., 2005a; Poveda et al., 2006; Wang et al., 2007). Interestingly, on glacial-interglacial timescales, the $\delta^{18}O$ values of CM show a close relationship rather to winter insolation, which is opposite to the expectation of a direct insolation-monsoon strength mechanism. This observation is shared with the Costa Rican speleothem record (Lachniet et al., 2009). The Puerto Rican record is too short to conduct a similar comparison, however, the similarities in the long-term variability between CM and PR-LA-1 support this pattern. The most probable interpretation explaining this phenomenon is, that high winter insolation leads to a prolonged wet season in the tropical Atlantic and Caribbean. This demonstrates the complexity of tropical hydrological cycle (section 6.4.2).

MIS5 appeared to have experienced the most variable climate compared to the other parts of the Cuban record (Figure 6.7). Interestingly, the transition into cooler and drier glacial conditions during MIS4 is very differently pronounced in the other archives, with the runoff

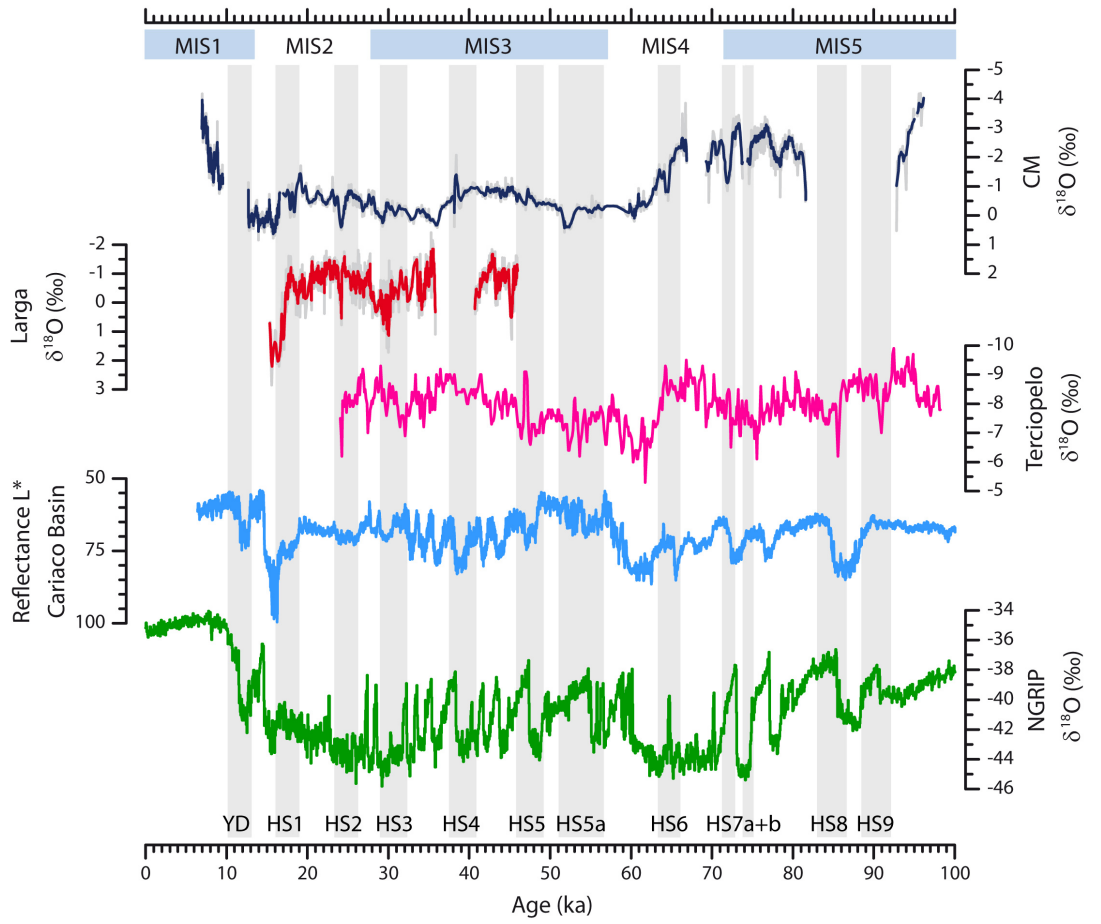

Figure 9.1: *Comparison of $\delta^{18}O$ records of CM (dark blue) and PR-LA-1 (red) with speleothem $\delta^{18}O$ values (magenta) from Terciopelo Cave, Costa Rica (Lachniet et al. (2009)), the reflectance record from the Cariaco basin (light blue) representative for the position of the ITCZ (Deplazes et al., 2013) and the NGRIP $\delta^{18}O$ ice core record (green, NGRIP members (2004)). Vertical gray bars indicate the timing of North Atlantic cold events (Younger Dryas (YD) and Heinrich stadials (HS)).*

in Northern Mexico decreasing very smoothly (Roy et al., 2013), and the rainfall in Cuba and Central America dropping much faster, but not simultaneously. On the one hand, this may be attributed to uncertainties in the age models or site-specific factors. On the other hand, this may suggest an interesting spatio-temporal feature in last Glacial climate variability, which might deserve further investigation.

During the Last Glacial Maximum (LGM), climate on Cuba was relatively cool, but not extraordinary dry. Nevertheless, P/Ca ratios demonstrated that environmental conditions were sufficiently unfavorable for the existing biosphere, resulting in a decline in vegetation and soil dynamics (section 6.4.3). The results are in concert with lacustrine sediments from Guatemala (Hodell et al., 2008; Escobar et al., 2012; Correa-Metrio et al., 2012; Grauel et al., 2016) or Mexico (Roy et al., 2013).

In contrast, the LGM marks no such pronounced interval in the Puerto Rican record. $\delta^{18}O$ values remain on a comparably stable level between 24 and 18 ka, with slightly higher values from 20.5 to 18 ka. These are accompanied by slightly higher Mg/Ca and lower P/Ca values, indicating drier conditions and a potential deterioration of vegetation and soil activity also in Puerto Rico. However, these environmental changes are not as pronounced as indicated by the proxy records in Cuba. This may be attributed to its location further north-west, which probably resulted in the severer climate changes due to the southern movement of the ITCZ. On Puerto Rico, the millennial scale fluctuations had a much stronger influence (section 9.1.2).

9.1.2 Abrupt North Atlantic climate changes on millennial scale

Despite CM covers most of the last Glacial cycle, the Dansgaard/Oeschger interstadials are pronounced in stalagmite CM only during MIS5, where the peak intervals also mark the warmest phases in the record besides the Holocene (Figure 6.7). In contrast, PR-LA-1 shows a clear response to warm interstadials during MIS2 and 3. The internal comparison of the $\delta^{18}O$ signatures reveals, that D/Os 7 and 11 were the warmest/wettest on Puerto Rico, with only slightly drier and cooler conditions compared to modern times (section 5.4.3).

Most NA cold events, such as the Younger Dryas and the Heinrich stadials were characterized by cooler and/or drier conditions on Cuba and Puerto Rico (sections 5.4.3 and 6.4.3). Similarly, in both records, HS 1 seems to be the coolest and driest interval. This phenomenon is observed also in other archives throughout the Caribbean realm, such as from Central America (e.g., (Escobar et al., 2012; Lachniet et al., 2013)) or the Bahamas (Arienzo et al., 2015), and may be associated with a near complete shut down of the AMOC (Böhm et al., 2015). Also the internal structure of HS 1 is coherent across the region, with two consecutive cold/dry spells interrupted by a short recovery to relatively warmer/wetter conditions.

In general, the $\delta^{18}O$ signatures during Heinrich stadials are much more pronounced in the Puerto Rican record than in western Cuba (Figure 9.1), with $\delta^{18}O$ values increasing by about 2-3 ‰ in PR-LA-1, compared to 1-2 ‰ in CM. This may be attributed to a spatial difference

in temperature and rainfall variability, or site-specific variable fractionation effects due to drip-rate variability or cave ventilation. The generally higher growth rates of PR-LA-1 and the high, persistent correlation with $\delta^{13}C$ values suggest, that this speleothem is probably more sensitive to disequilibrium fractionation effects than stalagmite CM. Thus, it may be suspected, that the difference in the $\delta^{18}O$ signal of these records may be largely attributed to 'kinetic' effects in Puerto Rico. However, rainfall variability and the associated amount effect in the tropics may be also regionally very different and site-specific. Additionally, the absolute decrease in last Glacial temperatures differs largely between marine and terrestrial records (Sachs and Lehman, 1999; Hagen and Keigwin, 2002; Correa-Metrio et al., 2012; Grauel et al., 2016), ranging from 2 - 3 °C in tropical Atlantic sea surface temperatures to 6 - 10 °C in the central American lowlands. Both presented speleothem records from Puerto Rico and Cuba suggest, that the temperature decrease during the last Glacial and the Heinrich stadials was comparable rather to the SST estimates and similar to the results obtained by Arienzo et al. (2015) (sections 5.4.3 and 6.4.3). This may be attributed to the insular locations, which could be responsible to the stronger marine imprint.

Regarding the amount effect, the estimated slope at Cueva Larga is roughly -0.4 to -1 ‰ per 100 mm on annual and monthly scale, respectively (Vieten et al. (in press) and section 5.4.2). For Panama, previous studies found a relationship of -1.6 to -2.85 ‰/100 mm between $\delta^{18}O$ and the amount of precipitation (Lachniet et al., 2004; Lachniet and Patterson, 2006). Similar values were found for Barbados (-2.2 to -2.75 ‰/100 mm, Jones et al. (2000)) and Panama and Belize (-1.24 ‰/100 mm, Lachniet and Patterson (2009)). Fensterer et al. (2012) derived a trend line between stalagmite $\delta^{18}O$ and rainfall of -0.19 ‰/100 mm whereas Medina-Elizalde et al. (2010) deduced a more negative slope of -0.57 ‰/100 mm for stalagmites from Mexico. This large range of slopes describing the amount effect throughout the Caribbean and Central American realm illustrates that the absolute differences in $\delta^{18}O$ signatures during supra-regional climate events such as the Heinrich stadials or the Dansgaard/Oeschger cycles cannot be directly compared without additional information such as independent temperature estimates (e.g., Arienzo et al. (2015)) and an estimation of the site-specific amount effect.

9.1.3 Conclusions

The both presented speleothem studies from Cuba and Puerto Rico provide a valuable amendment to the picture of last Glacial spatio-temporal climate variability in the Caribbean realm. Even if the temporal resolution of both records is partly very different, they share fundamental similarities, such as the long-term variability in $\delta^{18}O$ values, which may be attributed to changes in insolation, sea surface temperatures. Another feature present in both $\delta^{18}O$ signals is the response to North Atlantic cold events, which are pronounced as cool and dry intervals in the Caribbean region. The decrease in temperature and precipitation seems to be closely linked to a slowdown of the Atlantic meridional overturning circulation (AMOC)

due to enhanced fresh water input in the North Atlantic and associated lower SSTs.

The comparison of the absolute variability in $\delta^{18}O$ values, however, does not enable a quantitative estimation of the spatio-temporal differences of temperature and rainfall variability between both locations. Additional information, for example derived from fluid inclusions or clumped isotopes, might enable a more specific estimation of the effects of temperature, rainfall and disequilibrium effects during last Glacial climate oscillations.

Substantial differences are observed in the response to North Atlantic warm interstadials (D/O cycles) which are only partly pronounced in the Cuban record - and only during the relatively warm MIS5. Additionally, the Last Glacial Maximum seems to have been characterized by more severe environmental conditions on Cuba than on Puerto Rico, where the associated climate deteriorations appear to have been relatively mild. These differences could be linked with the latitudinal position of both locations and the relative distance to the position of the ITCZ which determines the strength of the trade wind zone at the cave sites. Puerto Rico is located further south, so a southern shift of the ITCZ during MIS2, MIS3 and especially the LGM may affect the hydrological cycle less than on the more northwesterly situated Cuba.

9.2 Late Holocene climate variability in eastern Europe

The main focus of Chapter 7 was the analysis and interpretation of trace elemental and stable isotopic records deduced from a late Holocene speleothem from Cloşani Cave, Romania. The correlation analysis demonstrated, that the Mg/Ca ratio in stalagmite C09-2 is strongly connected with winter precipitation in southwestern Romania and enabled a quantitative reconstruction of past winter rainfall for the last 3.6 ka. The deduced precipitation estimates from C09-2 were found to be in agreement with other rainfall reconstructions. Moreover, the most prominent anomalies recorded in European climate archives during the last 4 ka are also pronounced in this record. However, in Chapter 7, the discussion of past climate variability in eastern Europe and the associated processes was kept rather cursory. In this section, the emphasis is on assessing the influences of large-scale teleconnection patterns and a more comprehensive comparison of the generated climate record with other regional and European climate archives during the Medieval Climate Anomaly and the Little Ice Age.

9.2.1 Influence of large-scale circulation patterns

The climate over Eastern Europe region is dominated by the North Atlantic Oscillation (NAO) and the East Atlantic-West Russia (EAWR) pattern (Hurrell et al., 2003, 2006; Barnston and Livezey, 1987). Both teleconnection patterns were found to strongly influence climate parameters in Romania (e.g. Bojariu and Paliu (2001); Bojariu and Gimeno (2003); Rimbu et al. (2012); Drăguşin et al. (2014); Micu et al. (2015)). In general, a high NAO index appears to be associated with warmer temperatures and reduced precipitation in the Romanian area (Bojariu and Gimeno, 2003; Bojariu and Paliu, 2001). In contrast, positive anomalies of the EAWR index are related with cooler temperatures and drier conditions (Rimbu et al., 2012). However, model studies indicate, that these large-scale pressure systems interact and that the previously found associations with precipitation, snow variability or temperature may not be stationary in time (Ionita, 2014; Comas-Bru et al., 2016).

In Figure 9.2, the Mg/Ca and $\delta^{18}O$ values from C09-2 are compared to reconstructions of NAO and EAWR indices during the last 350 years (Luterbacher et al., 2001, 2002; Poirier et al., 2017). The plot illustrates the non-stationary relation of southwestern Romanian climate to the both teleconnection patterns. Despite all winter dry spells in the Cloşani region are associated with a positive phase of the EAWR, this connection is not valid in the other direction. Several intervals with high EAWR indices cannot be attributed with reduced precipitation in Romania. However, the driest phase in the plotted interval around 1680 AD is also characterized by extremely high values of the EAWR index. A similar picture is notable regarding the NAO. Only a few of the drier periods in Romania are accompanied by high NAO indices.

In Chapter 7, more Mediterranean influence on rainfall variability in southwestern Romania associated with warmer conditions is attributed with higher $\delta^{18}O$ values in the speleothem and vice versa. Thus, positive EAWR anomalies might coincide with lower $\delta^{18}O$ values. This relation is visible for many of the positive excursions of the $\delta^{18}O$ record. The long-term pat-

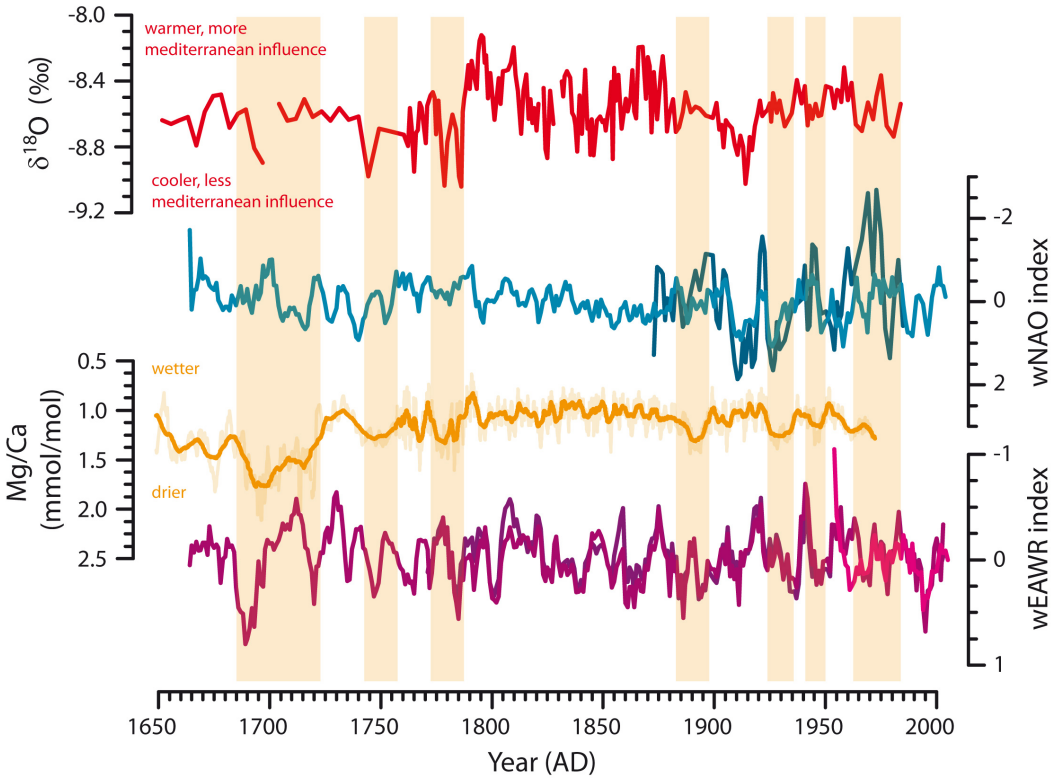

Figure 9.2: *Mg/Ca and $\delta^{18}O$ values from C09-2 are compared to the 5-year running means of DJF-NAO (Luterbacher et al., 2001) and DJF-EAWR indices (Poirier et al. (2017) with data from Luterbacher et al. (2001)) from 1660 until 2000 AD. The light orange bars indicate dry spells in southwestern Romania. Note that the axes are inverted.*

tern of the oxygen isotopic signature in C09-2 may be also related with NAO variability on multidecadal timescales. This connection to North Atlantic climate variability was suggested by a number of low-resolution speleothem records from the Holocene (e.g., (Onac et al., 2002; Constantin et al., 2007; Drăguşin et al., 2014)).

To summarize, despite some apparent connections of southwestern Romanian climate to the NAO and EAWR patterns, reconstructions from the southern Carpathian realm appear not to be appropriate to make inferences about past variability of these teleconnections.

9.2.2 Eastern European Holocene climate variability

For eastern Europe, a variety of climate reconstructions exist covering the last centuries and millennia. Many of them are based on tree-ring reconstructions, which rather reflect summer conditions (e.g., Popa and Kern (2008); Levanič et al. (2012); Trouet (2014); Levanič et al. (2015)). The C09-2 speleothem record however is biased to the cold season. Other climate records are available, but many are based on rather coarse resolution or cover relatively short intervals such as various speleothem (e.g., Onac et al. (2002); Constantin et al. (2007); Tămaş

et al. (2010); Rudzka et al. (2012); Drăguşin et al. (2014); Onac et al. (2014, 2015)) or lake sediment records (Feurdean and Bennike, 2004; Schnitchen et al., 2006; Magyari et al., 2009; Buczkó et al., 2013; Cristea et al., 2014).

In section 7.4.1, it was shown that the winter precipitation reconstruction for southwestern Romania agrees with several regional and supra-regional hydroclimate records. During the last 250 years, a number of dry spells prevailing in summer and winter seasons could be identified due to the comparison with a summer drought record from Levanič et al. (2012). A supra-regional connection was found to the autumn/winter rainfall reconstruction of Jex et al. (2011) from northern Turkey, which may be attributed to the strong influence of the EAWR on precipitation variability at both locations.

Medieval Climate Anomly and Roman Warm Period

Amongst the most prominent warm climate anomalies during the last 3500 years were the Medieval Climate Anomaly (MCA) between ca. 900 and 1400 AD and the Roman Warm Period (RWP) between ca. 250 BC to 400 AD. Across southern and eastern Europe, overall warm conditions are inferred for both intervals, the MCA (e.g., Rohling et al. (2002); Frisia et al. (2005); Cristea et al. (2014)) and the RWP (e.g., Martín-Chivelet et al. (2011); Cristea et al. (2014); Goudeau et al. (2015)), respectively. However, Bradley (2015) infer that there is little evidence, that global or hemispheric mean temperatures were higher during the MCA than in the latter half of the twentieth centuries. The author notes, that it is of greater significance, that there were significant precipitation anomalies during the period of the MCA, in particular, many areas experienced pronounced drought episodes (Diaz et al., 2011). The widespread nature of hydrologic anomalies during the MCA suggests that changes in particular circulation regimes (e.g., NAO and ENSO) may account for the unusual regimes during this interval. In stalagmites from NW Scotland, evidence was found for a persistent positive NAO during the MCA (Trouet et al., 2009; Baker et al., 2015), which might explain the existence of a dry period in the western and central Mediterranean (Moreno et al., 2012; Ramos-Román et al., 2016). However, other data suggests a more variable state of the NAO during the MCA (Wassenburg et al., 2013; Smith et al., 2016).

Also in the reconstructed precipitation estimates from SW Romania (Figure 7.14), climate during the MCA appears to be variable, with the beginning of the MCA being more humid than average, whereas during the second half conditions became slightly drier. This pattern was also observed by Onac et al. (2015) deduced from a cave guano sequence from a cave in SW Romania. Consistently, Feurdean et al. (2015) infer wet conditions between 800-1150 AD and a dry interval from 1300-1450 AD for the northern Carpathians. Goudeau et al. (2015) observe a warm early MCA (~950 AD) and colder conditions during the later part (1000-1200 AD). A similar pattern is found across the Mediterranean (Pla and Catalan, 2005; Frisia et al., 2006) and in the southern Alps (Frisia et al., 2005; Holzhauser et al., 2005). This interval also corresponds with a transition from dry conditions to more humid conditions in the western Mediterranean (Nieto-Moreno et al., 2013). A similar pattern appears during the

RWP, which was characterized by generally warmer and humid conditions in SW Romania, with a drier period from 0 to 200 AD.

Little Ice Age (LIA) and other dry intervals

The Little Ice Age (LIA) represents one of the strongest global climate instabilities during the late Holocene and is characterized by a multi-centennial-long cooling during the 14th to 19th centuries (e.g., Mayewski et al. (2004); Mann et al. (2009b); Büntgen et al. (2011); PAGES 2k Consortium (2013)). The cooling has been attributed to a reduction in solar activity, with the most prominent solar minima occurring between 1645-1715 AD and 1790-1830 AD. These excursions are known as Maunder and Dalton minima, respectively (Mann et al., 1998; Jones and Mann, 2004; Mann et al., 2009b). On the European continent, and especially in the circum-Mediterranean region, the climate during the LIA is characterized by a remarkable spatio-temporal heterogenity (Luterbacher et al., 2004; Xoplaki et al., 2005; Touchan et al., 2005; Griggs et al., 2007; Gogou et al., 2016). For instance, various climate records have documented more humid conditions in the western Mediterranean, and drier conditions in the East (Roberts et al., 2012).

Recent research on high-resolution records indicates also a non-consistent pattern across eastern and southeastern Europe during the LIA. In the northern Carpathians, generally cooler temperatures are inferred in a peat bog profile (Cristea et al., 2014), while Feurdean et al. (2015) report dry conditions during 1500 to 1850 AD. In C09-2, the LIA is a very pronounced period, with a gradual decrease in growth rates, precipitation and $\delta^{18}O$ values from approximately 1500 AD onwards (Figure 7.14). The severest winter conditions were identified between 1680 and 1760 AD, contemporary with the Maunder Minimum. The Dalton minimum, however, is not as pronounced in this record.

Interestingly, a bat guano $\delta^{13}C$ record from the Apuseni mountains northwest of the Carpathians shows a different picture of climate conditions during the LIA, indicating the strong influence of the topography of the mountain chain. In their record, evidence was found for two major cold spells occurring around 1400-1500 AD and ca. 1870 AD, which are both also prominent in the C09-2 record, even if not as pronounced. However, neither $\delta^{13}C$ values nor pollen association in guano changed strikingly over the MCA and LIA transition (Forray et al., 2015). The authors infer, that this region experienced generally a warmer and drier climate during the LIA, but colder and wetter than the MCA.

On the Balkan Peninsula, generally cooler conditions prevailed as inferred from tree-ring reconstructions (Trouet, 2014; Levanič et al., 2015). Sedimentological and geochemical data from Lake Butrint in the western Balkans (Albania) suggest that although the LIA was generally characterized by higher humidity relative to pre- and post-LIA times, maximum winter precipitation was recorded between 1600 and 1800 AD (Morellón et al., 2016). Another varved sediment record from Etoliko Lagoon (western Greece) suggests that wet conditions in winter prevailed during 1740-1790 AD, whereas dry winters marked the periods 1790-1830 AD (Dalton Minimum) and 1830-1930 AD, the latter being sporadically interrupted by wet winters

(Koutsodendris et al., 2017). This is apparently an opposite observation to the hydroclimatic variations reconstructed in the Cloşani area. Moreover, the relatively high $\delta^{18}O$ values in C09-2 indicate generally less Mediterranean influence during the LIA. Koutsodendris et al. (2017) assign the variability of precipitation in western Greece to North Atlantic Oscillation dynamics, which was found to have a generally less impact on climate variability in southwestern Romania than e.g., the EAWR. These observations support, that precipitation variability in southwestern Romania is the result of different competing circulation patterns.

Other dry intervals in the C09-2 record are recorded around 450-610 AD and at the end of the late Bronze Age from around 1300 to 1000 BC (Figure 7.14). The first one may be associated with a pronounced cooling recorded throughout the northern hemisphere from 536 to around 660 AD, which was recently described by Büntgen et al. (2016) and termed the 'Late Antique Little Ice Age' (LALIA). Cristea et al. (2014) also report a dry period in a peat bog profile from the northern Carpathians around 520 AD. The latter dry phase during the Bronze Age may be attributed to the '3.2 ka event' (Drake, 2012; Drăguşin et al., 2014), which is also associated with a minor dry phase in the northern Carpathian $\delta^{13}C$ record (Cristea et al., 2014).

9.2.3 Conclusions

Chapter 7 and this summary show, that the deduced proxy record and its interpretation is in agreement with other regional and supra-regional climate reconstructions. However, the mechanisms governing temperature and precipitation variability are very diverse and could not be unambiguously elucidated. Several patterns and processes could be identified which have an at least temporary strong influence on the climate in the region.

In general, air masses from the Mediterranean and the Atlantic ocean dominate the moisture sources, which probably determines the variability of the $\delta^{18}O$ values in the speleothem. This is supported by the connection of eastern European to North Atlantic climate variability. However, the comparison of the C09-2 proxy records with the reconstruction of NAO and EAWR indices has shown, that the climate in southwestern Romania cannot be attributed to the variability of a single large-scale teleconnection pattern. Despite the EAWR appears to exert more influence on winter climate in the Cloşani region than the NAO, the relation seems to be non-stationary.

10 Conclusions and Outlook

The central goal of this thesis was assessing the benefits and limitations of multi-proxy approaches in speleothem research. Hence, the aims were evaluating the environmental controls of speleothem proxies such as stable isotopes or trace elements, and the application to specific case studies from locations affected by complex climate interactions. Thus, the extraction of appropriate proxies and the improvement of their general understanding concerning their interpretation in terms of climate variability was a main task. A second focus was to evaluate the contribution of the generated records to increasing the knowledge and understanding of past climate conditions in the investigated regions.

All studies presented in the Chapters 5 to 7 demonstrate the strong benefits of the application of several proxies in speleothems. However, the chosen tracers reveal some limitations in terms of specific climate reconstruction, which require the assessment of potential further steps for an improvement of such approaches. The main results and consequences from this thesis concerning the interpretation of the applied proxies are summarized and discussed in Chapter 8.

The analysis of stable isotope $\delta^{18}O$ and $\delta^{13}C$ composition together with trace elemental signatures enables a broad survey of past environmental changes comprising temperature and rainfall variability as well as soil and vegetation dynamics. However, only under certain circumstances, a single proxy may be clearly associated with a climate parameter, and the comprehensive interpretation of several proxies is necessary to make climatological inferences.

For example, in tropical locations, the $\delta^{18}O$ values in speleothems may be reliable recorders of past rainfall variability. However, a number of processes affecting the oxygen isotopic composition of speleothems have to be evaluated prior to expressing a final conclusion. Since cave temperature variations influence the fractionation of oxygen isotopes, the absolute estimation of precipitation changes is not possible without additional proxies or other independent records providing information about temperature variations (section 8.1).

Trace elements such as Mg and Sr are found to constitute valuable tracers of hydrological variability (section 8.2), along with P, which is also commonly associated with soil and vegetation dynamics (section 8.3). For the Romanian record (Chapter 7), it is even possible to derive a quantitative transfer function between Mg/Ca in the speleothem and meteoric precipitation, which enables the reconstruction of past rainfall variability in southwestern Romania for the last 3.6 ka.

The interpretation of P/Ca is found to be diverse in the three case studies. In Chapter 6,

the P/Ca ratio is inversely connected with past environmental conditions on Cuba than previously observed in other publications as well as in the other case studies from Puerto Rico and Romania (section 8.3). The proposed mechanism applies only under site-specific conditions, but it shows that the 'established' interpretation of certain proxies may not always be appropriate and has to be questioned in every single case.

Since the environmental controls of the analyzed proxies and its interactions may differ significantly from site to site, speleothem studies strongly benefit from cave monitoring studies, which was shown for the Puerto Rican and Romanian sample (Chapters 5 and 7). However, in some remote locations, regular cave visits may not be realized. In these cases, the model of Sinclair et al. (2012) provides a useful tool to estimate the influence of calcite-water interactions on elemental ratios in speleothems.

A comprehensive evaluation of the results gains more importance and reliability by comparing them with other climate archives, such as for example instrumental or historical records, tree-ring chronologies (Chapter 7), lacustrine sediments (Chapter 6), or pollen assemblages (Drăguşin et al., 2014). Additional information may be also obtained by the application of independent proxies. For the investigated tropical speleothems, the analysis of fluid inclusions could provide valuable information about past dripwater or temperature variability (Arienzo et al., 2015). Clumped isotopes are regarded as paleo thermometer as well as indicators of kinetic effects during calcite precipitation. These methods may provide a reasonable complement to disentangle the effects of temperature, rainfall and kinetic fractionation on the variability of $\delta^{18}O$ values in tropical speleothems.

Regarding the climatological inferences, this thesis focuses on glacial-interglacial and millennial scale variability in the tropics as well as sub-annual to centennial scale climate variability in eastern Europe during the late Holocene (Chapter 9). This comprises a large range in timescales as well as very different climate systems.

The both speleothem records from the Caribbean realm provide valuable information about the last glacial hydrological cycle in the tropics (section 9.1). Similarities in both records and the agreement with independent archives confirm the previously demonstrated response of the Caribbean to North Atlantic climate variability as well as external and internal controls. The exhibited differences suggest a spatio-temporal variability in the distribution of rainfall and temperature, for whose better understanding the two studies provide an important step.

The $\delta^{18}O$ record from stalagmite PR-LA-1 (Chapter 5) is the first speleothem derived long-term reconstruction of rainfall variability from the western tropical Atlantic realm which demonstrates the imprint of both the Heinrich stadials as well as the Dansgaard/Oeschger cycles during the last Glacial (section 9.1.2). Stalagmite CM provides one of the longest speleothem records from the Caribbean region, and the geochemical evidence from the stable isotope and trace element signatures gives a comprehensive picture of past environmental variability over a long time interval (section 9.1.1).

The analysis of independent temperature proxies, as suggested above, could provide more

specific information about past temperature variability and thus enable the direct comparison of the response to North Atlantic climate fluctuations, such as the Heinrich stadials or the D/O cycles. Moreover, the Puerto Rican stalagmite has the potential to allow the possibility to study the internal variability of Heinrich stadials and D/O interstadials on multi-annual timescales, for example by increasing the resolution of the stable isotope records.

Stalagmite C09-2 from southwestern Romania emerged as one of the unique samples appropriate for quantitative reconstruction of past climate variability (Chapter 7). The Mg/Ca ratio was found to be strongly connected with past winter rainfall, and the reconstructed precipitation estimates are in agreement with other local and supra-regional records. However, the classification of the record in a climatological context was rather complex, since southwestern Romania is located in a transition zone of the influence of different teleconnection patterns and air masses.

This thesis demonstrates the benefits and limitations of multi-proxy approaches in speleothem research and provides an important contribution to the recent scientific discussion. All presented case studies are the first speleothem derived climate reconstructions in the investigated regions, respectively, combining both stable isotopes and trace elemental proxies. This approach enabled new insights in the analysis, interpretation and combination of speleothem proxies to make inferences about past climate variability.

For example, an important addition to the previous conventional interpretation of the P/Ca ratio was deduced from stalagmite CM. Moreover, useful guidelines for the interpretation of $\delta^{18}O$ and trace elements such as Mg/Ca in speleothems were developed and applied.

From the climatological point of view, the case studies provided an important step towards better understanding of the spatio-temporal variability of the tropical hydrological cycle during the last Glacial as well as late Holocene climate variability in southwestern Romania.

Part IV

Appendix

A Supplementary material to Paper I - Cueva Larga

A.1 Analytical details

Samples for ^{230}Th/U-dating were cut along the growth axis using a band saw. Analyses of U and Th isotopes was performed using multi-collector inductively coupled plasma mass spectrometry (MC-ICPMS) performed at the Max Planck Institute for Chemistry (MPIC) in Mainz). Chemical preparation of the samples at the MPIC is described in detail in Yang et al. (2015). The analytical methods are described by Obert et al. (2016). All MC-ICPMS ages and activity ratios were calculated using the half-lives reported by Cheng et al. (2000). We decided to use these half-lives instead of the more recent half-lives of Cheng et al. (2013) in order to preserve comparability with previous publications. Age uncertainties are quoted at the 2σ-level and do not include half-life uncertainties. As described in section 5.4.1, a ^{232}Th/^{238}U weight ratio of 0.14 ± 0.11 was found to be appropriate for correction of detrital contamination assuming ^{230}Th, ^{234}U and ^{238}U in secular equilibrium.

Stable carbon and oxygen isotope analysis was performed at the University of Innsbruck. The samples were micromilled at a spatial resolution of 1 mm. The carbonate powder was measured using an on-line, automated carbonate preparation system (Gasbench II) linked to a triple collector gas source ThermoFisher Delta^{plus}XL mass spectrometer. Raw data were calibrated against NBS19, and δ values are reported relative to Vienna Pee Dee Belemnite (VPDB) standard. Long-term precision of the δ^{13}C and δ^{18}O values, estimated as the 1σ-standard deviation of replicate analyses, is 0.06 and 0.08 ‰, respectively (Spötl and Vennemann, 2003; Spötl, 2011).

Elemental concentrations were measured by laser ablation ICPMS at the MPIC following the procedure of Jochum et al. (2012) and Yang et al. (2015), using the high-resolution sector-field ICPMS Thermo Element2, combined with the UP-213 Nd:YAG laser ablation system from New Wave. The analyzed isotopes were measured at low mass resolution ($m/\Delta m$ ~300) and are reported to be interference-free (Jochum et al., 2012). Trace element line scans were performed along the growth axis of PR-LA-1 using a spot size of 110 µm and a scan speed of 10 µm/s, resulting in a spatial resolution of 7 µm per data point (scan time 0.7 s). To avoid potential surface contamination, the scan path was pre-ablated with a scan speed of 80 µm/s. Trace element spot measurements on host rock samples were analyzed with a dwell time of 60 s, spot size 110 µm and repetition rate of 10 Hz. For spot measurements and line

scans warm up and wash out times are 23 and 30 s, respectively. In order to account for matrix effects, data reduction was carried out by calculating the blank corrected count rates of the analyzed isotopes relative to the simultaneously measured internal standard ^{43}Ca. The silicate reference glass NIST SRM 612 was used for external calibration of the trace element analyses (Jochum et al., 2012, 2011). Element to calcium ratios are given as molar ratios.

A.2 Supplementary tables to section 5.3.1 (^{230}Th/U dating)

Table A.1: *Activity ratios and $^{230}Th/U$-ages for section L1A. Uncertainties are given as 2σ range. All ages corrected with a detrital $^{232}Th/^{238}U$ weight ratio of 0.14 ± 0.11.*

Lab.No.	Sample ID	dft (cm)	^{238}U (µg/g)	^{232}Th (ng/g)	($^{230}Th/^{232}Th$) Act. ratio	($^{230}Th/^{238}U$) Act.ratio	($^{234}U/^{238}U$) Act.ratio	Age (uncorr.) (ka)	Age (corr.) (ka)
SW 111	L1A-0,5	0.5	0.295 ± 0.003	0.4468 ± 0.0049	313 ± 3	0.146 ± 0.002	1.1071 ± 0.0116	16.47 ± 0.28	15.40 ± 0.28
SW 1	L1A-1,5	1.5	0.281 ± 0.002	0.1056 ± 0.0015	1297 ± 19	0.157 ± 0.001	1.1018 ± 0.0018	17.02 ± 0.14	16.76 ± 0.13
SW 41	L1A-2,5	2.5	0.101 ± 0.001	0.0089 ± 0.0002	18566 ± 363	0.163 ± 0.001	1.0992 ± 0.0044	17.52 ± 0.18	17.51 ± 0.19
SW 9	L1A-5,3	5.3	0.317 ± 0.002	n.d.	n.d.	0.165 ± 0.001	1.0923 ± 0.0025	17.89 ± 0.17	17.89 ± 0.17
SW 2	L1A-6,5	6.5	0.301 ± 0.002	n.d.	n.d.	0.175 ± 0.001	1.0895 ± 0.0015	19.13 ± 0.16	19.13 ± 0.16
SW 17	L1A-9,5	9.5	0.329 ± 0.002	0.0278 ± 0.0004	6507 ± 93	0.179 ± 0.001	1.0913 ± 0.0016	19.60 ± 0.13	19.54 ± 0.13
SW 10	L1A-10,8	10.8	0.274 ± 0.002	0.4843 ± 0.0060	330 ± 4	0.180 ± 0.001	1.0978 ± 0.0043	20.78 ± 0.19	19.52 ± 0.19
SW 42	L1A-11,8	11.8	0.093 ± 0.001	0.0371 ± 0.0005	5289 ± 85	0.187 ± 0.002	1.0934 ± 0.0046	20.49 ± 0.25	20.41 ± 0.25
SW 11	L1A-16,1	16.1	0.295 ± 0.002	0.0496 ± 0.0024	3439 ± 164	0.188 ± 0.002	1.0848 ± 0.0047	20.85 ± 0.23	20.73 ± 0.23
SW 25	L1A-17,5	17.5	0.259 ± 0.002	0.0834 ± 0.0011	1811 ± 25	0.189 ± 0.002	1.0789 ± 0.0024	21.22 ± 0.19	20.99 ± 0.19
SW 3	L1A-19,5	19.5	0.390 ± 0.002	0.7091 ± 0.0075	341 ± 3	0.193 ± 0.001	1.0782 ± 0.0015	22.76 ± 0.13	21.44 ± 0.14
SW 33	L1A-20,3	20.3	0.298 ± 0.002	0.1864 ± 0.0028	954 ± 16	0.192 ± 0.002	1.0794 ± 0.0017	21.73 ± 0.21	21.28 ± 0.22
SW 43	L1A-21,3	21.3	0.133 ± 0.001	0.0198 ± 0.0003	9625 ± 161	0.192 ± 0.002	1.0807 ± 0.0033	21.33 ± 0.21	21.29 ± 0.21
SW 18	L1A-23,2	23.2	0.300 ± 0.002	1.7210 ± 0.0168	123 ± 1	0.197 ± 0.001	1.0812 ± 0.0013	26.09 ± 0.16	21.89 ± 0.17
SW 26	L1A-25,2	25.2	0.304 ± 0.002	2.0274 ± 0.0198	108 ± 1	0.197 ± 0.001	1.0809 ± 0.0022	26.83 ± 0.16	21.91 ± 0.19
SW 4	L1A-26,5	26.5	0.303 ± 0.002	0.1794 ± 0.0027	1042 ± 17	0.199 ± 0.002	1.0772 ± 0.0014	22.62 ± 0.24	22.19 ± 0.23
SW 12	L1A-31,7	31.7	0.331 ± 0.003	0.0208 ± 0.0022	9887 ± 1033	0.203 ± 0.002	1.0819 ± 0.0063	22.69 ± 0.27	22.64 ± 0.27
SW 19	L1A-32,5	32.5	0.307 ± 0.002	0.0451 ± 0.0006	4315 ± 58	0.206 ± 0.002	1.0808 ± 0.0016	23.16 ± 0.21	23.05 ± 0.21

continued on next page

continued from previous page

Lab.No.	Sample ID	dft (cm)	^{238}U (µg/g)	^{232}Th (ng/g)	(^{230}Th/^{232}Th) Act. ratio	(^{230}Th/^{238}U) Act.ratio	(^{234}U/^{238}U) Act.ratio	Age (uncorr.) (ka)	Age (corr.) (ka)
SW 5	L1A-35	35	0.349 ± 0.002	n.d.	n.d.	0.210 ± 0.001	1.0847 ± 0.0017	23.42 ± 0.18	23.42 ± 0.18
SW 6	L1A-41	41	0.321 ± 0.002	n.d.	n.d.	0.214 ± 0.001	1.0883 ± 0.0018	23.79 ± 0.16	23.79 ± 0.16
SW 13	L1A-47,8	47.8	0.284 ± 0.002	n.d.	n.d.	0.215 ± 0.002	1.0832 ± 0.0023	24.08 ± 0.25	24.08 ± 0.25
SW 14	L1A-49,3	49.3	0.254 ± 0.002	n.d.	n.d.	0.215 ± 0.002	1.0801 ± 0.0035	24.20 ± 0.26	24.20 ± 0.26
SW 20	L1A-50,8	50.8	0.257 ± 0.001	0.1518 ± 0.0020	1147 ± 16	0.218 ± 0.002	1.0790 ± 0.0017	24.99 ± 0.22	24.57 ± 0.23
SW 15	L1A-54,5	54.5	0.258 ± 0.002	0.1933 ± 0.0028	910 ± 13	0.218 ± 0.001	1.0760 ± 0.0032	25.25 ± 0.19	24.71 ± 0.19

Table A.2: *Activity ratios and ^{230}Th/U-ages for section L1B. Uncertainties are given as 2σ range. All ages corrected with a detrital ^{232}Th/^{238}U weight ratio of 0.14 ± 0.11.*

Lab.No.	Sample ID	dft (cm)	^{238}U (µg/g)	^{232}Th (ng/g)	(^{230}Th/^{232}Th) Act. ratio	(^{230}Th/^{238}U) Act.ratio	(^{234}U/^{238}U) Act.ratio	Age (uncorr.) (ka)	Age (corr.) (ka)
SW 29	L1B-0,0	55	0.292 ± 0.003	0.0230 ± 0.0006	8582 ± 239	0.221 ± 0.003	1.07 ± 0.01	25.14 ± 0.44	25.08 ± 0.45
SW 44	L1B-4,0	59	0.392 ± 0.002	0.0099 ± 0.0002	18277 ± 343	0.223 ± 0.002	1.0654 ± 0.0042	25.67 ± 0.26	25.64 ± 0.27
SW 49	L1B-5,5	60.5	0.271 ± 0.002	0.0550 ± 0.0014	3443 ± 102	0.228 ± 0.004	1.0624 ± 0.0066	26.44 ± 0.54	26.29 ± 0.53
SW 34	L1B-9,3	64.3	0.337 ± 0.002	0.0160 ± 0.0005	14834 ± 503	0.230 ± 0.002	1.0615 ± 0.0020	26.68 ± 0.27	26.65 ± 0.27
SW 50	L1B-10,8	65.8	0.328 ± 0.003	0.0306 ± 0.0007	7877 ± 193	0.240 ± 0.003	1.0661 ± 0.0061	27.81 ± 0.48	27.74 ± 0.48
SW 145	L1B-13.2	68.2	0.393 ± 0.002	0.0721 ± 0.0012	4000 ± 68	0.239 ± 0.002	1.0628 ± 0.0018	27.93 ± 0.26	27.79 ± 0.25
SW 27	L1B-17,7	72.7	0.404 ± 0.002	0.0292 ± 0.0007	10101 ± 264	0.238 ± 0.003	1.0646 ± 0.0025	27.65 ± 0.35	27.59 ± 0.35
SW 51	L1B-19,7	74.7	0.343 ± 0.004	0.0224 ± 0.0007	11404 ± 368	0.243 ± 0.004	1.07 ± 0.01	28.12 ± 0.58	28.08 ± 0.59
SW 45	L1B-24,0	79	0.112 ± 0.001	0.0367 ± 0.0005	7426 ± 105	0.257 ± 0.002	1.0977 ± 0.0039	29.03 ± 0.28	28.95 ± 0.29
SW 28	L1B-25,3	80.3	0.270 ± 0.002	0.0516 ± 0.0008	4162 ± 65	0.259 ± 0.002	1.0977 ± 0.0027	29.43 ± 0.28	29.30 ± 0.28

Table A.3: *Activity ratios and $^{230}Th/U$-ages for section L1C. Uncertainties are given as 2σ range. All ages corrected with a detrital $^{232}Th/^{238}U$ weight ratio of 0.14 ± 0.11. Samples marked with a * are not used for the age model (more details in sections 5.3.1 and 5.4.1).*

Lab.No.	Sample ID	dft (cm)	^{238}U (µg/g)	^{232}Th (ng/g)	($^{230}Th/^{232}Th$) Act. ratio	($^{230}Th/^{238}U$) Act.ratio	($^{234}U/^{238}U$) Act.ratio	Age (uncorr.) (ka)	Age (corr.) (ka)
SW 105	L1C-1,5	82	0.444 ± 0.003	n.d.	n.d.	0.258 ± 0.002	1.0987 ± 0.0045	29.13 ± 0.31	29.13 ± 0.31
SW 35	L1C-2,7	83.2	0.471 ± 0.003	0.0038 ± 0.0005	98840 ± 12050	0.259 ± 0.002	1.0995 ± 0.0018	29.23 ± 0.27	29.22 ± 0.26
SW 106	L1C-6,2	86.7	0.336 ± 0.003	n.d.	n.d.	0.262 ± 0.003	1.1000 ± 0.0084	29.53 ± 0.42	29.53 ± 0.42
SW 146	L1C-8.9	89.4	0.375 ± 0.002	0.0544 ± 0.0007	5552 ± 77	0.262 ± 0.002	1.1007 ± 0.0016	29.72 ± 0.25	29.62 ± 0.25
SW 46	L1C-10,6	91.1	0.094 ± 0.001	0.0056 ± 0.0001	54828 ± 1472	0.264 ± 0.003	1.1014 ± 0.0050	29.76 ± 0.38	29.75 ± 0.38
SW 52	L1C-6,7	92.2	0.353 ± 0.004	0.0010 ± 0.0003	292363 ± 85792	0.264 ± 0.003	1.1019 ± 0.0099	29.78 ± 0.53	29.78 ± 0.52
SW 147	L1C-14.2	94.7	0.347 ± 0.002	0.0365 ± 0.0006	7670 ± 123	0.264 ± 0.002	1.0973 ± 0.0017	29.95 ± 0.27	29.87 ± 0.27
SW 107	L1C-16,3	96.8	0.307 ± 0.003	0.0014 ± 0.0011	175481 ± 137687	0.268 ± 0.003	1.0930 ± 0.0088	30.62 ± 0.49	30.62 ± 0.48
SW 30	L1C-19,9	100.4	0.324 ± 0.002	0.0070 ± 0.0003	37507 ± 1603	0.266 ± 0.002	1.0915 ± 0.0040	30.35 ± 0.35	30.34 ± 0.36
SW 47	L1C-22,7	103.2	0.201 ± 0.001	0.0104 ± 0.0002	27485 ± 464	0.275 ± 0.002	1.0860 ± 0.0032	31.78 ± 0.29	31.76 ± 0.29
SW 108	L1C-24,3	104.8	0.311 ± 0.004	0.0126 ± 0.0014	20893 ± 2296	0.276 ± 0.003	1.085 ± 0.011	31.94 ± 0.60	31.91 ± 0.60
SW 36	L1C-26,1	106.6	0.341 ± 0.002	n.d.	n.d.	0.282 ± 0.003	1.0706 ± 0.0018	33.25 ± 0.37	33.25 ± 0.37
SW 109	L1C-28,3	108.8	0.337 ± 0.002	n.d.	n.d.	0.284 ± 0.002	1.0687 ± 0.0040	33.60 ± 0.36	33.60 ± 0.36
SW 148*	L1C-33.4	113.9	0.360 ± 0.002	0.0714 ± 0.0009	4501 ± 56	0.291 ± 0.002	1.0510 ± 0.0017	35.51 ± 0.28	35.37 ± 0.29*
SW 110*	L1C-35,5	116	0.314 ± 0.004	0.3373 ± 0.0039	836 ± 10	0.288 ± 0.003	1.0494 ± 0.011	35.79 ± 0.67	34.99 ± 0.65*
SW 149*	L1C-37.0	117.5	0.348 ± 0.002	0.0784 ± 0.0009	4030 ± 52	0.296 ± 0.002	1.0505 ± 0.0020	36.13 ± 0.36	35.97 ± 0.37*
SW 31	L1C-38,5	119	0.364 ± 0.002	0.0181 ± 0.0004	17384 ± 418	0.283 ± 0.003	1.0541 ± 0.0044	34.11 ± 0.50	34.08 ± 0.49

Table A.4: *Activity ratios and $^{230}Th/U$-ages for section L1D. Uncertainties are given as 2σ range. All ages corrected with a detrital $^{232}Th/^{238}U$ weight ratio of 0.14 ± 0.11. Samples marked with a * are not used for the age model (more details in sections 5.3.1 and 5.4.1).*

Lab.No.	Sample ID	dft (cm)	^{238}U (µg/g)	^{232}Th (ng/g)	($^{230}Th/^{232}Th$) Act. ratio	($^{230}Th/^{238}U$) Act.ratio	($^{234}U/^{238}U$) Act.ratio	Age (uncorr.) (ka)	Age (corr.) (ka)
SW 113	L1D-0,0	120.6	0.344 ± 0.002	n.d.	n.d.	0.276 ± 0.004	1.0469 ± 0.0015	33.32 ± 0.52	33.32 ± 0.52
SW 129*	L1D-3,2	123.8	0.268 ± 0.002	0.2061 ± 0.0025	1440 ± 19	0.359 ± 0.003	1.0719 ± 0.0016	44.82 ± 0.43	44.26 ± 0.44*
SW 114	L1D-7,4	128	0.348 ± 0.002	0.0016 ± 0.0009	190315 ± 110448	0.285 ± 0.004	1.0448 ± 0.0016	34.71 ± 0.57	34.71 ± 0.58
SW 130*	L1D-10,2	130.8	0.197 ± 0.001	1.4555 ± 0.0149	168 ± 2	0.374 ± 0.003	1.0812 ± 0.0017	51.57 ± 0.41	46.14 ± 0.45*
SW 115	L1D-13,0	133.6	0.340 ± 0.002	0.0301 ± 0.0011	9937 ± 382	0.287 ± 0.003	1.0529 ± 0.0017	34.76 ± 0.47	34.69 ± 0.49
SW 131*	L1D-17,1	137.7	0.236 ± 0.001	1.0287 ± 0.0105	276 ± 3	0.374 ± 0.002	1.0713 ± 0.0018	49.81 ± 0.34	46.62 ± 0.35*
SW 132*	L1D-18,3	138.9	0.227 ± 0.001	0.0506 ± 0.0009	4789 ± 86	0.349 ± 0.003	1.0719 ± 0.0017	42.99 ± 0.40	42.83 ± 0.41*
SW 116	L1D-23,7	144.3	0.378 ± 0.002	n.d.	n.d.	0.300 ± 0.003	1.0770 ± 0.0018	35.55 ± 0.41	35.55 ± 0.41

Table A.5: *Activity ratios and $^{230}Th/U$-ages for section L1E. Uncertainties are given as 2σ range. Ages marked with a † were corrected with a detrital $^{232}Th/^{238}U$ weight ratio of 0.30 ± 0.24. Ages marked with a ‡ were corrected with a detrital $^{232}Th/^{238}U$ weight ratio of 0.11 ± 0.09. All other ages corrected with a detrital $^{232}Th/^{238}U$ weight ratio of 0.14 ± 0.11. Samples marked with a * are not used for the age model (more details in sections 5.3.1 and 5.4.1).*

Lab.No.	Sample ID	dft (cm)	^{238}U (µg/g)	^{232}Th (ng/g)	($^{230}Th/^{232}Th$) Act. ratio	($^{230}Th/^{238}U$) Act.ratio	($^{234}U/^{238}U$) Act.ratio	Age (uncorr.) (ka)	Age (corr.) (ka)
SW 125	L1E-1,2	146.2	0.289 ± 0.002	0.0164 ± 0.0005	18345 ± 560	0.348 ± 0.002	1.0953 ± 0.0016	41.61 ± 0.34	41.57 ± 0.33
SW 133	L1E-5,9	150.9	0.202 ± 0.001	0.0091 ± 0.0004	23611 ± 1084	0.347 ± 0.002	1.0952 ± 0.0016	41.36 ± 0.34	41.33 ± 0.33
SW 134	L1E-10,9	155.9	0.296 ± 0.002	0.0316 ± 0.0006	10140 ± 200	0.354 ± 0.003	1.0778 ± 0.0018	43.34 ± 0.45	43.26 ± 0.46
SW 126	L1E-11,9	156.9	0.327 ± 0.002	0.0350 ± 0.0007	10026 ± 194	0.354 ± 0.003	1.0778 ± 0.0018	43.36 ± 0.45	43.29 ± 0.46
SW 127†	L1E-14,0	159	0.336 ± 0.002	0.4433 ± 0.0060	829 ± 12	0.355 ± 0.003	1.0793 ± 0.0017	43.83 ± 0.43	43.39 ± 0.41†
SW 124	L1E-19,2	164.2	0.335 ± 0.002	0.0776 ± 0.0013	4608 ± 77	0.350 ± 0.003	1.0720 ± 0.0017	43.17 ± 0.40	43.01 ± 0.41
SW 135†	L1Eb-0,7	166.8	0.323 ± 0.002	0.4264 ± 0.0058	829 ± 12	0.356 ± 0.003	1.0793 ± 0.0017	43.84 ± 0.42	43.40 ± 0.43†
SW 117*	L1Eb-2,2	168.3	0.333 ± 0.002	0.0479 ± 0.0015	7102 ± 240	0.333 ± 0.005	1.0709 ± 0.0016	40.64 ± 0.69	40.54 ± 0.69
SW 121	L1Eb-4,1	170.2	0.288 ± 0.002	0.2222 ± 0.0026	1437 ± 19	0.359 ± 0.003	1.0719 ± 0.0016	44.86 ± 0.42	44.30 ± 0.43*
SW 150†	L1Eb-8.2	174.3	0.295 ± 0.002	0.9855 ± .0099	333 ± 4	0.357 ± 0.003	1.0672 ± 0.0060	45.41 ± 0.58	44.27 ± 0.59†
SW 122‡	L1Eb-10,1	176.2	0.249 ± 0.001	1.8454 ± 0.0189	168 ± 2	0.365 ± 0.003	1.0825 ± 0.0017	51.65 ± 0.40	44.68 ± 0.48‡
SW 123‡	L1Eb11,1	177.2	0.239 ± 0.001	1.0377 ± 0.0106	276 ± 3	0.368 ± 0.002	1.0719 ± 0.0018	49.80 ± 0.34	45.73 ± 0.36‡
SW 151	L1Eb-12.5	178.6	0.248 ± 0.001	0.1712 ± 0.0023	1719 ± 26	0.386 ± 0.004	1.0696 ± 0.0023	49.09 ± 0.61	48.59 ± 0.60
SW 118	L1Eb-15,2	181.3	0.282 ± 0.002	0.1937 ± 0.0027	1643 ± 28	0.367 ± 0.004	1.0700 ± 0.0016	46.07 ± 0.64	45.57 ± 0.65
SW 119	L1Eb-20,7	186.8	0.308 ± 0.002	n.d.	n.d.	0.369 ± 0.004	1.0724 ± 0.0017	45.87 ± 0.65	45.87 ± 0.65

A.3 Supplementary figures to section 5.3.2 (Proxy analysis)

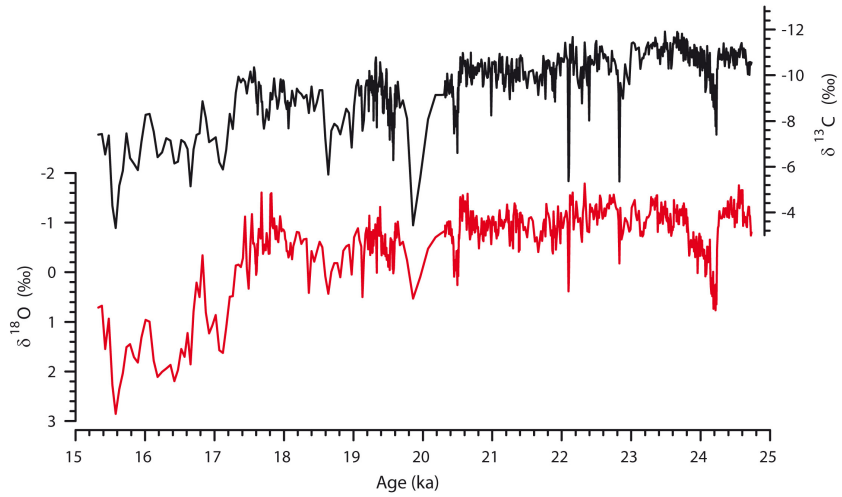

(a) *L1A (15 to 25 ka)*

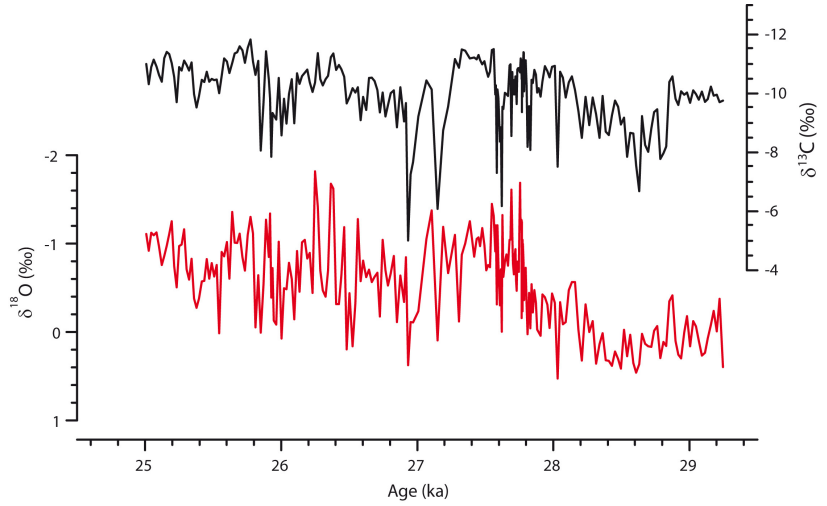

(b) *L1B (25 to 29.5 ka)*

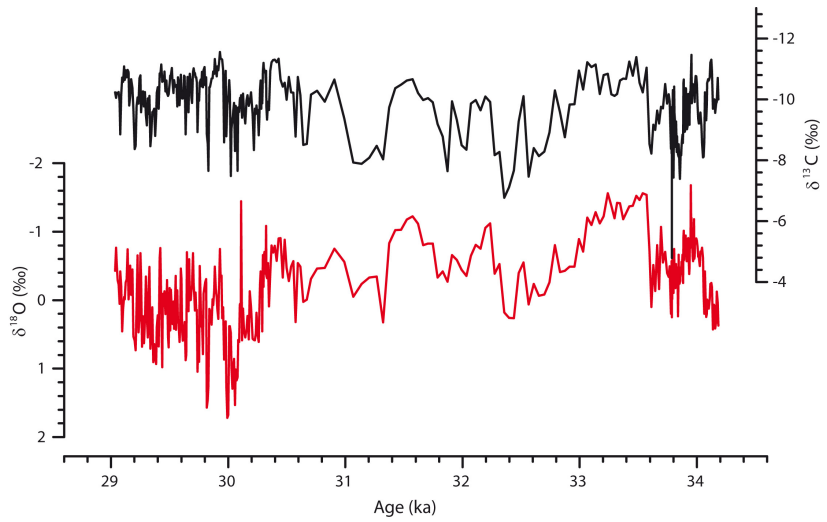

(c) *L1C (29 to 34.2 ka)*

Figure A.1: *Stable isotope records of PR-LA-1 with* $\delta^{18}O$ *values in red and* $\delta^{13}C$ *values in black.*

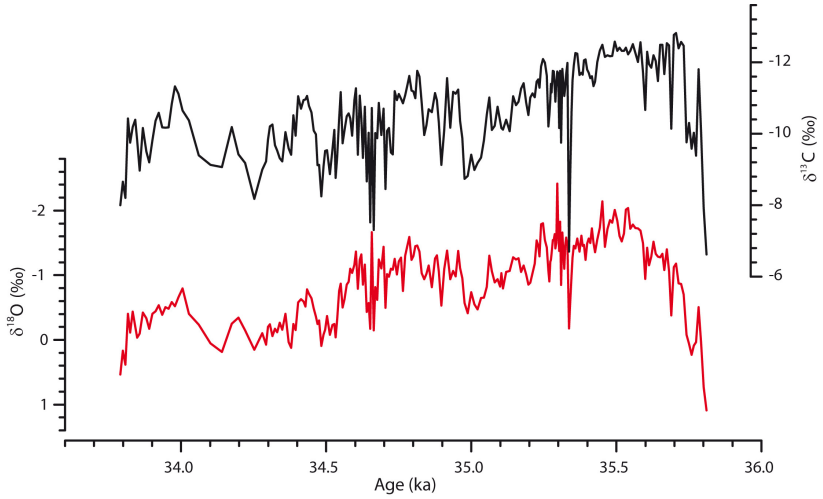

(a) *L1D (33.8 to 35.8 ka)*

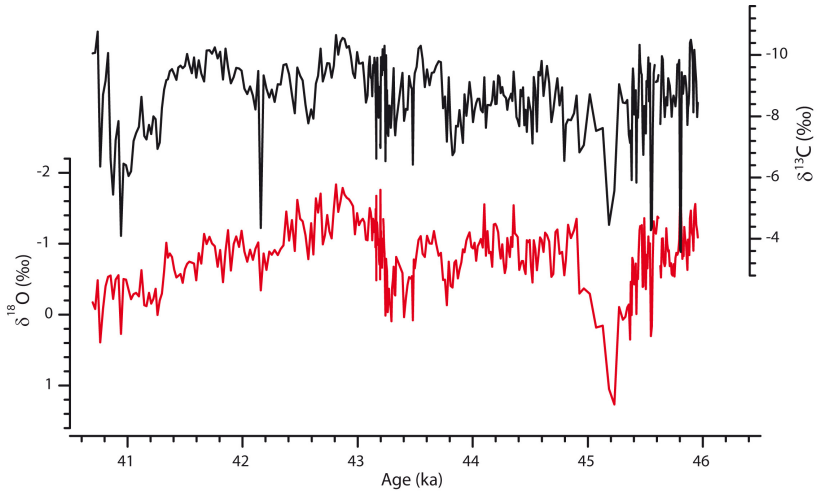

(b) *L1E (40.8 to 46 ka)*

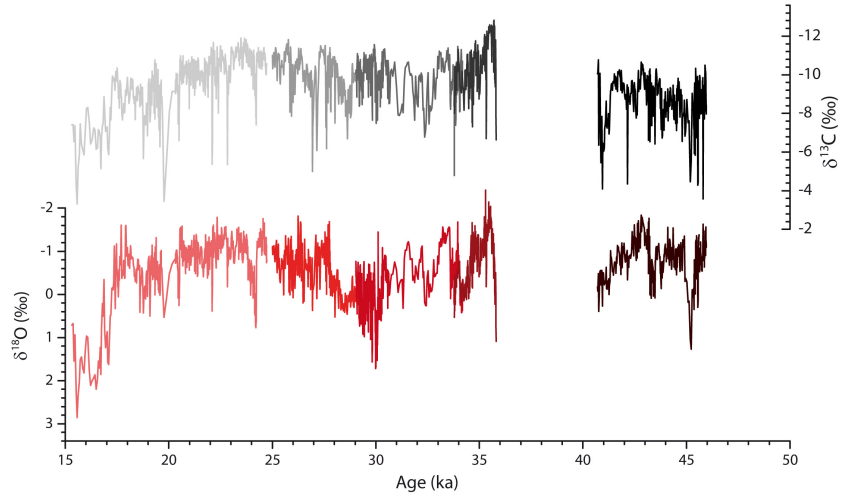

(c) *L1A to L1E from 15 to 46 ka.*

Figure A.2: *Stable isotope records of PR-LA-1 with* $\delta^{18}O$ *values in red and* $\delta^{13}C$ *values in black. In Figure A.2c,* $\delta^{18}O$ *values are displayed in light red (L1A) to dark red (L1E) and* $\delta^{13}C$ *values in light grey (L1A) to black (L1E).*

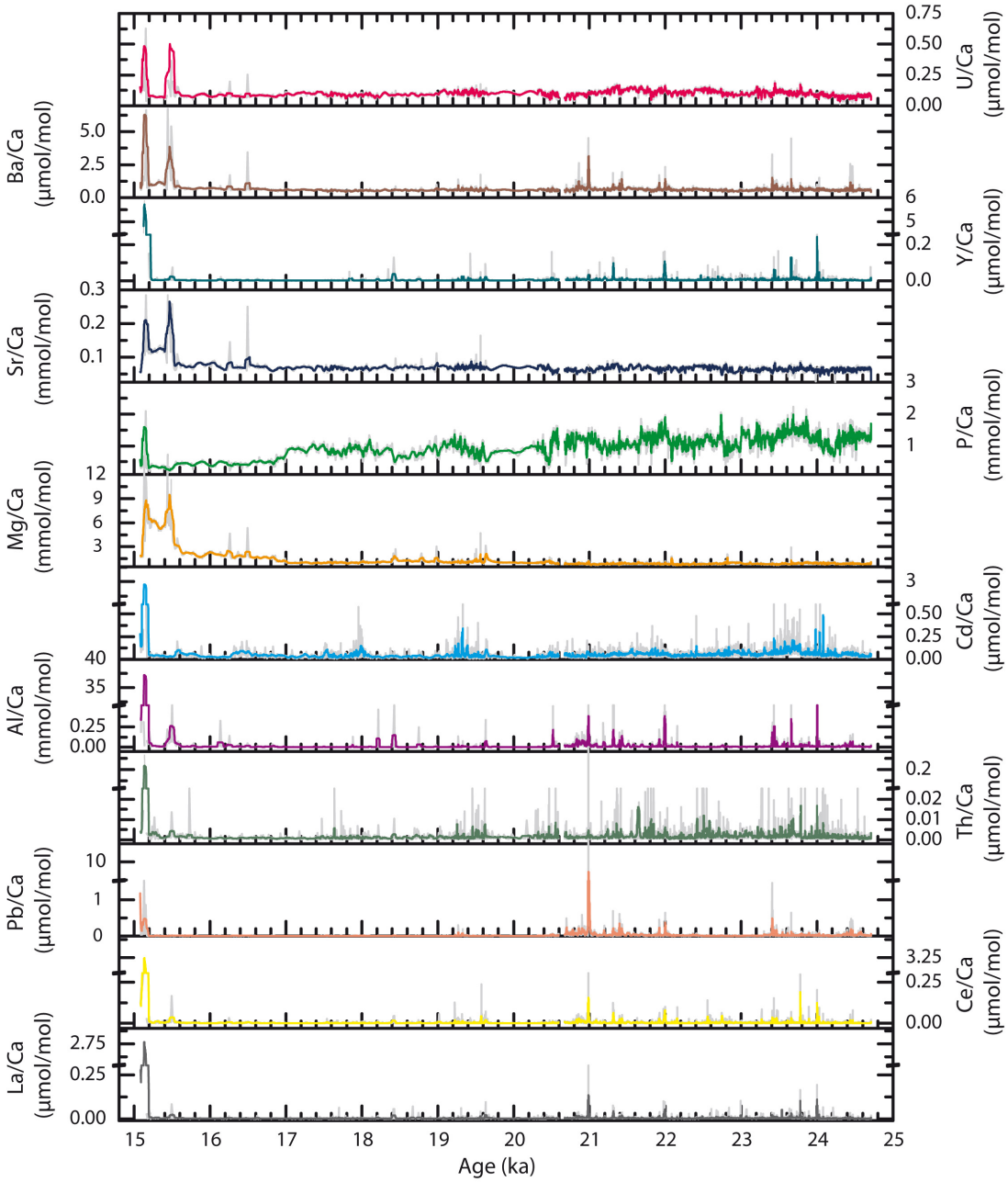

Figure A.3: *Element to calcium ratios of L1A (15 to 25 ka). Grey lines: Raw data (25 µm resolution), colored lines: 25p running mean.*

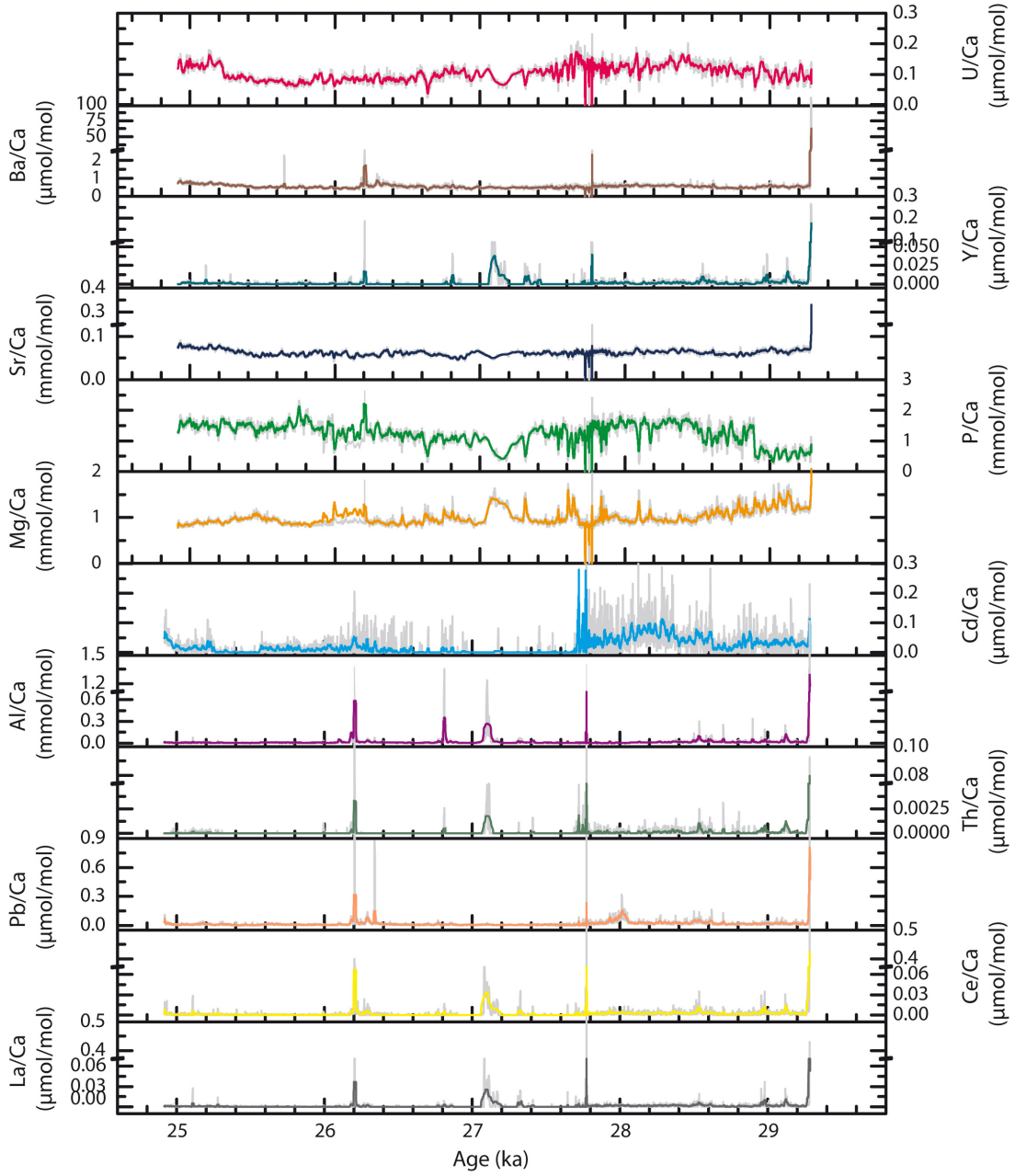

Figure A.4: *Element to calcium ratios of L1B (25 to 29.5 ka). Grey lines: Raw data (25 µm resolution), colored lines: 25p running mean.*

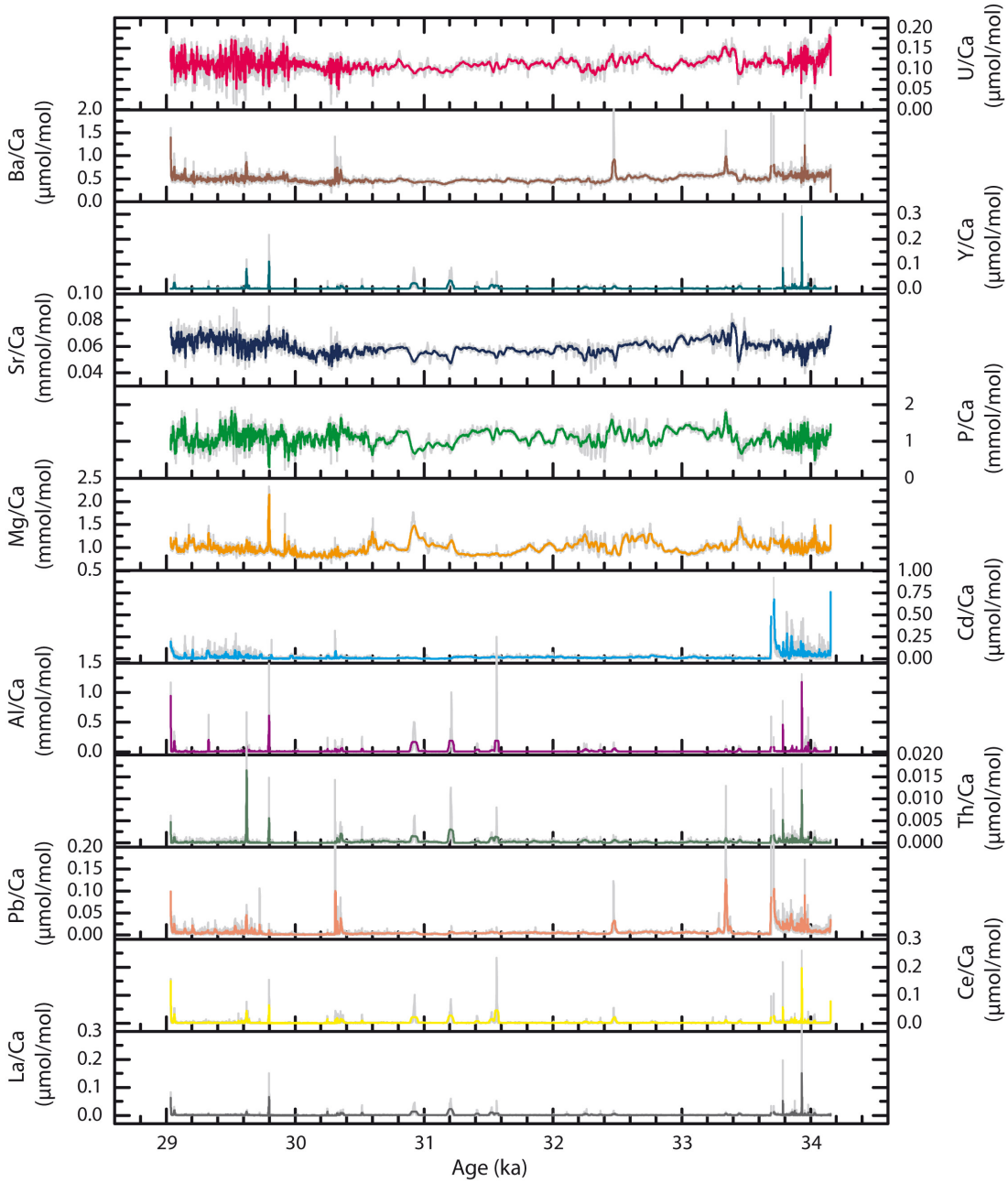

Figure A.5: *Element to calcium ratios of L1C (29 to 34.2 ka). Grey lines: Raw data (25 µm resolution), colored lines: 25p running mean.*

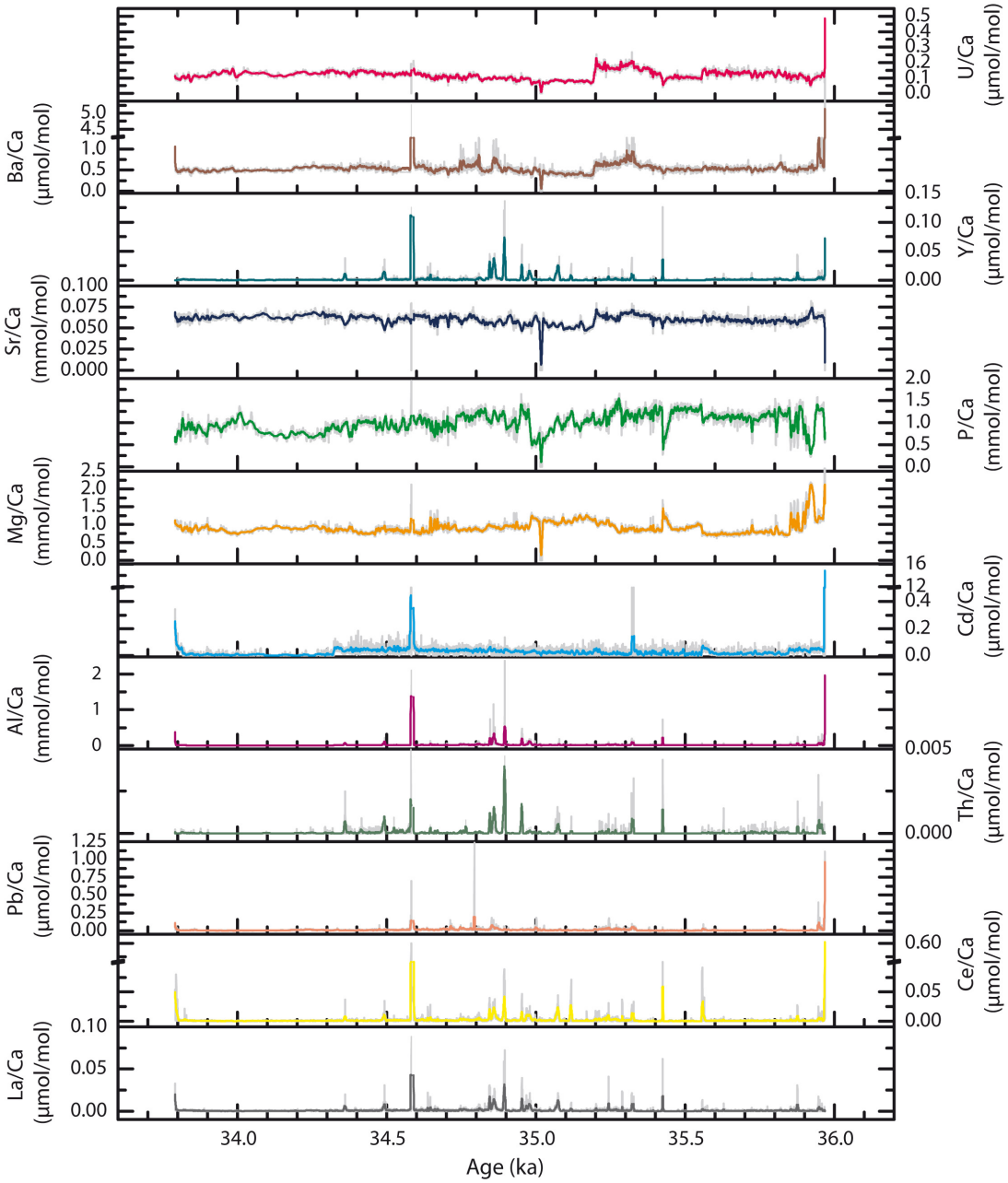

Figure A.6: *Element to calcium ratios of L1D (33.8 to 35.8 ka). Grey lines: Raw data (25 µm resolution), colored lines: 25p running mean.*

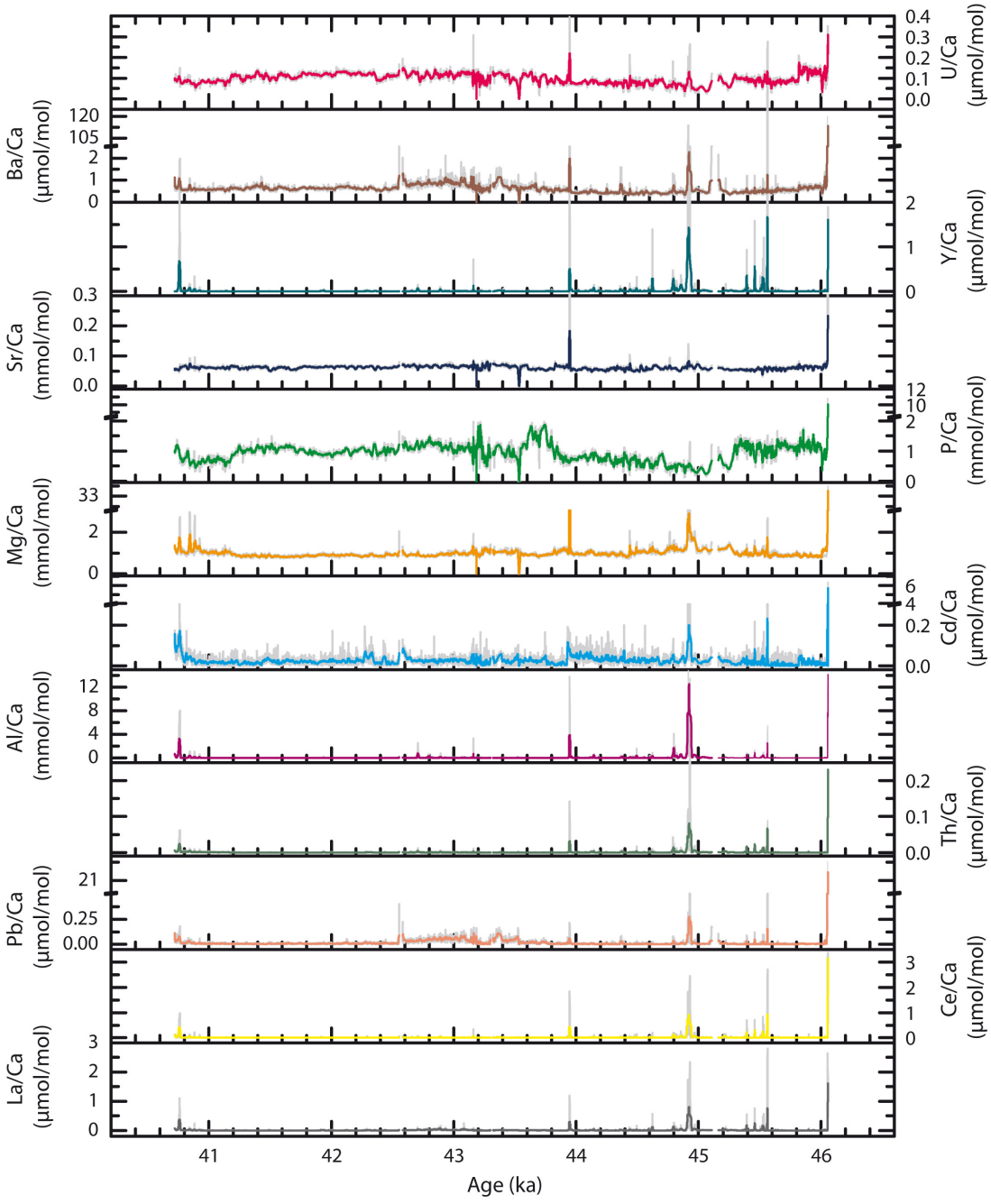

Figure A.7: *Element to calcium ratios of L1E (40.8 to 46 ka). Grey lines: Raw data (25 µm resolution), colored lines: 25p running mean.*

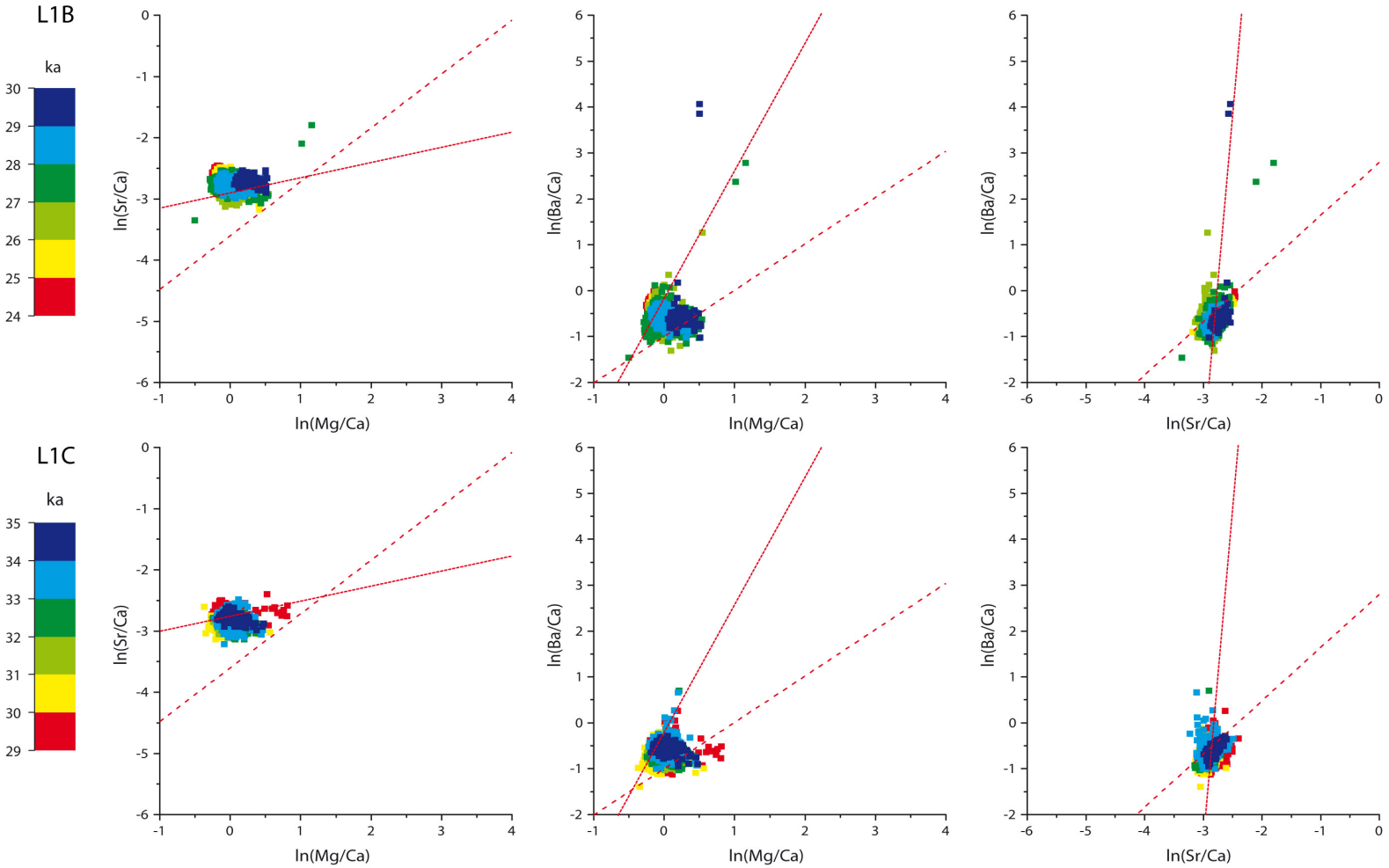

Figure A.8: *Cross plots of element to calcium ratios in speleothem calcite of section L1B (upper panels) and L1C (bottom panels) shown as ln(Sr/Ca) vs. ln(Mg/Ca) (left), ln(Ba/Ca) vs. ln(Mg/Ca) (middle) and ln(Ba/Ca) vs. ln(Sr/Ca) (right). The red lines indicate the theoretically expected slopes for PCP and/or ICD after Sinclair et al. (2012) calculated with the corresponding partition coefficients. The dotted lines show the same for the case of calcite recrystallization (Sinclair et al., 2012)*

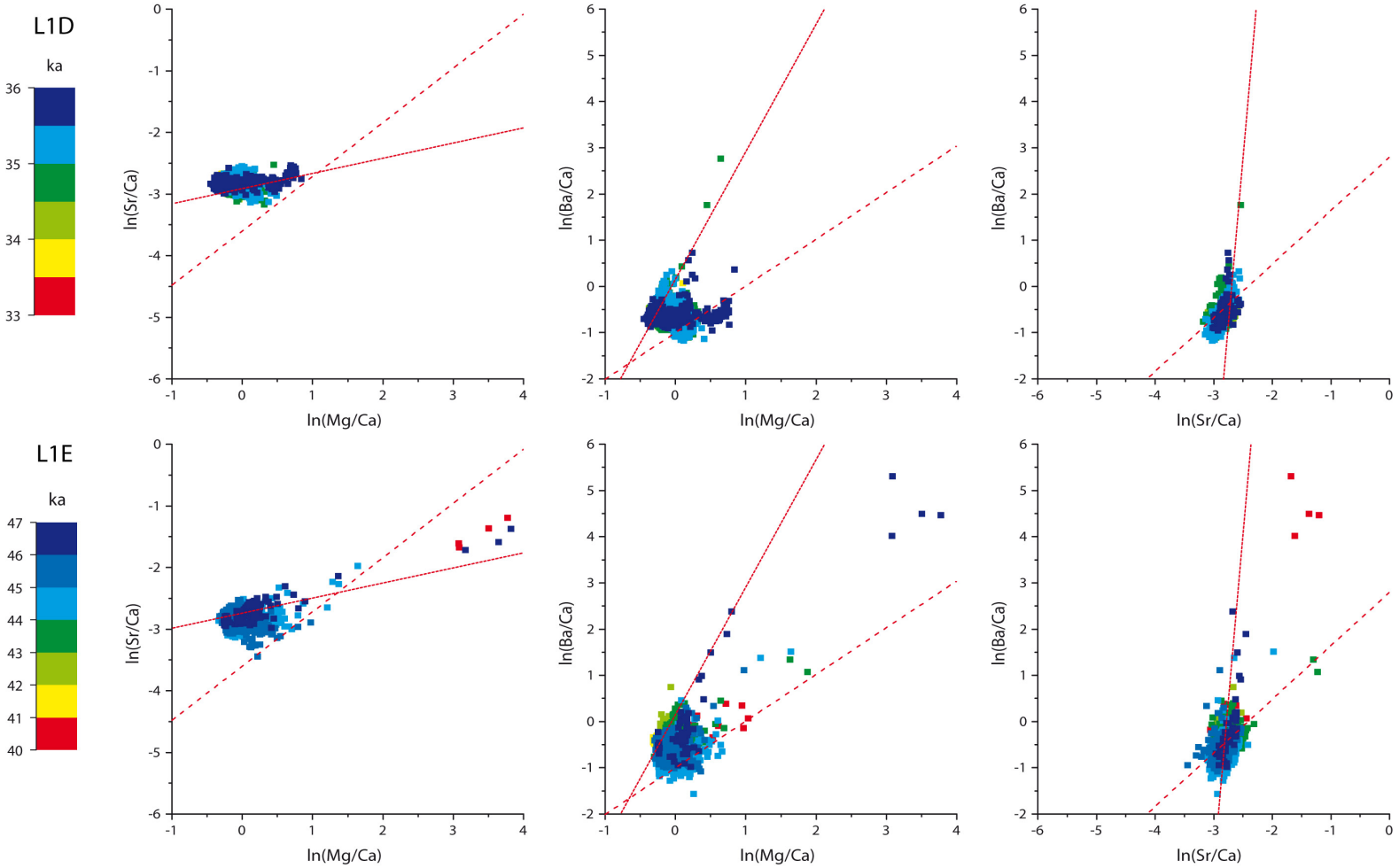

Figure A.9: *Cross plots of element to calcium ratios in speleothem calcite of section L1D (upper panels) and L1E (bottom panels) shown as ln(Sr/Ca) vs. ln(Mg/Ca) (left), ln(Ba/Ca) vs. ln(Mg/Ca) (middle) and ln(Ba/Ca) vs. ln(Sr/Ca) (right). The red lines indicate the theoretically expected slopes for PCP and/or ICD after Sinclair et al. (2012) calculated with the corresponding partition coefficients. The dotted lines show the same for the case of calcite recrystallization (Sinclair et al., 2012)*

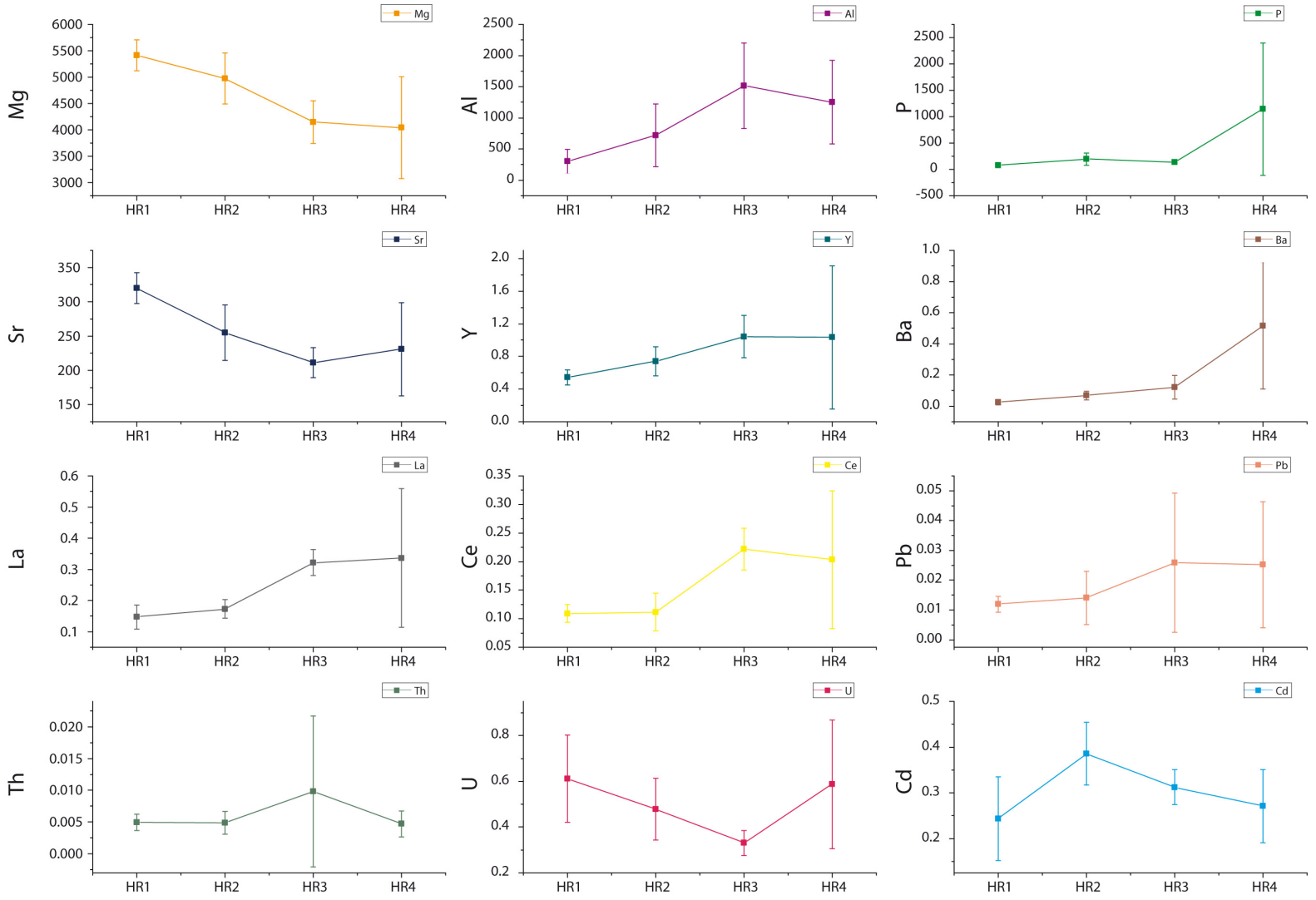

Figure A.10: *Mean element to calcium ratios (in mmol/mol) of the four host rock samples: HR1 (base weatherstation), HR2 (weatherstation), HR3 (Cueva Larga entrance) and HR4 (Cueva Larga SW1).*

B Supplementary material to Paper II - Santo Tomas Cave

B.1 Analytical details

Stalagmite CM was cut in two halves along its main growth axis. A slab was prepared from one half, which was subsequently cut into two further halves along the main growth axis. One half was used for ^{230}Th/U-dating, the opposite half for stable isotope and trace element measurements.

Samples for ^{230}Th/U-dating were cut along the growth axis using a band saw and a drill. Mass spectrometric analyses of U and Th isotopes was performed using two methods, thermal ionization mass spectrometry (TIMS, performed at the Heidelberg Academy of Sciences) and multi-collector inductively coupled plasma mass spectrometry (MC-ICPMS, performed at the Max Planck Institute for Chemistry (MPIC) in Mainz). Chemical preparation of the samples at the MPIC is described in detail in Yang et al. (2015). The analytical methods are described by Obert et al. (2016). Details of the procedures applied in Heidelberg are given in Scholz et al. (2004) for the TIMS method. ^{230}Th/U TIMS ages which were already published by Fensterer et al. (2013) are shown in Table B.1. The new TIMS samples were measured by adding a Th solution (Fohlmeister et al., 2012) due to the low U and Th content of the samples. The results are shown in Table B.2. Table B.3 shows the results of the MC-ICPMS analyses.

All TIMS and MC-ICPMS ages and activity ratios were calculated using the half-lives reported by Cheng et al. (2000). We decided to use these half-lives instead of the more recent half-lives of Cheng et al. (2013) in order to preserve comparability with previous publications. Similar to Fensterer et al. (2010) and Fensterer et al. (2012), a ^{232}Th/^{238}U weight ratio of 0.8 ± 0.5 was found to be appropriate for correction of detrital contamination assuming ^{230}Th, ^{234}U and ^{238}U in secular equilibrium. Age uncertainties are quoted at the 2σ-level and do not include half-life uncertainties.

Stable carbon and oxygen isotope analysis was performed at the University of Innsbruck. The samples were micro-milled at a resolution of 0.10-0.33 mm along the growth axis of CM, CMa and CMb. The carbonate powder was analyzed using an on-line, automated carbonate preparation system (Gasbench II) linked to a triple collector gas source ThermoFisher DeltaplusXL mass spectrometer. Raw data were calibrated against NBS19, and δ-values are reported relative to Vienna Pee Dee Belemnite (VPDB) standard. Long-term precision of the δ^{13}C and δ^{18}O values, estimated as the 1σ-standard deviation of replicate analyses, is 0.06

and 0.08 ‰, respectively (Spötl, 2011; Spötl and Vennemann, 2003).

Concentrations of the elements Mg, Al, P, Sr, Y, Ba, Th and U were measured along the growth axis CM by laser ablation ICPMS at the MPIC. The analytical procedure followed Jochum et al. (2012) and Yang et al. (2015), using the high-resolution sector-field ICPMS Thermo Element2, combined with the UP-213 Nd:YAG laser ablation system from New Wave. The analyzed isotopes were measured at low mass resolution ($m/\Delta m$ ~300) and are reported to be interference-free (Jochum et al., 2012). Trace element line scans were performed along the growth axis of CM using a spot size of 110 µm and a scan speed of 10 µm/s, resulting in a spatial resolution of 7 µm per data point (scan time 0.7 s). Warm up and wash out times are 23 and 30 s, respectively. To avoid potential surface contamination, the scan path was pre-ablated with a scan speed of 80 µm/s. In order to account for matrix effects, data reduction was carried out by calculating the blank corrected count rates of the analyzed isotopes relative to the simultaneously measured internal standard ^{43}Ca. The silicate reference glass NIST SRM 612 was used for external calibration of the trace element analyses (Jochum et al., 2011, 2012). Element to calcium ratios are given as molar ratios.

B.2 Supplementary data to section 6.3.1 (^{230}Th/U dating)

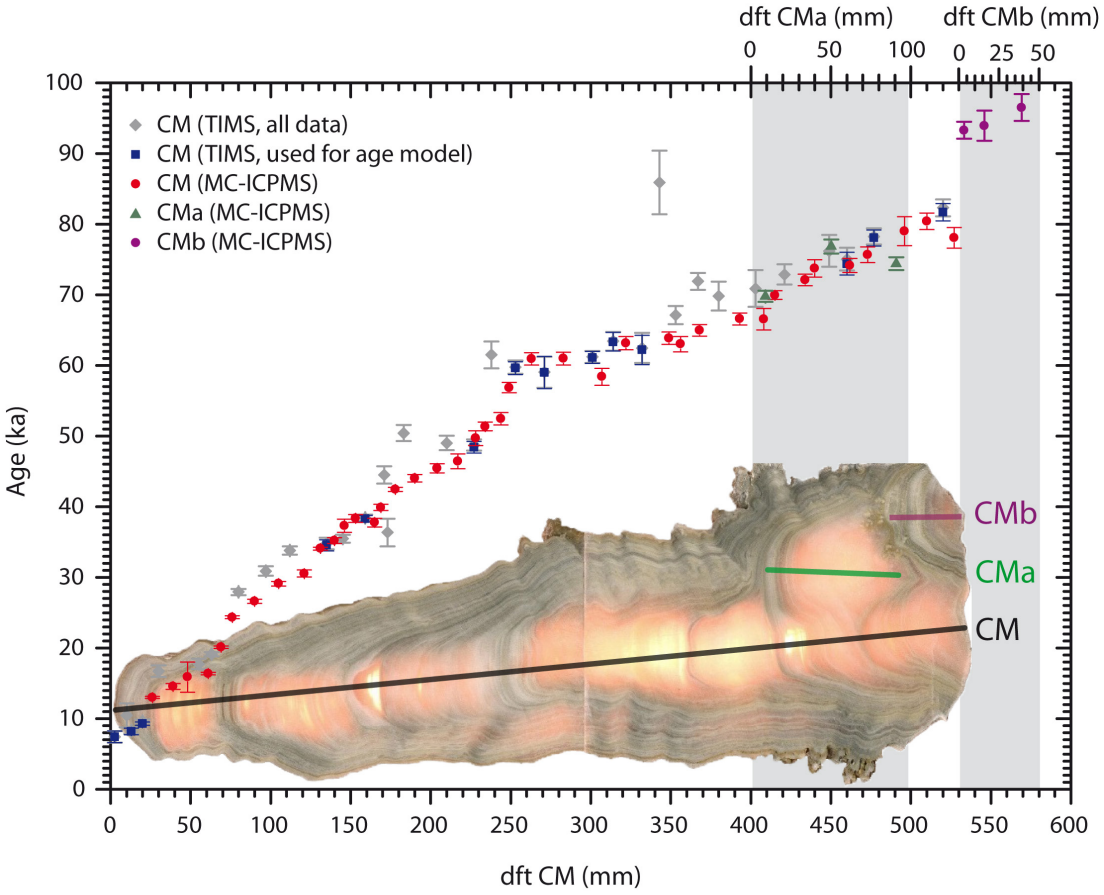

Figure B.1: *^{230}Th/U-ages measured along the growth axes CM, CMa (green triangles) and CMb (violet dots). Grey diamonds inidicate all measured TIMS data from CM, blue squares indicate the TIMS data which are used for constructing the age model. Red dots show the MC-ICPMS data from CM.*

Table B.1: *Activity ratios and $^{230}Th/U$-ages for growth axis CM obtained with TIMS. Uncertainties are given as 2σ range. Ages were corrected with a detrital $^{232}Th/^{238}U$ weight ratio of 0.38 ± 0.30. Samples marked with a * are not used for the age model (more details in section 6.3.1)*

Lab.No.	Sample ID	dft (cm)	^{238}U (µg/g)	^{232}Th (ng/g)	($^{230}Th/^{232}Th$) Act. ratio	($^{230}Th/^{238}U$) Act.ratio	($^{234}U/^{238}U$) Act.ratio	Age (uncorr.) (ka)	Age (corr.) (ka)
4743	CM-0,25	0.25	0.0911 ± 0.0001	0.014 ± 0.001	1975 ± 214	0.099 ± 0.011	1.508 ± 0.013	7.44 ± 0.81	7.41 ± 0.82
4597*	CM-1	1.0	0.1092 ± 0.0001	0.241 ± 0.006	189 ± 30	0.132 ± 0.021	1.486 ± 0.010	10.52 ± 1.73	10.10 ± 1.64
4744	CM-1,3	1.3	0.1028 ± 0.0001	0.067 ± 0.001	497 ± 28	0.105 ± 0.006	1.445 ± 0.008	8.32 ± 0.47	8.19 ± 0.46
4649	CM-2	2.0	0.0857 ± 0.0001	0.172 ± 0.001	191 ± 5	0.121 ± 0.003	1.475 ± 0.005	9.68 ± 0.24	9.29 ± 0.23
4650*	CM-3	3.0	0.0977 ± 0.0002	0.063 ± 0.001	966 ± 43	0.203 ± 0.009	1.427 ± 0.018	16.72 ± 0.81	16.59 ± 0.79
4651*	CM-5,5	5.5	0.1580 ± 0.0002	0.271 ± 0.002	377 ± 14	0.209 ± 0.008	1.404 ± 0.009	17.77 ± 0.73	17.42 ± 0.70
4807*	CM-8	8.0	0.2149 ± 0.0004	0.512 ± 0.002	421 ± 6	0.324 ± 0.004	1.437 ± 0.006	27.99 ± 0.44	27.52 ± 0.43
4808	CM-13,5	13.5	0.1815 ± 0.0004	0.268 ± 0.002	834 ± 17	0.400 ± 0.008	1.455 ± 0.008	34.82 ± 0.81	34.54 ± 0.79
4745*	CM-14,5	14.5	0.2408 ± 0.0001	0.449 ± 0.004	709 ± 11	0.430 ± 0.006	1.534 ± 0.006	35.51 ± 0.56	35.17 ± 0.55
4598*	CM-21	21.0	0.0983 ± 0.0002	0.503 ± 0.003	305 ± 5	0.505 ± 0.007	1.391 ± 0.013	49.12 ± 1.04	48.10 ± 1.04
4746	CM-46	46.0	0.0905 ± 0.0001	0.355 ± 0.002	592 ± 9	0.758 ± 0.011	1.486 ± 0.008	75.12 ± 1.62	74.41 ± 1.62
4747	CM-47,7	47.7	0.2652 ± 0.0002	0.364 ± 0.002	1757 ± 21	0.788 ± 0.008	1.491 ± 0.004	78.30 ± 1.15	78.05 ± 1.14
4863	CM-52	52.0	0.2722 ± 0.0001	1.090 ± 0.003	635 ± 7	0.830 ± 0.008	1.519 ± 0.003	82.39 ± 1.24	81.69 ± 1.21

Table B.2: *Activity ratios and $^{230}Th/U$-ages for growth axis CM obtained with TIMS. Uncertainties are given as 2σ range. Ages were corrected with a detrital $^{232}Th/^{238}U$ weight ratio of 0.38 ± 0.30. Samples are analyzed after Fohlmeister et al. (2012) (see section B.1 for more details). Samples marked with a * are not used for the age model (more details in section 6.3.1)*

Lab.No.	Sample ID	dft (cm)	^{238}U (µg/g)	^{232}Th (ng/g)	($^{230}Th/^{232}Th$) Act. ratio	($^{230}Th/^{238}U$) Act.ratio	($^{234}U/^{238}U$) Act.ratio	Age (uncorr.) (ka)	Age (corr.) (ka)
5639*	CM-6,3	6.3	0.3919 ± 0.0008	1.765 ± 0.032	160 ± 4	0.227 ± 0.003	1.457 ± 0.005	19.21 ± 0.28	18.33 ± 0.28
5638*	CM-9,7	9.7	0.0939 ± 0.0002	0.230 ± 0.025	444 ± 49	0.352 ± 0.007	1.426 ± 0.007	30.95 ± 0.69	30.47 ± 0.70
5580*	CM-11,2	11.2	0.1586 ± 0.0003	0.360 ± 0.030	522 ± 45	0.384 ± 0.005	1.435 ± 0.008	33.86 ± 0.57	33.41 ± 0.56
5637	CM-15,9	15.9	0.1171 ± 0.0002	0.080 ± 0.019	1910 ± 452	0.428 ± 0.004	1.424 ± 0.005	38.43 ± 0.48	38.30 ± 0.47
5656*	CM-17,1	17.1	0.1029 ± 0.0002	0.166 ± 0.032	896 ± 176	0.470 ± 0.011	1.389 ± 0.006	44.56 ± 1.27	44.23 ± 1.27
5579*	CM-18,3	18.3	0.0635 ± 0.0001	0.100 ± 0.032	1053 ± 336	0.540 ± 0.009	1.436 ± 0.011	50.46 ± 1.15	50.16 ± 1.13
5636	CM-22,7	22.7	0.0790 ± 0.0002	0.145 ± 0.026	870 ± 155	0.522 ± 0.006	1.428 ± 0.008	48.77 ± 0.82	48.42 ± 0.81
5581*	CM-23,8	23.8	0.0993 ± 0.0002	0.450 ± 0.036	422 ± 34	0.623 ± 0.013	1.425 ± 0.015	61.58 ± 1.83	60.71 ± 1.82
5657	CM-25,3	25.3	0.1552 ± 0.0003	0.129 ± 0.032	2202 ± 550	0.599 ± 0.007	1.392 ± 0.005	59.79 ± 0.93	59.62 ± 0.92
5562	CM-27,1	27.1	0.1698 ± 0.0003	0.037 ± 0.035	8166 ± 7812	0.581 ± 0.018	1.362 ± 0.005	59.05 ± 2.33	59.00 ± 2.30
5635	CM-30,1	30.1	0.1587 ± 0.0003	0.060 ± 0.018	4842 ± 1451	0.601 ± 0.006	1.370 ± 0.005	61.21 ± 0.84	61.14 ± 0.84
5658	CM-31,4	31.4	0.1401 ± 0.0003	0.076 ± 0.039	3457 ± 1752	0.615 ± 0.009	1.366 ± 0.006	63.45 ± 1.32	63.34 ± 1.31
5563	CM-33,2	33.2	0.1143 ± 0.0002	0.178 ± 0.026	1179 ± 175	0.600 ± 0.015	1.352 ± 0.006	62.51 ± 2.10	62.20 ± 2.08
5659*	CM-34,3	34.3	0.0983 ± 0.0002	n.d.	n.d.	0.767 ± 0.027	1.365 ± 0.007	85.90 ± 4.45	85.98 ± 4.45
5578*	CM-35,3	35.3	0.1040 ± 0.0002	0.046 ± 0.031	4387 ± 2959	0.640 ± 0.007	1.363 ± 0.010	67.13 ± 1.22	67.04 ± 1.21
5577*	CM-36,7	36.7	0.1056 ± 0.0002	0.053 ± 0.027	4234 ± 2175	0.689 ± 0.006	1.391 ± 0.010	71.92 ± 1.18	71.82 ± 1.16
5634*	CM-40,3	40.3	0.1007 ± 0.0002	0.072 ± 0.038	2958 ± 1556	0.696 ± 0.019	1.419 ± 0.010	70.92 ± 2.70	70.78 ± 2.70
5633*	CM-42,1	42.1	0.1427 ± 0.0003	0.019 ± 0.025	16149 ± 20586	0.721 ± 0.009	1.437 ± 0.007	72.88 ± 1.39	72.85 ± 1.41
5660*	CM-44,9	44.9	0.0864 ± 0.0002	0.081 ± 0.038	2374 ± 1109	0.726 ± 0.015	1.405 ± 0.007	76.24 ± 2.24	76.06 ± 2.18

Table B.3: *Activity ratios and $^{230}Th/U$-ages for growth axis CM obtained with MC-ICPMS. Uncertainties are given as 2σ range. Ages were corrected with a detrital $^{232}Th/^{238}U$ weight ratio of 0.38 ± 0.30.*

Lab.No.	Sample ID	dft (cm)	^{238}U (µg/g)	^{232}Th (ng/g)	($^{230}Th/^{232}Th$) Act. ratio	($^{230}Th/^{238}U$) Act.ratio	($^{234}U/^{238}U$) Act.ratio	Age (uncorr.) (ka)	Age (corr.) (ka)
SW 73	CM-2,6	2.6	0.086 ± 0.001	n.d.	n.d.	0.166 ± 0.002	1.465 ± 0.006	13.00 ± 0.16	13.00 ± 0.16
SW 89	CM-3,9	3.9	0.178 ± 0.001	0.139 ± 0.002	714 ± 20	0.182 ± 0.005	1.434 ± 0.002	14.71 ± 0.42	14.55 ± 0.42
SW 142	CM-4.8	4.80	0.197 ± 0.001	0.186 ± 0.003	1447 ± 34	0.852 ± 0.013	1.421 ± 0.002	16.08 ± 2.12	15.89 ± 2.13
SW 97	CM-6,1	6.1	0.194 ± 0.001	0.695 ± 0.007	177 ± 2	0.207 ± 0.002	1.419 ± 0.005	17.11 ± 0.16	16.39 ± 0.17
SW 60	CM-6,9	6.9	0.442 ± 0.003	3.057 ± 0.032	117 ± 1	0.265 ± 0.002	1.475 ± 0.002	21.44 ± 0.16	20.11 ± 0.19
SW 74	CM-7,6	7.6	0.324 ± 0.002	0.767 ± 0.009	387 ± 4	0.299 ± 0.002	1.457 ± 0.006	24.79 ± 0.20	24.34 ± 0.21
SW 86	CM-9,0	9	0.163 ± 0.001	0.153 ± 0.002	1028 ± 17	0.315 ± 0.003	1.429 ± 0.003	26.80 ± 0.30	26.62 ± 0.30
SW 87	CM-10,5	10.5	0.135 ± 0.001	0.214 ± 0.003	662 ± 11	0.343 ± 0.003	1.435 ± 0.003	29.42 ± 0.33	29.11 ± 0.33
SW 90	CM-12,1	12.1	0.212 ± 0.001	0.270 ± 0.004	867 ± 16	0.360 ± 0.005	1.446 ± 0.002	30.80 ± 0.50	30.55 ± 0.50
SW 143	CM-13.1	13.10	0.111 ± 0.001	0.090 ± 0.002	612 ± 11	0.189 ± 0.002	1.369 ± 0.002	34.22 ± 0.22	34.07 ± 0.22
SW 98	CM-14,0	14	0.263 ± 0.002	0.221 ± 0.004	1551 ± 27	0.426 ± 0.004	1.515 ± 0.006	35.35 ± 0.41	35.20 ± 0.41
SW 99	CM-14,6	14.6	0.069 ± 0.001	0.133 ± 0.002	667 ± 12	0.423 ± 0.007	1.427 ± 0.017	37.67 ± 0.94	37.29 ± 0.94
SW 100	CM-15,3	15.3	0.100 ± 0.001	0.024 ± 0.001	5489 ± 130	0.426 ± 0.005	1.414 ± 0.005	38.38 ± 0.59	38.34 ± 0.57
SW 37	CM-16,5	16.5	0.138 ± 0.001	0.923 ± 0.012	198 ± 3	0.431 ± 0.006	1.413 ± 0.002	39.07 ± 0.59	37.75 ± 0.62
SW 85	CM-16,9	16.9	0.113 ± 0.001	0.677 ± 0.007	234 ± 3	0.459 ± 0.003	1.441 ± 0.004	41.07 ± 0.38	39.91 ± 0.43
SW 38	CM-17,8	17.8	0.122 ± 0.001	0.458 ± 0.005	378 ± 4	0.466 ± 0.002	1.401 ± 0.002	43.21 ± 0.28	42.46 ± 0.30
SW 61	CM-19,0	19	0.129 ± 0.001	0.401 ± 0.006	477 ± 8	0.486 ± 0.005	1.422 ± 0.002	44.64 ± 0.53	44.03 ± 0.54
SW 75	CM-20,4	20.4	0.062 ± 0.001	n.d.	n.d.	0.489 ± 0.005	1.410 ± 0.007	45.44 ± 0.65	45.44 ± 0.65
SW 91	CM-21,7	21.7	0.103 ± 0.001	0.653 ± 0.007	251 ± 5	0.518 ± 0.009	1.437 ± 0.003	47.66 ± 1.02	46.44 ± 1.03
SW 101	CM-22,8	22.8	0.085 ± 0.001	0.218 ± 0.004	635 ± 15	0.532 ± 0.008	1.414 ± 0.006	50.21 ± 1.03	49.71 ± 1.03

continued on next page

continued from previous page

Lab.No.	Sample ID	dft (cm)	^{238}U (µg/g)	^{232}Th (ng/g)	(^{230}Th/^{232}Th) Act. ratio	(^{230}Th/^{238}U) Act.ratio	(^{234}U/^{238}U) Act.ratio	Age (uncorr.) (ka)	Age (corr.) (ka)
SW 62	CM-23,4	23.4	0.086 ± 0.001	0.200 ± 0.003	704 ± 12	0.536 ± 0.005	1.389 ± 0.003	51.83 ± 0.59	51.37 ± 0.61
SW 39	CM-24,4	24.4	0.136 ± 0.001	2.286 ± 0.023	105 ± 1	0.577 ± 0.003	1.416 ± 0.003	55.76 ± 0.40	52.45 ± 0.86
SW 76	CM-24,9	24.9	0.115 ± 0.001	n.d.	n.d.	0.573 ± 0.005	1.381 ± 0.007	56.87 ± 0.71	56.87 ± 0.71
SW 92	CM-26,3	26.3	0.162 ± 0.001	0.103 ± 0.001	2945 ± 47	0.613 ± 0.007	1.397 ± 0.002	61.07 ± 0.87	60.94 ± 0.86
SW 57	CM-28,3	28.3	0.116 ± 0.001	0.093 ± 0.002	2258 ± 48	0.592 ± 0.007	1.352 ± 0.002	61.13 ± 0.90	60.97 ± 0.90
SW 93	CM-30,7	30.7	0.185 ± 0.001	0.178 ± 0.004	1859 ± 49	0.585 ± 0.009	1.378 ± 0.002	58.60 ± 1.19	58.40 ± 1.22
SW 84	CM-32,2	32.2	0.096 ± 0.001	0.093 ± 0.002	1947 ± 48	0.616 ± 0.007	1.367 ± 0.003	63.36 ± 0.99	63.16 ± 0.95
SW 58	CM-34,9	34.9	0.105 ± 0.001	0.068 ± 0.001	2948 ± 64	0.623 ± 0.006	1.373 ± 0.003	63.96 ± 0.87	63.84 ± 0.87
SW 78	CM.35,6	35.6	0.089 ± 0.001	n.d.	n.d.	0.617 ± 0.007	1.374 ± 0.009	63.02 ± 1.09	63.02 ± 1.09
SW 77	CM-36,8	36.8	0.120 ± 0.001	0.208 ± 0.004	1145 ± 22	0.650 ± 0.005	1.408 ± 0.008	65.29 ± 0.83	64.96 ± 0.82
SW 59	CM-39,3	39.3	0.109 ± 0.001	0.072 ± 0.001	3055 ± 60	0.662 ± 0.006	1.410 ± 0.002	66.71 ± 0.85	66.59 ± 0.85
SW 79	CM-40,8	40.8	0.114 ± 0.001	n.d.	n.d.	0.665 ± 0.010	1.419 ± 0.010	66.57 ± 1.52	66.57 ± 1.52
SW 81	CM-41,5	41.5	0.162 ± 0.001	0.465 ± 0.005	760 ± 8	0.712 ± 0.004	1.455 ± 0.004	70.49 ± 0.59	69.96 ± 0.62
SW 63	CM-43,4	43.4	0.191 ± 0.001	0.455 ± 0.006	933 ± 14	0.725 ± 0.006	1.449 ± 0.003	72.56 ± 0.81	72.11 ± 0.83
SW 94	CM-44,0	44	0.135 ± 0.001	0.655 ± 0.010	460 ± 8	0.727 ± 0.008	1.426 ± 0.003	74.66 ± 1.17	73.74 ± 1.21
SW 83	CM-46,2	46.2	0.086 ± 0.001	0.863 ± 0.009	229 ± 2	0.752 ± 0.004	1.455 ± 0.003	76.02 ± 0.64	74.16 ± 0.99
SW 82	CM-47,3	47.3	0.167 ± 0.001	0.476 ± 0.009	836 ± 17	0.779 ± 0.008	1.500 ± 0.003	76.17 ± 1.09	75.67 ± 1.12
SW 95	CM-49,6	49.6	0.186 ± 0.001	0.133 ± 0.004	3414 ± 114	0.797 ± 0.015	1.494 ± 0.003	79.11 ± 2.05	78.98 ± 2.04
SW 71	CM-51,0	51	0.233 ± 0.001	0.168 ± 0.005	3421 ± 101	0.807 ± 0.008	1.493 ± 0.002	80.54 ± 1.14	80.41 ± 1.15
SW 102	CM-52,7	52.7	2.818 ± 0.030	1.596 ± 0.016	4257 ± 38	0.789 ± 0.008	1.491 ± 0.013	78.17 ± 1.49	78.07 ± 1.49

Table B.4: *Activity ratios and $^{230}Th/U$-ages for growth axis CMa obtained with MC-ICPMS. Uncertainties are given as 2σ range. Ages were corrected with a detrital $^{232}Th/^{238}U$ weight ratio of 0.38 ± 0.3.*

Lab.No.	Sample ID	dft (cm)	^{238}U (µg/g)	^{232}Th (ng/g)	($^{230}Th/^{232}Th$) Act. ratio	($^{230}Th/^{238}U$) Act.ratio	($^{234}U/^{238}U$) Act.ratio	Age (uncorr.) (ka)	Age (corr.) (ka)
SW137	CMa-1.2	1.2	0.203 ± 0.001	1.580 ± 0.016	277 ± 3	0.705 ± 0.004	1.431 ± 0.002	71.27 ± 0.59	69.79 ± 0.79
SW138	CMa-5.4	5.4	0.139 ± 0.001	0.011 ± 0.000	28218 ± 1054	0.753 ± 0.007	1.443 ± 0.002	76.85 ± 0.99	76.84 ± 1.00
SW139b	CMa-9.7	9.7	0.191 ± 0.001	1.677 ± 0.017	267 ± 3	0.767 ± 0.004	1.481 ± 0.002	76.01 ± 0.60	74.41 ± 0.90

Table B.5: *Activity ratios and $^{230}Th/U$-ages for growth axis CMb obtained with MC-ICPMS. Uncertainties are given as 2σ range. Ages were corrected with a detrital $^{232}Th/^{238}U$ weight ratio of 0.38 ± 0.3.*

Lab.No.	Sample ID	dft (cm)	^{238}U (µg/g)	^{232}Th (ng/g)	($^{230}Th/^{232}Th$) Act. ratio	($^{230}Th/^{238}U$) Act.ratio	($^{234}U/^{238}U$) Act.ratio	Age (uncorr.) (ka)	Age (corr.) (ka)
SW140	CMb-0.3	0.3	1.171 ± 0.009	3.083 ± 0.031	1017 ± 9	0.876 ± 0.006	1.462 ± 0.007	93.77 ± 1.17	93.30 ± 1.18
SW141	CMb-1.5	1.5	0.138 ± 0.001	0.248 ± 0.005	1447 ± 34	0.852 ± 0.013	1.421 ± 0.002	94.27 ± 2.12	93.93 ± 2.13
SW103	CMb-3.4	3.4	0.135 ± 0.001	0.030 ± 0.001	11793 ± 229	0.850 ± 0.008	1.396 ± 0.010	96.56 ± 1.86	96.52 ± 1.90

B.3 Supplementary data to section 6.3.3 (Proxy variability)

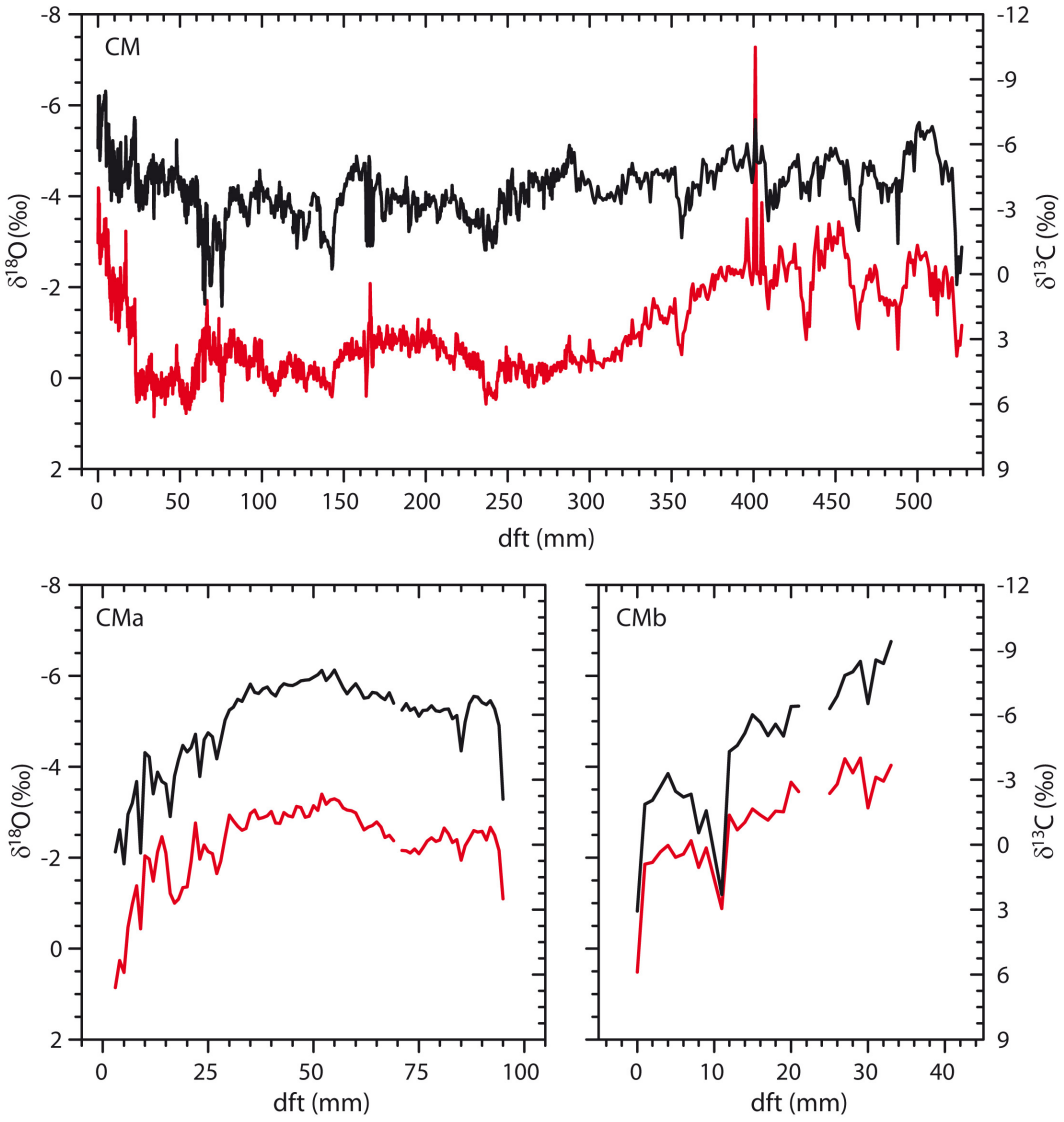

Figure B.2: *Stable isotope records $\delta^{13}C$ (black) and $\delta^{18}O$ (red) for growth axis CM (0 - 520 mm dft, upper panel), CMa (0 - 100 mm dft, bottom left) and CMb (0 - 40 mm dft, bottom right).*

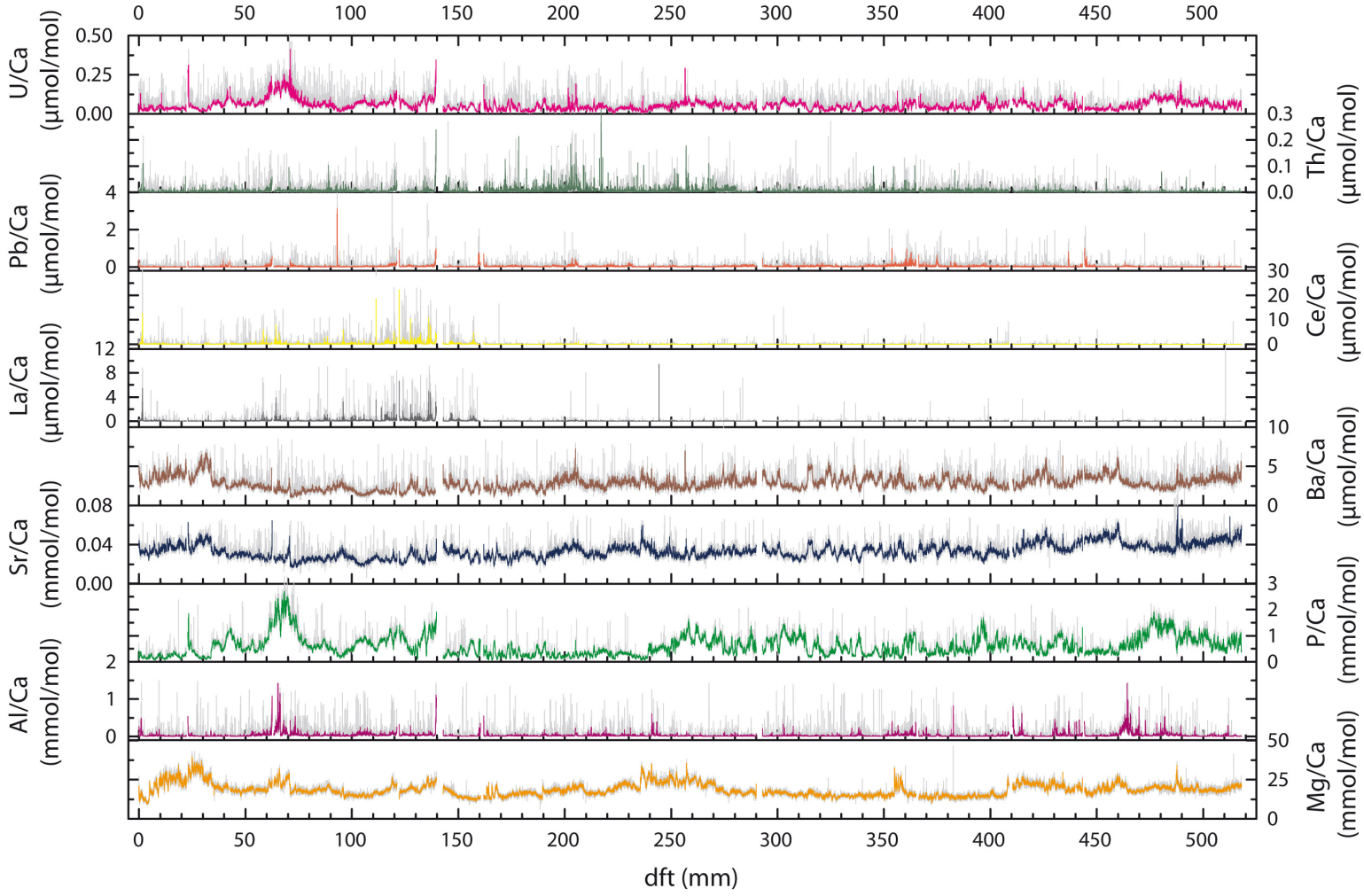

Figure B.3: *Element to calcium ratios measured along CM (0 - 520 mm dft). Outlier corrected raw data (10 µm resolution, grey lines), 5p running median (colored lines).*

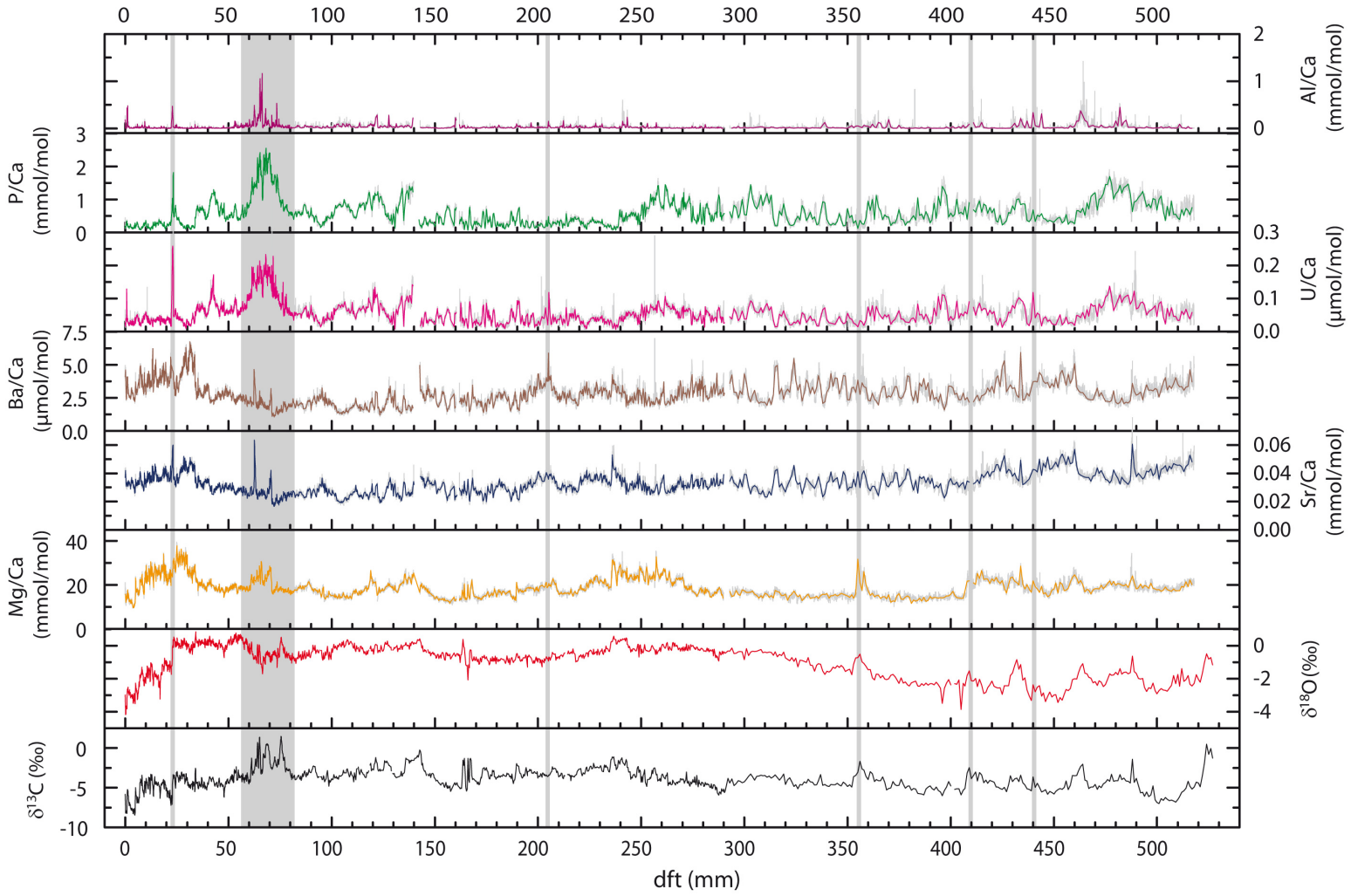

Figure B.4: *From top to bottom: Element to calcium ratios of Al/Ca, P/Ca, U/Ca, Ba/Ca, Sr/Ca and Mg/Ca in comparison with stable isotope values $\delta^{18}O$ (red) and $\delta^{13}C$ (black) measured along growth axis CM (0 - 520 mm dft). The elemental ratios are shown as outlier corrected raw data (grey lines) and 5p running median (colored lines). The grey vertical bars indicate the positon of potential hiatuses or sections with low growth rates indicated also in the age model (Figure 6.2).*

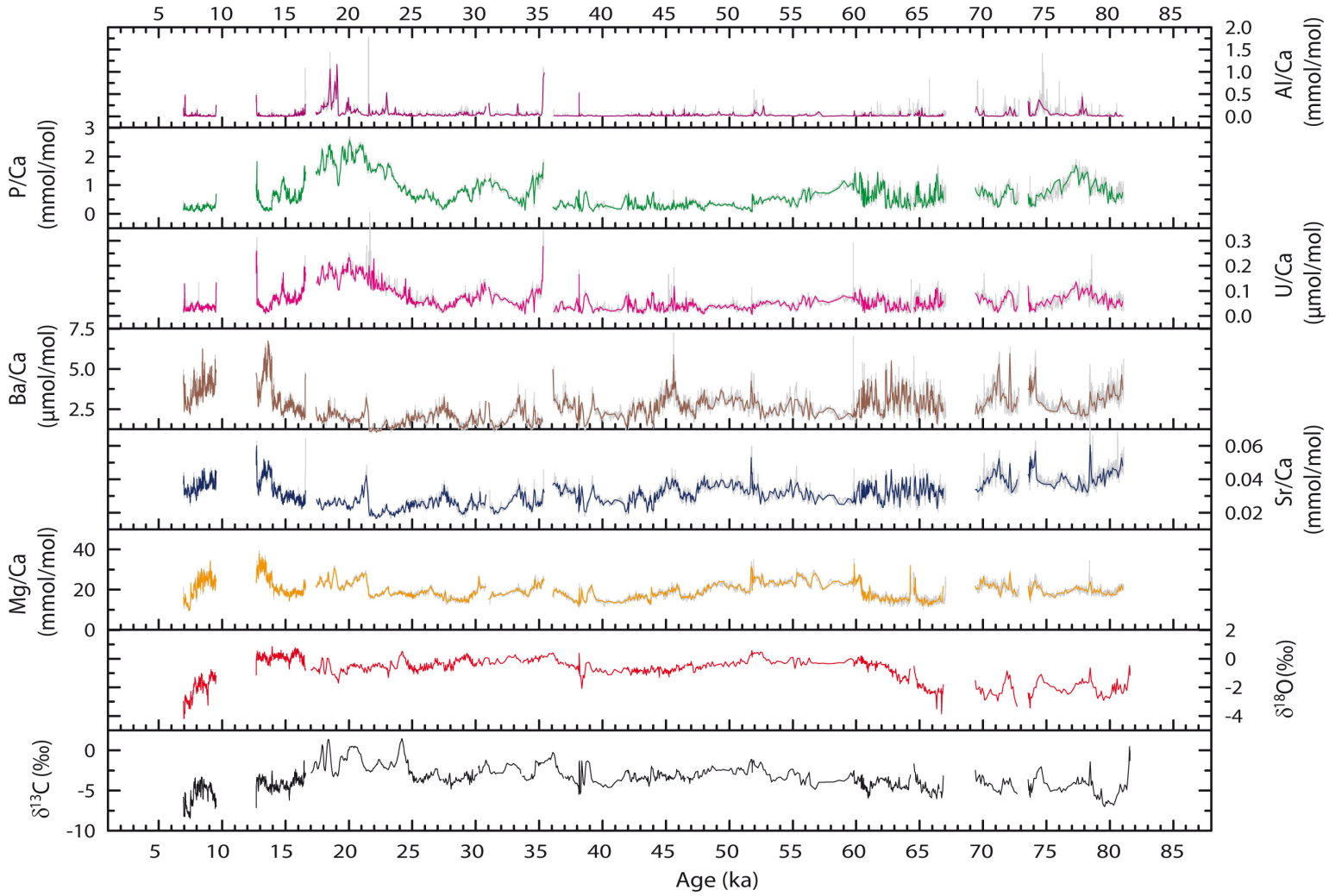

Figure B.5: *Element to calcium ratios and $\delta^{13}C$ (black) and $\delta^{18}O$ (red) values measured along CM (7 - 82 ka). Elemental ratios: Outlier corrected raw data (10 µm resolution, grey lines), 5p running median (colored lines).*

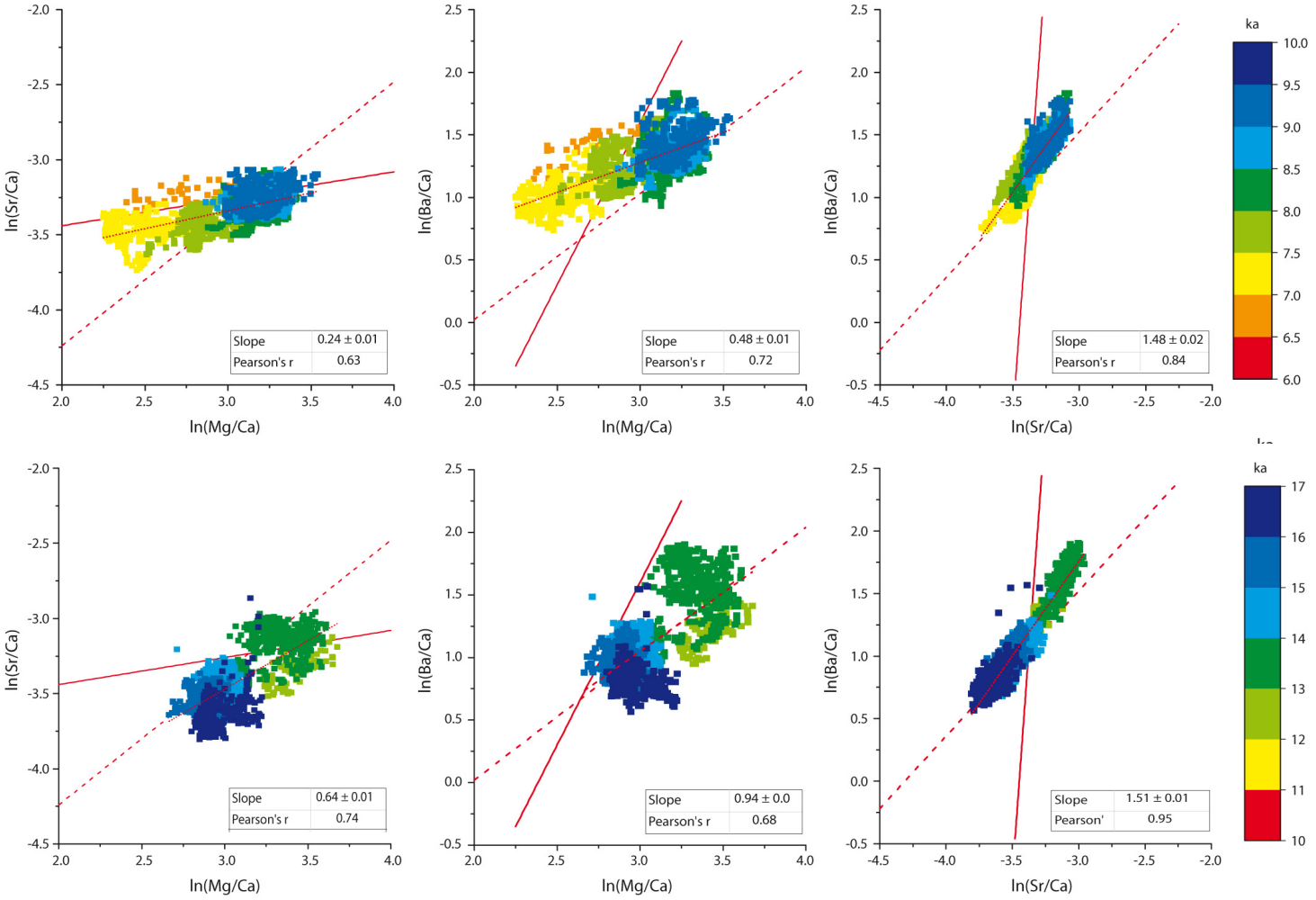

Figure B.6: *Cross plots of element to calcium ratios in speleothem calcite of CM shown as ln(Sr/Ca) vs. ln(Mg/Ca) (left), ln(Ba/Ca) vs. ln(Mg/Ca) (middle) and ln(Ba/Ca) vs. ln(Sr/Ca) (right) for different time slices during MIS 1 (upper panel: Holocene (10 - 7 ka), bottom panel: deglaciation (17 - 12 ka)). The red lines indicate the theoretically expected slopes for PCP and/or ICD after Sinclair et al. (2012) calculated with the corresponding partition coefficients. The dashed lines show the same for the case of calcite recrystallization (Sinclair et al., 2012). The dotted lines show the fitted slope of the data points.*

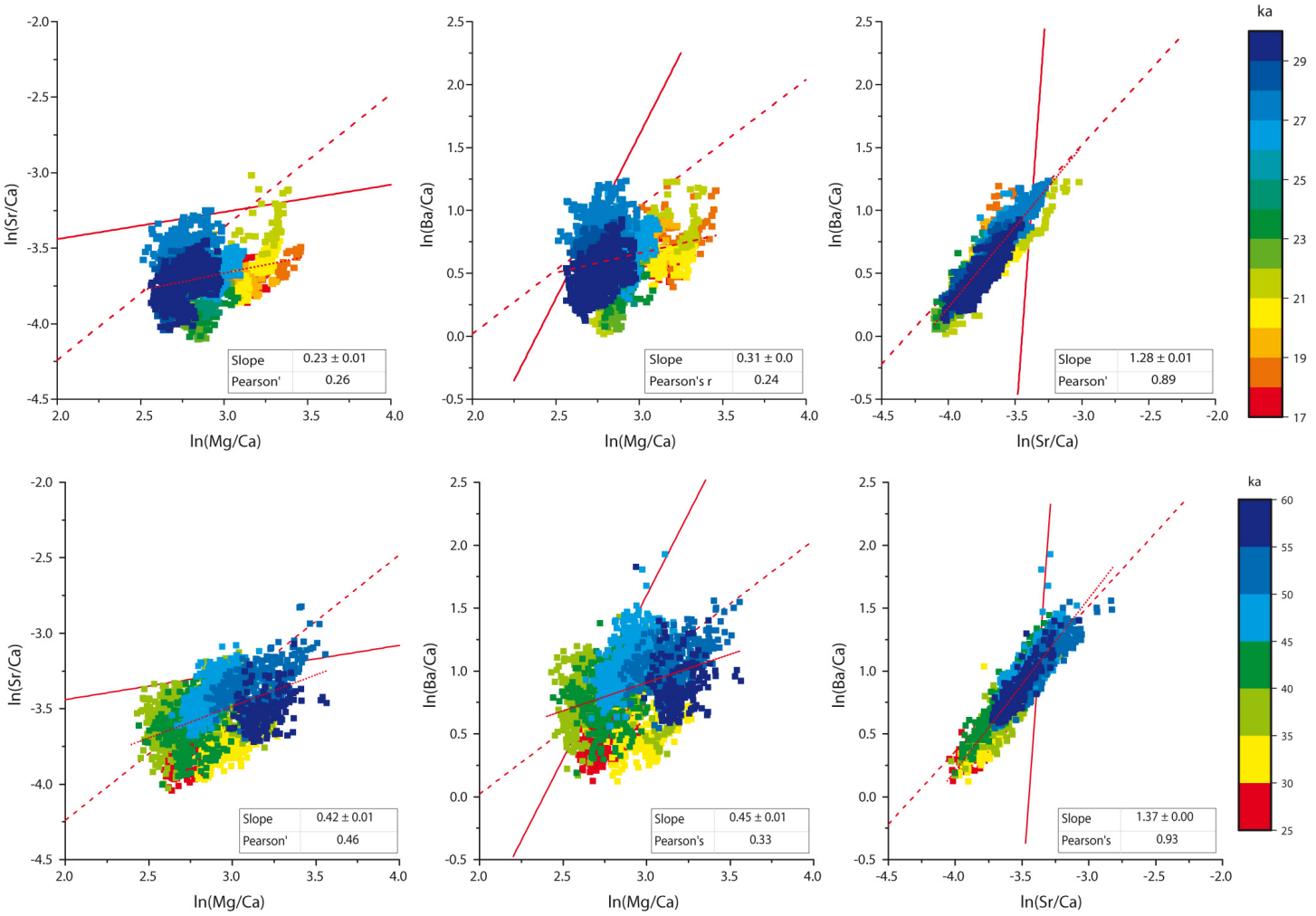

Figure B.7: *Cross plots of element to calcium ratios in speleothem calcite of CM shown as ln(Sr/Ca) vs. ln(Mg/Ca) (left), ln(Ba/Ca) vs. ln(Mg/Ca) (middle) and ln(Ba/Ca) vs. ln(Sr/Ca) (right) for different time slices MIS 2 (29 - 17 ka, upper panel) and MIS 3 (57 - 29 ka, bottom panel). The red lines indicate the theoretically expected slopes for PCP and/or ICD after Sinclair et al. (2012) calculated with the corresponding partition coefficients. The dashed lines show the same for the case of calcite recrystallization (Sinclair et al., 2012). The dotted lines show the fitted slope of the data points.*

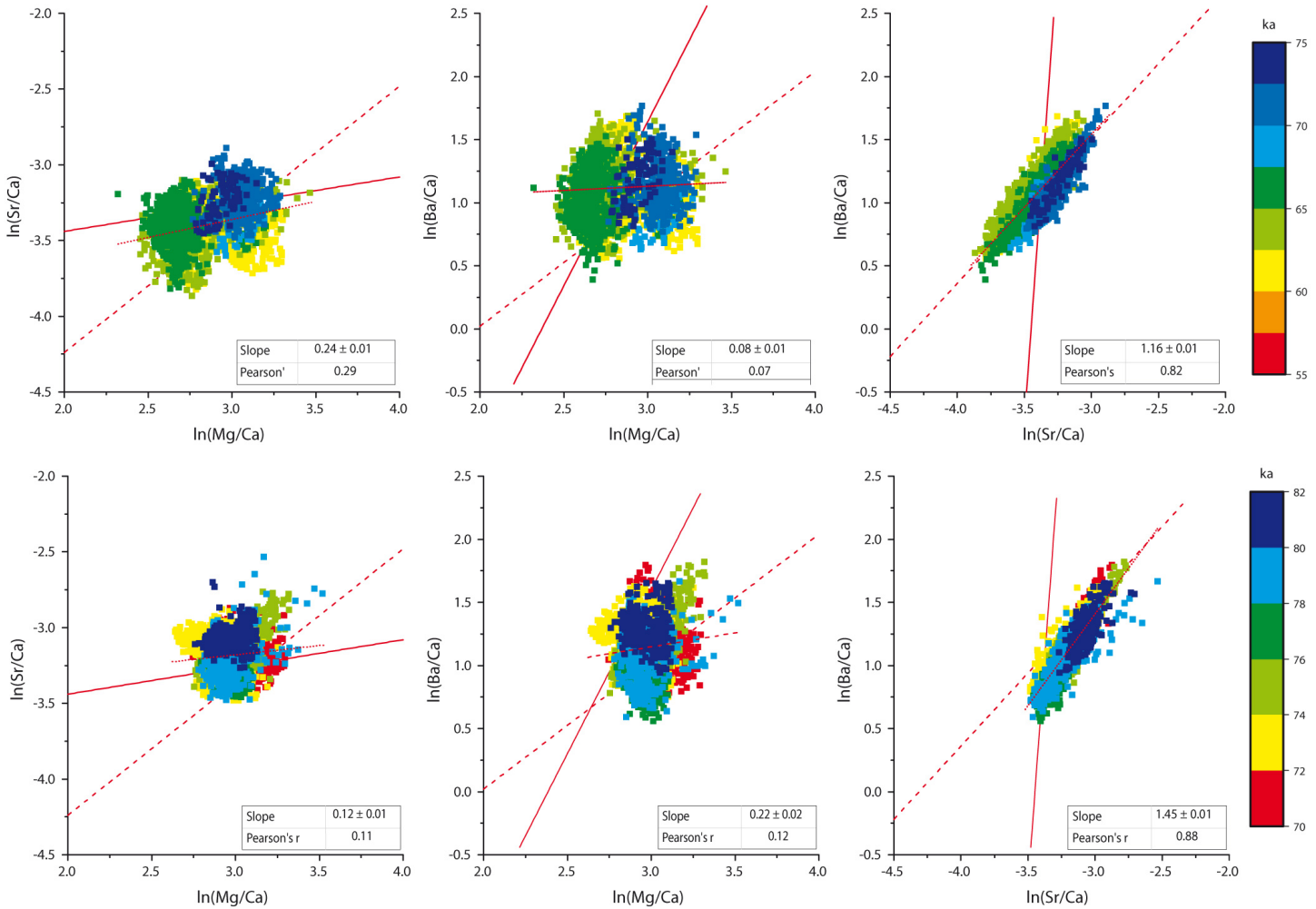

Figure B.8: *Cross plots of element to calcium ratios in speleothem calcite of CM shown as ln(Sr/Ca) vs. ln(Mg/Ca) (left), ln(Ba/Ca) vs. ln(Mg/Ca) (middle) and ln(Ba/Ca) vs. ln(Sr/Ca) (right) for different time slices MIS 4 (73 - 57 ka, upper panel) and MIS 5 (82 - 71 ka, bottom panel). The red lines indicate the theoretically expected slopes for PCP and/or ICD after Sinclair et al. (2012) calculated with the corresponding partition coefficients. The dashed lines show the same for the case of calcite recrystallization (Sinclair et al., 2012). The dotted lines show the fitted slope of the data points.*

C Supplementary material to Paper III - Cloşani Cave

C.1 Analytical details

Sample preparation and ^{230}Th/U-dating were performed at the Institute of Environmental Physics, Heidelberg. Samples were cut with a band-saw close to the growth axis. The methods of sample preparation and mass spectrometric analysis follow the procedure of Douville et al. (2010) and Matos et al. (2015). Activity ratios were analysed with a Thermo Fisher Neptune MC-ICP-MS in Heidelberg. The calibration of the used ^{233}U, ^{236}U and ^{229}Th spikes is described in Hoffmann et al. (2007). Replicated measurements of the HU-1 standard yield a reproducibility of the activity ratios of (^{234}U/^{238}U) of 0.9997 ± 0.0003 and for (^{230}Th/^{238}U) 1.0002 ± 0.0005 (weighted mean and 2σ standard deviation of 113 measurements between June 2015 and July 2016). Blanks are smaller than 0.4 ± 0.1 fg for ^{234}U and 0.04 ± 0.03 fg for ^{230}Th (1σ standard deviation). Ages were calculated using the half-lives of Cheng et al. (2000). We decided to use these half-lives instead of the more recent half-lives of Cheng et al. (2013) in order to preserve comparability with previous publications. Correction for detrital contamination assumes a ^{232}Th/^{238}U weight ratio of 3.8 ± 1.9 and ^{230}Th, ^{234}U and ^{238}U in secular equilibrium. Age uncertainties are quoted at the 2σ-level and do not include half-life uncertainties.

Samples for radiocarbon dating were obtained with a micro-mill at a spatial resolution of 0.4 mm. Subsamples yielded approximately 6 to 7 mg of $CaCO_3$. The $CaCO_3$ powder was acidified (HCl) under vacuum, and the resulting CO_2 was combusted with H_2 to C on a Fe catalyst at 575 °C. The detailed sample preparation is described in (Fohlmeister et al., 2011). The samples were measured with the MICADAS (Synal et al., 2007) operated at the Klaus-Tschira-Facility (Mannheim, Germany). Typically, the precision of modern samples is at the 2 ‰ level.

Stable carbon and oxygen isotope analysis was performed at the University of Innsbruck. The samples were micromilled at a spatial resolution of 250 µm. The carbonate powder was measured using an on-line, automated carbonate preparation system (Gasbench II) linked to a triple collector gas source ThermoFisher DeltaplusXL mass spectrometer. Raw data were calibrated against NBS19, and δ values are reported relative to Vienna Pee Dee Belemnite (VPDB) standard. Long-term precision of the δ^{13}C and δ^{18}O values, estimated as the 1σ-standard deviation of replicate analyses, is 0.06 and 0.08 ‰, respectively (Spötl and Venne-

mann, 2003; Spötl, 2011).

For trace element analyses, thin slabs (about 4 cm long and approx. 0.5 cm wide) had to be cut along the growth axis, which were mounted with epoxy resin onto glass plates and polished (Figure 7.2 C). If possible, these slabs were taken from pieces of the sample which had already been broken apart in order to keep the sample loss at the transition of the laser ablation tracks at a minimum. If necessary, the slabs were cut with a band saw, which implies a sample loss of 1 mm, which was taken into account in the composite record. Elements were measured parallel to the growth axis, and the continuous profile is located at less than 2 mm distance from the stable isotope track.

Trace element concentrations were measured by Laser Ablation ICP-MS at Goethe University Frankfurt, Germany, using a Resolution M-50 (Resonetics) 193 nm ArF Excimer laser (CompexPro 102, Coherent) equipped with a two-volume ablation cell (Laurin Technic, Australia, Mueller et al. (2009)) coupled to a Thermo Scientific Element 2 sector field ICP-MS (Gerdes and Zeh, 2006). The signal was tuned for maximum sensitivity for Ce and U while maintaining oxide production, monitored as $^{238}U^{16}O/^{238}U$, below 0.5 %. Element data were continuously acquired using a rectangular, 100 x 20 µm wide ablation slit and a scan speed of 10 µm/s. The method yields a spatial resolution of 12.5 µm. A continuous sample scan has a maximum length of 4 cm. Background counts were measured with the laser in off mode and subtracted from the raw data. Trace element data were normalized to the Ca content of the speleothem and standardized against the NIST SRM 612 glass standard using the concentrations published by Pearce et al. (1997). Measured Sr, Ba, and Mg concentrations are well above the detection limits of 0.03 ppm (Sr), 0.02 ppm (Ba) and 0.2 ppm (Mg), respectively. Element to Ca ratios are given as molar ratios. The uppermost 1 mm of the trace element record is missing, because it was lost during sample preparation. The bottom 30 mm of C09-2 could not be analyzed and are missing in the trace element record.

C.2 Supplementary material to section 7.3.4 (Correlation analysis)

Correlation analysis (section 7.3.4) for the speleothem proxies was performed with a test statistic based on Pearson's product moment correlation coefficient r (x,y) and follows a t distribution with length (x)-2 degrees of freedom. Asymptotic confidence intervals are given based on Fisher's Z transform. Table C.1 shows the relevant information concerning the statistics of the correlation analysis between the different speleothem proxies. For the calculation of the correlation coefficients between stalagmite proxies and instrumental data, the software PearsonT3 was used in order to account for autocorrelation (Ólafsdóttir and Mudelsee, 2014). Table C.2 shows the results for the computed cross-correlations.

Table C.1: *Summary of statistical results for the correlation coefficients presented in section 7.3.4.*

$r_{x/y}$	estimate	95% conf. int.		df	t value	p value	time frame (yrs BP)	reference resolution
		upper	lower					
$r_{Sr/Ba}$	0.96	0.96	0.96	34175	664.26	<10E-5	3600 - 27	trace elements
$r_{Mg/Sr}$	-0.45	-0.46	-0.44	34113	-92.72	<10E-5	3600 - 27	trace elements
$r_{Mg/Ba}$	-0.46	-0.47	-0.45	34112	-96.47	<10E-5	3600 - 27	trace elements
$r_{Sr/Ba}$	0.95	0.94	0.97	212	46.73	<10E-5	241 - 26	trace elements
$r_{Mg/Sr}$	-0.23	-0.35	-0.10	212	-3.42	7.40E-04	241 - 26	trace elements
$r_{Mg/Ba}$	-0.32	-0.43	-0.19	212	-4.91	<10E-5	241 - 26	trace elements
$r_{gr/Sr}$	0.57	0.47	0.65	212	9.98	<10E-5	241 - 26	annual
$r_{gr/Mg}$	-0.67	-0.74	-0.59	212	-13.13	<10E-5	241 - 26	annual
$r_{gr/Ba}$	0.62	0.53	0.69	212	11.39	<10E-5	241 - 26	annual
$r_{\delta^{13}C/\delta^{18}O}$	-0.31	-0.35	-0.27	1830	-14.12	<10E-5	3800 - 19	stable isotopes
$r_{\delta^{13}C/Sr}$	0.33	0.29	0.38	1707	14.68	<10E-5	3600 - 19	stable isotopes
$r_{\delta^{13}C/Mg}$	0.01	-0.04	0.06	1707	0.49	0.62	3600 - 19	stable isotopes
$r_{\delta^{13}C/Ba}$	0.33	0.29	0.37	1707	14.37	<10E-5	3600 - 19	stable isotopes
$r_{\delta^{18}O/Sr}$	-0.29	-0.33	-0.25	1707	-12.58	<10E-5	3600 - 19	stable isotopes
$r_{\delta^{18}O/Mg}$	0.13	0.08	0.17	1707	5.28	<10E-5	3600 - 19	stable isotopes
$r_{\delta^{18}O/Ba}$	-0.32	-0.36	-0.27	1707	-13.82	<10E-5	3600 - 19	stable isotopes
$r_{gr/\delta^{18}O}$	-0.15	-0.29	0.00	180	-1.99	0.05	241 - 26	stable isotopes
$r_{gr/\delta^{13}C}$	0.31	0.17	0.43	180	4.31	2.68E-05	241 - 26	stable isotopes

Table C.2: *Summary of results obtained by PearsonT3 (Ólafsdóttir and Mudelsee, 2014) for the correlation analysis between stalagmite proxies and instrumental data and the 5-point linear weighted running means of temperature and precipitation with the bootstrap confidence intervals and the persistence times τ, respectively.*

$r_{x/x}$	estimate	95% conf. int.		τ_x	τ_y	Time period	n
r_{Mg/P_lin}	-0.583	-0.848	-0.084	6.401	2.529	1922 - 1973	51
r_{Sr/P_lin}	0.095	-0.409	0.555	2.216	2.529	1922 - 1973	51
r_{gr/P_lin}	0.369	0.011	0.642	4.963	2.529	1922 - 1973	51
r_{Mg/T_lin}	0.368	-0.136	0.72	3.354	2.607	1905 - 1973	63
r_{Sr/T_lin}	-0.276	-0.69	0.273	2.554	2.607	1905 - 1973	63
r_{gr/T_lin}	-0.437	-0.793	0.142	4.714	2.607	1905 - 1973	63
$r_{Mg/P}$	-0.424	-0.614	-0.189	6.762	0.427	1918 - 1973	55
$r_{Sr/P}$	0.033	-0.278	0.338	2.369	0.427	1918 - 1973	55
$r_{gr/P}$	0.306	-0.003	0.561	5.114	0.427	1918 - 1973	55
$r_{Mg/T}$	0.181	-0.076	0.416	3.599	0.567	1901 - 1973	69
$r_{Sr/T}$	-0.232	-0.484	0.055	5.694	0.542	1901 - 1973	69
$r_{gr/T}$	-0.258	-0.518	0.047	5.052	0.542	1901 - 1973	69

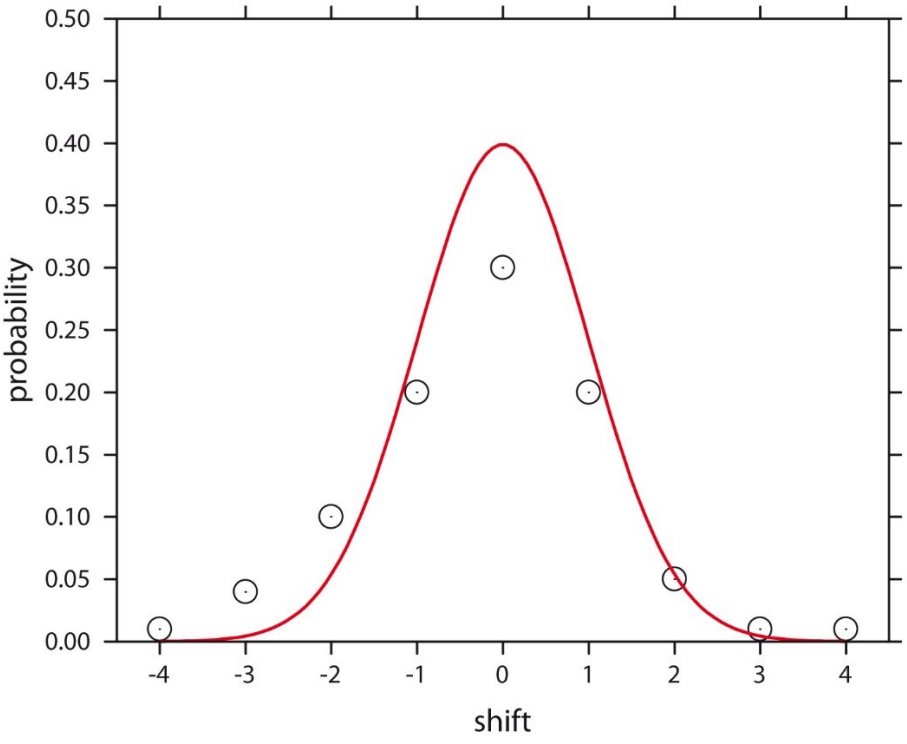

Figure C.1: *Probability distribution chosen for the shift of the reference point for the Monte Carlo simulation of the correlation coefficients in section 7.3.4 (open symbols). The red line indicates a normal distribution (mean = 0, sd = 1).*

D Featured publications: Paper V

The following pages include the accepted version of Paper V - Vieten et al. (in press):

Vieten R., Winterhalder S., Winter A., Scholz D., Miller T., Spötl C. and Schröder-Ritzrau A. (in press). Monitoring of Cueva Larga, Puerto Rico - a First Step to Decode Speleothem Climate Records. Karst Groundwater Contamination and Public Health. Selected papers and abstracts of the symposium held January 27 through 30, 2016, San Juan, Puerto Rico. Karst Waters Institute Special Publication, 19: 74.

Monitoring of Cueva Larga, Puerto Rico – a First Step to Decode Speleothem Climate Records

Rolf Vieten, Sophie Winterhalder, Amos Winter, Denis Scholz, Thomas Miller, Christoph Spötl and Andrea Schröder-Ritzrau

Abstract

This study presents results of an ongoing cave monitoring study at Cueva Larga, Puerto Rico. The monitoring includes monthly analysis of stable isotope ratios of rain and drip water, trace element ratios of drip water and cave air parameters. Drip sites are above growing speleothems offering the unique chance to calibrate geochemical variations in speleothems in order to reconstruct past climate conditions.

Seasonal rainfall patterns above Cueva Larga show characteristic stable isotope values. The wet season is characterized by more negative $\delta^{18}O$ and δD values and a maritime deuterium excess (+10‰). The dry season has more positive $\delta^{18}O$ and δD values and elevated deuterium excess (>15%). The seasonal variations in the $\delta^{18}O$ and δD values are smoothed by the soil and karst system which acts as a low-pass filter, indicating that climate proxies derived from speleothems growing in Cueva Larga may only show multi-annual changes. The seepage water reservoir appears to be well-mixed. The transmission time of atmospheric signals into the drip water is site specific ranging most likely from several months to years.

R. Vieten
A. Winter
Department of Marine Sciences
University of Puerto Rico, Mayagüez
259 Blvd. Alfonso Valdés Physics, Geology and Marine Sci. Building – Office F-205
Mayagüez, PR 00680
E-mail: rolf-martin.vieten@upr.edu

S. Winterhalder
D. Scholz
Institut für Geowissenschaften
Johannes Gutenberg Universität Mainz
Johann-Joachim-Becherweg 21, D-55199 Mainz, Germany

S. Winterhalder
A. Schröder-Ritzrau
Institut für Umweltphysik
Ruprecht-Karls-Universität Heidelberg
Im Neuenheimer Feld 229 D - 69120 Heidelberg, Germany

T. Miller
Department of Geology, University of Puerto Rico, Mayagüez
Call Box 9000 Mayaguez, Puerto Rico 00681-9000

C. Spötl
Institut für Geologie
Universität Innsbruck
Innrain 52, 6020 Innsbruck, Austria

1.0. INTRODUCTION

Here we present results from a cave monitoring program at Cueva Larga. The goal of monitoring the Cueva Larga (CL) cave system is to understand and quantify the processes controlling the geochemical composition of cave drip waters which is ultimately recorded in speleothems. Calibrating the speleothems' geochemical composition to climate variables is the key to correctly interpret the proxy record encoded in speleothems in terms of past climate variability.

Speleothems have successfully been used as paleoclimate records (e.g., Fairchild and Baker, 2012; Fairchild et al., 2006a; Lachniet, 2009). Stable oxygen isotopes and trace element ratios have proven to be reliable paleoclimate proxies in many settings (e.g. Winter et al., 2011; Lachniet, 2004; Wang et al., 2001; Spötl and Mangini, 2002; Fairchild and Treble, 2009; Cruz et al., 2009). However, interpretation of these proxies is not always straight forward. Cave and drip site monitoring play a key role prior to paleo-climate reconstruction based on speleothems (James et al., 2015; Lachniet, 2009; Riechelmann et al., 2013, 2011).

Speleothem geochemical composition and growth are affected by the seepage water flow systematics through the soil and karst as well as the cave environment (Fairchild and Baker, 2012). Seasonal variations in the cave environment can bias the recorded signal and might lead to aliasing if not resolved at a sufficiently high resolution (Banner et al., 2007; James et al., 2015; Weedon, 2003). Moreover, processes such as evaporation, temperature variations, prior calcite precipitation (PCP), and changes in drip rate and pCO_2 can potentially alter the geochemical composition of speleothems, including trace elements and stable isotopes (Deininger et al., 2012; Fairchild and Baker, 2012; Mickler et al., 2006). Cave monitoring results, as presented here, are important to understand the transmission of climate signals from the surface through the vegetation cover, soil and karst into the cave (Fairchild and Baker, 2012, Fairchild et al., 2007).

In the tropics, the speleothem $\delta^{18}O$ value is commonly used to reconstruct variations in local rainfall amount over time (Lachniet, 2009). Variations in $\delta^{18}O$ and δD values of rainfall in the tropics are inversely correlated with the monthly rainfall amount, which is referred to as the "amount effect" (section 2.1; Dansgaard, 1964). The "amount effect" is variable and other processes such as temperature, seasonality and moisture source can modulate the "amount effect" and result in a more complex $\delta^{18}O$ signal (Dansgaard, 1964; Rozanski et al., 1993). Trace element ratios of Sr/Ca and Mg/Ca show high potential as a complementary recorder of rainfall changes (Fairchild and Treble, 2009; Fairchild et al., 2000; Stoll et al., 2012).

Adjustments of rainfall patterns to future climate change scenarios are still uncertain and changes in the hydrological cycle will affect freshwater supplies (Intergovernmental Panel on Climate Change, 2014; Winter et al., 2015). Multiproxy paleo-rainfall records offer a unique opportunity to evaluate climate models (Braconnot et al., 2012) and speleothem records can elucidate important climate forcings on regional rainfall (e.g. Asmerom et al., 2007; Cruz et al., 2005).

Our study investigates the transmission of the atmospheric signal into cave drip water feeding growing speleothems in Cueva Larga, Puerto Rico. The focus lies on tracing variations in the water cycle, expressed by changes in local precipitation. One part is to

investigate the "amount effect" to ensure that variations recorded by speleothem isotopes can be linked to changes in past rainfall amount. Rainfall samples are collected above the cave site in the northern karst region of Puerto Rico and in Mayaguez at the western coast of the island to detect the stable isotope signal of precipitation. Another part is to characterize the cave environment and record changes in drip water chemistry to study if there is a connection to atmospheric rainfall anomalies.

Cueva Larga appears ideal for paleoclimate studies due to its remote location, the lack of an active water stream and its small entrance limiting cave ventilation. In addition, the cave is unknown to the public restricting the risk of measurement disturbances. The monitoring results are documenting the natural undisturbed conditions in Cueva Larga and provide important insight into the climate signal transmission into the cave.

2.0. BACKGROUND

2.1. Isotopic "Amount Effect"

Rainwater $\delta^{18}O$ values depend on complex interactions in the hydrological cycle (Dansgaard, 1964; Lachniet, 2009; Rozanski et al., 1993). In the tropics the "amount effect", first described by Dansgaard (1964), usually outweighs other stable isotope effects. The "amount effect" describes a negative correlation between the monthly rainfall amount and its $\delta^{18}O$ values. Deep vertical convection systems, including tropical storms and hurricanes, have more negative $\delta^{18}O$ values than most other tropical rain events (Dansgaard, 1964; Lawrence and Gedzelman, 1996). In tropical cyclonic systems, atmospheric water ascends to high altitudes and Rayleigh distillation in the deep convection leads to an enrichment in light isotopes during the system's evolution (Lachniet, 2009). Furthermore, the extent of sub-cloud raindrop evaporation has also been related to rainfall amount and intensity (Dansgaard, 1964; Lachniet, 2009).

In Puerto Rico, easterly waves and low pressure systems during the rainy season have higher cloud altitudes and lower condensation temperatures than trade wind orographic rainfall of high-pressure systems during the dry season. More recent results obtained in Puerto Rico have shown a stronger correlation between $\delta^{18}O$ values of precipitation and maximal cloud heights (Scholl et al., 2009). This implies that condensation temperature of precipitation also plays a role in the "amount effect". Speleothem $\delta^{18}O$ values record variations in the stable isotope composition of rainfall over time allowing to reconstruct changes in rainfall amount and weather patterns in the tropics (Fairchild and Baker, 2012; Lachniet, 2009).

2.2. Global Meteoric Water Line (GMWL) and Deuterium Excess (d-excess)

The global meteoric water line (GMWL) was defined Craig (1961) as the relationship between the δD and $\delta^{18}O$ values of monthly rainfall water samples around the globe (equation 1). It results from the proportional fractionation difference during phase changes between δD and $\delta^{18}O$ and kinetic isotope fractionation during evaporation at relative humidity below 100% creating ad-excess. The d-excess (equation 2) is caused by the higher diffusivity for the lighter deuterium carrying molecule $^{2}H^{1}H^{16}O$ than for the heavier $^{1}H^{1}H^{18}O$. The d-excess of 10‰ in the GMWL represents an average relative humidity of 85% at the water source region (Clark and Fritz, 1997; Merlivat and Jouzel, 1979).

$$\delta D = 8 * \delta^{18}O + 10‰ \quad (1)$$

$$d = \delta D - 8 * \delta^{18}O \quad (2)$$

During condensation the d-excess does not change and it is an indicator of the water vapor source region (Merlivat and Jouzel, 1979).

2.3. Speleothem Trace Element Ratios (Sr/Ca and Mg/Ca)

Trace element ratios of Sr/Ca and Mg/Ca in cave drip water and speleothem may be used as hydrological proxies in (Fairchild and Baker, 2012). In certain cave settings (Fairchild et al., 2006a, 2000) it has been shown that seepage water during drier conditions exhibits higher ratios due to increased prior calcite precipitation (PCP) and selective leaching due to longer water residence times. PCP occurs upstream from the drip site and preferentially incorporates Ca in the crystal's lattice increasing the trace element ratio downstream. This may also be the case in Cueva Larga.

3.0. SITE DESCRIPTION

Puerto Rico is the most eastern island of the Greater Antilles located in the northeastern Caribbean between the island of Hispaniola and the Virgin Islands (Fig. 1). From east to west, the northern karst region stretches along the north coast reaching heights of more than 400 m. Cueva Larga (CL), also known as Cueva Coroso (Fig. 1), is located in the north-central karst region (N 18°19; W 66°48) at a height of 350 msl. The area is a developed holokarst characterized by sinkholes and mogotes. A thick tropical forest covers the surface above the cave. The cave is dominantly vadose with some phreatic features. It developed in the Oligocene Lares Limestone (Monroe, 1980). The entrance of CL is located along the flank of a sinkhole at the lower edge of a small hill. A narrow vertical pit forms the entrance, followed by two U-shaped depressions along the cave ceiling (Fig. 1). The main passage is nearly horizontal, strikes west-east, and forms a tube with ceiling heights of up to 30 m. The cave ends in the Collapse Room, a chamber whose roof collapsed, which is separated from the main chamber by a rise in the cave passage floor. The Collapse Room splits up in a small lower and a large upper level passage which reconnect at the end of the cave (Fig. 1). The horizontal extent of CL is about1440 m (Miller, 2010). Here we discuss the drip water data of drip site SW-2, located in the main passage, and site C-2, located in the Collapse Room (Fig. 1). Both sites were chosen because they feed actively growing speleothems and their drip rate is fast enough to allow instantaneous drip water sampling during each cave visit. Site SW-2 is in close proximity to a fallen speleothem which grew during the last 35 to 17 ka.

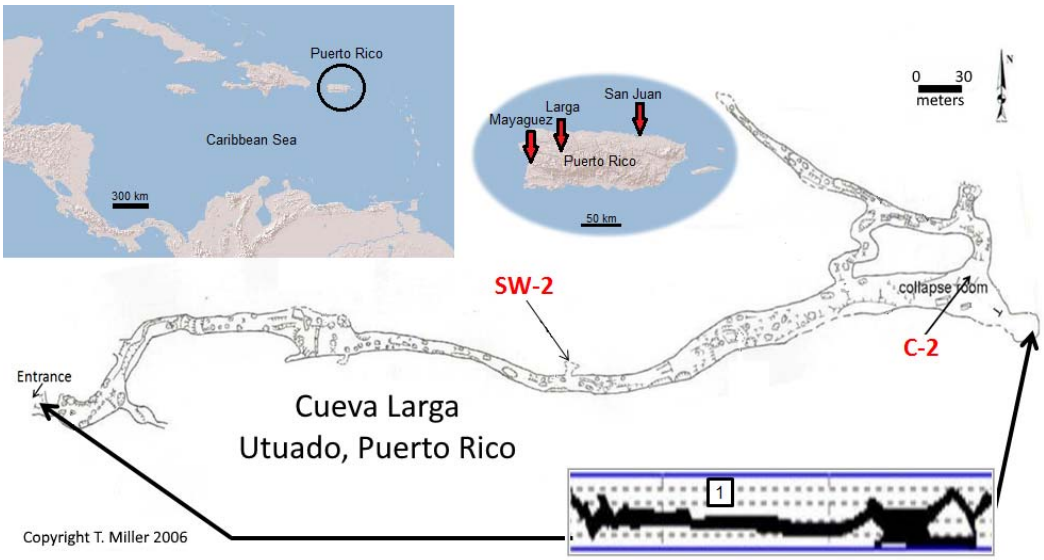

Fig. 1. Plan view of Cueva Larga (after Miller, 2010) with monitored drip sites SW-2 and C-2 (marked in red). Also shown is an overview map of the Caribbean and a map of Puerto Rico with the locations of Cueva Larga, Mayaguez and San Juan (red arrows). Insert 1: Longitudinal section of the cave (Miller, 2010).

Monthly rain water samples were collected both above the cave site and at the University of Puerto Rico in Mayaguez (N 18°12; W 66°08, 10 msl).

Most of the Caribbean shows a dry (Dec–Mar/Apr) and wet (Apr/May–Nov) season. The hurricane season starts at beginning of June and ends in November. During the wet season precipitation declines during the summer months, which is referred to as the mid-summer drought (Chen and Taylor, 2002; Magaña et al., 1999). This rainfall pattern is also visible at Mayaguez and the Arecibo Observatory (Fig. 2). At the Arecibo Observatory the annual rainfall amount is larger with 2137 mm per year compared to 1510 mm per year in Mayaguez. The mid-summer drought is very pronounced at the mountainous Arecibo Observatory site with highest monthly rainfall amounts occurring during May. In Mayaguez, the mid-summer drought is marked by a slight rainfall decrease in June, and the rainfall maximum is reached in September. Trade winds are the dominant control (85%) of air flow over Puerto Rico (Jury and Chiao, 2013). In Mayaguez, the diurnal land and sea breeze are pronounced (Bennett et al., 1998), and the topography of Puerto Rico weakens the trade wind flow creating a wake to the west of the islands, which promotes the formation of high convective afternoon thunderstorms (Jury and Chiao, 2013).

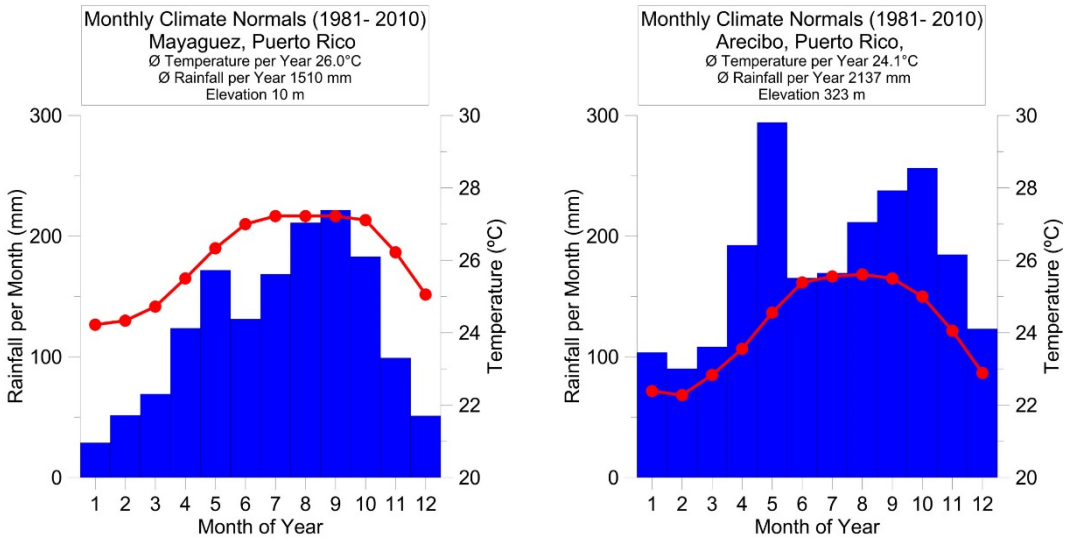

Fig. 2. Monthly climate normal 1981-2010 for Mayaguez (left) and Arecibo Observatory (right). The data were downloaded from the data-query tool xmACIS (http://xmacis.rcc-acis.org/) developed and maintained by NOAA's Northeast Regional Climate Center.

Different weather patterns cause rain events throughout the year. Low pressure systems embedded in easterly waves, tropical storms and occasional cold fronts from the north are the main contributors of Caribbean rainfall. During the rainy season, easterly waves and low pressure systems with cloud altitudes reaching up to 8000 m deliver the majority of rainfall, while during the dry season trade wind orographic rainfall of high-pressure systems with significantly lower cloud heights occurs (Scholl et al., 2009).

4.0. METHODS

4.1. Sampling Procedure

Cueva Larga was visited every month in 2013 and 2014 and about every two months in 2015. The monitored drip site SW-2 is located in the middle section of CL about 425 m inside the cave and site C-2 is located in the Collapse Room on top of a boulder field at the end of the cave about 790 m inside (Fig. 1). During each cave visit, pCO_2, temperature (T) and relative humidity (RH) measurements were recorded at each site. An Amprobe CO_2-100 handheld carbon dioxide meter (precision of ±30 ppm, ±5% of the reading for pCO_2 between 0 and 5000 ppm; ±0.6 °C for T and ±5% for RH above 90%) was used from January 2013 to July 2013, whereas from July 2013 to January 2015, a handheld Vaisala GM 70 with a 2000 ppm CO_2 probe (accuracy ±30 ppm + 2% of reading for pCO_2 between 0 and 2000 ppm) and a HM70 humidity and temperature probe (precision ±0.2 °C for T and ±1.7% for RH above 90%) were used. During two cave visits, both devices were used and the measurements agreed within uncertainty.

Outside atmospheric temperature data for Cueva Larga were taken from the Arecibo Observatory weather station, located at 323 msl (about 7 m lower than the entrance of CL) about 10 km north of the cave site. (data source: http://xmacis.rcc-acis.org/). Rain water samples were collected according to the GNIP (Global Network of Isotopes in Precipitation) station operation manual (IAEA, 2012). At the beginning of each sampling period the collection bucket was filled with paraffin oil that covered the buckets surface area by a height of at least 0.5 cm to prevent evaporation of the rainwater stored inside the

bucket over the sampling period. After a settling period of about one week, to allow the oil to separate completely from the rainwater, the monthly rain water sample was transferred via syphoning into transportation vials. For the Cueva Larga site, the weighted average rainfall δD and $\delta^{18}O$ value (Fig. 4) was calculated. At the cave site, rainfall samples were collected during each cave visit. In Mayaguez, rainwater samples were taken in close temporal relation to the cave site visitation in 2013. Starting in 2014, the rainwater samples in Mayaguez were taken at the beginning of each month.

Cave drip water samples were collected during each field trip. Depending on the drip rate the collection of enough water took up to 1.5 hours. Drip rates were determined via counting the number of drips within 1 min. For cation analyses, pre-acidified 15 ml Falcon tubes were used.

4.2. Analytical Methods

Monthly rain water samples from Mayaguez were measured in the Isotope Hydrology Laboratory of the IAEA (International Atomic Energy Agency) in Vienna. Hydrogen and oxygen isotope analyses were conducted by off-axis integrated cavity output laser spectroscopy and/or dual-inlet isotope-ratio mass spectrometry.

Stable isotope ratios of rain and drip water from the CL site were analyzed at the University of Innsbruck, Austria. A first set of samples was analyzed for $\delta^{18}O$ using the CO_2 equilibration method (Thermo Scientific Delta^{plus}XL with Gasbench II) and for δD using a Thermo Scientific Thermal Combustion/Elemental Analyzer (TC/EA) and a Delta V Advantage mass spectrometer. The uncertainty was 0.15‰ for $\delta^{18}O$ and 1‰ for δD. Later samples were analyzed on a Picarro L2140-*i* CRDS. The uncertainty is 0.08‰ for $\delta^{18}O$ and 0.5‰ for δD. All results are reported relative to VSMOW.

The analyses of the cation concentrations of drip waters were performed at Heidelberg University with a VISTA MXP ICP-OES (Varian) with an internal 1σ-standard deviation of <1% for Ca^{2+}, Mg^{2+} and Sr^{2+}.An external standards, the SPS SW2 with a long-term 1sigma-reproducibility of 2.2% for Ca^{2+} (conc. 10mg/l), 3.4% for Mg^{2+} (conc. 2mg/l) and 3.6% for Sr^{2+} (conc. 250µg/l) were used.

5.0. RESULTS

At both sites, Mayaguez and Cueva Larga, the rain water $\delta^{18}O$ values more negative with increasing amount of rainfall (Fig.3). The sample period has not always been exactly one month. For Cueva Larga the rain water sampling period varied between 16 and 58 days and for Mayaguez the sampling period started to be monthly in the year 2014 but varied between 15 and 48 days in 2013. To account for different sampling durations the average daily rainfall amount over the sampling period has been calculated and was multiplied by 30.4 days (the length of an average month) to express the average rainfall intensity over the sampling period in terms of monthly rainfall amount. In Figure 3, the raw results (rainfall amounts over initial variable sampling periods) and normalized monthly results (normalized to 30.4 days) are shown together with data from San Juan between the years 1968 and 1973 by the GNIP. The monthly rainfall $\delta^{18}O$ values show a wide scatter, but in general, lower values are observed during periods of higher rainfall amount. The linear trend indicates that a decrease of 1‰ in $\delta^{18}O$ roughly corresponds to a rainfall increase of about 220 mm/month in Mayaguez and 250 mm/month at Cueva Larga.

All data from Mayaguez plot close to the GMWL (Fig. 4). The rainfall measurements from Cueva Larga split up into two groups. One group is located near the GMWL, while the other group plots above the GMWL with elevated d-excess values between 15 and 20‰ (blue box in Fig. 4). Some of the cave drip water samples from drip sites SW-2 and C-2 were analyzed for both δD and $\delta^{18}O$. These results are also shown in Figure 4. Only one result falls on the GMWL. The other drip water samples plot between the GMWL and the elevated d-excess. These have been sampled between April and August 2014. All drip water values show lower stable isotope values than the weighted mean of rainfall $\delta^{18}O$ and δD ($\delta^{18}O$=-2.04‰ and δD=-5.24 ‰).

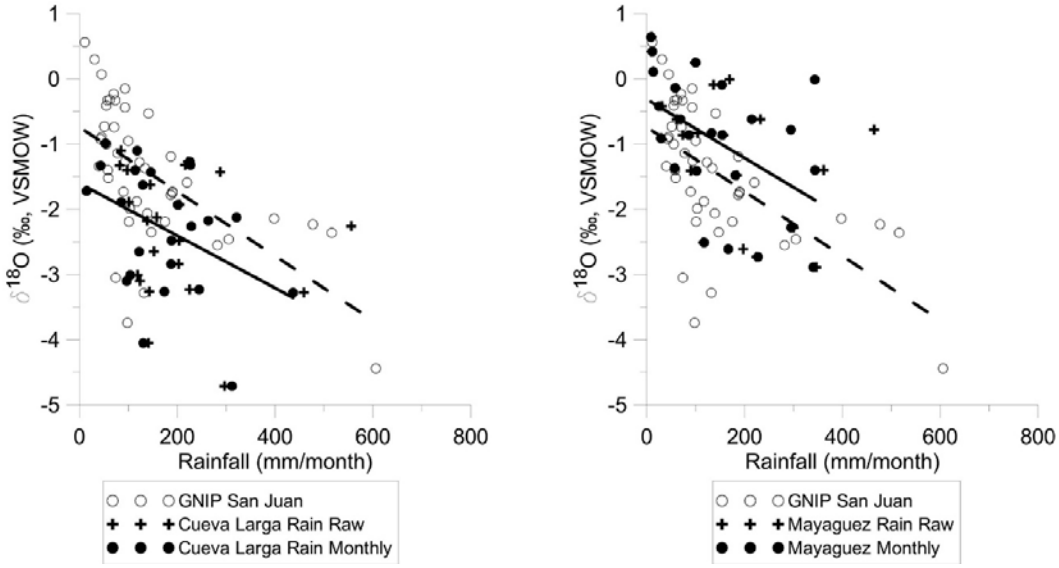

Fig. 3. $\delta^{18}O$ values of rainfall collected at Cueva Larga (left) and in Mayaguez (right). Crosses show the measured values for each sampling period (raw data). Filled circles show the rainfall $\delta^{18}O$ value relative to the normalized to rainfal amounts occuring over one month (30.4 day sampling period). Open circles show GNIP rainfall data from San Juan between 1968 and 1973 (downloaded from GNIP's WISER data-platform https://nucleus.iaea.org/wiser IAEA/WMO, 2015). The solid and dashed line shows the linear trends of the normalized data from our measurments and the GNIP data from San Juan, respectively.

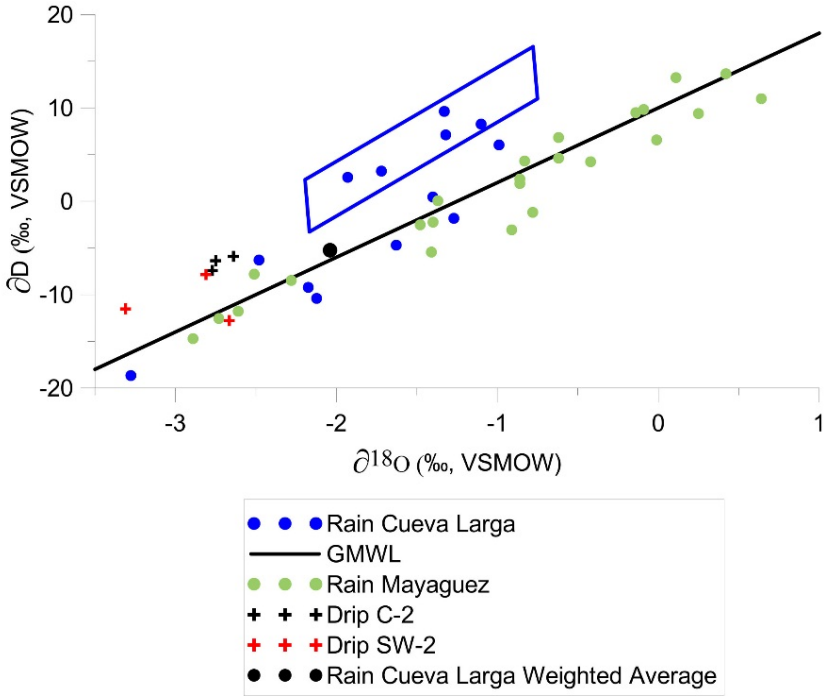

Fig. 4. Comparison of rain (points) and drip water data (diamonds). The Global Meteoric Water Line (GMWL: δD=8*δ^{18}O+10‰) is represented by the black solid line. The blue box marks elevated rainwater d-excess values >15‰ at Cueva Larga. The black filled circle shows the average isotopic composition of the rainfall weighted by rainfall amount (δ^{18}O=-2.04‰ and δD=-5.24 ‰).

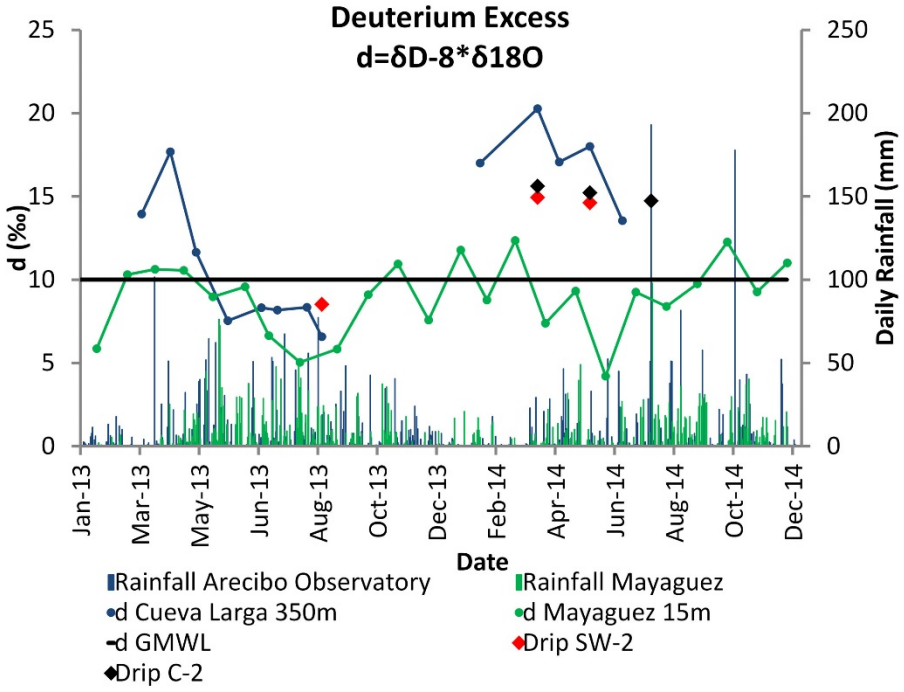

Fig. 5. Deuterium excess (d) of rain water compared to the daily rainfall amount. The time series for Cueva Larga shows gaps, because some monthly samples have been measured only for δ^{18}O.

The d-excess values have been plotted against time to investigate the temporal distribution of both rainfall groups at Cueva Larga in Figure 5. The rainfall measurements with an elevated deuterium excess (d-excess > 15‰) were taken during the end of the dry season and early wet season (February to May; Fig. 5). While Fig. 4 and 5 point out that there is a seasonality of the deuterium excess, yet insufficient data are available to establish seasonal meteoric water lines for the Cueva Larga mountain site.

Figure 6 shows the results of cave monitoring compared to the temperature and rainfall outside the cave. The rainfall pattern shows the dry season in the winter and wet season in the summer period. Extreme daily rainfall events are related to tropical depressions and hurricanes. The highest daily rainfall amount (193 mm) was measured during hurricane Bertha (3 August 2014). Tropical depressions delivered large rainfall amounts of 178 mm (27 October 2014) and 142 mm (16 May 2015). The monthly rainfall anomaly is the difference between the observed monthly rainfall to the rainfall normals from 1981 to 2010. Figure 6 shows that monthly rainfall anomaly was negative during summer 2013 and early 2014. This trend is interrupted by the strong positive anomaly in August 2014 when hurricane Bertha passed by Puerto Rico. The following month showed normal rainfall amounts and some positive and negative anomalies at the end of 2015.

Inside Cueva Larga, the variations in drip rate are site-specific. The monthly observations at drip site C-2 show constant trends exceeding the annual period. Drip rate increased from November 2013 to May 2014 and then continuously decreased until October 2015. In contrast, drip site SW-2 shows variations on a shorter time scale. Rapid increases of drip rate were observed in November 2013, February 2014, July 2014 and July 2015. Followed by drip rate decreases occuring over time frames of several months (Fig. 6). Assuming a drip volume of 0.23 ml/drip (Collister and Mattey, 2008) we calculated the drip rate in L/sec and were able to classify both drips after Fairchild et al.(2006b) as dominated by seepage flow.

Rainfall $\delta^{18}O$ values show a seasonal signal. More negative values (down to -4.7‰) are recorded during the wet season and vice versa. In 2013, one negative peak in May (-3.28‰) is observed followed by a second negative peak (below -3‰). At the end of the rainfall season (September to December). In 2014 the negative $\delta^{18}O$ values of the summer season do not show the bimodal signal observed in 2013. More negative values are measured from July to December/January. The most negative values are up to 1.4‰ more negative than in 2013 and occur during October and November. The drip water $\delta^{18}O$ composition of drip sites C-2 and SW-2 inside Cueva Larga do not reflect the surface pattern between dry and wet season. The drip water of drip site C-2 shows no significant variations and has an average $\delta^{18}O$ value of -2.59±0.12‰. Similar $\delta^{18}O$ values were measured in drip water at site SW-2 (-2.69±0.23‰). Except for April and May 2014, when drip water $\delta^{18}O$ values were more negative.

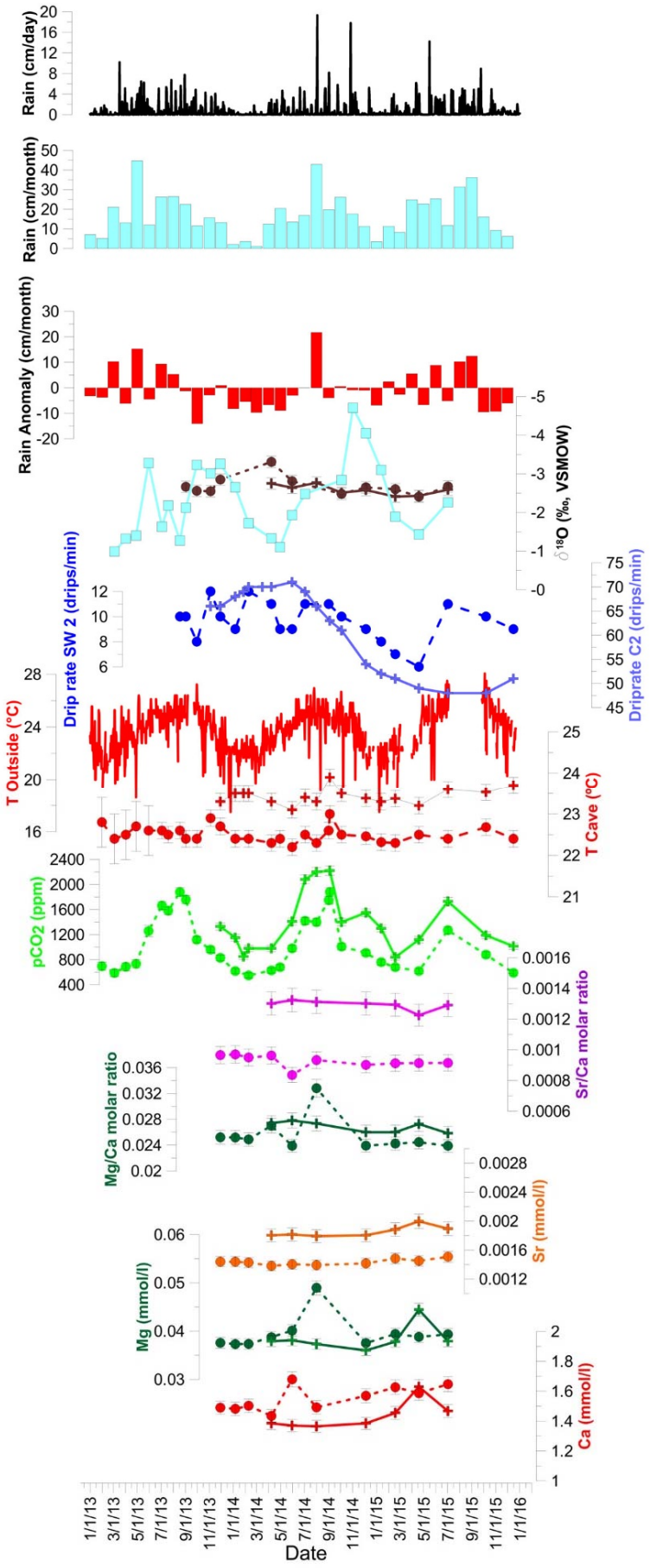

Fig. 6. Weather observation and cave monitoring results in Cueva Larga from 2013 to 2015. Data are shown for drip site SW-2 (circles on dashed line) and C-2 (crosses on solid line). The first three plots show the daily rainfall amount, the monthly rainfall amount and the rainfall anomaly of each month compared to the monthly climate normal from 1981 to 2010 from the Arecibo Observatory weather station (Fig. 2). The blue squares show $\delta^{18}O$ results of rain water compared to the $\delta^{18}O$ results of drip water (in brown). This is followed by the temperature outside and inside Cueva Larga (red), the cave atmospheric pCO_2 at each site (green) and the Sr/Ca (pink) and Mg/Ca (dark green) values. The lowest plots show the concentrations of Sr (orange), Mg (green) and Ca (red) in the drip water.

Temperatures in Cueva Larga are nearly constant over time compared to the annual cycle outside the cave. In the main cave passage at site SW-2, the average temperature is 22.51±0.18°C. This is similar to the avarage annual temperature outside the cave 22.5±0.1°C (calculated for two years from 4 November 2012 to 3 November 2013 and 4 November 2013 to 3 November 2013). At site C-2 in the collapsed room near the end of Cueva Larga, the average temperature is almost 1°C higher (23.43±0.19°C). At the transition from summer to winter (September and October), a short-lived temperature maximum was observed where temperatures increase by +0.5°C. This is probably related to a change in cave air circulation.

Cave pCO_2 values follow the seasonal temperature cycle at the surface. Summer maxima reach up to 1880 ppm at drip site SW-2 and up to 2220 ppm at drip site C-2. Winter minima are as low as 550 ppm at srip site SW-2 and 850 ppm at drip site C-2. In contrast to temperature, the annual pCO_2 pattern is asymmetrical showing a gradual rise from May to August and a relative rapid decrease in September.

The trace element to Ca ratios are nearly-constant over the monitoring period. At drip site C-2 the average Sr/Ca ratio is $1.293x10^{-3}±0.029x10^{-3}$ and thus higher than at drip site SW-2 with an average of $9.25\ x10^{-4}±0.38x10^{-4}$. The Mg/Ca ratio is similar at both sites with an average of $2.55x10^{-2}\ ±0.26x10^{-2}$ at site SW-2 and $2.681x10^{-2}±0.077x10^{-2}$ at site C-2. The Ca concentration is generally higher at drip site SW-2.

6.0 DISCUSSION

Rainfall and temperature outside Cueva Larga show a seasonal cycle with increased rainfall during the summer season (Fig. 6). Plotting the $\delta^{18}O$ values of rainfall against rainfall amount (Fig. 3) reveals that periods of increased rainfall amount correspond to more negative $\delta^{18}O$ values. The linear trend at both sites shows a rainfall "amount effect" of about $4.5x10^{-3}$ to $4.0x10^{-3}$‰/mm monthly rainfall. This "amount effect" is in agreement with the trend observed in rainfall collected in San Juan between 1968 and 1973 (Fig. 3). Unfortunately the rainfall data (Fig. 3) show a large scatter, which makes quantification of absolute rainfall amounts from the rainfall's isotopic composition difficult. Nonetheless the rainfall results document the general isotopic "amount effect", suggesting that $\delta^{18}O$ values recorded in speleothems from Cueva Larga reflect primarily variations in rainfall amount similar to other speleothem records from tropical regions (e.g. Lachniet, 2004; Winter et al., 2015).

The differences in rainfall $\delta^{18}O$ values between 2013 and 2014 above Cueva Larga appear to be related to different weather patterns reaching the site. In 2014, maximum daily rainfall amounts are larger than in 2013 due to large convective rainfall systems including hurricane Bertha. Large tropical convective systems may have $\delta^{18}O$ values lower than -6‰ (Lawrence and Gedzelman, 1996). The contribution of these systems seems to be responsible for the lower $\delta^{18}O$ values in 2014. The observed bimodal summer in the $\delta^{18}O$ values of 2013 may be related to the lack of large convective rainfall systems allowing the mid-summer drought to appear in the rainfall $\delta^{18}O$ data. In the summer of 2014, the sampling interval was larger than in 2013 which may also have prohibited the detection of a bimodal $\delta^{18}O$ rainfall signal.

The currently available two years of observations from Cueva Larga indicate inter-annual variations in rainfall $\delta^{18}O$ values. Extending the observations to several years might

resolve inter-annual isotopic rainfall variations, which are likely to be recorded in speleothems. Detailed rainfall stable isotope studies in Puerto Rico revealed that the $\delta^{18}O$ value of rainfall is complex (Scholl et al., 2009; Scholl and Murphy, 2014). The correlation between maximum cloud height and rainfall $\delta^{18}O$ values is larger than the correlation to rainfall amount (Scholl et al., 2009) indicating that condensation temperature plays an important role. The evolution of rainfall downstream of Puerto Rico leads to characteristic rainfall $\delta^{18}O$ values distinguishing trade-wind orographic showers, low pressure systems and convective systems (Scholl and Murphy, 2014). Thus, changes in weather patterns over multi-annual timespans seem to have an influence on the isotopic signal of drip water in Cueva Larga, highlighting the potential for speleothem $\delta^{18}O$ time series from this site for revealing changes in paleo-climate and rainfall amounts. However, the complexity of the process occurring in the soil and karst above the cave as well as inside the cave during precipitation of speleothem calcite may make the interpretation of speleothem $\delta^{18}O$ values on inter-annual time-scales difficult (Mischel et al., 2015).

In Mayaguez, $\delta^{18}O$ and δD values of the rainwater plot close to the GMWL (Fig. 4). These samples seem to be primarily controlled by different degrees of Rayleigh-fractionation during rainout (Rozanski et al., 1993). At the location of Cueva Larga, the rainwater samples appear to form two groups, one group plotting on the GMWL and the other group plotting above the GMWL with d-excess values between +15‰ and +20‰. Currently we do not have enough data to establish a seasonal Local Meteoric Water Line (LMWL) but it appears that the season of elevated d-excess agrees well to a LMWL ($\delta D=8.2*\delta^{18}O+14$) established for the mountainous Eastern Puerto Rico by Scholl and Murphy (2014). Elevated d-excess values occur between the middle and end of the dry season and have been measured in April 2013 and from February to end of May 2014 (Fig.5). The seasonality might be related to a greater fraction of recycled rainwater via the process of evaporation from surface and forest-canopy (Lee et al., 2009; Victoria et al., 1991) among other processes.

Since elevated d-excess values have not been observed at Mayaguez (Fig. 5), rainwater recycling seems to be negligible during both seasons. Mayaguez lies on the west coast of Puerto Rico in the trade wind wake zone of the island. At this location, winds typically come from the west (Jury and Chiao, 2013) bringing marine moisture with a d-excess of about 10‰. Similar observations have been made at the south coast of Puerto Rico where the primary moisture source is also maritime (Govender et al., 2013).

Inside Cueva Larga drip water $\delta^{18}O$ and δD results indicate that the wet season rainfall contributes proportionally more to the drip water than the rainfall during the dry season because all drip water measurements are more negative than the amount weighted average isotopic composition of the rainfall (Fig. 4). This seems plausible because during the dry season a greater fraction of the rainfall will be lost to evapo-transpiration than during the wet season. Currently, only three drip water samples at each site have been analyzed for δD. These results are insufficient to reveal drip water seasonality. More frequent cave drip water $\delta^{18}O$ and δD values could be used to investigate the transmission of seasonal atmospheric signals into the cave drip water in addition to the $\delta^{18}O$ drip water time series at this site. An indication of the transmission of d-excess seasonality into Cueva Larga is the observation that during the wet season in September 2013 the drip water at site SW-2 falls near the GMWL, having similar d-excess values than the rainwater at that time (Fig. 5). The rest of the few drip water d-excess observations have been made during the end of the dry season (April and May 2014) and show elevated d-excess values similar to

the rainfall at that time. Additional drip water δD data with monthly sampling resolution are required for more meaningful interpretations concerning the transmission of the seasonal d-excess signal from the rainwater into the cave drip water.

Cave atmosphere pCO_2 shows an annual cycle. It reaches a minimum during winter and a maximum during summer season. Comparing the buoyancy of cave air to the outside atmosphere reveals that the combination of the seasonal temperature cycle outside the cave and the cave geometry of Cueva Larga are the main driver of alternation between a well-ventilated winter mode and a near-stagnant summer mode (Vieten et al., under review). Especially during winter nights, the buoyancy of the cold outside air drops markedly below the cave atmosphere's buoyancy, leading to maximal cave ventilation. During the summer mode cave ventilation is at a minimum because most of the time the buoyancy of the cave air is lower than outside leading to stagnant ventilation conditions. Similar observations in the seasonality and magnitude of pCO_2 have been documented in temperate regions (Frisia et al., 2011; Spötl et al., 2005). Other caves show similar seasonal ventilation systematics, but different pCO_2 amplitudes, such as in Austria (Boch and Spötl, 2008), Ireland (Baldini et al., 2008), France (Bourges et al., 2006), Arizona, USA (Buecher, 1999), Texas, USA (Cowan et al., 2013) and Germany (Meisner et al., 2010).

The documented cave atmosphere seasonality probably leads to seasonal variations in carbonate precipitation (e.g.: Kaufmann and Dreybrodt, 2004; Fairchild et al., 2006; Baldini et al., 2008) because cave pCO_2 is directly linked to the growth rate of speleothems where lower pCO_2 values result in higher supersaturation with respect to calcite and increasing carbonate precipitation rates (Baker et al., 2014; Dreybrodt, 2012). Variations in growth rate might cause a bias towards the fast growing season in climate records deduced from speleothems and also affect the incorporation of trace elements into the crystal lattice (Fairchild et al., 2006a; Gabitov and Watson, 2006). Assuming all other factors being equal, seasonal ventilation appears to cause increased growth rates during the low pCO_2 winter season even though it rains more in the summer. In the most extreme case, speleothems in Cueva Larga would only grow during winter when the cave pCO_2 falls below a threshold value allowing carbonate precipitation. Carbonate precipitation seasonality is especially important for drip sites which feed from seepage water with short transition times and negligible water mixing along the seepage path from the surface to the cave. Such sites usually exhibit seasonal variations in the drip water geochemistry linked to the seasonality above the cave. The drip water stable isotope and trace element data from Cueva Larga do not show seasonal patterns (Fig. 6). Thus, the soil and karst above the cave appears to act as a low pass filter.

A seasonal signal similar to the rainfall $\delta^{18}O$ seasonality is not clearly detectable in the drip water data. Drip site SW-2 appears to show a slight response to rainfall seasonality in early 2014. More negative $\delta^{18}O$ values are recorded at site SW-2 (Fig. 6.). This could be the signal transmitted of 2013 summer rainfall. Delay times of similar length have been observed at other cave sites (e.g. Riechelmann et al., 2011). In 2015, a corresponding signal is not visible in the drip water of site SW-2. This might be related to the relatively dry year in 2014 with most months showing a negative rainfall amount anomaly (Fig. 6). A lack of recharge during 2014 is also indicated by the decreasing drip rates at both drip sites starting in summer 2014. At site SW-2, drip rates decrease by about 45% from 11 drips/min in September 2015 to 6 drips/min in April 2015. Thus, less recharge of more negative summer rainfall during the drier summer 2014 might be the reason for the missing negative peak in drip water $\delta^{18}O$ values at drip site SW-2 in 2015. At drip site C-2, drip rates decrease by

about 40% from 69 drips/min in July 2014 to 48 drips/min in July 2015 and remain low, while drip site SW-2 shows an increase in drip rate in July 2015. The increase in drip rate at drip site SW-2 seems to be related to a large rainfall event in May 2015 (140 mm rain on May 16th 2015). During 2013/2014, drip site SW-2 also shows higher drip rate variability than drip site C-2 indicating that drip site SW-2 responds more directly to rainfall and recharge events above the cave.

Trace element ratios indicate that the residence time and/or the host rock composition is different above both drip sites. Sr/Ca are higher at drip site C-2 (Fig. 6) indicating longer residence times above drip site C-2 than above drip site SW-2 (Verheyden et al., 2000). This is in agreement with the slower responding drip rates and the lack of any seasonality at drip site C-2.

Sr/Ca and Mg/Ca show no seasonal variation. We do not find evidence for varying degrees in PCP. Figure 7 shows a comparison of the drip water results from both drip sites at Cueva Larga to drip water data from Brown's Folly Mine, UK (Fairchild et al., 2006b). The varible drip water composition in Brown's Folley Mine is represented by the outlined area in figure 7 and has been interpreted to be the result of varying degrees of PDP. In Cueva Larga there is no evidence for such variable degrees of PCP above the cave on the annual time scale.

The water reservoir above Cueva Larga seems to be large enough to buffer seasonal rainfall variations causing no detectable changes in PCP over the monitored period. However, trace element variability in speleothems from Cueva Larga may be related to long-term changes in climate above the cave.

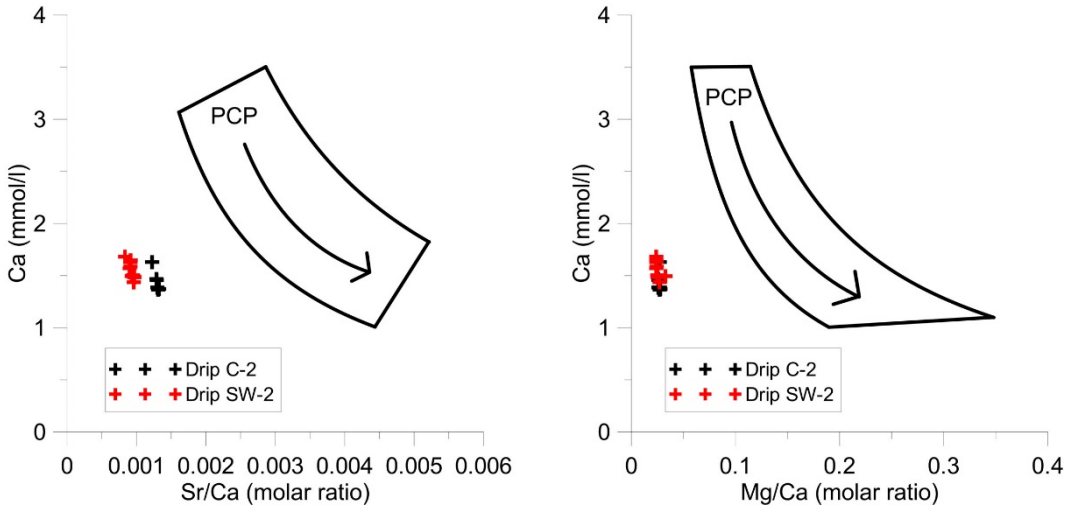

Fig. 7. Geochemical relationships of trace element ratios (Sr/Ca left and Mg/Ca right) to Ca-concentration for drip sites SW-2 and C-2 in Cueva Larga. The outlined area in each plot shows similar evaluation in Brown's Folly Mine, UK (Fairchild et al., 2006). The arrow labeled with PCP (Prior Calcite Precipitation) show the direction in which higher degrees of PCP along the seepage water flow path would shift the results.

7.0. CONCLUSIONS

Two years of cave monitoring in Cueva Larga, Puerto Rico, represent a first step to investigate the response of cave drip water to climate fluctuations above the cave. The drip water geochemistry provides insight into seepage water flow and mixing processes resulting in important implications for speleothem climate records. The isotopic rainfall "amount effect" has been detected in rainfall above the cave and in Mayaguez. This is an important prerequisite for speleothem $\delta^{18}O$ values to reflect changes in the rainfall amount over Puerto Rico. Rainfall deuterium excess shows elevated values during the dry season only at Cueva Larga, whereas Mayaguez seems to be dominated by maritime water vapor sources. Drip water d-excess may enable to estimate seepage water transition time.

Seasonality in cave ventilation results in low cave air pCO_2 in the winter season which might cause accelerated speleothem growth rates and bias speleothem climate records towards the winter season. Drip water trace element ratios lack variations implying PCP along the seepage flow path does not have a significant effect over the monitored period.

Both drip sites seem to be fed by well-mixed sources. The lack of clear seasonality makes estimations of residence and transmission time difficult. Drip site SW-2 appears to show a response to annual rainfall changes indicating a transmission time of several months, while the transmission time for drip site C-2 appears to be larger. The well-mixed and slowly responding drip sites monitored here favor speleothems to record multi-annual paleo-climate changes because the seepage water system acts as a low-pass filter.

This study shows that monitoring of drip sites is useful to decipher the effects influencing the climate signal recorded in speleothems. Environmental observations will improve speleothem paleo-climate interpretations and may even enable to calibrate the speleothem proxy record to absolute changes above the cave. Some of the here presented results are preliminary and need to be verified by continuation of the cave monitoring program in Cueva Larga.

ACKNOWLEDGMENTS

This research was supported by grant AGS 1003502 from the National Science Foundation. We are grateful to the International Association of Sedimentologist for a graduate student grant. S.W. and D.S. are thankful to the Deutsche Forschungsgemeinschaft (DFG) for funding (SCHO 1274/6-1). We gratefully acknowledge Stefan Terzer (IAEA, Vienna) for providing isotopic data and comments on the manuscript and we thank Augusto Mangini for his support inside and outside the cave. We thank Sylvia Riechelmann and Adrian Immenhauser from the Ruhr University Bochum and Eric Harmsen from the University of Puerto Rico, Mayaguez for their technical support. We thank Felipe Rodriguez-Morales and his family for their support and Nestor Aponte and Phil Perillat from the Arecibo Observatory. We also thank the following people for their assistance in the field: Flora Sperberg, Michael A. Casciano Kotick, Juan Estrella Martínez, Sarymar Barreto Saavedra, Jose A. Santiago-Saez, and Adam Haydock.

REFERENCES

Aemisegger, F., Pfahl, S., Sodemann, H., Lehner, I., Seneviratne, S.I., Wernli, H., 2014. Deuterium excess as a proxy for continental moisture recycling and plant transpiration. Atmos. Chem. Phys. 14, 4029–4054. doi:10.5194/acp-14-4029-2014

Asmerom, Y., Polyak, V., Burns, S., Rassmussen, J., 2007. Solar forcing of Holocene climate: New insights from a speleothem record, southwestern United States. Geology 35, 1. doi:10.1130/G22865A.1

Baker, A.J., Mattey, D.P., Baldini, J.U.L., 2014. Reconstructing modern stalagmite growth from cave monitoring, local meteorology, and experimental measurements of dripwater films. Earth Planet. Sci. Lett. 392, 239–249. doi:10.1016/j.epsl.2014.02.036

Baldini, J.U.L., McDermott, F., Hoffmann, D.L., Richards, D.A., Clipson, N., 2008. Very high-frequency and seasonal cave atmosphere PCO2 variability: Implications for stalagmite growth and oxygen isotope-based paleoclimate records. Earth Planet. Sci. Lett. 272, 118–129. doi:10.1016/j.epsl.2008.04.031

Banner, J.L., Guilfoyle, a., James, E.W., Stern, L. a., Musgrove, M., 2007. Seasonal Variations in Modern Speleothem Calcite Growth in Central Texas, U.S.A. J. Sediment. Res. 77, 615–622. doi:10.2110/jsr.2007.065

Bennett, S.P., Grubi si c, V., Rasmussen, R.M., 1998. Gravity waves, rainbands, and deep convection induced by trade wind flow over Puerto Rico, in: 12th Conf. on Numerical Weather Prediction. Amer. Meteor. Soc., Phoenix, AZ, pp. 98–102.

Boch, R., Spötl, C., 2008. The origin of lamination in stalagmites from Katerloch Cave, Austria: Towards a seasonality proxy. Pages News 16, 21–22. doi:10.1111/j.1365-3091.2010.01173.x

Bourges, F., Genthon, P., Mangin, A., D'Hulst, D., 2006. Microclimates of l'Aven d'Orgnac and other French limestone caves (Chauvet, Esparros, Marsoulas). Int. J. Climatol. 26, 1651–1670. doi:10.1002/joc.1327

Braconnot, P., Harrison, S.P., Kageyama, M., Bartlein, P.J., Masson-Delmotte, V., Abe-Ouchi, A., Otto-Bliesner, B., Zhao, Y., 2012. Evaluation of climate models using palaeoclimatic data. Nat. Clim. Chang. 2, 417–424. doi:10.1038/nclimate1456

Buecher, R.H., 1999. Microclimate Study of Kartchner Caverns, Arizona. J. Archaeol. Sci. 61, 108–120.

Chen, A.A., Taylor, M. a., 2002. Investigating the link between early season Caribbean rainfall and the El Nino + 1 year. Int. J. Climatol. 22, 87–106. doi:10.1002/joc.711

Clark, I., Fritz, P., 1997. Environmental Isotopes in Hydrogeology. Lewis Publisher, New York.

Collister, C., Mattey, D., 2008. Controls on water drop volume at speleothem drip sites: An experimental study. J. Hydrol. 358, 259–267. doi:10.1016/j.jhydrol.2008.06.008

Cowan, B.D., Osborne, M.C., Banner, J.L., 2013. Temporal Variability of Cave-Air CO2 in Central Texas. J. Cave Karst Stud. 75, 38–50. doi:10.4311/2011ES0246

Craig, H., 1961. Isotopic variations in meteoric waters. Science (80-.). 133, 1702–1703.

Cruz, F.W., Burns, S.J., Karmann, I., Sharp, W.D., Vuille, M., Cardoso, A.O., Ferrari, J.A., Silva Dias, P.L., Viana, O., 2005. Insolation-driven changes in atmospheric circulation over the past 116,000 years in subtropical Brazil. Nature 434, 63–66. doi:10.1038/nature03365

Cruz, F.W., Vuille, M., Burns, S.J., Wang, X., Cheng, H., Werner, M., Lawrence Edwards, R., Karmann, I., Auler, A.S., Nguyen, H., 2009. Orbitally driven east–west antiphasing of South American precipitation. Nat. Geosci. 2, 210–214. doi:10.1038/ngeo444

Dansgaard, W., 1964. Stable isotopes in precipitation. Tellus 16, 436–468. doi:10.1111/j.2153-3490.1964.tb00181.x

Deininger, M., Fohlmeister, J., Scholz, D., Mangini, A., 2012. Isotope disequilibrium effects: The influence of evaporation and ventilation effects on the carbon and oxygen isotope composition of speleothems – A model approach. Geochim. Cosmochim. Acta 96, 57–79. doi:10.1016/j.gca.2012.08.013

Dreybrodt, W., 2012. Speleothem Deposition, in: White, W.B., C., C.D. (Eds.), Encyclopedia of Caves. Elsevier Inc., pp. 769–777. doi:10.1016/B978

Fairchild, I.J., Baker, A., 2012. Speleothem Science: From Proces to Past Environments, 1st ed. John Wiley & Sons.

Fairchild, I.J., Borsato, A., Tooth, A.F., Frisia, S., Hawkesworth, C.J., Huang, Y., McDermott, F., Spiro, B., 2000. Controls on trace element (Sr–Mg) compositions of carbonate cave waters: implications for speleothem climatic records. Chem. Geol. 166, 255–269. doi:10.1016/S0009-2541(99)00216-8

Fairchild, I.J., Frisia, S., Borsato, A., Tooth, A.F., 2007. Speleothems, in: Nash, D.J., McLaren, S.J. (Eds.), Geochemical Sediments and Landscapes. Blackwell, Oxford, pp. 200–245.

Fairchild, I.J., Smith, C.L., Baker, A., Fuller, L., Spötl, C., Mattey, D., McDermott, F., 2006a. Modification and preservation of environmental signals in speleothems. Earth Planet. Sci. Lett. 75, 105–153. doi:10.1016/j.earscirev.2005.08.003

Fairchild, I.J., Treble, P.C., 2009. Trace elements in speleothems as recorders of environmental change. Quat. Sci. Rev. 28, 449–468. doi:10.1016/j.quascirev.2008.11.007

Fairchild, I.J., Tuckwell, G.W., Baker, A., Tooth, A.F., 2006b. Modelling of dripwater hydrology and hydrogeochemistry in a weakly karstified aquifer (Bath, UK): Implications for climate change studies. J. Hydrol. 321, 213–231. doi:10.1016/j.jhydrol.2005.08.002

Gabitov, R.I., Watson, E.B., 2006. Partitioning of strontium between calcite and fluid. Geochemistry, Geophys. Geosystems 7, n/a–n/a. doi:10.1029/2005GC001216

Gat, J.R., Bowser, C.J., Kendall, C., 1994. The contribution of evaporation from the Great Lakes to the continental atmosphere: estimate based on stable isotope data. Geophys. Res. Lett. 21, 557–560. doi:10.1029/94GL00069

Gat, J.R., Matsui, E., 1991. Atmospheric water balance in the Amazon basin: An isotopic evapotranspiration model. J. Geophys. Res. 96, 13179. doi:10.1029/91JD00054

Govender, Y., Cuevas, E., Sternberg, L.D.S., Jury, M.R., 2013. Temporal Variation in Stable Isotopic Composition of Rainfall and Groundwater in a Tropical Dry Forest in the Northeastern Caribbean. Earth Interact. 17, 1–20. doi:10.1175/2013EI000534.1

IAEA, 2012. Technical Procedures for GNIP Stations. International Atomic Energy Agency, Vienna, Austria.

IAEA/WMO, 2015. Global Network of Isotopes in Precipitation. The GNIP Database. Avaialble via. https://nucleus.iaea.org/wiser.

Intergovernmental Panel on Climate Change (Ed.), 2014. Climate Change 2013 - The Physical Science Basis. Cambridge University Press, Cambridge. doi:10.1017/CBO9781107415324

James, E.W., Banner, J.L., Hardt, B., 2015. A global model for cave ventilation and seasonal bias in speleothem paleoclimate records. Geochemistry, Geophys. Geosystems n/a–n/a. doi:10.1002/2014GC005658

Jury, M.R., Chiao, S., 2013. Leeside boundary layer confluence and afternoon thunderstorms over mayaguez, puerto rico. J. Appl. Meteorol. Climatol. 52, 439–454. doi:10.1175/JAMC-D-11-087.1

Katsuyama, M., Yoshioka, T., Konohira, E., 2015. Spatial distribution of oxygen-18 and deuterium in stream waters across the Japanese archipelago. Hydrol. Earth Syst. Sci. 19, 1577–1588. doi:10.5194/hess-19-1577-2015

Kaufmann, G., Dreybrodt, W., 2004. Stalagmite growth and palaeo-climate: an inverse approach. Earth Planet. Sci. Lett. 224, 529–545. doi:10.1016/j.epsl.2004.05.020

Lachniet, M.S., 2004. A 1500-year El Niño/Southern Oscillation and rainfall history for the Isthmus of Panama from speleothem calcite. J. Geophys. Res. 109, 1–8. doi:10.1029/2004JD004694

Lachniet, M.S., 2009. Climatic and environmental controls on speleothem oxygen-isotope values. Quat. Sci. Rev. 28, 412–432. doi:10.1016/j.quascirev.2008.10.021

Lawrence, J.R., Gedzelman, S.D., 1996. Low stable isotope ratios of tropical cyclone rains. Geophys. Res. Lett. 23, 527–530.

Lee, X., Griffis, T.J., Baker, J.M., Billmark, K. a., Kim, K., Welp, L.R., 2009. Canopy-scale kinetic fractionation of atmospheric carbon dioxide and water vapor isotopes. Global Biogeochem. Cycles 23, n/a–n/a. doi:10.1029/2008GB003331

Magaña, V., Amador, J.A., Medina, S., 1999. The Midsummer Drought over Mexico and Central America. J. Clim. 12, 1577–1588. doi:10.1175/1520-0442(1999)012<1577:TMDOMA>2.0.CO;2

Meisner, P., Riechelmann, S., Jansen, K., Richter, D.K., Voigt, S., 2010. CO2- Monitoring in drei Höhlen des Bergischen Landes–Aggertalhöhle, Kluterthöhle und Bismarckhöhle. Mitt. Verb. dt. Höhlen u. Karstforsch 56, 25–51.

Merlivat, L., Jouzel, J., 1979. Global climatic interpretation of the deuterium-oxygen 18 relationship for precipitation. J. Geophys. Res. 84, 5029. doi:10.1029/JC084iC08p05029

Mickler, P.J., Stern, L. a., Banner, J.L., 2006. Large kinetic isotope effects in modern speleothems. Geol. Soc. Am. Bull. 118, 65–81. doi:10.1130/B25698.1

Miller, T.E., 2010. Stream Pirates of the Caribbean: Tanamá and Camuy Rivers in the Northern Karst of Puerto Rico. Espeleorevista Puerto Rico 8–13.

Monroe, W.H., 1980. Some Tropical Landforms of Puerto Rico. USGS Prof. Pap. 1159.

Peng, T.-R., Wang, C.-H., Huang, C.-C., Fei, L.-Y., Chen, C.-T.A., Hwong, J.-L., 2010. Stable isotopic characteristic of Taiwan's precipitation: A case study of western Pacific monsoon region. Earth Planet. Sci. Lett. 289, 357–366. doi:10.1016/j.epsl.2009.11.024

Price, R.M., Swart, P.K., Willoughby, H.E., 2008. Seasonal and spatial variation in the stable isotopic composition (δ18O and δD) of precipitation in. FCE LTER 193–205.

Riechelmann, D.F.C., Deininger, M., Scholz, D., Riechelmann, S., Schröder-Ritzrau, A., Spötl, C., Richter, D.K., Mangini, A., Immenhauser, A., 2013. Disequilibrium carbon and oxygen isotope fractionation in recent cave calcite: Comparison of cave precipitates and model data. Geochim. Cosmochim. Acta 103, 232–244. doi:10.1016/j.gca.2012.11.002

Riechelmann, D.F.C., Schröder-Ritzrau, A., Scholz, D., Fohlmeister, J., Spötl, C., Richter, D.K., Mangini, A., 2011. Monitoring Bunker Cave (NW Germany): A prerequisite to interpret geochemical proxy data of speleothems from this site. J. Hydrol. 409, 682–695. doi:10.1016/j.jhydrol.2011.08.068

Rozanski, K., Aragua's, L., Gonfiantini, R., 1993. Isotopic patterns in modern global precipitation, in: Swart, P.K., Lohmann, K.L., Savin, S., McKenzie, K.L. (Eds.), Climate Change in Continental Isotopic Records. American Geophysical Union, Washington, DC, pp. 1–37.

Salati, E., Dall'Olio, A., Matsui, E., Gat, J.R., 1979. Recycling of water in the Amazon Basin: An isotopic study. Water Resour. Res. 15, 1250–1258. doi:10.1029/WR015i005p01250

Scholl, M. a., Shanley, J.B., Zegarra, J.P., Coplen, T.B., 2009. The stable isotope amount effect: New insights from NEXRAD echo tops, Luquillo Mountains, Puerto Rico. Water Resour. Res. 45, W12407. doi:10.1029/2008WR007515

Scholl, M.A., Murphy, S.F., 2014. Precipitation isotopes link regional climate patterns to water supply in a tropical mountain forest, eastern Puerto Rico. Water Resour. Res. 50, 4305–4322. doi:10.1002/2013WR014413

Spötl, C., Fairchild, I.J., Tooth, A.F., 2005. Cave air control on dripwater geochemistry, Obir Caves (Austria): Implications for speleothem deposition in dynamically ventilated caves. Geochim. Cosmochim. Acta 69, 2451–2468. doi:10.1016/j.gca.2004.12.009

Spötl, C., Mangini, A., 2002. Stalagmite from the Austrian Alps reveals Dansgaard–Oeschger events during isotope stage 3: Earth Planet. Sci. Lett. 203, 507–518. doi:10.1016/S0012-821X(02)00837-3

Stoll, H.M., Müller, W., Prieto, M., 2012. I-STAL, a model for interpretation of Mg/Ca, Sr/Ca and Ba/Ca variations in speleothems and its forward and inverse application on seasonal to millennial scales. Geochemistry, Geophys. Geosystems 13. doi:10.1029/2012GC004183

Verheyden, S., Keppens, E., Fairchild, I.J., McDermott, F., Weis, D., 2000. Mg, Sr and Sr isotope geochemistry of a Belgian Holocene speleothem: implications for paleoclimate reconstructions. Chem. Geol. 169, 131–144. doi:10.1016/S0009-2541(00)00299-0

Victoria, R.L., Martinelli, L.A., Mortatti, J., Richey, J., 1991. Mechanisms of Water Recycling in the Amazon Basin: Isotopic Insights. AMBIO-A J. Hum. Environ. 20, 384–387.

Vieten, R., Winter, A., Winterhalder, S., Schröder-Ritzrau, A., Miller, T.E., n.d. Seasonal temperature variations control cave ventilation processes in Cueva Larga, Puerto Rico. under Rev. by Int. J. Speleol.

Wang, Y.J., Cheng, H., Edwards, R.L., An, Z.S., Wu, J.Y., Shen, C.C., Dorale, J. a, 2001. A high-resolution absolute-dated late Pleistocene Monsoon record from Hulu Cave, China. Science 294, 2345–2348. doi:10.1126/science.1064618

Weedon, G.P., 2003. Time-series analysis and cyclostratigraphy: examining stratigraphic records of environmental cycles. Cambrige Univ Pr.

Winter, A., Miller, T., Kushnir, Y., Sinha, A., Timmermann, A., Jury, M.R., Gallup, C., Cheng, H., Edwards, R.L., 2011. Evidence for 800years of North Atlantic multi-decadal variability from a Puerto Rican speleothem. Earth Planet. Sci. Lett. 308, 23–28. doi:10.1016/j.epsl.2011.05.028

Winter, A., Zanchettin, D., Miller, T., Kushnir, Y., Black, D., Lohmann, G., Burnett, A., Haug, G.H., Estrella-Martínez, J., Breitenbach, S.F.M., Beaufort, L., Rubino, A., Cheng, H., 2015. Persistent drying in the tropics linked to natural forcing. Nat. Commun. 6, 7627. doi:10.1038/ncomms8627

Bibliography

Affek H.P., Bar-Matthews M., Ayalon A., Matthews A. and Eiler J.M. (**2008**). "Glacial/interglacial temperature variations in Soreq cave speleothems as recorded by clumped isotope thermometry." *Geochimica et Cosmochimica Acta*, 72(22): 5351–5360.

Affolter S., Fleitmann D. and Leuenberger M. (**2014**). "New online method for water isotope analysis of speleothem fluid inclusions using laser absorption spectroscopy (WS-CRDS)." *Climate of the Past*, 10(4): 1291–1304.

Affolter S., Häuselmann A.D., Fleitmann D., Häuselmann P. and Leuenberger M. (**2015**). "Triple isotope (δD, δ^{17}O, δ^{18}O) study on precipitation, drip water and speleothem fluid inclusions for a Western Central European cave (NW Switzerland)." *Quaternary Science Reviews*, 127: 73–89.

Alexander M. and Scott J. (**2002**). "The influence of ENSO on air-sea interaction in the Atlantic." *Geophysical Research Letters*, 29(14): 46–1–46–4.

Alley R., Meese D., Shuman C., Gow A., Taylor K., Grootes P., White J., Ram M., Waddington E., Mayewski P. et al. (**1993**). "Abrupt increase in Greenland snow accumulation at the end of the Younger Dryas event." *Nature*, 362: 527–529.

Amador J.A. (**1998**). "A climatic feature of the tropical Americas: The trade wind easterly jet." *Tópicos meteorológicos y oceanográficos*, 5(2): 91–102.

Amador J.A. and Magana V., "Dynamics of the low level jet over the Caribbean Sea." In "Preprints, Third Conference on Hurricanes and Tropical Meteorology," **1999**.

Arbuszewski J.A., Cléroux C., Bradtmiller L. and Mix A. (**2013**). "Meridional shifts of the Atlantic intertropical convergence zone since the Last Glacial Maximum." *Nature Geoscience*, 6(11): 959–962.

Arellano-Torres E., Ganeshram R.S., Pichevin L.E. and Salas-de Leon D.A. (**2015**). "Persistent millennial-scale climate variability in the eastern tropical North Pacific over the last two glacial cycles." *Paleoceanography*, 30(6): 682–701.

Arienzo M.M., Swart P.K., Pourmand A., Broad K., Clement A.C., Murphy L.N., Vonhof H.B. and Kakuk B. (**2015**). "Bahamian speleothem reveals temperature decrease associated with Heinrich stadials." *Earth and Planetary Science Letters*, 430: 377–386.

Arienzo M.M., Swart P.K. and Vonhof H.B. (**2013**). "Measurement of $\delta^{18}O$ and $\delta^{2}H$ values of fluid inclusion water in speleothems using cavity ring-down spectroscopy compared with isotope ratio mass spectrometry." *Rapid Communications in Mass Spectrometry*, 27(23): 2616–2624.

Ashraf I. (**2015**). "Phosphate ageing in soil and bioavailability of aged phosphates." Ph.D. thesis, Justus Liebig University Giessen.

Asmerom Y., Polyak V.J. and Burns S.J. (**2010**). "Variable winter moisture in the southwestern United States linked to rapid glacial climate shifts." *Nature Geoscience*, 3(2): 114–117.

Atkinson T. (**1977**). "Carbon dioxide in the atmosphere of the unsaturated zone: an important control of groundwater hardness in limestones." *Journal of Hydrology*, 35(1): 111–123.

Baker A., Asrat A., Fairchild I.J., Leng M.J., Wynn P.M., Bryant C., Genty D. and Umer M. (**2007**). "Analysis of the climate signal contained within $\delta^{18}O$ and growth rate parameters in two Ethiopian stalagmites." *Geochimica et Cosmochimica Acta*, 71(12): 2975–2988.

Baker A. and Bradley C. (**2010**). "Modern stalagmite $\delta^{18}O$: Instrumental calibration and forward modelling." *Global and Planetary Change*, 71(3): 201–206.

Baker A., C. Hellstrom J., Kelly B.F.J., Mariethoz G. and Trouet V. (**2015**). "A composite annual-resolution stalagmite record of North Atlantic climate over the last three millennia." *Scientific Reports*, 5: 10307.

Baker A., Genty D. and Fairchild I.J. (**2000**). "Hydrological characterisation of stalagmite dripwaters at Grotte de Villars, Dordogne, by the analysis of inorganic species and luminescent organic matter." *Hydrology and Earth System Sciences Discussions*, 4(3): 439–449.

Baker A., Smart P.L., Edwards R.L. and Richards D.A. (**1993**). "Annual growth banding in a cave stalagmite." *Nature*, 364(6437): 518–520.

Baker A., Smith C.L., Jex C., Fairchild I.J., Genty D. and Fuller L. (**2008**). "Annually laminated speleothems: a review." *International Journal of Speleology*, 37(3): 4.

Baker A.J., Mattey D.P. and Baldini J.U. (**2014**). "Reconstructing modern stalagmite growth from cave monitoring, local meteorology, and experimental measurements of dripwater films." *Earth and Planetary Science Letters*, 392: 239–249.

Baker P.A. and Fritz S.C. (**2015**). "Nature and causes of Quaternary climate variation of tropical South America." *Quaternary Science Reviews*, 124: 31–47.

Baker P.A., Rigsby C.A., Seltzer G.O., Fritz S.C., Lowenstein T.K., Bacher N.P. and Veliz C. (**2001**). "Tropical climate changes at millennial and orbital timescales on the Bolivian Altiplano." *Nature*, 409(6821): 698–701.

Baldini J., McDermott F. and Fairchild I. (**2006**). "Spatial variability in cave drip water hydrochemistry: Implications for stalagmite paleoclimate records." *Chemical Geology*, 235(3): 390–404.

Baldini J.U., McDermott F. and Fairchild I.J. (**2002**). "Structure of the 8200-year cold event revealed by a speleothem trace element record." *Science*, 296(5576): 2203–2206.

Bard E., Rostek F., Turon J.L. and Gendreau S. (**2000**). "Hydrological impact of Heinrich events in the subtropical northeast Atlantic." *Science*, 289(5483): 1321–1324.

Barnston A.G. and Livezey R.E. (**1987**). "Classification, seasonality and persistence of low-frequency atmospheric circulation patterns." *Monthly weather review*, 115(6): 1083–1126.

Baskaran M. and Krishnamurthy R.V. (**1993**). "Speleothems as proxy for the carbon isotope composition of atmospheric CO2." *Geophysical Research Letters*, 20(24): 2905–2908.

Beck J.W., Richards D.A., Edwards R.L., Silverman B.W., Smart P.L., Donahue D.J., Hererra-Osterheld S., Burr G.S., Calsoyas L., Jull A.J. and Biddulph D. (**2001**). "Extremely large variations of atmospheric ^{14}C concentration during the last glacial period." *Science*, 292(5526): 2453–8.

Bieleski R. (**1973**). "Phosphate pools, phosphate transport, and phosphate availability." *Annual review of plant physiology*, 24(1): 225–252.

Blyth A.J., Baker A., Collins M.J., Penkman K.E., Gilmour M.A., Moss J.S., Genty D. and Drysdale R.N. (**2008**). "Molecular organic matter in speleothems and its potential as an environmental proxy." *Quaternary Science Reviews*, 27(9): 905–921.

Boch R., Cheng H., Spötl C., Edwards R.L., Wang X. and Häuselmann P. (**2011**). "NALPS: a precisely dated European climate record 120–60 ka." *Climate of the Past*, 7(4): 1247–1259.

Böhm E., Lippold J., Gutjahr M., Frank M., Blaser P., Antz B., Fohlmeister J., Frank N., Andersen M. and Deininger M. (**2015**). "Strong and deep Atlantic meridional overturning circulation during the last glacial cycle." *Nature*, 517(7532): 73–76.

Bojariu R. and Gimeno L. (**2003**). "The role of snow cover fluctuations in multiannual NAO persistence." *Geophysical Research Letters*, 30(4).

Bojariu R. and Paliu D.M., "North Atlantic Oscillation projection on Romanian climate fluctuations in the cold season." In "Detecting and Modelling Regional Climate Change," Springer, **2001**, 345–356.

Bond G. (**1997**). "A Pervasive Millennial-Scale Cycle in North Atlantic Holocene and Glacial Climates." *Science*, 278(5341): 1257–1266.

Bond G., Broecker W., Johnsen S., McManus J., Labeyrie L., Jouzel J., Bonani G. et al. (**1993**). "Correlations between climate records from North Atlantic sediments and Greenland ice." *Nature*, 365(6442): 143–147.

Bond G., Heinrich H., Broecker W., Labeyrie L., McManus J., Andrews J., Huon S., Jantschik R., Clasen S., Simet C. et al. (**1992**). "Evidence for massive discharges of icebergs into the North Atlantic ocean during the last glacial period."

Bond G., Kromer B., Beer J., Muscheler R., Evans M.N., Showers W., Hoffmann S., Lotti-Bond R., Hajdas I. and Bonani G. (**2001**). "Persistent solar influence on North Atlantic climate during the Holocene." *Science*, 294(5549): 2130–2136.

Borsato A., Frisia S., Fairchild I.J., Somogyi A. and Susini J. (**2007**). "Trace element distribution in annual stalagmite laminae mapped by micrometer-resolution X-ray fluorescence: Implications for incorporation of environmentally significant species." *Geochimica et Cosmochimica Acta*, 71(6): 1494–1512.

Bradley R.S., *Paleoclimatology: Reconstructing Climates of the Quaternary*. Elsevier Inc., **2015**, third edn.

Broccoli A.J., Dahl K.A. and Stouffer R.J. (**2006**). "Response of the ITCZ to Northern Hemisphere cooling." *Geophysical Research Letters*, 33(1).

Broecker W.S., Olson E.A. and ORR P.C. (**1960**). "Radiocarbon measurements and annual rings in cave formations." *Nature*, 185.

Buczkó K., Magyari E.K., Braun M. and Bálint M. (**2013**). "Diatom-inferred lateglacial and Holocene climatic variability in the South Carpathian Mountains (Romania)." *Quaternary International*, 293: 123–135.

Büntgen U., Myglan V.S., Ljungqvist F.C., McCormick M., Di Cosmo N., Sigl M., Jungclaus J., Wagner S., Krusic P.J., Esper J. et al. (**2016**). "Cooling and societal change during the Late Antique Little Ice Age from 536 to around 660 AD." *Nature Geoscience*.

Büntgen U., Tegel W., Nicolussi K., McCormick M., Frank D., Trouet V., Kaplan J.O., Herzig F., Heussner K.U., Wanner H. et al. (**2011**). "2500 years of European climate variability and human susceptibility." *Science*, 331(6017): 578–582.

Bush M.B., Correa-metrio A.Y., Hodell D.A., Brenner M., Anselmetti F.S., Ariztegui D., Mueller A.D., Curtis J.H., Grzesik D.A., Burton C. et al., "Re-evaluation of climate change in lowland Central America during the Last Glacial Maximum using new sediment cores from Lake Petén Itzá, Guatemala." In "Past Climate Variability in South America and Surrounding Regions," Springer, **2009**, 113–128.

Busuioc A., Dobrinescu A., Birsan M.V., Dumitrescu A. and Orzan A. (**2014**). "Spatial and temporal variability of climate extremes in Romania and associated large-scale mechanisms." *International Journal of Climatology*.

Casteel R.C. and Banner J.L. (**2015**). "Temperature-driven seasonal calcite growth and drip water trace element variations in a well-ventilated Texas cave: Implications for speleothem paleoclimate studies." *Chemical Geology*, 392: 43–58.

Channell J., Hodell D. and Curtis J. (**2012**). "ODP Site 1063 (Bermuda Rise) revisited: oxygen isotopes, excursions and paleointensity in the Brunhes Chron." *Geochemistry, Geophysics, Geosystems*, 13(2).

Charles C.D., Rind D.V., Jouzel J., Koster R.D. and Fairbanks R.G. (**1994**). "Glacial-interglacial changes in moisture sources for Greenland: Influences on the ice core record of climate." *Science*, 263(5146): 508–511.

Chen A.A. and Taylor M.A. (**2002**). "Investigating the link between early season Caribbean rainfall and the El Niño+ 1 year." *International Journal of Climatology*, 22(1): 87–106.

Cheng H., Edwards R., Hoff J., Gallup C., Richards D. and Asmerom Y. (**2000**). "The half-lives of uranium-234 and thorium-230." *Chemical Geology*, 169(1): 17–33.

Cheng H., Edwards R.L., Shen C.C., Polyak V.J., Asmerom Y., Woodhead J., Hellstrom J., Wang Y., Kong X., Spötl C. et al. (**2013**). "Improvements in ^{230}Th dating, ^{230}Th and ^{234}U half-life values, and U–Th isotopic measurements by multi-collector inductively coupled plasma mass spectrometry." *Earth and Planetary Science Letters*, 371: 82–91.

Chiang J.C. and Koutavas A. (**2004**). "Climate change: tropical flip-flop connections." *Nature*, 432(7018): 684–685.

Chiang J.C.H. (**2003**). "Sensitivity of the Atlantic Intertropical Convergence Zone to Last Glacial Maximum boundary conditions." *Paleoceanography*, 18(4).

Chiang J.C.H. (**2009**). "The Tropics in Paleoclimate." *Annual Review of Earth and Planetary Sciences*, 37(1): 263–297.

Chiang J.C.H. and Bitz C.M. (**2005**). "Influence of high latitude ice cover on the marine Intertropical Convergence Zone." *Climate Dynamics*, 25(5): 477–496.

Clark I.D. and Fritz P., *Environmental isotopes in hydrogeology*. CRC press, **1997**.

Clement A.C. and Peterson L.C. (**2008**). "Mechanisms of abrupt climate change of the last glacial period." *Reviews of Geophysics*, 46(4).

Coladarci T., Cobb C.D., Minium E.W. and Clarke R.C., *Fundamentals of statistical reasoning in education*. John Wiley & Sons, **2010**.

Cole J.E., Rind D., Webb R.S., Jouzel J. and Healy R. (**1999**). "Climatic controls on interannual variability of precipitation δ^{230}O: Simulated influence of temperature, precipitation amount, and vapor source region." *Journal of Geophysical Research: Atmospheres*, 104(D12): 14223–14235.

Collins J.A., Schefuß E., Heslop D., Mulitza S., Prange M., Zabel M., Tjallingii R., Dokken T.M., Huang E. and Mackensen A. (**2011**). "Interhemispheric symmetry of the tropical African rainbelt over the past 23,000 years." *Nature Geoscience*, 4(1): 42–45.

Comas-Bru L. and McDermott F. (**2014**). "Impacts of the EA and SCA patterns on the European twentieth century NAO-winter climate relationship." *Quarterly Journal of the Royal Meteorological Society*, 140(679): 354–363.

Comas-Bru L., McDermott F. and Werner M. (**2016**). "The effect of the East Atlantic pattern on the precipitation δ^{18}O-NAO relationship in Europe." *Climate Dynamics*: 1–11.

Comboul M., Emile-Geay J., Evans M., Mirnateghi N., Cobb K.M. and Thompson D.M. (**2014**). "A probabilistic model of chronological errors in layer-counted climate proxies: applications to annually banded coral archives." *Climate of the Past*, 10(2): 825–841.

Constantin S. (**2003**). "Paleoclimatic evolution during the Quaternary as derived from speleothem records from the karst of Banat and Mehedinti Mountains (Romania)." Ph.D. thesis, University of Bucharest.

Constantin S., Bojar A.V., Lauritzen S.E. and Lundberg J. (**2007**). "Holocene and Late Pleistocene climate in the sub-Mediterranean continental environment: A speleothem record from Poleva Cave (Southern Carpathians, Romania)." *Palaeogeography, Palaeoclimatology, Palaeoecology*, 243(3-4): 322–338.

Constantin S. and Lauritzen S.E. (**1998**). "Speleothem datings in SW Romania." *Theoretical and Applied Karstology*, 11(1999): 35–45.

Coplen T.B. (**2007**). "Calibration of the calcite–water oxygen-isotope geothermometer at Devils Hole, Nevada, a natural laboratory." *Geochimica et Cosmochimica Acta*, 71(16): 3948–3957.

Correa-Metrio A., Bush M.B., Cabrera K.R., Sully S., Brenner M., Hodell D.A., Escobar J. and Guilderson T. (**2012**). "Rapid climate change and no-analog vegetation in lowland Central America during the last 86,000 years." *Quaternary Science Reviews*, 38: 63–75.

Craig H. (**1961**). "Isotopic variations in meteoric waters." *Science*, 133(3465): 1702–1703.

Cristea G., Cuna S.M., Fărcaş S., Tanţău I., Dordai E. and Măgdaş D.A. (**2014**). "Carbon isotope composition as indicator for climatic changes during the middle and late Holocene in a peat bog from Maramureş Mountains (Romania)." *The Holocene*, 24(1): 15–23.

Cruz F., Burns S., Karmann I., Sharp W., Vuille M., Cardoso A., Ferrari J., Dias P. and Viana O. (**2005**a). "Insolation-driven changes in atmospheric circulation over the past 116,000 years in subtropical Brazil." *Nature*, 434(7029): 63–66.

Cruz F.W., Burns S.J., Jercinovic M., Karmann I., Sharp W.D. and Vuille M. (**2007**). "Evidence of rainfall variations in Southern Brazil from trace element ratios (Mg/Ca and Sr/Ca) in a Late Pleistocene stalagmite." *Geochimica et Cosmochimica Acta*, 71(9): 2250–2263.

Cruz F.W., Burns S.J., Karmann I., Sharp W.D. and Vuille M. (**2006**). "Reconstruction of regional atmospheric circulation features during the late Pleistocene in subtropical Brazil from oxygen isotope composition of speleothems." *Earth and Planetary Science Letters*, 248(1-2): 495–507.

Cruz F.W., Karmann I., Viana O., Burns S.J., Ferrari J.A., Vuille M., Sial A.N. and Moreira M.Z. (**2005**b). "Stable isotope study of cave percolation waters in subtropical Brazil: Implications for paleoclimate inferences from speleothems." *Chemical Geology*, 220(3): 245–262.

Cruz F.W., Wang X., Auler A., Vuille M., Burns S.J., Edwards L.R., Karmann I. and Cheng H., *Orbital and Millennial-Scale Precipitation Changes in Brazil from Speleothem Records*. Springer Netherlands, Dordrecht, **2009**, 29–60.

Daëron M., Guo W., Eiler J., Genty D., Blamart D., Boch R., Drysdale R., Maire R., Wainer K. and Zanchetta G. (**2011**). "^{13}C ^{18}O clumping in speleothems: Observations from natural caves and precipitation experiments." *Geochimica et Cosmochimica Acta*, 75(12): 3303–3317.

Dansgaard W. (**1964**). "Stable isotopes in precipitation." *Tellus*, 16(4): 436–468.

Dansgaard W., Johnsen S., Clausen H., Dahl-Jensen D., Gundestrup N., Hammer C. and Oeschger H. (**1984**). "North Atlantic climatic oscillations revealed by deep Greenland ice cores." *Climate processes and climate sensitivity*: 288–298.

Daroub S.H., Gerakis A., Ritchie J.T., Friesen D.K. and Ryan J. (**2003**). "Development of a soil-plant phosphorus simulation model for calcareous and weathered tropical soils." *Agricultural Systems*, 76(3): 1157 – 1181.

Dasgupta S., Saar M.O., Edwards R.L., Shen C.C., Cheng H. and Alexander E.C. (**2010**). "Three thousand years of extreme rainfall events recorded in stalagmites from Spring Valley Caverns, Minnesota." *Earth and Planetary Science Letters*, 300(1): 46–54.

Day C.C. and Henderson G.M. (**2013**). "Controls on trace-element partitioning in cave-analogue calcite." *Geochimica et Cosmochimica Acta*, 120: 612–627.

Dee S., Emile-Geay J., Evans M., Allam A., Steig E. and Thompson D. (**2015**). "PRYSM: An open-source framework for PRoxY System Modeling, with applications to oxygen-isotope systems." *Journal of Advances in Modeling Earth Systems*, 7(3): 1220–1247.

Deines P., Langmuir D. and Harmon R.S. (**1974**). "Stable carbon isotope ratios and the existence of a gas phase in the evolution of carbonate ground waters." *Geochimica et Cosmochimica Acta*, 38(7): 1147–1164.

Deininger M., Fohlmeister J., Scholz D. and Mangini A. (**2012**). "Isotope disequilibrium effects: The influence of evaporation and ventilation effects on the carbon and oxygen isotope composition of speleothems – A model approach." *Geochimica et Cosmochimica Acta*, 96: 57–79.

Delgado-Baquerizo M., Maestre F.T., Gallardo A., Bowker M.A., Wallenstein M.D., Quero J.L., Ochoa V., Gozalo B., García-Gómez M., Soliveres S. et al. (**2013**). "Decoupling of soil nutrient cycles as a function of aridity in global drylands." *Nature*, 502(7473): 672–676.

deMenocal P., Ortiz J., Guilderson T. and Sarnthein M. (**2000**). "Coherent High- and Low-Latitude Climate Variability During the Holocene Warm Period." *Science*, 288(5474): 2198–2202.

Deplazes G., Lückge A., Peterson L.C., Timmermann A., Hamann Y., Hughen K.A., Röhl U., Laj C., Cane M.A. and Sigman D.M. (**2013**). "Links between tropical rainfall and North Atlantic climate during the last glacial period." *Nature Geoscience*, 6(3): 213–217.

Deplazes G., Lückge A., Stuut J.B.W., Pätzold J., Kuhlmann H., Husson D., Fant M. and Haug G.H. (**2014**). "Weakening and strengthening of the Indian monsoon during Heinrich events and Dansgaard-Oeschger oscillations." *Paleoceanography*, 29(2): 99–114.

Desmarchelier J.M., Hellstrom J.C. and McCulloch M.T. (**2006**). "Rapid trace element analysis of speleothems by ELA-ICP-MS." *Chemical Geology*, 231(1): 102–117.

Diaconu G., *Cloşani Cave. Mineralogic and genetic study of carbonate and clays*, vol. 2 of *Miscellanea Speologica Romanica*. Inst. Speol. "E. Racoviţă", Bucureşti, **1990**.

Diaz H.F., Trigo R., Hughes M.K., Mann M.E., Xoplaki E. and Barriopedro D. (**2011**). "Spatial and temporal characteristics of climate in medieval times revisited." *Bulletin of the American Meteorological Society*, 92(11): 1487–1500.

Donders T.H., de Boer H.J., Finsinger W., Grimm E.C., Dekker S.C., Reichart G.J. and Wagner-Cremer F. (**2011**). "Impact of the Atlantic Warm Pool on precipitation and temperature in Florida during North Atlantic cold spells." *Climate Dynamics*, 36(1-2): 109–118.

Dorale J.A., Edwards R.L., Alexander Jr E.C., Shen C.C., Richards D.A. and Cheng H., "Uranium-series dating of speleothems: current techniques, limits, & applications." In "Studies of Cave Sediments," Springer, **2004**, 177–197.

Dorale J.A., González L.A., Reagan M.K., Pickett D.A., Murrell M.T. and Baker R.G. (**1992**). "A high-resolution record of Holocene climate change in speleothem calcite from Cold Water Cave, northeast Iowa." *Science*, 258(5088): 1626–1630.

Douville E., Sallé E., Frank N., Eisele M., Pons-Branchu E. and Ayrault S. (**2010**). "Rapid and accurate U-Th dating of ancient carbonates using inductively coupled plasma-quadrupole mass spectrometry." *Chemical Geology*, 272(1-4): 1–11.

Drăguşin V., Staubwasser M., Hoffmann D., Ersek V., Onac B.P. and Vereş D. (**2014**). "Constraining Holocene hydrological changes in the Carpathian–Balkan region using speleothem $\delta^{18}O$ and pollen-based temperature reconstructions." *Climate of the Past*, 10: 1363.

Drake B.L. (**2012**). "The influence of climatic change on the Late Bronze Age Collapse and the Greek Dark Ages." *Journal of Archaeological Science*, 39(6): 1862–1870.

Drake J.J. (**1983**). "The effects of geomorphology and seasonality on the chemistry of carbonate groundwater." *Journal of Hydrology*, 61(1): 223–236.

Dreybrodt W. (**1988**). "Processes in Karst Systems: Physics." *Chemistry, and Geology, Springer, Berlin*.

Dreybrodt W. (**1999**). "Chemical kinetics, speleothem growth and climate." *Boreas*, 28(3): 347–356.

Dreybrodt W. (**2008**). "Evolution of the isotopic composition of carbon and oxygen in a calcite precipitating H_2O-CO_2-$CaCO_3$ solution and the related isotopic composition of calcite in stalagmites." *Geochimica et Cosmochimica Acta*, 72(19): 4712–4724.

Dreybrodt W. and Scholz D. (**2011**). "Climatic dependence of stable carbon and oxygen isotope signals recorded in speleothems: From soil water to speleothem calcite." *Geochimica et Cosmochimica Acta*, 75(3): 734–752.

Drysdale R., Zanchetta G., Hellstrom J., Maas R., Fallick A., Pickett M., Cartwright I. and Piccini L. (**2006**). "Late Holocene drought responsible for the collapse of Old World civilizations is recorded in an Italian cave flowstone." *Geology*, 34(2): 101–104.

Dublyansky Y.V. and Spötl C. (**2009**). "Hydrogen and oxygen isotopes of water from inclusions in minerals: design of a new crushing system and on-line continuous-flow isotope ratio mass spectrometric analysis." *Rapid Communications in Mass Spectrometry*, 23(17): 2605–2613.

Eiler J.M. (**2007**). ""Clumped-isotope" geochemistry - The study of naturally-occurring, multiply-substituted isotopologues." *Earth and Planetary Science Letters*, 262(3): 309–327.

Emiliani C. (**1955**). "Pleistocene temperatures." *The Journal of Geology*, 63(6): 538–578.

Enfield D.B. and Alfaro E.J. (**1999**). "The dependence of Caribbean rainfall on the interaction of the tropical Atlantic and Pacific Oceans." *Journal of Climate*, 12(7): 2093–2103.

Escobar J., Hodell D.A., Brenner M., Curtis J.H., Gilli A., Mueller A.D., Anselmetti F.S., Ariztegui D., Grzesik D.A., Pérez L., Schwalb A. and Guilderson T.P. (**2012**). "A 43-ka record of paleoenvironmental change in the Central American lowlands inferred from stable isotopes of lacustrine ostracods." *Quaternary Science Reviews*, 37: 92–104.

Fairchild I.J. and Baker A., *Speleothem science: from process to past environments*, vol. 3. John Wiley & Sons, **2012**.

Fairchild I.J., Baker A., Borsato A., Frisia S., Hinton R.W., McDermott F. and Tooth A.F. (**2001**). "Annual to sub-annual resolution of multiple trace-element trends in speleothems." *Journal of the Geological Society*, 158(5): 831–841.

Fairchild I.J., Borsato A., Tooth A.F., Frisia S., Hawkesworth C.J., Huang Y., McDermott F. and Spiro B. (**2000**). "Controls on trace element (Sr-Mg) compositions of carbonate cave waters: implications for speleothem climatic records." *Chemical Geology*, 166(3): 255–269.

Fairchild I.J., Smith C.L., Baker A., Fuller L., Spötl C., Mattey D., McDermott F. and E.I.M.F (**2006**a). "Modification and preservation of environmental signals in speleothems." *Earth-Science Reviews*, 75(1-4): 105–153.

Fairchild I.J., Spötl C., Frisia S., Borsato A., Susini J., Wynn P.M., Cauzid J. et al. (**2010**). "Petrology and geochemistry of annually laminated stalagmites from an Alpine cave (Obir, Austria): seasonal cave physiology." *Geological Society, London, Special Publications*, 336(1): 295–321.

Fairchild I.J. and Treble P.C. (**2009**). "Trace elements in speleothems as recorders of environmental change." *Quaternary Science Reviews*, 28(5-6): 449–468.

Fairchild I.J., Tuckwell G.W., Baker A. and Tooth A.F. (**2006**b). "Modelling of dripwater hydrology and hydrogeochemistry in a weakly karstified aquifer (Bath, UK): implications for climate change studies." *Journal of Hydrology*, 321(1): 213–231.

Fensterer C. (**2011**). "Holocene caribbean Climate Variability reconstructed from Speleothems from Western Cuba." Ph.D. thesis, Ruperto-Carola University of Heidelberg.

Fensterer C., Scholz D., Hoffmann D., Mangini A. and Pajón J.M. (**2010**). "^{230}Th/U-dating of a late Holocene low uranium speleothem from Cuba." *IOP Conference Series: Earth and Environmental Science*, 9: 012015.

Fensterer C., Scholz D., Hoffmann D., Spötl C., Pajón J.M. and Mangini A. (**2012**). "Cuban stalagmite suggests relationship between Caribbean precipitation and the Atlantic Multidecadal Oscillation during the past 1.3 ka." *The Holocene*, 22(12): 1405–1412.

Fensterer C., Scholz D., Hoffmann D.L., Spötl C., Schröder-Ritzrau A., Horn C., Pajón J.M. and Mangini A. (**2013**). "Millennial-scale climate variability during the last 12.5 ka recorded in a Caribbean speleothem." *Earth and Planetary Science Letters*, 361: 143–151.

Feurdean A. and Bennike O. (**2004**). "Late Quaternary palaeoecological and palaeoclimatological reconstruction in the Gutaiului Mountains, northwest Romania." *Journal of Quaternary Science*, 19(8): 809–827.

Feurdean A., Galka M., Kuske E., Tantau I., Lamentowicz M., Florescu G., Liakka J., Hutchinson S.M., Mulch A. and Hickler T. (**2015**). "Last millennium hydro-climate variability in Central–Eastern Europe (northern Carpathians, Romania)." *The Holocene*, 25(7): 1179–1192.

Feurdean A., Klotz S., Mosbrugger V. and Wohlfarth B. (**2008**). "Pollen-based quantitative reconstructions of Holocene climate variability in NW Romania." *Palaeogeography, Palaeoclimatology, Palaeoecology*, 260(3-4): 494–504.

Finch A.A., Shaw P.A., Weedon G.P. and Holmgren K. (**2001**). "Trace element variation in speleothem aragonite: potential for palaeoenvironmental reconstruction." *Earth and Planetary Science Letters*, 186(2): 255–267.

Fleitmann D., Burns S.J., Mudelsee M., Neff U., Kramers J., Mangini A. and Matter A. (**2003**). "Holocene forcing of the Indian monsoon recorded in a stalagmite from southern Oman." *Science*, 300(5626): 1737–9.

Fleitmann D., Burns S.J., Neff U., Mudelsee M., Mangini A. and Matter A. (**2004**). "Palaeoclimatic interpretation of high-resolution oxygen isotope profiles derived from annually laminated speleothems from Southern Oman." *Quaternary Science Reviews*, 23(7): 935–945.

Fleitmann D., Cheng H., Badertscher S., Edwards R.L., Mudelsee M., Göktürk O.M., Fankhauser A., Pickering R., Raible C.C., Matter A., Kramers J. and Tüysüz O. (**2009**). "Timing and climatic impact of Greenland interstadials recorded in stalagmites from northern Turkey." *Geophysical Research Letters*, 36(19).

Fohlmeister J., Scholz D., Kromer B. and Mangini A. (**2011**). "Modelling carbon isotopes of carbonates in cave drip water." *Geochimica et Cosmochimica Acta*, 75(18): 5219–5228.

Fohlmeister J., Schröder-Ritzrau A., Scholz D., Spötl C., Riechelmann D.F., Mudelsee M., Wackerbarth A., Gerdes A., Riechelmann S. and Immenhauser A. (**2012**).

"Bunker Cave stalagmites: an archive for central European Holocene climate variability." *Climate of the Past*, 8(5): 1751–1764.

Fohlmeister J., Vollweiler N., Spötl C. and Mangini A. (**2013**). "COMNISPA II: Update of a mid-European isotope climate record, 11 ka to present." *The Holocene*, 23(5): 749–754.

Forray F.L., Onac B.P., Tanţău I., Wynn J.G., Tămaş T., Coroiu I. and Giurgiu A.M. (**2015**). "A Late Holocene environmental history of a bat guano deposit from Romania: an isotopic, pollen and microcharcoal study." *Quaternary Science Reviews*, 127: 141–154.

Frisia S. (**2015**). "Microstratigraphic logging of calcite fabrics in speleothems as tool for palaeoclimate studies." *International Journal of Speleology*, 44(1): 1.

Frisia S., Borsato A., Drysdale R., Paul B., Greig A. and Cotte M. (**2012**). "A re-evaluation of the palaeoclimatic significance of phosphorus variability in speleothems revealed by high-resolution synchrotron micro XRF mapping." *Climate of the Past*, 8(6): 2039–2051.

Frisia S., Borsato A., Fairchild I.J. and Longinelli A., "Aragonite precipitation at Grotte de Clamouse (Herault, France): role of magnesium and drip rate." In "Proceedings of the 12th International Congress of Speleology," vol. 7. **1997**, 247–250.

Frisia S., Borsato A., Fairchild I.J. and McDermott F. (**2000**). "Calcite fabrics, growth mechanisms, and environments of formation in speleothems from the Italian Alps and southwestern Ireland." *Journal of Sedimentary Research*, 70(5).

Frisia S., Borsato A., Mangini A., Spötl C., Madonia G. and Sauro U. (**2006**). "Holocene climate variability in Sicily from a discontinuous stalagmite record and the Mesolithic to Neolithic transition." *Quaternary Research*, 66(3): 388–400.

Frisia S., Borsato A., Spötl C., Villa I.M. and Cucchi F. (**2005**). "Climate variability in the SE Alps of Italy over the past 17 000 years reconstructed from a stalagmite record." *Boreas*, 34(4): 445–455.

Frisia S., Fairchild I.J., Fohlmeister J., Miorandi R., Spötl C. and Borsato A. (**2011**). "Carbon mass-balance modelling and carbon isotope exchange processes in dynamic caves." *Geochimica et Cosmochimica Acta*, 75(2): 380–400.

Fritts H. (**1976**). "Tree rings and climate, 567 pp." *Academic, San Diego, Calif.*

Gabitov R. and Watson E. (**2006**). "Partitioning of strontium between calcite and fluid." *Geochemistry, Geophysics, Geosystems*, 7(11).

Gardi C., Angelini M., Barceló S., Comerma J., Gaistardo C.C., Rojas A.E., Jones A., Krasilnikov P., Brefin M.M.S., Montanarella L. et al., *Atlas de suelos de América Latina y el Caribe*. Publications Office, **2014**.

Garrels R.M. and Christ C.L., *Solutions, minerals, and equilibria*. Harper's geoscience series. Harper & Row, **1965**.

Gascoyne M. (**1983**). "Trace-element partition coefficients in the calcite-water system and their paleoclimatic significance in cave studies." *Journal of Hydrology*, 61(1): 213–222.

Genty D., Baker A., Massault M., Proctor C., Gilmour M., Pons-Branchu E. and Hamelin B. (**2001**). "Dead carbon in stalagmites: carbonate bedrock paleodissolution vs. ageing of soil organic matter. Implications for ^{13}C variations in speleothems." *Geochimica et Cosmochimica Acta*, 65(20): 3443–3457.

Genty D., Blamart D., Ouahdi R., Gilmour M., Baker A., Jouzel J. and Van-Exter S. (**2003**). "Precise dating of Dansgaard–Oeschger climate oscillations in western Europe from stalagmite data." *Nature*, 421(6925): 833–837.

Genty D., Labuhn I., Hoffmann G., Danis P., Mestre O., Bourges F., Wainer K., Massault M., Van Exter S., Régnier E. et al. (**2014**). "Rainfall and cave water isotopic relationships in two South-France sites." *Geochimica et Cosmochimica Acta*, 131: 323–343.

Genty D. and Massault M. (**1999**). "Carbon transfer dynamics from bomb-^{14}C and $\delta^{13}C$ time series of a laminated stalagmite from SW France - modelling and comparison with other stalagmite records." *Geochimica et Cosmochimica Acta*, 63(10): 1537–1548.

Genty D., Massault M., Gilmour M., Baker A., Verheyden S. and Keppens E. (**1999**). "Calculation of past dead carbon proportion and variability by the comparison of AMS ^{14}C and TIMS U/ Th ages on two Holocene stalagmites." *Radiocarbon*, 41(3).

Genty D., Vokal B., Obelic B. and Massault M. (**1998**). "Bomb 14 C time history recorded in two modern stalagmites-importance for soil organic matter dynamics and bomb ^{14}C distribution over continents." *Earth and Planetary Science Letters*, 160(3): 795–809.

Gerdes A. and Zeh A. (**2006**). "Combined U-Pb and Hf isotope LA-(MC-)ICP-MS analyses of detrital zircons: Comparison with SHRIMP and new constraints for the provenance and age of an Armorican metasediment in Central Germany." *Earth and Planetary Science Letters*, 249(1-2): 47–61.

Geyh M. (**1970**). "Zeitliche Abgrenzung von Klimaänderungen mit ^{14}C-Daten von Kalksinter und organischen Substanzen." *Beihefte zum geologischen Jahrbuch*, 98: 15–22.

Ghosh P., Adkins J., Affek H., Balta B., Guo W., Schauble E.A., Schrag D. and Eiler J.M. (**2006**). "^{13}C–^{18}O bonds in carbonate minerals: A new kind of paleothermometer." *Geochimica et Cosmochimica Acta*, 70(6): 1439 – 1456.

Giannini A., Kushnir Y. and Cane M.A. (**2000**). "Interannual variability of Caribbean rainfall, ENSO, and the Atlantic Ocean." *Journal of Climate*, 13(2): 297–311.

Giusti E.V., *Hydrogeology of the karst of Puerto Rico*, vol. 1012. US Govt. Print. Off., **1978**.

Godwin H. (**1962**). "Half-life of radiocarbon." *Nature*, 195.

Goede A., McCulloch M., McDermott F. and Hawkesworth C. (**1998**). "Aeolian contribution to strontium and strontium isotope variations in a Tasmanian speleothem." *Chemical Geology*, 149(1): 37–50.

Gogou A., Triantaphyllou M., Xoplaki E., Izdebski A., Parinos C., Dimiza M., Bouloubassi I., Luterbacher J., Kouli K., Martrat B. et al. (**2016**). "Climate variability and socio-environmental changes in the northern Aegean (NE Mediterranean) during the last 1500 years." *Quaternary Science Reviews*, 136: 209–228.

Gonfiantini R., Roche M.A., Olivry J.C., Fontes J.C. and Zuppi G.M. (**2001**). "The altitude effect on the isotopic composition of tropical rains." *Chemical Geology*, 181(1): 147–167.

Goudeau M.L.S., Reichart G.J., Wit J., de Nooijer L., Grauel A.L., Bernasconi S. and de Lange G. (**2015**). "Seasonality variations in the Central Mediterranean during climate change events in the Late Holocene." *Palaeogeography, Palaeoclimatology, Palaeoecology*, 418: 304 – 318.

Grauel A.L., Hodell D.A. and Bernasconi S.M. (**2016**). "Quantitative estimates of tropical temperature change in lowland Central America during the last 42 ka." *Earth and Planetary Science Letters*, 438: 37–46.

Gray S.T., Graumlich L.J., Betancourt J.L. and Pederson G.T. (**2004**). "A tree-ring based reconstruction of the Atlantic Multidecadal Oscillation since 1567 A.D." *Geophysical Research Letters*, 31(12). L12205.

Griffiths M.L., Drysdale R.N., Vonhof H.B., Gagan M.K., Zhao J.x., Ayliffe L.K., Hantoro W.S., Hellstrom J.C., Cartwright I. and Frisia S. (**2010**). "Younger Dryas-Holocene temperature and rainfall history of southern Indonesia from $\delta^{18}O$ in speleothem calcite and fluid inclusions." *Earth and Planetary Science Letters*, 295(1-2): 30–36.

Griggs C., DeGaetano A., Kuniholm P. and Newton M. (**2007**). "A regional high-frequency reconstruction of May–June precipitation in the north Aegean from oak tree rings, AD 1089–1989." *International Journal of Climatology*, 27(8): 1075–1089.

Grimm E.C., Watts W.A., Jacobson Jr G.L., Hansen B.C.S., Almquist H.R. and Dieffenbacher-Krall A.C. (**2006**). "Evidence for warm wet Heinrich events in Florida." *Quaternary Science Reviews*, 25(17-18): 2197–2211.

Hagen S. and Keigwin L.D. (**2002**). "Sea-surface temperature variability and deep water reorganisation in the subtropical North Atlantic during Isotope Stage 2–4." *Marine Geology*, 189(1): 145–162.

Hansen M., Dreybrodt W. and Scholz D. (**2013**). "Chemical evolution of dissolved inorganic carbon species flowing in thin water films and its implications for (rapid) degassing of CO_2 during speleothem growth." *Geochimica et Cosmochimica Acta*, 107: 242–251.

Hartung J. and Elpelt B. (**1992**). "Multivariate Statistik: Lehr-und Handbuch der angewandten Statistik. München."

Haslett J. and Parnell A. (**2008**). "A simple monotone process with application to radiocarbon-dated depth chronologies." *Journal of the Royal Statistical Society: Series C (Applied Statistics)*, 57(4): 399–418.

Haug G.H., Hughen K.A., Sigman D.M., Peterson L.C. and Rohl U. (**2001**). "Southward migration of the intertropical convergence zone through the Holocene." *Science*, 293(5533): 1304–8.

Heinrich H. (**1988**). "Origin and consequences of cyclic ice rafting in the northeast Atlantic Ocean during the past 130,000 years." *Quaternary research*, 29(2): 142–152.

Hellstrom J. (**2003**). "Rapid and accurate U/Th dating using parallel ion-counting multi-collector ICP-MS." *Journal of Analytical Atomic Spectrometry*, 18(11): 1346–1351.

Hellstrom J. (**2006**). "U-Th dating of speleothems with high initial ^{230}Th using stratigraphical constraint." *Quaternary Geochronology*, 1(4): 289–295.

Hellstrom J. and McCulloch M. (**2000**). "Multi-proxy constraints on the climatic significance of trace element records from a New Zealand speleothem." *Earth and Planetary Science Letters*, 179(2): 287–297.

Hemming S.R. (**2004**). "Heinrich events: Massive late Pleistocene detritus layers of the North Atlantic and their global climate imprint." *Reviews of Geophysics*, 42(1).

Henderson-Sellers A. and Robinson P.J., *Contemporary Climatology.* Longman, Essex (UK), **1986**.

Hendy C.H. (**1971**). "The isotopic geochemistry of speleothems–I. The calculation of the effects of different modes of formation on the isotopic composition of speleothems and their applicability as palaeoclimatic indicators." *Geochimica et cosmochimica Acta*, 35(8): 801–824.

Hinsinger P. (**2001**). "Bioavailability of soil inorganic P in the rhizosphere as affected by root-induced chemical changes: a review." *Plant and soil*, 237(2): 173–195.

Hodell D.A., Anselmetti F.S., Ariztegui D., Brenner M., Curtis J.H., Gilli A., Grzesik D.A., Guilderson T.J., Müller A.D., Bush M.B., Correa-Metrio A., Escobar J. and Kutterolf S. (**2008**). "An 85-ka record of climate change in lowland Central America." *Quaternary Science Reviews*, 27(11–12): 1152–1165.

Hoffmann D.L. (**2008**). "^{230}Th isotope measurements of femtogram quantities for U-series dating using multi ion counting (MIC) MC-ICPMS." *International Journal of Mass Spectrometry*, 275(1-3): 75–79.

Hoffmann D.L., Beck J.W., Richards D.A., Smart P.L., Singarayer J.S., Ketchmark T. and Hawkesworth C.J. (**2010**). "Towards radiocarbon calibration beyond 28ka using speleothems from the Bahamas." *Earth and Planetary Science Letters*, 289(1-2): 1–10.

Hoffmann D.L., Prytulak J., Richards D.A., Elliott T., Coath C.D., Smart P.L. and Scholz D. (**2007**). "Procedures for accurate U and Th isotope measurements by high precision MC-ICPMS." *International Journal of Mass Spectrometry*, 264(2-3): 97–109.

Hoffmann D.L., Spötl C. and Mangini A. (**2009**). "Micromill and in situ laser ablation sampling techniques for high spatial resolution MC-ICPMS U-Th dating of carbonates." *Chemical Geology*, 259(3-4): 253–261.

Holzhauser H., Magny M. and Zumbuühl H.J. (**2005**). "Glacier and lake-level variations in west-central Europe over the last 3500 years." *The Holocene*, 15(6): 789–801.

Hossner L., Freeouf J. and Folsom B. (**1973**). "Solution phosphorus concentration and growth of rice (Oryza sativa L.) in flooded soils." *Soil Science Society of America Journal*, 37(3): 405–408.

Hua Q. (**2009**). "Radiocarbon: a chronological tool for the recent past." *Quaternary Geochronology*, 4(5): 378–390.

Hua Q., Barbetti M. and Rakowski A.Z. (**2013**). "Atmospheric radiocarbon for the period 1950–2010." *Radiocarbon*, 55(4): 2059–2072.

Huang Y. and Fairchild I.J. (**2001**). "Partitioning of Sr^{2+} and Mg^{2+} into calcite under karst-analogue experimental conditions." *Geochimica et Cosmochimica Acta*, 65(1): 47–62.

Huang Y., Fairchild I.J., Borsato A., Frisia S., Cassidy N.J., McDermott F. and Hawkesworth C.J. (**2001**). "Seasonal variations in Sr, Mg and P in modern speleothems (Grotta di Ernesto, Italy)." *Chemical Geology*, 175(3): 429–448.

Hurrell J.W., Kushnir Y., Ottersen G. and Visbeck M., *An overview of the North Atlantic oscillation*. Wiley Online Library, **2003**.

Hurrell J.W., Visbeck M., Busalacchi A., Clarke R., Delworth T., Dickson R., Johns W.E., Koltermann K., Kushnir Y. and Marshall D. (**2006**). "Atlantic climate variability and predictability: A CLIVAR perspective." *Journal of Climate*, 19(20): 5100–5121.

Imbrie J. and Imbrie K.P., *Ice ages: solving the mystery*. Harvard University Press, **1986**.

Ionita M. (**2014**). "The impact of the East Atlantic/Western Russia pattern on the hydroclimatology of Europe from mid-winter to late spring." *Climate*, 2(4): 296–309.

Ionita M., Chelcea S., Rimbu N. and Adler M.J. (**2014**). "Spatial and temporal variability of winter streamflow over Romania and its relationship to large-scale atmospheric circulation." *Journal of Hydrology*, 519: 1339–1349.

Ivanovich M. and Harmon R.S., eds., *Uranium-series disequilibrium: applications to earth, marine, and environmental sciences. 2.* Clarendon Press, Oxford (United Kingdom), **1992**.

Jaeschke A., Rühlemann C., Arz H., Heil G. and Lohmann G. (**2007**). "Coupling of millennial–scale changes in sea surface temperature and precipitation off northeastern Brazil with high–latitude climate shifts during the last glacial period." *Paleoceanography*, 22(4).

Jex C.N., Baker A., Eden J.M., Eastwood W.J., Fairchild I.J., Leng M.J., Thomas L. and Sloane H.J. (**2011**). "A 500yr speleothem-derived reconstruction of late autumn-winter precipitation, northeast Turkey." *Quaternary Research*, 75(3): 399–405.

Jex C.N., Baker A., Fairchild I.J., Eastwood W.J., Leng M.J., Sloane H.J., Thomas L. and Bekaroğlu E. (**2010**). "Calibration of speleothem $\delta^{18}O$ with instrumental climate records from Turkey." *Global and Planetary Change*, 71(3): 207–217.

Jochum K.P., Scholz D., Stoll B., Weis U., Wilson S.A., Yang Q., Schwalb A., Börner N., Jacob D.E. and Andreae M.O. (**2012**). "Accurate trace element analysis of speleothems and biogenic calcium carbonates by LA-ICP-MS." *Chemical Geology*, 318–319: 31–44.

Jochum K.P., Weis U., Stoll B., Kuzmin D., Yang Q., Raczek I., Jacob D.E., Stracke A., Birbaum K., Frick D.A., Günther D. and Enzweiler J. (**2011**). "Determination of Reference Values for NIST SRM 610-17 Glasses Following ISO Guidelines." *Geostandards and Geoanalytical Research*, 35(4): 397–429.

Johnson K., Hu C., Belshaw N. and Henderson G. (**2006**). "Seasonal trace-element and stable-isotope variations in a Chinese speleothem: The potential for high-resolution paleomonsoon reconstruction." *Earth and Planetary Science Letters*, 244(1-2): 394–407.

Jones B. (**2009**). "Phosphatic precipitates associated with actinomycetes in speleothems from Grand Cayman, British West Indies." *Sedimentary Geology*, 219(1): 302–317.

Jones I.C., Banner J.L., Humphrey J.D. et al. (**2000**). "Estimating recharge in a tropical karst aquifer." *Water Resources Research*, 36(5): 1289–1299.

Jones P.D. and Mann M.E. (**2004**). "Climate over past millennia." *Reviews of Geophysics*, 42(2).

Jury M., Malmgren B.A. and Winter A. (**2007**). "Subregional precipitation climate of the Caribbean and relationships with ENSO and NAO." *Journal of Geophysical Research*, 112(D16).

Kaniewski D., Paulissen E., Van Campo E., Weiss H., Otto T., Bretschneider J. and Van Lerberghe K. (**2010**). "Late second–early first millennium BC abrupt climate changes in coastal Syria and their possible significance for the history of the Eastern Mediterranean." *Quaternary Research*, 74(2): 207–215.

Kaniewski D., Van Campo E., Guiot J., Le Burel S., Otto T. and Baeteman C. (**2013**). "Environmental roots of the Late Bronze Age crisis." *PLoS One*, 8(8): e71004.

Kanner L.C., Burns S.J., Cheng H. and Edwards R.L. (**2012**). "High-latitude forcing of the South American summer monsoon during the last glacial." *Science*, 335(6068): 570–573.

Karmann I., Cruz F.W., Viana O. and Burns S.J. (**2007**). "Climate influence on geochemistry parameters of waters from Santana–Pérolas cave system, Brazil." *Chemical Geology*, 244(1): 232–247.

Kaufmann G. (**2003**). "Stalagmite growth and palaeo-climate: the numerical perspective." *Earth and Planetary Science Letters*, 214(1–2): 251 – 266.

Keigwin L.D. and Boyle E.A. (**1999**). "Surface and deep ocean variability in the northern Sargasso Sea during marine isotope stage 3." *Paleoceanography*, 14(2): 164–170.

Kim S.T. and O'Neil J.R. (**1997**). "Equilibrium and nonequilibrium oxygen isotope effects in synthetic carbonates." *Geochimica et Cosmochimica Acta*, 61(16): 3461–3475.

Klein Tank et al. (**2002**). "Daily dataset of 20th-century surface air temperature and precipitation series for the European Climate Assessment." *International Journal of Climatology*, 22: 1441–1453.

Kluge T., Affek H., Marx T., Aeschbach-Hertig W., Riechelmann D., Scholz D., Riechelmann S., Immenhauser A., Richter D., Fohlmeister J. et al. (**2013**). "Reconstruction of drip-water $\delta^{18}O$ based on calcite oxygen and clumped isotopes of speleothems from Bunker Cave (Germany)." *Climate of the Past*, 9(1): 377.

Kluge T. and Affek H.P. (**2012**). "Quantifying kinetic fractionation in Bunker Cave speleothems using $\Delta 47$." *Quaternary Science Reviews*, 49: 82–94.

Kluge T., Affek H.P., Zhang Y.G., Dublyansky Y., Spötl C., Immenhauser A. and Richter D.K. (**2014**). "Clumped isotope thermometry of cryogenic cave carbonates." *Geochimica et Cosmochimica Acta*, 126: 541–554.

Kluge T., Marx T., Scholz D., Niggemann S., Mangini A. and Aeschbach-Hertig W. (**2008**). "A new tool for palaeoclimate reconstruction: Noble gas temperatures from fluid inclusions in speleothems." *Earth and Planetary Science Letters*, 269(3-4): 408–415.

Koutsodendris A., Brauer A., Reed J.M., Plessen B., Friedrich O., Hennrich B., Zacharias I. and Pross J. (**2017**). "Climate variability in {SE} Europe since 1450 {AD}

based on a varved sediment record from Etoliko Lagoon (Western Greece)." *Quaternary Science Reviews*, 159: 63 – 76.

Krichak S., Kishcha P. and Alpert P. (**2002**). "Decadal trends of main Eurasian oscillations and the Eastern Mediterranean precipitation." *Theoretical and Applied Climatology*, 72(3): 209–220.

Krichak S.O. and Alpert P. (**2005**). "Decadal trends in the east Atlantic–west Russia pattern and Mediterranean precipitation." *International Journal of Climatology*, 25(2): 183–192.

Krüger Y., Marti D., Staub R.H., Fleitmann D. and Frenz M. (**2011**). "Liquid–vapour homogenisation of fluid inclusions in stalagmites: Evaluation of a new thermometer for palaeoclimate research." *Chemical Geology*, 289(1–2): 39 – 47.

Ku T. and Li H. (**1998**). "Speleothems as high-resolution paleoenvironment archives: records from northeastern China." *Proceedings of the Indian Academy of Sciences-Earth and Planetary Sciences*, 107(4): 321–330.

Kushnir Y., Seager R., Ting M., Naik N. and Nakamura J. (**2010**). "Mechanisms of Tropical Atlantic SST Influence on North American Precipitation Variability." *Journal of Climate*, 23(21): 5610–5628.

Labuhn I., Genty D., Vonhof H., Bourdin C., Blamart D., Douville E., Ruan J., Cheng H., Edwards R.L., Pons-Branchu E. et al. (**2015**). "A high-resolution fluid inclusion $\delta^{18}O$ record from a stalagmite in SW France: modern calibration and comparison with multiple proxies." *Quaternary Science Reviews*, 110: 152–165.

Lachniet M.S. (**2009**a). "Climatic and environmental controls on speleothem oxygen-isotope values." *Quaternary Science Reviews*, 28(5-6): 412–432.

Lachniet M.S. (**2009**b). "Sea surface temperature control on the stable isotopic composition of rainfall in Panama." *Geophysical Research Letters*, 36(3).

Lachniet M.S., Asmerom Y., Bernal J.P., Polyak V.J. and Vazquez-Selem L. (**2013**). "Orbital pacing and ocean circulation-induced collapses of the Mesoamerican monsoon over the past 22,000 y." *Proceedings of the National Academy of Sciences*, 110(23): 9255–9260.

Lachniet M.S., Burns S.J., Piperno D.R., Asmerom Y., Polyak V.J., Moy C.M. and Christenson K. (**2004**). "A 1500-year El Niño/Southern Oscillation and rainfall history for the isthmus of Panama from speleothem calcite." *Journal of Geophysical Research: Atmospheres*, 109(D20).

Lachniet M.S., Johnson L., Asmerom Y., Burns S.J., Polyak V., Patterson W.P., Burt L. and Azouz A. (**2009**). "Late Quaternary moisture export across Central America and to Greenland: evidence for tropical rainfall variability from Costa Rican stalagmites." *Quaternary Science Reviews*, 28(27-28): 3348–3360.

Lachniet M.S. and Patterson W.P. (**2006**). "Use of correlation and stepwise regression to evaluate physical controls on the stable isotope values of Panamanian rain and surface waters." *Journal of Hydrology*, 324(1-4): 115–140.

Lachniet M.S. and Patterson W.P. (**2009**). "Oxygen isotope values of precipitation and surface waters in northern Central America (Belize and Guatemala) are dominated by temperature and amount effects." *Earth and Planetary Science Letters*, 284(3-4): 435–446.

Land L.S. (**1967**). "Diagenesis of skeletal carbonates." *Journal of Sedimentary Research*, 37(3).

Lea D.W., Martin P.A., Pak D.K. and Spero H.J. (**2002**). "Reconstructing a 350ky history of sea level using planktonic Mg/Ca and oxygen isotope records from a Cocos Ridge core." *Quaternary Science Reviews*, 21(1): 283–293.

Lea D.W., Pak D.K., Peterson L.C. and Hughen K.A. (**2003**). "Synchroneity of Tropical and High-Latitude Atlantic Temperatures over the Last Glacial Termination." *Science*, 301(5638): 1361–1364.

Lead J.R. and Wilkinson K.J. (**2006**). "Aquatic colloids and nanoparticles: current knowledge and future trends." *Environmental Chemistry*, 3(3): 159–171.

Leeman W. and Sisson V. (**1996**). "Geochemistry of boron and its implications for crustal and mantle processes." *Reviews in mineralogy and geochemistry*, 33(1): 645–707.

Levanič T., Poljanšek S. and Toromani E. (**2015**). "Early summer temperatures reconstructed from black pine (Pinus nigra Arnold) tree-ring widths from Albania." *The Holocene*, 25(3): 469–481.

Levanič T., Popa I., Poljanšek S. and Nechita C. (**2012**). "A 323-year long reconstruction of drought for SW Romania based on black pine (Pinus Nigra) tree-ring widths." *International Journal of Biometeorology*, 57(5): 703–714.

Levin I., Naegler T., Kromer B., Diehl M., Francey R.J., Gomez-Pelaez A.J., Steele L., Wagenbach D., Weller R. and Worthy D.E. (**2010**). "Observations and modelling of the global distribution and long-term trend of atmospheric 14CO2." *Tellus B*, 62(1): 26–46.

Lewis S.C., Gagan M.K., Ayliffe L.K., Zhao J.x., Hantoro W.S., Treble P.C., Hellstrom J.C., LeGrande A.N., Kelley M., Schmidt G.A. and Suwargadi B.W. (**2011**). "High-resolution stalagmite reconstructions of Australian-Indonesian monsoon rainfall variability during Heinrich stadial 3 and Greenland interstadial 4." *Earth and Planetary Science Letters*, 303(1-2): 133–142.

Lorens R.B. (**1981**). "Sr, Cd, Mn and Co distribution coefficients in calcite as a function of calcite precipitation rate." *Geochimica et Cosmochimica Acta*, 45(4): 553–561.

Luterbacher J., Dietrich D., Xoplaki E., Grosjean M. and Wanner H. (**2004**). "European seasonal and annual temperature variability, trends, and extremes since 1500." *Science*, 303(5663): 1499–503.

Luterbacher J., Xoplaki E., Dietrich D., Jones P., Davies T., Portis D., Gonzalez-Rouco J., Von Storch H., Gyalistras D., Casty C. et al. (**2001**). "Extending North Atlantic oscillation reconstructions back to 1500." *Atmospheric Science Letters*, 2(1-4): 114–124.

Luterbacher J., Xoplaki E., Dietrich D., Rickli R., Jacobeit J., Beck C., Gyalistras D., Schmutz C. and Wanner H. (**2002**). "Reconstruction of sea level pressure fields over the Eastern North Atlantic and Europe back to 1500." *Climate Dynamics*, 18(7): 545–561.

Magyari E., Buczkó K., Jakab G., Braun M., Pßl Z., Karßtson D. and Pap I. (**2009**). "Palaeolimnology of the last crater lake in the Eastern Carpathian Mountains: a multiproxy study of Holocene hydrological changes." *Hydrobiologia*, 631(1): 29–63.

Mangini A., Spötl C. and Verdes P. (**2005**). "Reconstruction of temperature in the Central Alps during the past 2000 yr from a $\delta^{18}O$ stalagmite record." *Earth and Planetary Science Letters*, 235(3-4): 741–751.

Mann M.E., Bradley R.S. and Hughes M.K. (**1998**). "Global-scale temperature patterns and climate forcing over the past six centuries." *Nature*, 392(6678): 779–787.

Mann M.E., Woodruff J.D., Donnelly J.P. and Zhang Z. (**2009**a). "Atlantic hurricanes and climate over the past 1,500 years." *Nature*, 460(7257): 880–3.

Mann M.E., Zhang Z., Rutherford S., Bradley R.S., Hughes M.K., Shindell D., Ammann C., Faluvegi G. and Ni F. (**2009**b). "Global signatures and dynamical origins of the Little Ice Age and Medieval Climate Anomaly." *Science*, 326(5957): 1256–60.

Martín-Chivelet J., Muñoz-García M.B., Edwards R.L., Turrero M.J. and Ortega A.I. (**2011**). "Land surface temperature changes in Northern Iberia since 4000yrBP, based on $\delta^{13}C$ of speleothems." *Global and Planetary Change*, 77(1): 1–12.

Martis A., van Oldenborgh G.J. and Burgers G. (**2002**). "Predicting rainfall in the Dutch Caribbean - more than El Niño?" *International Journal of Climatology*, 22(10): 1219–1234.

Mason H.E., Frisia S., Tang Y., Reeder R.J. and Phillips B.L. (**2007**). "Phosphorus speciation in calcite speleothems determined from solid-state NMR spectroscopy." *Earth and Planetary Science Letters*, 254(3): 313–322.

Matos L., Mienis F., Wienberg C., Frank N., Kwiatkowski C., Groeneveld J., Thil F., Abrantes F., Cunha M.R. and Hebbeln D. (**2015**). "Interglacial occurrence of cold-water corals off Cape Lookout (NW Atlantic): First evidence of the Gulf Stream influence." *Deep Sea Research Part I: Oceanographic Research Papers*, 105: 158–170.

Mattey D., Lowry D., Duffet J., Fisher R., Hodge E. and Frisia S. (**2008**). "A 53-year seasonally resolved oxygen and carbon isotope record from a modern Gibraltar speleothem: Reconstructed drip water and relationship to local precipitation." *Earth and Planetary Science Letters*, 269(1-2): 80–95.

Mattey D.P., Fairchild I.J., Atkinson T.C., Latin J.P., Ainsworth M. and Durell R. (**2010**). "Seasonal microclimate control of calcite fabrics, stable isotopes and trace elements in modern speleothem from St Michaels Cave, Gibraltar." *Geological Society, London, Special Publications*, 336(1): 323–344.

Mayewski P.A., Rohling E.E., Curt Stager J., KarlÃ©n W., Maasch K.A., David Meeker L., Meyerson E.A., Gasse F., van Kreveld S., Holmgren K., Lee-Thorp J., Rosqvist G., Rack F., Staubwasser M., Schneider R.R. and Steig E.J. (**2004**). "Holocene climate variability." *Quaternary Research*, 62(3): 243–255.

McDermott F. (**2004**). "Palaeo-climate reconstruction from stable isotope variations in speleothems: a review." *Quaternary Science Reviews*, 23(7-8): 901–918.

McDonald J., Drysdale R. and Hill D. (**2004**). "The 2002–2003 El Niño recorded in Australian cave drip waters: implications for reconstructing rainfall histories using stalagmites." *Geophysical Research Letters*, 31(22).

McGarry S.F. and Baker A. (**2000**). "Organic acid fluorescence: applications to speleothem palaeoenvironmental reconstruction." *Quaternary Science Reviews*, 19(11): 1087–1101.

McGee D., Donohoe A., Marshall J. and Ferreira D. (**2014**). "Changes in ITCZ location and cross-equatorial heat transport at the Last Glacial Maximum, Heinrich Stadial 1, and the mid-Holocene." *Earth and Planetary Science Letters*, 390: 69–79.

McGee D., Quade J., Edwards R.L., Broecker W.S., Cheng H., Reiners P.W. and Evenson N. (**2012**). "Lacustrine cave carbonates: Novel archives of paleohydrologic change in the Bonneville Basin (Utah, USA)." *Earth and Planetary Science Letters*, 351: 182–194.

McGillen M.R. and Fairchild I.J. (**2005**). "An experimental study of incongruent dissolution of $CaCO_3$ under analogue glacial conditions." *Journal of Glaciology*, 51(174): 383–390.

McManus J.F., Francois R., Gherardi J.M., Keigwin L.D. and Brown-Leger S. (**2004**). "Collapse and rapid resumption of Atlantic meridional circulation linked to deglacial climate changes." *Nature*, 428(6985): 834–837.

McMillan E.A., Fairchild I.J., Frisia S., Borsato A. and McDermott F. (**2005**). "Annual trace element cycles in calcite-aragonite speleothems: evidence of drought in the western Mediterranean 1200-1100 yr BP." *Journal of Quaternary Science*, 20(5): 423–433.

Meckler A.N., Affolter S., Dublyansky Y.V., Krüger Y., Vogel N., Bernasconi S.M., Frenz M., Kipfer R., Leuenberger M., Spötl C. et al. (**2015**). "Glacial–interglacial temperature change in the tropical West Pacific: A comparison of stalagmite-based paleothermometers." *Quaternary Science Reviews*, 127: 90–116.

Meckler A.N., Ziegler M., Millán M.I., Breitenbach S.F. and Bernasconi S.M. (**2014**). "Long-term performance of the Kiel carbonate device with a new correction scheme for clumped isotope measurements." *Rapid Communications in Mass Spectrometry*, 28(15): 1705–1715.

Medina-Elizalde M., Burns S.J., Lea D.W., Asmerom Y., von Gunten L., Polyak V., Vuille M. and Karmalkar A. (**2010**). "High resolution stalagmite climate record from the Yucatán Peninsula spanning the Maya terminal classic period." *Earth and Planetary Science Letters*, 298(1-2): 255–262.

Medina-Elizalde M., Burns S.J., Polanco-Martínez J., Beach T., Lases-Hernández F., Shen C.C. and Wang H.C. (**2016**). "High-resolution speleothem record of precipitation from the Yucatán Peninsula spanning the Maya Preclassic Period." *Global and Planetary Change*, 138: 93–102.

Merlivat L. and Jouzel J. (**1979**). "Global climatic interpretation of the deuterium-oxygen 18 relationship for precipitation." *Journal of Geophysical Research: Oceans*, 84(C8): 5029–5033.

Mestas-Nuñez A.M., Enfield D.B. and Zhang C. (**2007**). "Water Vapor Fluxes over the Intra-Americas Sea: Seasonal and Interannual Variability and Associations with Rainfall." *Journal of Climate*, 20(9): 1910–1922.

Mestas-Nuñez A.M. and Miller A.J. (**2006**). "Interdecadal variability and climate change in the eastern tropical Pacific: A review." *Progress in Oceanography*, 69(2-4): 267–284.

Meyer K.W., Feng W., Breecker D.O., Banner J.L. and Guilfoyle A. (**2014**). "Interpretation of speleothem calcite $\delta^{13}C$ variations: evidence from monitoring soil CO_2, drip water, and modern speleothem calcite in central Texas." *Geochimica et Cosmochimica Acta*, 142: 281–298.

Meyer M.C., Faber R. and Spötl C. (**2006**). "The WinGeol Lamination Tool: new software for rapid, semi-automated analysis of laminated climate archives." *The Holocene*, 16(5): 753–761.

Mickler P.J., Banner J.L., Stern L., Asmerom Y., Edwards R.L. and Ito E. (**2004**). "Stable isotope variations in modern tropical speleothems: Evaluating equilibrium vs. kinetic isotope effects." *Geochimica et Cosmochimica Acta*, 68(21): 4381–4393.

Micu D.M., Dumitrescu A., Cheval S. and Birsan M.V., *Climate of the Romanian Carpathians*. Springer, **2015**.

Milankovitch M. (**1941**). "Kanon der Erdbestrahlung und seine Anwendung auf das Eiszeitenproblem." *Académie Royale Serbe Editions Speciales Section des Sciences Mathématiques et Naturelles*, 133.

Miller T. (**2010**). "Stream pirates of the Caribbean: Tanamá and Camuy Rivers in the northern karst of Puerto Rico." *Espeleorevista Puerto Rico*, 2: 8 – 13.

Mischel S.A., Scholz D. and Spötl C. (**2015**). "$\delta^{18}O$ values of cave drip water: a promising proxy for the reconstruction of the North Atlantic Oscillation?" *Climate Dynamics*, 45(11): 3035–3050.

Mischel S.A., Scholz D., Spötl C., Jochum K.P., Schröder-Ritzrau A. and Fiedler S. (**in press**). "Holocene climate variability in Central Germany and a potential link to the polar North Atlantic: A replicated record from three coeval speleothems." *The Holocene*, 0(0): 0959683616670246.

Monroe W.H., *Some tropical landforms of Puerto Rico.* US Government Printing Office, **1980**.

Moore C.H., *Carbonate Reservoirs: Porosity, Evolution & Diagenesis in a Sequence Stratigraphic Framework*, vol. 55. Elsevier, **2001**.

Morellón M., Anselmetti F.S., Ariztegui D., Brushulli B., Sinopoli G., Wagner B., Sadori L., Gilli A. and Pambuku A. (**2016**). "Human–climate interactions in the central Mediterranean region during the last millennia: The laminated record of Lake Butrint (Albania)." *Quaternary Science Reviews*, 136: 134–152.

Moreno A., Pérez A., Frigola J., Nieto-Moreno V., Rodrigo-Gámiz M., Martrat B., González-Sampériz P., Morellón M., Martín-Puertas C., Corella J.P. et al. (**2012**). "The Medieval Climate Anomaly in the Iberian Peninsula reconstructed from marine and lake records." *Quaternary Science Reviews*, 43: 16–32.

Morse J.W. and Mackenzie F.T., *Geochemistry of sedimentary carbonates*, vol. 48. Elsevier, **1990**.

Mucci A. and Morse J.W. (**1983**). "The incorporation of Mg^{2+} and Sr^{2+} into calcite overgrowths: influences of growth rate and solution composition." *Geochimica et Cosmochimica Acta*, 47(2): 217–233.

Mueller A.D., Islebe G.A., Hillesheim M.B., Grzesik D.A., Anselmetti F.S., Ariztegui D., Brenner M., Curtis J.H., Hodell D.A. and Venz K.A. (**2009**). "Climate drying and associated forest decline in the lowlands of northern Guatemala during the late Holocene." *Quaternary Research*, 71(2): 133–141.

Mühlinghaus C., Scholz D. and Mangini A. (**2007**). "Modelling stalagmite growth and $\delta^{13}C$ as a function of drip interval and temperature." *Geochimica et Cosmochimica Acta*, 71(11): 2780–2790.

Mühlinghaus C., Scholz D. and Mangini A. (**2009**). "Modelling fractionation of stable isotopes in stalagmites." *Geochimica et Cosmochimica Acta*, 73(24): 7275–7289.

Murphy L.N., Clement A.C., Albani S., Mahowald N.M., Swart P. and Arienzo M.M. (**2014**). "Simulated changes in atmospheric dust in response to a Heinrich stadial." *Paleoceanography*, 29(1): 30–43.

Musgrove M. and Banner J.L. (**2004**). "Controls on the spatial and temporal variability of vadose dripwater geochemistry: Edwards Aquifer, central Texas." *Geochimica et Cosmochimica Acta*, 68(5): 1007–1020.

Neff U. (**2001**). "Massenspektrometrische Th/U-Datierung von Höhlensintern aus dem Oman: Klimaarchive des asiatischen Monsuns, Universität Heidelberg." Ph.D. thesis, Dissertation.

Nehrke G., Reichart G.J., Van Cappellen P., Meile C. and Bijma J. (**2007**). "Dependence of calcite growth rate and Sr partitioning on solution stoichiometry: Non-Kossel crystal growth." *Geochimica et Cosmochimica Acta*, 71(9): 2240–2249.

NGRIP members (**2004**). "High-resolution record of Northern Hemisphere climate extending into the last interglacial period." *Nature*, 431(7005): 147–151.

Nieto-Moreno V., Martínez-Ruiz F., Willmott V., García-Orellana J., Masqué P. and Damsté J.S. (**2013**). "Climate conditions in the westernmost Mediterranean over the last two millennia: An integrated biomarker approach." *Organic Geochemistry*, 55: 1–10.

Nissen K., Leckebusch G., Pinto J.G., Renggli D., Ulbrich S. and Ulbrich U. (**2010**). "Cyclones causing wind storms in the Mediterranean: characteristics, trends and links to large-scale patterns." *Natural Hazards and Earth System Science*, 10(7): 1379–1391.

Noronha A.L., Johnson K.R., Southon J.R., Hu C., Ruan J. and McCabe-Glynn S. (**2015**). "Radiocarbon evidence for decomposition of aged organic matter in the vadose zone as the main source of speleothem carbon." *Quaternary Science Reviews*, 127: 37–47.

Nürnberg D., Ziegler M., Karas C., Tiedemann R. and Schmidt M.W. (**2008**). "Interacting Loop Current variability and Mississippi River discharge over the past 400 kyr." *Earth and Planetary Science Letters*, 272(1): 278–289.

Obert J.C., Scholz D., Felis T., Brocas W.M., Jochum K.P. and Andreae M.O. (**2016**). "^{230}Th/U dating of Last Interglacial brain corals from Bonaire (southern Caribbean) using bulk and theca wall material." *Geochimica et Cosmochimica Acta*, 178: 20–40.

Ólafsdóttir K. and Mudelsee M. (**2014**). "More accurate, calibrated bootstrap confidence intervals for estimating the correlation between two time series." *Mathematical Geosciences*, 46(4): 411–427.

Onac B.P., Constantin S., Lundberg J. and Lauritzen S.E. (**2002**). "Isotopic climate record in a Holocene stalagmite from Ursilor Cave (Romania)." *Journal of Quaternary Science*, 17(4): 319–327.

Onac B.P., Forray F.L., Wynn J.G. and Giurgiu A.M. (**2014**). "Guano-derived δ^{13}C-based paleo-hydroclimate record from Gaura cu Musca Cave, SW Romania." *Environmental Earth Sciences*, 71(9): 4061–4069.

Onac B.P., Hutchinson S.M., Geantă A., Forray F.L., Wynn J.G., Giurgiu A.M. and Coroiu I. (**2015**). "A 2500-yr late Holocene multi-proxy record of vegetation and hydrologic changes from a cave guano-clay sequence in SW Romania." *Quaternary Research*, 83(3): 437–448.

O'Neil J.R., Clayton R.N. and Mayeda T.K. (**1969**). "Oxygen isotope fractionation in divalent metal carbonates." *The Journal of Chemical Physics*, 51(12): 5547–5558.

Orland I.J., Burstyn Y., Bar-Matthews M., Kozdon R., Ayalon A., Matthews A. and Valley J.W. (**2014**). "Seasonal climate signals (1990-2008) in a modern Soreq Cave stalagmite as revealed by high-resolution geochemical analysis." *Chemical Geology*, 363: 322–333.

PAGES 2k Consortium (**2013**). "Continental-scale temperature variability during the past two millennia." *Nature Geoscience*, 6(5): 339.

Paillard D. (**2001**). "Glacial cycles: toward a new paradigm." *Reviews of Geophysics*, 39(3): 325–346.

Pajón J., Hernández I., Ortega F. and Macle J., *Period of wet climate in Cuba: evaluation of expression in karst of Sierra de San Carlos*, chap. 13. Academic Press San Diego, **2001**, 217–226.

Papula L., *Mathematik für Ingenieure und Naturwissenschaftler Band 3.* Springer Fachmedien Wiesbaden, **2016**.

Paquette J. and Reeder R.J. (**1995**). "Relationship between surface structure, growth mechanism, and trace element incorporation in calcite." *Geochimica et Cosmochimica Acta*, 59(4): 735–749.

Parise M., Valdes Suarez M.V., Potenza R., Del Vecchio U., Marangella A., Maurano F. and Torrez Mirabal L.D. (**2005**). "Geological and morphological observations in the eastern part of the Gran Caverna de Santo Tomas, Cuba (results of the "Santo Tomas 2003" speleological expedition)." *Cave and Karst Science, Transactions of the British cave Research Association*, 32(1): 19.

Pearce N.J., Perkins W.T., Westgate J.A., Gorton M.P., Jackson S.E., Neal C.R. and Chenery S.P. (**1997**). "A compilation of new and published major and trace element data

for NIST SRM 610 and NIST SRM 612 glass reference materials." *Geostandards newsletter*, 21(1): 115–144.

Peterson L.C. (**2000**). "Rapid Changes in the Hydrologic Cycle of the Tropical Atlantic During the Last Glacial." *Science*, 290(5498): 1947–1951.

Pett-Ridge J.C. (**2009**). "Contributions of dust to phosphorus cycling in tropical forests of the Luquillo Mountains, Puerto Rico." *Biogeochemistry*, 94(1): 63–80.

Pla S. and Catalan J. (**2005**). "Chrysophyte cysts from lake sediments reveal the submillennial winter/spring climate variability in the northwestern Mediterranean region throughout the Holocene." *Climate Dynamics*, 24(2-3): 263–278.

Poage M.A. and Chamberlain C.P. (**2001**). "Empirical relationships between elevation and the stable isotope composition of precipitation and surface waters: considerations for studies of paleoelevation change." *American Journal of Science*, 301(1): 1–15.

Poirier C., Tessier B., Chaumillon É., Bertin X., Fruergaard M., Mouazé D., Noël S., Weill P. and Wöppelmann G. (**2017**). "Decadal changes in North Atlantic atmospheric circulation patterns recorded by sand spits since 1800CE." *Geomorphology*, 281: 1–12.

Polag D., Scholz D., Mühlinghaus C., Spötl C., Schröder-Ritzrau A., Segl M. and Mangini A. (**2010**). "Stable isotope fractionation in speleothems: Laboratory experiments." *Chemical Geology*, 279(1): 31–39.

Popa I. and Kern Z. (**2008**). "Long-term summer temperature reconstruction inferred from tree-ring records from the Eastern Carpathians." *Climate Dynamics*, 32(7-8): 1107–1117.

Poveda G., Waylen P.R. and Pulwarty R.S. (**2006**). "Annual and inter-annual variability of the present climate in northern South America and southern Mesoamerica." *Palaeogeography, Palaeoclimatology, Palaeoecology*, 234(1): 3–27.

Proctor C., Baker A. and Barnes W. (**2002**). "A three thousand year record of North Atlantic climate." *Climate Dynamics*, 19(5): 449–454.

Qayyum M.F., Ashraf I., Abid M. and Steffens D. (**2015**). "Effect of biochar, lime, and compost application on phosphorus adsorption in a Ferralsol." *Journal of Plant Nutrition and Soil Science*, 178(4): 576–581.

Rahmstorf S. (**2003**). "Timing of abrupt climate change: A precise clock." *Geophysical Research Letters*, 30(10).

Railsback L. (**2008**). "Speciation of inorganic carbon in aqueous solution."

Ramos-Román M., Jiménez-Moreno G., Anderson R., García-Alix A., Toney J., Jiménez-Espejo F. and Carrión J. (**2016**). "Centennial-scale vegetation and North Atlantic Oscillation changes during the Late Holocene in the southern Iberia." *Quaternary Science Reviews*, 143: 84–95.

Ramsey C.B. (**1995**). "Radiocarbon calibration and analysis of stratigraphy; the OxCal program." *Radiocarbon*, 37(2): 425–430.

Rasbury E.T. and Cole J.M. (**2009**). "Directly dating geologic events: U-Pb dating of carbonates." *Reviews of Geophysics*, 47(3).

Rayner N., Brohan P., Parker D., Folland C., Kennedy J., Vanicek M., Ansell T. and Tett S. (**2006**). "Improved analyses of changes and uncertainties in sea surface temperature measured in situ since the mid-nineteenth century: the HadSST2 dataset." *Journal of Climate*, 19(3): 446–469.

Reeve A.S. and Perry E.C. (**1994**). "Carbonate geochemistry and the concentrations of aqueous Mg^{2+}, Sr^{2+} and Ca^{2+}: western north coast of the Yucatan, Mexico." *Chemical Geology*, 112(1-2): 105–117.

Regattieri E., Zanchetta G., Drysdale R., Isola I., Hellstrom J. and Dallai L. (**2014**). "Lateglacial to Holocene trace element record (Ba, Mg, Sr) from Corchia Cave (Apuan Alps, central Italy): paleoenvironmental implications." *Journal of Quaternary Science*, 29(4): 381–392.

Richards D.A. and Dorale J.A. (**2003**). "Uranium-series chronology and environmental applications of speleothems." *Reviews in Mineralogy and Geochemistry*, 52(1): 407–460.

Riechelmann D.F.C., Schröder-Ritzrau A., Scholz D., Fohlmeister J., Spötl C., Richter D.K. and Mangini A. (**2011**). "Monitoring Bunker Cave (NW Germany): A prerequisite to interpret geochemical proxy data of speleothems from this site." *Journal of Hydrology*, 409(3-4): 682–695.

Rimbu N., Onac B.P. and Racovita G. (**2012**). "Large-scale anomaly patterns associated to temperature variability inside Scarisoara Ice Cave." *International Journal of Climatology*, 32(10): 1495–1502.

Roberts M.S., Smart P.L. and Baker A. (**1998**). "Annual trace element variations in a Holocene speleothem." *Earth and Planetary Science Letters*, 154(1-4): 237–246.

Roberts N., Moreno A., Valero-Garcés B.L., Corella J.P., Jones M., Allcock S., Woodbridge J., Morellón M., Luterbacher J., Xoplaki E. et al. (**2012**). "Palaeolimnological evidence for an east–west climate see-saw in the Mediterranean since AD 900." *Global and Planetary Change*, 84: 23–34.

Roberts W.H.G., Valdes P.J. and Payne A.J. (**2014**). "Topography's crucial role in Heinrich Events." *Proceedings of the National Academy of Sciences*, 111(47): 16688–16693.

Roche P., Grière L., Babre D., Calba H. and Fallavier P. (**1978**). "La carence en phosphore des sols intertropicaux et ses méthodes d'appréciation." *Bulletin de l'Association Française pour l'étude du Sol*, (4): 251–268.

Rohling E., Mayewski P., Abu-Zied R., Casford J. and Hayes A. (**2002**). "Holocene atmosphere-ocean interactions: records from Greenland and the Aegean Sea." *Climate Dynamics*, 18(7): 587–593.

Román-Más A. and Lee R.W. (**1987**). "Geochemical evolution of waters within the north coast limestone aquifers of Puerto Rico: A conceptualization based on a flow path in the Barceloneta area." *U.S. Geological Survey Water Resources Investigations Report*, 86-4080.

Romanov D., Kaufmann G. and Dreybrodt W. (**2008**). "Modeling stalagmite growth by first principles of chemistry and physics of calcite precipitation." *Geochimica et Cosmochimica Acta*, 72(2): 423–437.

Roy P.D., Quiroz-Jiménez J.D., Pérez-Cruz L.L., Lozano-García S., Metcalfe S.E., Lozano-Santacruz R., López-Balbiaux N., Sánchez-Zavala J.L. and Romero F.M. (**2013**). "Late Quaternary paleohydrological conditions in the drylands of northern Mexico: a summer precipitation proxy record of the last 80 cal ka BP." *Quaternary Science Reviews*, 78: 342–354.

Rozanski K., Araguás-Araguás L. and Gonfiantini R. (**1993**). "Isotopic patterns in modern global precipitation." *Climate change in continental isotopic records*: 1–36.

Rudloff W., *World-climates, with tables of climatic data and practical suggestions*. Wissenschaftliche Verlagsgesellschaft, **1981**.

Rudzka D., McDermott F. and Surić M. (**2012**). "A late Holocene climate record in stalagmites from Modrič Cave (Croatia)." *Journal of Quaternary Science*, 27(6): 585–596.

Rudzka-Phillips D., McDermott F., Jackson A. and Fleitmann D. (**2013**). "Inverse modelling of the ^{14}C bomb pulse in stalagmites to constrain the dynamics of soil carbon cycling at selected European cave sites." *Geochimica et Cosmochimica Acta*, 112: 32–51.

Sabatier P., Dezileau L., Colin C., Briqueu L., Bouchette F., Martinez P., Siani G., Raynal O. and Von Grafenstein U. (**2012**). "7000years of paleostorm activity in the NW Mediterranean Sea in response to Holocene climate events." *Quaternary Research*, 77(1): 1–11.

Sachs J.P. and Lehman S.J. (**1999**). "Subtropical North Atlantic Temperatures 60,000 to 30,000 Years Ago." *Science*, 286(5440): 756–759.

Sanchez P.A. and Uehara G. (**1980**). "Management considerations for acid soils with high phosphorus fixation capacity." *The role of phosphorus in agriculture*: 471–514.

Schmidt M.W. and Spero H.J. (**2011**). "Meridional shifts in the marine ITCZ and the tropical hydrologic cycle over the last three glacial cycles." *Paleoceanography*, 26(1).

Schmidt M.W., Spero H.J. and Lea D.W. (**2004**). "Links between salinity variation in the Caribbean and North Atlantic thermohaline circulation." *Nature*, 428(6979): 160–163.

Schmidt M.W., Vautravers M.J. and Spero H.J. (**2006**). "Western Caribbean sea surface temperatures during the late Quaternary." *Geochemistry, Geophysics, Geosystems*, 7(2).

Schnitchen C., Charman D., Magyari E., Braun M., Grigorszky I., Tóthmérész B., Molnár M. and Szántó Z. (**2006**). "Reconstructing hydrological variability from testate amoebae analysis in Carpathian peatlands." *Journal of Paleolimnology*, 36(1): 1–17.

Scholl M.A., Shanley J.B., Zegarra J.P. and Coplen T.B. (**2009**). "The stable isotope amount effect: new insights from NEXRAD echo tops, Luquillo Mountains, Puerto Rico." *Water resources research*, 45(12).

Scholz D., Frisia S., Borsato A., Spötl C., Fohlmeister J., Mudelsee M., Miorandi R. and Mangini A. (**2012**). "Holocene climate variability in north-eastern Italy: potential influence of the NAO and solar activity recorded by speleothem data." *Climate of the Past*, 8(4): 1367–1383.

Scholz D. and Hoffmann D. (**2008**). "^{230}Th/U-dating of fossil corals and speleothems." *Quat. Sci. J*, 57: 52.

Scholz D. and Hoffmann D.L. (**2011**). "StalAge - An algorithm designed for construction of speleothem age models." *Quaternary Geochronology*, 6(3-4): 369–382.

Scholz D., Mangini A. and Felis T. (**2004**). "U-series dating of diagenetically altered fossil reef corals." *Earth and Planetary Science Letters*, 218(1-2): 163–178.

Scholz D., Mühlinghaus C. and Mangini A. (**2009**). "Modelling δ^{13}C and δ^{18}O in the solution layer on stalagmite surfaces." *Geochimica et Cosmochimica Acta*, 73(9): 2592–2602.

Scholz D., Tolzmann J., Hoffmann D.L., Jochum K.P., Spötl C. and Riechelmann D.F. (**2014**). "Diagenesis of speleothems and its effect on the accuracy of ^{230}Th/U-ages." *Chemical Geology*, 387: 74–86.

Schrag D.P., Adkins J.F., McIntyre K., Alexander J.L., Hodell D.A., Charles C.D. and McManus J.F. (**2002**). "The oxygen isotopic composition of seawater during the Last Glacial Maximum." *Quaternary Science Reviews*, 21(1): 331–342.

Schroeder J.H. (**1969**). "Experimental dissolution of calcium, magnesium, and strontium from recent biogenic carbonates: a model of diagenesis." *Journal of Sedimentary Research*, 39(3).

Schulte A. and Ruhiyat D., *Soils of tropical forest ecosystems: characteristics, ecology and management*. Springer Science & Business Media, **1998**.

Schwarcz H.P., Harmon R.S., Thompson P. and Ford D.C. (**1976**). "Stable isotope studies of fluid inclusions in speleothems and their paleoclimatic significance." *Geochimica et Cosmochimica Acta*, 40(6): 657–665.

Shackleton N. (**1974**). "Attainment of isotopic equilibrium between ocean water and the benthonic foraminifera genus Uvigerina: isotopic changes in the ocean during the last glacial." *Colloques Internationaux du C.N.R.S*, (219).

Sharp Z., *Principles of stable isotope geochemistry*. Pearson Education Upper Saddle River, NJ, **2007**.

Sharpley A. and Rekolainen S. (**1997**). "Phosphorus in agriculture and its environmental implications."

Shopov Y., Ford D. and Schwarcz H. (**1994**). "Luminescent microbanding in speleothems: High-resolution chronology and paleoclimate." *Geology*, 22(5): 407–410.

Sims J.T. and Pierzynski G.M. (**2005**). "Chemistry of phosphorus in soils." *Chemical processes in soils*: 151–192.

Sinclair D.J. (**2011**). "Two mathematical models of Mg and Sr partitioning into solution during incongruent calcite dissolution: implications for dripwater and speleothem studies." *Chemical Geology*, 283(3): 119–133.

Sinclair D.J., Banner J.L., Taylor F.W., Partin J., Jenson J., Mylroie J., Goddard E., Quinn T., Jocson J. and Miklavič B. (**2012**). "Magnesium and strontium systematics in tropical speleothems from the Western Pacific." *Chemical Geology*, 294-295: 1–17.

Smeck N.E. (**1985**). "Phosphorus dynamics in soils and landscapes." *Geoderma*, 36(3): 185 – 199.

Smith A.C., Wynn P.M., Barker P.A., Leng M.J., Noble S.R. and Tych W. (**2016**). "North Atlantic forcing of moisture delivery to Europe throughout the Holocene." *Scientific reports*, 6.

Smith C.L., Fairchild I.J., Spötl C., Frisia S., Borsato A., Moreton S.G. and Wynn P.M. (**2009**). "Chronology building using objective identification of annual signals in trace element profiles of stalagmites." *Quaternary Geochronology*, 4(1): 11–21.

Spivack A., Palmer M. and Edmond J. (**1987**). "The sedimentary cycle of the boron isotopes." *Geochimica et Cosmochimica Acta*, 51(7): 1939–1949.

Spooner P.T., Chen T., Robinson L.F. and Coath C.D. (**2016**). "Rapid uranium-series age screening of carbonates by laser ablation mass spectrometry." *Quaternary Geochronology*, 31: 28–39.

Spötl C. (**2011**). "Long-term performance of the Gasbench isotope ratio mass spectrometry system for the stable isotope analysis of carbonate microsamples." *Rapid Commun Mass Spectrom*, 25(11): 1683–5.

Spötl C., Fairchild I.J. and Tooth A.F. (**2005**). "Cave air control on dripwater geochemistry, Obir Caves (Austria): Implications for speleothem deposition in dynamically ventilated caves." *Geochimica et Cosmochimica Acta*, 69(10): 2451 – 2468.

Spötl C. and Vennemann T.W. (**2003**). "Continuous-flow isotope ratio mass spectrometric analysis of carbonate minerals." *Rapid Commun Mass Spectrom*, 17(9): 1004–6.

Stager J.C., Ryves D.B., Chase B.M. and Pausata F.S. (**2011**). "Catastrophic drought in the Afro-Asian monsoon region during Heinrich event 1." *Science*, 331(6022): 1299–1302.

Steffens D., Leppin T., Luschin-Ebengreuth N., Min Yang Z. and Schubert S. (**2010**). "Organic soil phosphorus considerably contributes to plant nutrition but is neglected by routine soil-testing methods." *Journal of Plant Nutrition and Soil Science*, 173(5): 765–771.

Strikis N.M., Cruz F.W., Cheng H., Karmann I., Edwards R.L., Vuille M., Wang X., de Paula M.S., Novello V.F. and Auler A.S. (**2011**). "Abrupt variations in South American monsoon rainfall during the Holocene based on a speleothem record from central-eastern Brazil." *Geology*, 39(11): 1075–1078.

Stumm W. and Morgan J.J., "Aquatic chemistry: an introduction emphasizing chemical equilibria in natural waters." In "Aquatic chemistry: An introduction emphasizing chemical equilibria in natural waters," **1981**, 795–795.

Sundqvist H.S., Holmgren K., Fohlmeister J., Zhang Q., Matthews M.B., Spötl C. and Körnich H. (**2013**). "Evidence of a large cooling between 1690 and 1740 AD in southern Africa." *Scientific reports*, 3.

Swart P.K., Lohmann K.C., McKenzie J. and Savin S. (**1993**). "Climate change in continental isotopic records." *Washington DC American Geophysical Union Geophysical Monograph Series*, 78.

Synal H.A., Stocker M. and Suter M. (**2007**). "MICADAS: a new compact radiocarbon AMS system." *Nuclear Instruments and Methods in Physics Research Section B: Beam Interactions with Materials and Atoms*, 259(1): 7–13.

Tămaş T., Onac B.P. and Bojar A.V. (**2010**). "Lateglacial-Middle Holocene stable isotope records in two coeval stalagmites from the Bihor Mountains, NW Romania." *Geological Quarterly*, 49(2): 185–194.

Tan L., Shen C.C., Cai Y., Lo L., Cheng H. and An Z. (**2014**). "Trace-element variations in an annually layered stalagmite as recorders of climatic changes and anthropogenic pollution in Central China." *Quaternary Research*, 81(2): 181–188.

Tan L., Yi L., Cai Y., Shen C.C., Cheng H. and An Z. (**2013**). "Quantitative temperature reconstruction based on growth rate of annually-layered stalagmite: a case study from central China." *Quaternary Science Reviews*, 72: 137–145.

Tan M., Baker A., Genty D., Smith C., Esper J. and Cai B. (**2006**). "Applications of stalagmite laminae to paleoclimate reconstructions: comparison with dendrochronology/climatology." *Quaternary Science Reviews*, 25(17): 2103–2117.

Tang J., Dietzel M., Böhm F., Köhler S.J. and Eisenhauer A. (**2008**). "Sr^{2+}/Ca^{2+} and $^{44}Ca/^{40}Ca$ fractionation during inorganic calcite formation: II. Ca isotopes." *Geochimica et Cosmochimica Acta*, 72(15): 3733–3745.

Tesoriero A.J. and Pankow J.F. (**1996**). "Solid solution partitioning of Sr^{2+}, Ba^{2+}, and Cd^{2+} to calcite." *Geochimica et Cosmochimica Acta*, 60(6): 1053–1063.

Thornthwaite C.W. (**1948**). "An approach toward a rational classification of climate." *Geographical review*, 38(1): 55–94.

Tomozeiu R., Stefan S. and Busuioc A. (**2005**). "Winter precipitation variability and large-scale circulation patterns in Romania." *Theoretical and Applied Climatology*, 81(3-4): 193–201.

Tooth A.F. and Fairchild I.J. (**2003**). "Soil and karst aquifer hydrological controls on the geochemical evolution of speleothem-forming drip waters, Crag Cave, southwest Ireland." *Journal of Hydrology*, 273(1): 51–68.

Touchan R., Xoplaki E., Funkhouser G., Luterbacher J., Hughes M.K., Erkan N., Akkemik Ü. and Stephan J. (**2005**). "Reconstructions of spring/summer precipitation for the Eastern Mediterranean from tree-ring widths and its connection to large-scale atmospheric circulation." *Climate dynamics*, 25(1): 75–98.

Treble P., Chappell J., Gagan M.K., McKeegan K.D. and Harrison T.M. (**2005**). "In situ measurement of seasonal δ 18 O variations and analysis of isotopic trends in a modern speleothem from southwest Australia." *Earth and Planetary Science Letters*, 233(1): 17–32.

Treble P., Shelley J.M.G. and Chappell J. (**2003**). "Comparison of high resolution sub-annual records of trace elements in a modern (1911-1992) speleothem with instrumental

climate data from southwest Australia." *Earth and Planetary Science Letters*, 216(1-2): 141–153.

Tremaine D.M. and Froelich P.N. (**2013**). "Speleothem trace element signatures: a hydrologic geochemical study of modern cave dripwaters and farmed calcite." *Geochimica et Cosmochimica Acta*, 121: 522–545.

Tremaine D.M., Froelich P.N. and Wang Y. (**2011**). "Speleothem calcite farmed in situ: modern calibration of $\delta^{18}O$ and $\delta^{13}C$ paleoclimate proxies in a continuously-monitored natural cave system." *Geochimica et Cosmochimica Acta*, 75(17): 4929–4950.

Trouet V. (**2014**). "A tree-ring based late summer temperature reconstruction (AD 1675–1980) for the northeastern Mediterranean." *Radiocarbon*, 56(4): S69–S78.

Trouet V., Esper J., Graham N.E., Baker A., Scourse J.D. and Frank D.C. (**2009**). "Persistent positive North Atlantic oscillation mode dominated the Medieval Climate Anomaly." *Science*, 324(5923): 78–80.

van Beynen P. and Febbroriello P. (**2006**). "Seasonal isotopic variability of precipitation and cave drip water at Indian Oven Cave, New York." *Hydrological processes*, 20(8): 1793–1803.

van Breukelen M., Vonhof H., Hellstrom J., Wester W. and Kroon D. (**2008**). "Fossil dripwater in stalagmites reveals Holocene temperature and rainfall variation in Amazonia." *Earth and Planetary Science Letters*, 275(1 - 2): 54 – 60.

Vieten R., Winter A., Warken S.F., Schröder-Ritzrau A., Miller T.E. and Scholz D. (**2016**). "Seasonal temperature variations controlling cave ventilation processes in Cueva Larga, Puerto Rico." *International Journal of Speleology*, 45(3): 7.

Vieten R., Winterhalder S., Winter A., Scholz D., Miller T., Spötl C. and Schröder-Ritzrau A. (**in press**). "Monitoring of Cueva Larga, Puerto Rico - a First Step to Decode Speleothem Climate Records." *Karst Groundwater Contamination and Public Health. Selected papers and abstracts of the symposium held January 27 through 30, 2016, San Juan, Puerto Rico. Karst Waters Institute Special Publication*, 19: 74.

Vogel N., Brennwald M.S., Fleitmann D., Wieler R., Maden C., Süsli A. and Kipfer R. (**2013**). "A combined vacuum crushing and sieving (CVCS) system designed to determine noble gas paleotemperatures from stalagmite samples." *Geochemistry, geophysics, geosystems*, 14(7): 2432–2444.

von Storch H. and Zwiers F.W., *Statistical analysis in climate research.* Cambridge University Press, **1999**.

Vuille M. (**2003**). "Modeling $\delta^{18}O$ in precipitation over the tropical Americas: 2. Simulation of the stable isotope signal in Andean ice cores." *Journal of Geophysical Research*, 108(D6).

Wackerbarth A., Scholz D., Fohlmeister J. and Mangini A. (**2010**). "Modelling the $\delta^{18}O$ value of cave drip water and speleothem calcite." *Earth and Planetary Science Letters*, 299(3-4): 387–397.

Wada K., "The distinctive properties of Andosols." In "Advances in soil science," Springer, **1985**, 173–229.

Wainer K., Genty D., Blamart D., Daëron M., Bar-Matthews M., Vonhof H., Dublyansky Y., Pons-Branchu E., Thomas L., Van Calsteren P. et al. (**2011**). "Speleothem record of the last 180 ka in Villars cave (SW France): investigation of a large $\delta^{18}O$ shift between MIS6 and MIS5." *Quaternary Science Reviews*, 30(1): 130–146.

Walker T. and Syers J.K. (**1976**). "The fate of phosphorus during pedogenesis." *Geoderma*, 15(1): 1–19.

Wang H. and Fu R. (**2007**). "The Influence of Amazon Rainfall on the Atlantic ITCZ through Convectively Coupled Kelvin Waves." *Journal of Climate*, 20(7): 1188–1201.

Wang X., Auler A.S., Edwards R.L., Cheng H., Cristalli P.S., Smart P.L., Richards D.A. and Shen C.C. (**2004**). "Wet periods in northeastern Brazil over the past 210 kyr linked to distant climate anomalies." *Nature*, 432(7018): 740–743.

Wang X., Auler A.S., Edwards R.L., Cheng H., Ito E. and Solheid M. (**2006**). "Interhemispheric anti-phasing of rainfall during the last glacial period." *Quaternary Science Reviews*, 25(23): 3391–3403.

Wang X., Auler A.S., Edwards R.L., Cheng H., Ito E., Wang Y., Kong X. and Solheid M. (**2007**). "Millennial-scale precipitation changes in southern Brazil over the past 90,000 years." *Geophysical Research Letters*, 34(23).

Wang X., Edwards R.L., Auler A.S., Cheng H., Kong X., Wang Y., Cruz F.W., Dorale J.A. and Chiang H.W. (**2017**). "Hydroclimate changes across the Amazon lowlands over the past 45,000 years." *Nature*, 541(7636): 204–207.

Wang Y., Cheng H., Edwards R., Kong X., Shao X., Chen S., Wu J., Jiang X., Wang X. and An Z. (**2008**). "Millennial-and orbital-scale changes in the East Asian monsoon over the past 224,000 years." *Nature*, 451(7182): 1090–1093.

Wang Y.J., Cheng H., Edwards R.L., An Z.S., Wu J.Y., Shen C.C. and Dorale J.A. (**2001**). "A high-resolution absolute-dated late Pleistocene Monsoon record from Hulu Cave, China." *Science*, 294(5550): 2345–8.

Wanner H., Brönnimann S., Casty C., Gyalistras D., Luterbacher J., Schmutz C., Stephenson D.B. and Xoplaki E. (**2001**). "North Atlantic Oscillation – concepts and studies." *Surveys in geophysics*, 22(4): 321–381.

Wassenburg J., Immenhauser A., Richter D., Niedermayr A., Riechelmann S., Fietzke J., Scholz D., Jochum K., Fohlmeister J., Schröder-Ritzrau A. et al. (**2013**). "Moroccan speleothem and tree ring records suggest a variable positive state of the North Atlantic Oscillation during the Medieval Warm Period." *Earth and Planetary Science Letters*, 375: 291–302.

Wassenburg J., Scholz D., Jochum K., Cheng H., Oster J., Immenhauser A., Richter D., Häger T., Jamieson R., Baldini J., Hoffmann D. and Breitenbach S. (**2016**). "Determination of aragonite trace element distribution coefficients from speleothem calcite-aragonite transitions." *Geochimica et Cosmochimica Acta*, 190: 347 – 367.

Wassenburg J.A., Immenhauser A., Richter D.K., Jochum K.P., Fietzke J., Deininger M., Goos M., Scholz D. and Sabaoui A. (**2012**). "Climate and cave control on Pleistocene/Holocene calcite-to-aragonite transitions in speleothems from Morocco: Elemental and isotopic evidence." *Geochimica et Cosmochimica Acta*, 92: 23–47.

Webb M., Dredge J., Barker P., Mueller W., Jex C., Desmarchelier J., Hellstrom J. and Wynn P. (**2014**). "Quaternary climatic instability in south-east Australia from a multi-proxy speleothem record." *Journal of Quaternary Science*, 29(6): 589–596.

Wedepohl K.H. (**1995**). "The composition of the continental crust." *Geochimica et cosmochimica Acta*, 59(7): 1217–1232.

Winter A., Miller T., Kushnir Y., Sinha A., Timmermann A., Jury M.R., Gallup C., Cheng H. and Edwards R.L. (**2011**). "Evidence for 800years of North Atlantic multi-decadal variability from a Puerto Rican speleothem." *Earth and Planetary Science Letters*, 308(1-2): 23–28.

Winter A., Zanchettin D., Miller T., Kushnir Y., Black D., Lohmann G., Burnett A., Haug G.H., Estrella-Martínez J., Breitenbach S.F. et al. (**2015**). "Persistent drying in the tropics linked to natural forcing." *Nature communications*, 6.

Wolff E., Chappellaz J., Blunier T., Rasmussen S. and Svensson A. (**2010**). "Millennial-scale variability during the last glacial: The ice core record." *Quaternary Science Reviews*, 29(21 - 22): 2828 – 2838.

Woodhead J., Hellstrom J., Maas R., Drysdale R., Zanchetta G., Devine P. and Taylor E. (**2006**). "U–Pb geochronology of speleothems by MC-ICPMS." *Quaternary Geochronology*, 1(3): 208–221.

Xoplaki E., Luterbacher J., Paeth H., Dietrich D., Steiner N., Grosjean M. and Wanner H. (**2005**). "European spring and autumn temperature variability and change of extremes over the last half millennium." *Geophysical Research Letters*, 32(15).

Yang Q., Scholz D., Jochum K.P., Hoffmann D.L., Stoll B., Weis U., Schwager B. and Andreae M.O. (**2015**). "Lead isotope variability in speleothems-A promising new proxy for hydrological change? First results from a stalagmite from western Germany." *Chemical Geology*, 396: 143–151.

Zarriess M., Johnstone H., Prange M., Steph S., Groeneveld J., Mulitza S. and Mackensen A. (**2011**). "Bipolar seesaw in the northeastern tropical Atlantic during Heinrich stadials." *Geophysical Research Letters*, 38(4).

Zhang R. and Delworth T.L. (**2005**). "Simulated tropical response to a substantial weakening of the Atlantic thermohaline circulation." *Journal of Climate*, 18(12): 1853–1860.

Ziegler M., Nürnberg D., Karas C., Tiedemann R. and Lourens L.J. (**2008**). "Persistent summer expansion of the Atlantic Warm Pool during glacial abrupt cold events." *Nature Geoscience*, 1(9): 601–605.

Zwiers F.W. and von Storch H. (**1995**). "Taking serial correlation into account in tests of the mean." *Journal of Climate*, 8(2): 336–351.